

**Synthesis and Evaluation of Glycomimetic Antagonists
for the Lectins DC-SIGN and FimH**

Inauguraldissertation

zur

Erlangung der Würde eines Doktors der Philosophie

vorgelegt der

Philosophisch-Naturwissenschaftlichen Fakultät

der Universität Basel

von

Katharina Mayer

aus Reutlingen, Deutschland

Basel, 2014

Genehmigt von der Philosophisch-Naturwissenschaftlichen Fakultät
auf Antrag von:

Prof. Dr. Beat Ernst, Institut für Molekulare Pharmazie, Universität Basel

Prof. Dr. Karl-Heinz Altmann, Institut für Pharmazeutische Wissenschaften, ETH Zürich

Basel, den 11.12.2012

Prof. Dr. Jörg Schibler
Dekan

ACKNOWLEDGEMENT

First and foremost, I would like to express my sincere gratitude to Prof. Dr. Beat Ernst for giving me the opportunity to perform my PhD studies under his supervision. I am grateful for your guidance, your support, and the scientific discussions. You created an outstanding interdisciplinary environment with a great atmosphere and it was an exceptional experience for me to be part of it. Thank you!

I would like to thank Prof. Dr. Karl-Heinz Altmann for accepting to be the co-referee of this thesis.

I am thankful to Dr. Oliver Schwardt for the scientific advice and support and his hands-on help with equipment.

Many thanks also to PD Dr. Brian Cutting for his support and patience while introducing me to STD NMR and for the numerous scientific and non-scientific discussions.

I would like to thank Bea Wagner for her help in all kinds of ways, such as many practical tricks and providing me with laboratory equipment and the precious building blocks.

I am very grateful to my lab mates Flo, Mirko, Lijuan, and Xiaohua for the good atmosphere in lab 4007. It was great to have you around!

Thank you very much Gabi Lichtenhahn and Claudia Huber for your help with daily organizational issues.

Many thanks go to all those who contributed directly to this thesis: Dr. Meike Scharenberg and Dr. Said Rabbani for performing the competitive binding assays, Sameh Eid and Adam Zalewski for the molecular modeling studies and generating beautiful pictures which make this thesis much more colorful, Dr. Katrin Lemme, Roland Preston and Pascal Zihlmann for the ITC experiments, and Simon Kleeb and Jacqueline Bezençon for the *in vitro* PK profiling.

Furthermore, I would like to thank Prof. Dr. Angelo Vedani for his support and input on the various projects.

I would like to thank all former and present members of the IMP for the good (working) atmosphere and especially Jacqueline, Steffi, Flo, Mirko, Simon, Jonas, Gian, Roland, Arjan, Meike, Wojtek, Giulio, Lijuan, Daniela, Fan, Martin, Céline, Mo, and Matthias for the nice moments spent together outside of the lab.

Many thanks also to my friends for their support and for distracting me from science.

Last but not least, I would like to thank my family: I am very grateful to my parents and my brother for the constant support at all levels and for always being there for me.

ABSTRACT

Lectins are carbohydrate-binding proteins that are widely spread in nature and crucially involved in a multitude of biological processes. This thesis addresses the design of glycomimetic antagonists for the human lectin DC-SIGN (chapter 2) and the bacterial lectin FimH (chapter 3), which are both involved in infectious diseases.

Dendritic cell-specific ICAM-3-grabbing non-integrin (DC-SIGN) is a C-type lectin expressed on immature dendritic cells (DCs) prevalent in mucosal tissue. Besides its function as an adhesion molecule enabling the migration of DCs and binding to T cells, DC-SIGN is one of the major pathogen recognition receptors on DCs. In general, pathogen binding leads to phagocytosis, DC maturation, and migration to the lymph nodes, where antigenic fragments are presented to resting T cells which finally initiate a specific immune response. However, a variety of pathogens, such as viruses (e.g. HIV-1), bacteria (e.g. *Mycobacterium tuberculosis*), and parasites (e.g. *Schistosoma mansoni*), exploit this initial interaction with DC-SIGN to evade the immune system and, instead, efficiently infect the host. With its Ca^{2+} -dependent carbohydrate recognition domain (CRD), DC-SIGN binds oligomannosides or fucose-containing Lewis antigens such as Lewis^x ($\text{Le}^x = \text{Gal}\beta(1-4)[\text{Fuc}\alpha(1-3)]\text{GlcNAc}$) present on the surface of microbial cells or on viral envelop proteins. Blocking the first interaction between the microorganisms and DC-SIGN by suitable antagonists is therefore a promising therapeutic approach towards the prevention of infectious diseases.

The first part of this thesis addresses the development of fucose-based glycomimetic antagonists for DC-SIGN. To this end, the interaction of Lewis-type structures with DC-SIGN was elucidated. STD NMR experiments were conducted to determine the binding epitopes of Lewis trisaccharides bearing different aglycones. This study revealed a switch of the binding mode upon introduction of aromatic aglycones as a result of an additional hydrophobic interaction (chapter 2.2).

A series of trisaccharide mimics of Le^x was synthesized to elucidate the role of D-Gal and D-GlcNAc in Lewis-type structures for binding to DC-SIGN. For this purpose, the central D-GlcNAc was replaced with (1*R*,2*R*)-cyclohexane-1,2-diol based moieties and the D-Gal moiety was replaced with various deoxy analogues. Affinity data including thermodynamic binding parameters indicate that, first, D-Gal is not crucial for binding and, second, mimicking of one sugar moiety enhances binding affinity (chapters 2.3.1 and 2.3.2).

Based on the preliminary results, further glycomimetics were developed to enable the interaction with the hydrophobic area in the binding site and tested for their potential as DC-SIGN antagonists (chapter 2.3.3).

FimH is a bacterial, mannose-specific lectin expressed on the tip of filamentous surface organelles of uropathogenic *Escherichia coli*. The CRD of FimH interacts with glycoconjugates such as uroplakin Ia present on urothelial cells. This bacterial adhesion is the initial and most crucial step in the establishment of urinary tract infections (UTIs), since it prevents the bacteria from being washed out by the bulk flow of urine. UTIs are among the most common infectious diseases affecting millions of people every year. The treatment with antibiotics encounters increasing bacterial resistance and demands for alternative strategies to prevent and treat UTIs. The development of anti-adhesive agents that are able to inhibit the crucial interaction of FimH with the urothelial cells presents a promising, alternative therapeutic approach.

Intestinal absorption and renal clearance are key issues for orally dosed FimH antagonists to reach the therapeutic target in the human bladder. Besides high affinity and selectivity for the target, a potent FimH antagonist thus must exhibit favourable pharmacokinetic (PK) properties. The second part of this thesis covers three studies that aim at improving these characteristics in mannose-based FimH antagonists.

The first study was directed towards the replacement of a conserved water molecule within the CRD of FimH. For this purpose, an appropriately modified α -D-mannoside was synthesized and biologically evaluated. The unexpected loss in affinity towards FimH could be explained by detailed molecular dynamics studies (chapter 3.2.1).

A *Topliss*-based structure-activity relationship study was conducted for the investigation of biphenyl mannosides as FimH antagonists. The π - π stacking of the aromatic aglycone with Tyr48 at the rim of the binding site was elucidated and a group of high-affinity antagonists with promising physico-pharmacological properties was identified (chapter 3.2.2). One of these compounds was further investigated as part of a bioisosteres study for its potential as orally available FimH antagonist. In addition to the optimal *in vitro* PK/PD profile, this antagonist showed an excellent PK profile *in vivo* (chapter 3.2.3).

TABLE OF CONTENT

1. Lectins	1
2. DC-SIGN	5
2.1 Introduction	7
2.2 STD NMR with DC-SIGN	27
2.2.1 Manuscript 1: Binding of Lewis ^{a/x} to DC-SIGN – Nature of Aglycone Determines Binding Mode.....	28
2.2.1.1 Supporting Information.....	51
2.3 Synthesis of Glycomimetic Antagonists for DC-SIGN	61
2.3.1 Manuscript 2: Le ^x Mimics: The Role of <i>N</i> -Acetylglucosamine and D-Galactose in Binding to DC-SIGN.....	62
2.3.1.1 Synthesis of (1 <i>R</i> ,2 <i>R</i> ,3 <i>S</i>)-3-methyl-cyclohexane-1,2-diol as D-GlcNAc mimic.....	100
2.3.2 (1 <i>R</i> ,2 <i>R</i>)-cyclohexadiol as D-GlcNAc mimic.....	102
2.3.3 Synthesis of tetrahydropyran-based DC-SIGN antagonists.....	106
3. FimH	133
3.1 Introduction	135
3.2 Synthesis of Antagonists for FimH	151
3.2.1 Manuscript 3: Water: to be or not to be displaced?	152
3.2.2 Manuscript 4: <i>Topliss</i> Approach Applied to FimH Antagonists.....	167
3.2.3 Manuscript 5: FimH Antagonists - Bioisosteres to improve the <i>in vitro</i> and <i>in vivo</i> PK/PD Profile.....	203
4. Compound Index	251

1. Lectins

Lectins are carbohydrate-binding proteins widely spread throughout nature. The term lectin originates from the latin word “legere” which means “to choose” and reflects the major characteristic of these proteins, namely their carbohydrate specificity.¹ A second characteristic of lectins is their agglutinating effect on erythrocytes, which was first noted over 100 years ago.² Early studies focused on plant-derived lectins. The research on mammalian lectins started to gain popularity only in the 1970’s, as their role in biological processes became gradually apparent and the first hepatic lectin was successfully isolated.³ It was early noted that the lectin-mediated agglutination of cells can be inhibited by carbohydrates or oligosaccharides.⁴ Consequently, lectins were initially classified according to their carbohydrate-specificity. Later, Drickamer suggested a more standardized classification based on the sequence homology in the carbohydrate recognition domain (CRD).^{5,6} According to this classification system, important members of mammalian lectins include the following:

- C-type lectins which have a Ca^{2+} -dependent CRD (e.g. selectins and DC-SIGN).⁵
- S-lectins (galectins) which show specificity towards β -galactosides and have several conserved amino acid residues in their CRD.²
- I-type lectins that are members of the immunoglobulin superfamily (e.g. the Siglec family of sialic acid-binding lectins).⁷

Lectins are widely distributed in mammalian tissues and serve many different biological functions as they are involved in cell adhesion, cell recognition, cell signaling, and host immune response.⁸ Hence, a dysfunction of lectins can lead to serious diseases, such as infections, inflammatory diseases, and cancer, highlighting the potential of mammalian lectins as drug target.

Microbial lectins are an important virulence factor of bacteria. They are located on bacterial fimbriae and mediate the initial adhesion to glycoproteins present on endo- and epithelial cells of a host. Lectins of the enterobacteriaceae family are among the best-characterized bacterial lectins and were shown to play a major role in urinary tract infections and infections of the kidney. Members of this family are for example FimH, PapG, and F17G.⁹

This thesis focuses on the C-type lectin DC-SIGN (Chapter 2) and the microbial lectin FimH (Chapter 3). Both are involved in infectious diseases and therefore, constitute putative therapeutic targets for treatment and prevention.

References

1. Boyd, W.C. & Shapleigh, E. Specific Precipitating Activity of Plant Agglutinins (Lectins). *Science* **119**, 419-419 (1954).
2. Kilpatrick, D.C. Animal lectins: a historical introduction and overview. *Biochim. Biophys. Acta, Gen. Subj.* **1572**, 187-197 (2002).
3. Ashwell, G. & Morell, A. Role of role of surface carbohydrates in the hepatic recognition and transport of circulating glycoproteins. *Adv. Enzymol. Relat. Areas Mol. Biol.* **41**, 99-128 (1974).
4. Sumner, J.B. & Howell, S.F. The identification of the hemagglutinin of the jack bean with concanavalin A. *J. Bacteriol.* **32**, 227-237 (1936).
5. Drickamer, K. Ca²⁺-Dependent Carbohydrate-Recognition Domains in Animal Proteins. *Curr. Opin. Struct. Biol.* **3**, 393-400 (1993).
6. Drickamer, K. C-type lectin-like domains. *Curr. Opin. Struct. Biol.* **9**, 585-590 (1999).
7. Powell, L. & Varki, A. I-type Lectins. *J. Biol. Chem.* **270**, 14243-14246 (1995).
8. Crocker, P.R. & Feizi, T. Carbohydrate recognition systems: Functional triads in cell-cell interactions. *Curr. Opin. Struct. Biol.* **6**, 679-691 (1996).
9. Hartmann, M. & Lindhorst, T.K. The Bacterial Lectin FimH, a Target for Drug Discovery - Carbohydrate Inhibitors of Type 1 Fimbriae-Mediated Bacterial Adhesion. *Eur. J. Org. Chem.* 3583-3609 (2011).

2. DC-SIGN

2.1 Introduction

Dendritic Cells and their Role in Immune Response

Dendritic cells (DCs), termed due to their unusual tree-like shape (Greek, *dendron*, tree), were discovered in 1973 by Steinman and Cohn.¹ DCs play a major role in initiation and modulation of an immune response operating at the interface of innate and adaptive immunity. They are present in tissues (skin, mucosa, inner-lining of nose, intestines etc.) and fluids (blood) and can be described as sentinels of the immune system patrolling the body for invaders.²

There are two main types of DCs: myeloid DCs, also including Langerhans cells (LCs), and plasmacytoid DCs. Depending on their tissue location and differentiation state, DCs express various pattern recognition receptors (PRRs) on their surface, such as Toll-like receptors (TLRs)³ and C-type lectin receptors (CTLs).⁴ Immature DCs present the largest variety in CTLs. They are found in peripheral mucosal tissue and are among the first defense barrier to be encountered by invading pathogenic microorganisms.²

Once the DC captures a pathogen via receptor-mediated phagocytosis, it starts to migrate to the lymphoid organs. Meanwhile, the DC matures, processes the antigen in lysosomal compartments, and expresses co-stimulatory molecules such as cytokines and receptors that can modulate the effector functions of responding T cells.⁵ At the lymph nodes, the DC presents the degraded antigenic fragments on its surface on major histocompatibility complex (MHC) class I and II molecules to resting T cells. This results in T cell activation and initiation of an adaptive immune response, i.e. interaction with B cells for antibody formation or macrophages for cytokine release. Hence, they are called professional antigen-presenting cells.^{2,6,7}

The PRRs on DCs recognize specific pathogen-associated molecular patterns (PAMPs) of the microorganisms, e.g. viral and bacterial nucleic acids or fungal and bacterial cell wall components, such as lipopolysaccharides (LPS). The recognition of PAMPs by PRRs triggers a specific signaling pathway which contributes to the adaptive immune response. In this way, distinct PAMPs on a certain pathogen induce a specific immune response via signal transduction and receptor cross talk, as described later in this chapter.⁸

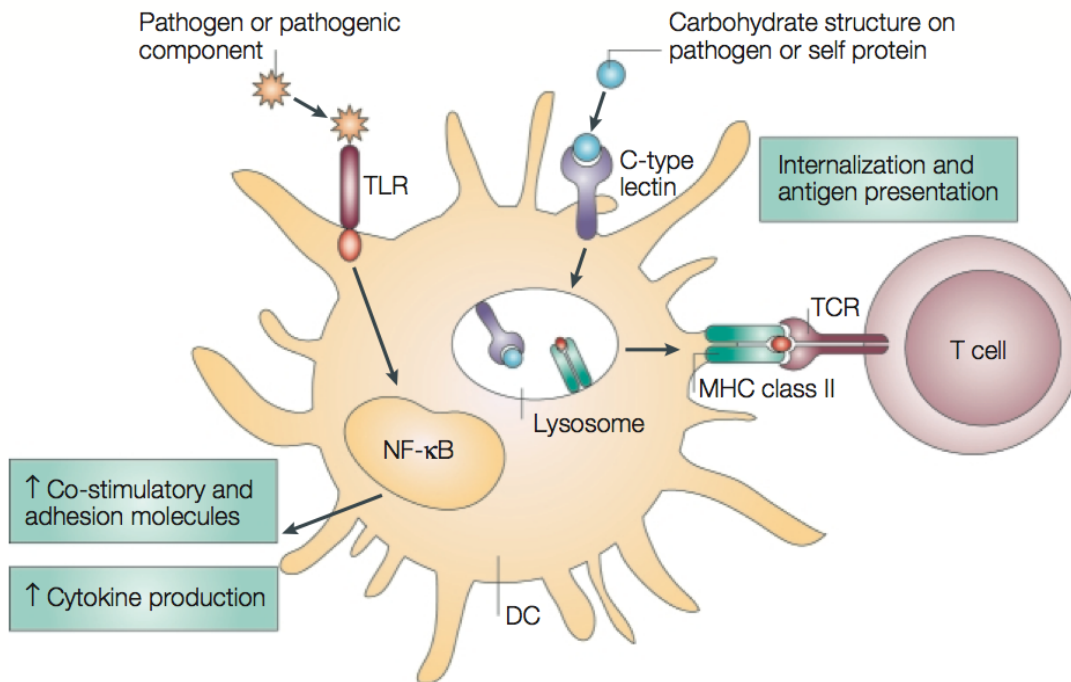


Figure 1. Scheme of a DC with its pattern-recognition receptors, such as Toll-like receptors (TLRs) and C-type lectins (CTLs). Microorganisms recognized by CTLs are internalized into lysosomal compartments where they are processed to peptidic fragments and presented as major histo-compatibility complex (MHC) to resting T cells. Binding to TLRs leads to activation of a signaling cascade triggering upregulation of co-stimulators and cytokine production, which facilitates DC maturation, taken from Geijtenbeek and van Kooyk⁹.

C-type Lectins

CTLs represent an important group of PRRs on DCs besides TLRs and scavenger receptors.¹⁰ The classification of lectins is based on primary structural homology of their carbohydrate recognition domain (CRD). The characteristic for CTLs is their Ca^{2+} -dependent carbohydrate binding.¹¹ However, the members of this lectin family differ in the type of carbohydrate structures they recognize with high affinity. The majority of CTLs are transmembrane proteins, though, soluble proteins exist as well, such as the collectins lung surfactant protein A (SP-A) and mannose binding protein (MBP).¹² One can further distinguish between type I and type II transmembrane CTLs with two and more CRD-like domains or with only one CRD, respectively. Another difference is the location of the N-terminus; in type I transmembrane proteins it is located outside the cell, whereas in type II transmembrane proteins the N-terminus is pointing into the cytoplasm.

By recognition of carbohydrate structures that are present on pathogens or self-antigens and by regulation of signaling pathways, CTLs are involved in many immune system functions.

Furthermore, they enable cell-cell adhesion and, in case of endocytic receptors, internalization of pathogens.¹³ The CTLs expressed on DCs are almost exclusively type II transmembrane proteins, such as DC-SIGN (CD209), the related DC-SIGNR (CD299)¹⁴, dectin-1, and Langerhans-cell-specific C-type lectin (Langerin, CD207).¹⁵

DC-SIGN

In 1992, Curtis *et al.* described a membrane associated PRR that has high affinity for the glycoprotein gp120 present on HIV-1.¹⁶ In 2000, the same receptor was discovered to mediate intercellular interactions with ICAM-3 on T cells by Geijtenbeek *et al.*¹⁷ They termed this transmembrane protein “dendritic cell-specific intercellular adhesion molecule (ICAM) 3-grabbing nonintegrin” (DC-SIGN). Up to now, DC-SIGN has gained more and more popularity, in particular because its crucial involvement in infections caused by HIV, Ebola virus, *Mycobacterium tuberculosis* (*M. tuberculosis*), SARS and many other microorganisms.¹⁸ DC-SIGN is one of the main receptors on DCs for recognition and uptake of various pathogens and therewith heavily involved in modulation of the immune response.^{19,20}

DC-SIGN is preferentially expressed on immature myeloid DCs and is found on dermal, interstitial, a subset of blood DCs, and on *in vitro* differentiated monocyte-derived DCs.^{21,22} Due to its highly restricted expression, DC-SIGN is considered a DC-specific phenotypic marker acquired during DC differentiation.²³

Endogenous ligands of DC-SIGN are the glycoproteins intercellular adhesion molecule-2 and -3 (ICAM-2 and ICAM-3). Besides its function as a cell-adhesion receptor for the control of DC migration via ICAM-2,^{22,24} DC-SIGN regulates the DC–T cell interactions via ICAM-3 that is present on the surface of T cells.^{18,25,26} It furthermore stabilizes the formation of synapses between the MHC class II molecules and the T cell receptor.

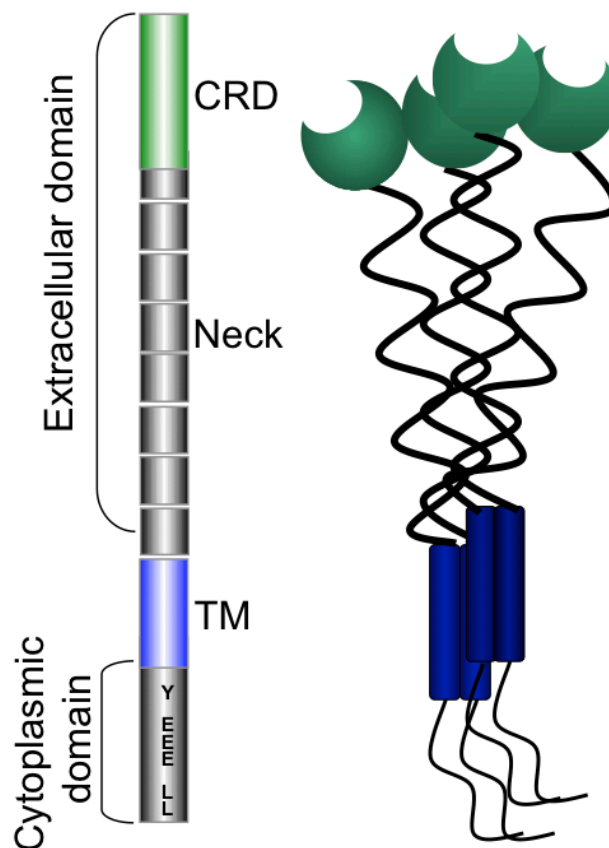


Figure 2. Schematic representation of the type II transmembrane protein DC-SIGN (taken from the dissertation of Meike Scharenberg, University of Basel²⁷). DC-SIGN consists of three domains: The cytoplasmic domain, the transmembrane domain (TM), and the extracellular domain. The cytoplasmic domain contains a di-leucine motif, a tri-acidic internalization motif and a tyrosin residue. The extracellular domain neck region is formed by seven and a half repeats of a 23 amino acid motif and induces tetramerisation of DC-SIGN monomers stabilized by hydrophobic interactions. The Ca^{2+} -dependent carbohydrate recognition domain (CRD) is located at the top.²⁰

The type II transmembrane protein DC-SIGN is part of the C-type lectin family. Figure 2 displays a schematic representation of DC-SIGN. DC-SIGN can be divided into three domains: the cytoplasmic region, the transmembrane domain and the extracellular domain. The CRD of DC-SIGN is located at the extracellular C-terminus on top of a seven and a half repeat unit of a 23 amino acid motif. This extended neck region is responsible for tetramerisation of the receptor. The α -helical structure of this extracellular unit stabilizes the tetramer via coiled-coil interactions.²⁸ Furthermore this region functions as a spacer placing the CRD away from the cell-surface, reachable for glycan structures, and allowing for multivalent interactions. The neck domain also has the function of a pH sensor. Variations in

pH encountered in physiological surrounding affect the oligomerisation state and can in particular lead to ligand release and receptor recycling.²⁹ The neck region passes on to the transmembrane region followed by a cytoplasmic tail that contains recycling and internalization motifs, such as a di-leucine based motif (Leu-Leu), a triacidic cluster (Glu-Glu-Glu), and an incomplete immunoreceptor tyrosine-based activation motif (ITAM, Tyr-x-x-Leu) which is an internalization loop associated with signaling.^{10,30}

Multimerization of the receptor enables recognition of multivalent epitope presentation, as it is the case for most pathogenic antigens. Besides increasing binding avidity, it promotes ligand specificity and is a determining factor for a specific immune response.³¹ It was shown that DC-SIGN tetramers further multimerize into so-called microdomains or lipid rafts within the membrane. This feature is associated with ligand recognition and specificity as well as internalization and signal transduction.^{32,33}

The CRD of DC-SIGN located at the top of the extracellular domain has a globular overall structure and is composed of 12 β -strands, two α -helices, and three disulfide-bridges.²⁸ Two calcium binding sites are present: one Ca^{2+} ion is essential for the tertiary protein conformation, the other one is directly involved in ligand-binding.³⁴ The CRD of DC-SIGN recognizes high D-mannose (D-Man) structures³⁵ and L-fucose (L-Fuc) containing Lewis antigens (Le), i.e. Le^a , Le^x , and Le^y present on viral envelope proteins or microbial membranes.^{36,37}

DC-SIGNR

DC-SIGNR is termed according to its close relation to DC-SIGN and shares 77% sequence identity with the latter. However, it shows distinct tissue tropism. It is not expressed in DCs but is mainly found on endothelia of liver sinusoids, lymph node sinuses, and placental villi.^{38,39} DC-SIGN and DC-SIGNR have been shown to have markedly different ligand binding characteristics. Both receptors bind to *N*-linked high-mannose oligosaccharides, however, DC-SIGNR has a diminished binding affinity for L-Fuc-containing oligosaccharides.⁴⁰

Langerin

Another protein related to DC-SIGN is Langerin, expressed exclusively on LCs.⁴¹ Langerin recognizes as well gp120 on HIV-1 but is much less susceptible to infection with the virus.⁴²

Furthermore, there is no transmission of HIV-1 to T cells via Langerin.⁴³ Internalization of virus into LCs leads to degradation of the virus and it was shown that inhibition of Langerin leads to infection of LCs. Therefore, Langerin is an important antiviral immune receptor, although signaling processes have not been elucidated yet.⁴⁴

Signaling and Involvement in Infection

The normal immunoregulatory response of DCs following pathogen recognition includes pathogen uptake, degradation, and antigen presentation. The latter together with costimulation determines CD4⁺ T helper cell differentiation as well as cytokine excretion. T helper 1 cells (T_h1) secrete Interferon- γ to activate macrophages to fight intracellular microbes. Activation of T_h2 cells leads to excretion of cytokines for a humoral immune response. T_h17 cells mobilize phagocytes for elimination of fungi or bacteria.⁴⁵ However, some microorganisms circumvent the normal degradation mechanisms and instead exploit the binding to DC-SIGN to efficiently infect the host. Among these pathogens are viruses, such as HIV-1¹⁸, Ebola virus^{46,47}, Hepatitis C virus (HCV)^{48,49}, Dengue virus⁵⁰, Herpes simplex virus⁵¹, and SARS corona virus⁵², bacteria, such as *M. tuberculosis*^{53,54} and *H. pylori*, fungi such as *C. albicans*⁵⁵, and parasites, such as *Leishmania*^{36,56} and *Schistosoma mansoni* (*S. mansoni*)³⁶. They bind with Fuc-containing Le^x epitope (*H. pylori*, *S. mansoni* egg antigen)^{36,57-59} or via high-Man structures (*M. tuberculosis*, HIV-1, and *Candida albicans*)^{54,60,61} to the CRD of DC-SIGN. It was found that each of these epitope types triggers a specific immune responses.⁵⁷ Elucidation of the exact mechanisms including signaling pathways downstream of CTLs has just begun and many details are still speculative.^{9,62} A simplified overview is given in Figure 3.

For most of the mentioned pathogens the interaction with DC-SIGN leads to interference with the transcription factor nuclear factor κ B (NF- κ B). The activation of NF- κ B is crucial for the development of an immune response.⁶³ p65 is a transcriptional active subunit of the NF- κ B family and is phosphorylated, i.e. activated, at Ser276 in DC-SIGN mediated signaling. Activation leads to translocation into the nucleus and to acetylation of p65 at a Lys residue. The latter is pivotal for p65 activity and modulates the transcription activity. In case of DC-SIGN mediated activation of p65, the gene transcription of the IL-10 promoter is prolonged which results in high levels of the immunosuppressive IL-10.¹⁹ Notably, DC-SIGN alone is not able to activate p65, however, it is instrumental in modulation of p65 activity.⁶⁴

Activation of Raf-1 via TLRs appears to be the prerequisite for induction of an immune response.

HIV-1 is one of the best-investigated examples of co-evolution to evade the eradication by host immune response. This virus targets CD4⁺ T cells by fusion to CD4 and chemokine receptors (CCR5 and CXCR4) on T cells. The envelope protein gp120 in HIV-1 interacts via its mannan structures with DC-SIGN in the mucosal tissue at the port of entry. It is then transported by DC-SIGN⁺ DCs to lymph nodes where the virus can efficiently infect CD4⁺ T cells via viral synapses.⁶⁵ Efficient virus production is mediated by CD4⁺ T cells, however infection of the DC itself was noted as well.⁶⁶ Internalization of the virus into the DC leads to triggering of endosomal TLR8 via viral ssRNA and results in activation of NF-κB and translocation into the nucleus. This initiates the transcription of short viral DNA. Binding of gp120 to DC-SIGN activates Raf-1. Phosphorylation and acetylation of p65 lead to transcription elongation of IL-10, which is crucial for synthesis of full-length HIV-1 transcripts and therewith the production and dissemination of virions.⁵⁷

A modulation of the T_h1/T_h2 balance, i.e. a shift of the immune response towards T_h2 resulting in immune evasion, is regarded as another feature pathogens evolved to favor their persistence.⁹ Infection with *M. tuberculosis* presents one example where the infection reaches a latent chronic state. The bacterium presumably subverts the elimination by suppressing the cellular immune response through induction of a specific DC-SIGN mediated signaling.⁶⁰ Mannosylated lipoarabinomannan (ManLAM) and bacterial cell-wall structures bind to DC-SIGN and TLR, respectively. Binding of ManLAM to DC-SIGN does not induce an effective immune modulation. But simultaneous triggering of TLR4 and TLR2 induces the activation of p65 and its translocation into the nucleus where DC-SIGN signaling results in phosphorylation and acetylation. This leads to a modulation of transcription of the immunosuppressive IL-10 but also of pro-inflammatory cytokines such as IL-6, IL-12, and IL-12p70.⁵⁷ Ultimately, this results in a disturbed T_h1/T_h2 balance, which might be the reason for persistence of *M. tuberculosis*.^{57,60}

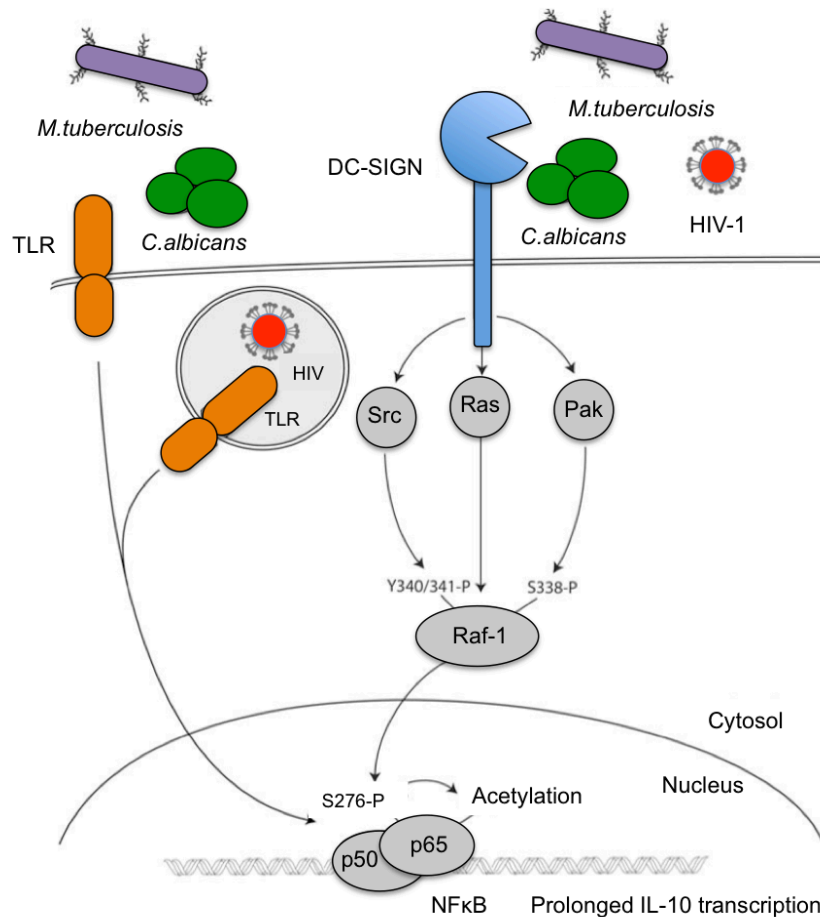


Figure 3. Schematic representation of DC with DC-SIGN-mediated signaling induced by mycobacteria, viruses and fungi (taken from the dissertation of Meike Scharenberg, University of Basel²⁷). Mannose-expressing pathogens such as *M. tuberculosis*, *C. albicans* and *HIV-1* activates *Raf-1* (activation of Ras leads to binding to *Raf-1* and induces conformational changes that allow for subsequent phosphorylation of *Raf-1* by Src and Pak kinases; Src kinases induce the phosphorylation of *Raf-1* at residue Tyr340/341, whereas Rho GTPase-dependent activation of Pak kinases results in phosphorylation of *Raf-1* at Ser338). After translocation of NF-κB by TLR-stimulation, DC-SIGN-induced *Raf-1* activation mediates the phosphorylation of NF-κB subunit p65 at Ser276, which in turn leads to p65-acetylation. Acetylation of p65 prolongs and increases the IL-10 transcription, resulting in increased IL-10 production.⁵⁷

In contrast to D-Man-induced signaling, immune responses induced by L-Fuc-containing ligands (e.g. *H. pylori*) are independent of *Raf-1* activation, i.e. do not need TLR triggering and as a consequence upregulate IL-10 but downregulate IL-6 and IL-12.⁵⁷ The reduction of IL-12 levels induced by ligands presenting Le antigens is associated with the shift of Th1 to Th2 immune response, which results in persistence (e.g. *S. mansoni* and *H. pylori*).^{67,68}

Binding of self-antigens such as ICAM-2 and ICAM-3 does not lead to DC maturation or cytokine production. Obviously, for the latter effect a secondary stimulation is necessary,

which is offered by the PAMPs of pathogens. This demonstrates the complex network and the fine tuning of these signaling cascades enabled by cross talk between different PRRs.²⁰

Co-crystallization Studies with DC-SIGN

The CRD of DC-SIGN was co-crystallized with ligand bearing D-Man (Man₂ (2IT6)⁶⁹, Man₆(2IT5)⁶⁹, Man₄ (1SL4)⁴⁰, GlcNAc₂Man₃ (1K9I)³⁴ or L-Fuc (LNFP III, 1SL5)⁴⁰. These crystallographic data reveal a rather shallow binding site. The hallmark of sugars binding to DC-SIGN is the coordination of the Ca²⁺ in the primary binding site. Five protein residues (Glu347, Asn349, Glu354, Asn365 and Asp366) define the principal Ca²⁺ binding site and contribute five of the seven coordination sites (Figure 4).⁴⁰ The coordination sphere is completed by two vicinal hydroxyl groups of the ligand, i.e. of a D-Man or a L-Fuc moiety. Analysis of different crystal structures shows that the CRD maintains almost the same geometry independent of the bound ligand. However, the distinct configuration of hydroxyl groups in D-Man and L-Fuc entails differences in Ca²⁺-coordination (Figure 4) influencing the orientation of the ligand in the binding site.

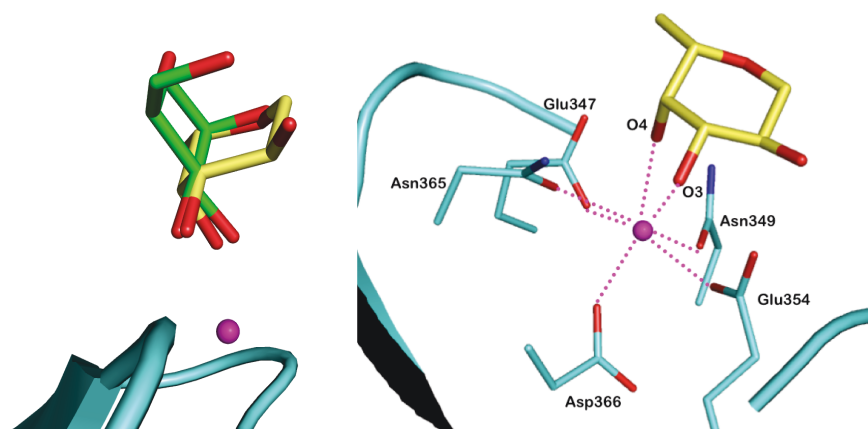


Figure 4. Comparison of the Ca²⁺-coordination (magenta sphere) in equatorial-equatorial manner by D-Man (green carbons) and a equatorial-axial manner by L-Fuc (yellow carbons). L-Fuc is tipped (yellow carbons) compared to D-Man (left). Coordination of Ca²⁺ by the equatorial 3-OH and the axial 4-OHs of L-Fuc in LNFP III (right). (PDB 1SL5⁴⁰, modeled by Sameh Eid, Institute of Molecular Pharmacy, University of Basel).

D-Man-bearing ligands coordinate the Ca²⁺ in an equatorial-equatorial manner via the 3- and 4-OH group of a Man α 1-3(Man α 1-6)Man α -motif. DC-SIGN recognizes this trimannose

substructure only if the central D-Man is linked in the α -anomeric configuration.³⁴ Figure 5 depicts the binding mode of GlcNAc₂Man₃ in complex with DC-SIGN.

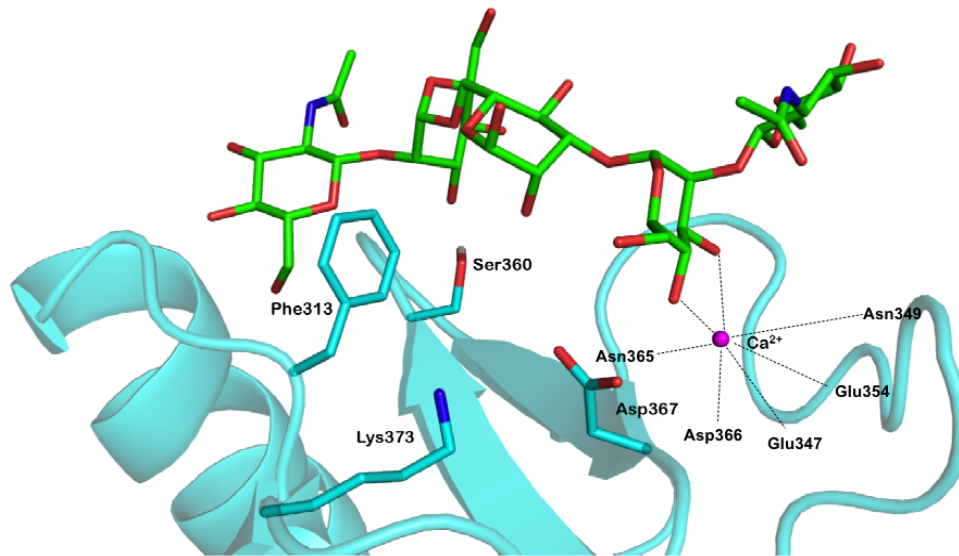


Figure 5. Binding mode of the resolved part of GlcNAc₂Man₃ (green carbons). Dashed lines show Ca²⁺-coordination by the 3-OH and the 4-OH of D-Man. D-GlcNAc and D-Man-3 are interacting with a secondary binding site lined by Phe313. (PDB 1K9I³⁴, modeled by Sameh Eid, University of Basel).

In Le^x as part of lacto-*N*-fucopentaose III (LNFP III = Le^x-D-Gal-D-Glc) the calcium is complexed by the terminal L-Fuc residue via the equatorial 3-OH and the axial 4-OH (PDB 1SL5, Figure 6)⁴⁰. Consequently, the L-Fuc is tipped and differently oriented compared to the D-Man moiety (Figure 4). This enables a van der Waals contact through C2 with Val351. The terminal D-Gal is involved in an H-bond network with Asp367 and Leu371 via its 6- and 4-OH group respectively (not shown). The D-GlcNAc moiety with the D-Gal and (unresolved) D-Glc residues points towards the solvent without efficiently contributing to binding. Hence, L-Fuc-containing ligands elevate in an upright position from the binding site and point towards the solvent (Figure 6), whereas D-Man-bearing ligands lie rather flat on the protein surface (Figure 5). Furthermore, there are differences in occupation of the binding site. L-Fuc-containing Le^x solely interacts with the main binding site surrounding the principal Ca²⁺. Mannosides use an enlarged binding site addressing also a secondary binding site lined by Phe313. This amino acid residue contributes to both ligand selectivity as well as affinity.⁴⁰ The differences in binding site accommodation and occupation might also be a reason for the distinct effects on signaling cascades downstream of DC-SIGN and therewith, on immune modulation.⁵⁷

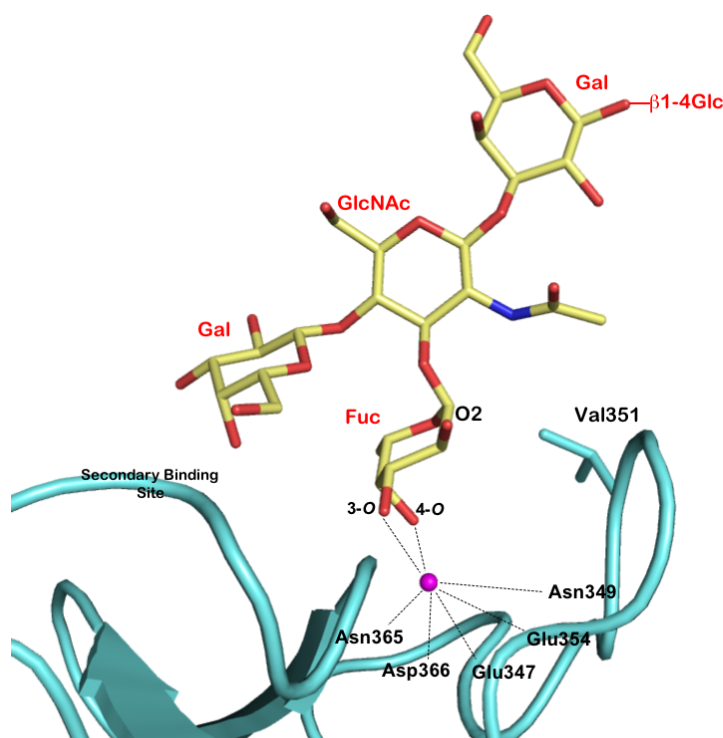


Figure 6. DC-SIGN CRD in complex with LNFP III (PDB 1SL5⁴⁰, modeled by Sameh Eid, Institute of Molecular Pharmacy, University of Basel). L-Fuc coordinates the calcium via its 3-OH and 4-OH in an equatorial-axial manner. The terminal D-Gal establishes a water mediated H-bond with Glu358 via the 4-OH. The 6-OH of D-Gal exhibits a H-bond to Asp367, which is stabilized by an interaction with Lys373. The D-GlcNAc moiety points towards the solvent.

DC-SIGN Antagonists

DC-SIGN interacts with a broad variety of pathogens, which indicates its meaningful role as an immunomodulatory receptor. Development of anti-infective agents that block the first contact between DC-SIGN and the pathogens is a promising therapeutic approach towards prevention of infectious diseases.⁷⁰⁻⁷²

Many efforts have been made to develop DC-SIGN antagonists and investigate their inhibitory potential by *in vitro* assays.^{47,73} In general, monovalent carbohydrate-lectin interactions are weak. Pathogens benefit from an avidity increase due to multivalent presentation of carbohydrate motifs. The design of DC-SIGN antagonists includes two main concepts: 1) monovalent glycomimetics and 2) multimeric presentation of oligosaccharides or respective glycomimetics.

The majority of pathogens bear D-Man-containing structures, such as GlcNAc₂Man₉ (**1**, Figure 7). This epitope is found on glycoprotein gp120 and binds to DC-SIGN with

micromolar affinity.^{69,74} The development of oligomannose glycodendrons has been proven successful in blocking DC-SIGN in a glycan array with an improved binding affinity in the nanomolar range.⁷⁵ Furthermore, gold-nanoparticles were functionalized with glycodendrons and were shown to efficiently prevent DC-SIGN-mediated *trans*-infection of T cells with HIV-1 at nanomolar concentrations.⁷⁶ In fact, already a tetravalent presentation of the linear trimannose mimic **2** is able to inhibit *trans*-infection at low micromolar concentrations (Figure 7).^{73,77} Similarly, a ROMP-derived glycopolymer with multimeric presentation of a shikimic acid based glycomimetic exhibited IC₅₀ values in the low micromolar range.⁷⁸ Furthermore, this demonstrated that shikimic acid is a suitable replacement for the D-Man moiety and hence, represents a non-carbohydrate based approach.

In many studies an increased binding avidity due to multimeric presentation of the binding epitope was proven.^{37,75,79} The multivalent presentation of oligosaccharides and mimetics makes a systemic administration difficult. However, a topical administration at the site of infection, such as mucosal surfaces, presents a possible therapeutic approach.⁸⁰

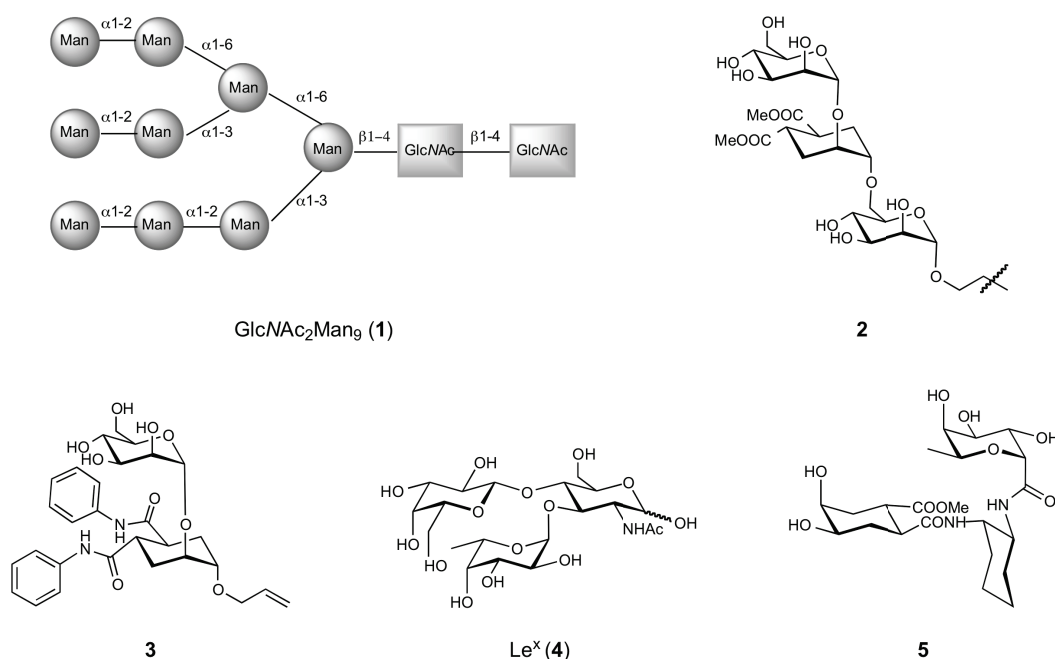


Figure 7. DC-SIGN ligands and glycomimetic antagonists. Multimeric presentation of D-Man-based glycomimetic **2**⁷³, monovalent ligand **3**⁸¹, and L-Fuc-based mimic **5**⁸² lead to affinities in the micro-molar range.

Monosaccharides, such as D-Man and L-Fuc, have low affinities to DC-SIGN with K_D values in the millimolar range.³⁵ Due to their polarity carbohydrates show no ideal drug-like properties concerning pharmacokinetics. Therefore, the development of monovalent DC-

SIGN antagonists is based on the design of glycomimetic compounds. In general, one monosaccharide anchor is chosen to establish the crucial Ca^{2+} coordination in the CRD of DC-SIGN and additional substituents are attached to make use of areas in the binding site that are not or only partially addressed by the natural ligands. In this manner, Obermajer *et al.* reported a series of potent monovalent D-man-based antagonist with low micromolar affinities (**3**, Figure 7).⁸¹ These inhibitors interact via aromatic substituents with the hydrophobic region lined by Phe313. Moreover, D-Man-containing di- or trisaccharide mimics have been designed with a cyclohexadiol moiety replacing D-man, which improved affinity.^{73,83,84}

Binding affinities of L-Fuc-containing ligands have not been determined extensively in the past. Lewis antigen, such as Le^x (**4**) and Le^y are epitopes presented by pathogens (*H. pylori*) or endogenous ligands of DC-SIGN (ICAM-2).^{24,58,85} Le^x (**1**) in a monovalent manner was determined to bind in the millimolar range.⁸² Multivalent presentation, as in human milk, leads to higher affinities and was shown to efficiently inhibit HIV-1 *trans*-infection of CD4+ lymphocytes.³⁷ In a glycan array Le^a exhibited a slightly higher relative binding affinity to DC-SIGN than the Le^x motif.⁷⁴ Lewis antigens sulfated or sialylated at the 3-O-position of D-Gal show no binding to DC-SIGN.⁷⁴ Considering the crystal structures of DC-SIGN, these extensions seem to clash with Phe313.⁴⁰ Recently, the development of L-Fuc-containing ligands has gained more interest. Bernardi *et al.* displaced the metabolically unstable α -glycosidic linkage of L-Fuc by a fucosylamide anchor.^{86,87} These ligands (e.g. **5**) exhibited slightly improved affinities compared to Le^x .^{86,87,88} Lewis-type structures are especially advantageous regarding their specificity. Whereas D-Man-containing ligands might be recognized by various other lectins as well, the mentioned L-Fuc-containing mimics were shown not to inhibit Langerin which is eligible in case of HIV-1 infection.⁸⁶

Besides the carbohydrate-based approach also screening approaches of small molecule libraries have been undertaken. In a high-throughput fluorescence-based competition assay monovalent non-carbohydrate ligands were identified with affinities in the low-micromolar range.⁸⁹ They proved to be effective in DC-SIGN dependent cell-adhesion assays, however, the precise binding mechanism was not being clarified and an allosteric binding cannot be excluded.⁷¹

A major challenge in the design and development of DC-SIGN ligands is the unpredictable outcome. Up to now no integral assay has been developed that allows for clear identification of a ligand as antagonist or agonist. Understanding of signal transduction processes and

involvement of receptor cross-talk has just begun and many details are still to be elucidated. Although much can be learned from *in vitro* data, the elaboration of suitable assay formats to elucidate DC-SIGN-related processes is a serious future task. For this matter, the design and synthesis of new ligands with high affinity and selectivity is substantial and presents the prerequisite for the development of drug-like anti-infectives.

References

1. Steinman, R.M. & Cohn, Z.A. Identification of a novel cell type in peripheral lymphoid organs of mice. *J. Exp. Med.* **139**, 380-397 (1974).
2. Banchereau, J. & Steinman, R.M. Dendritic cells and the control of immunity. *Nature* **392**, 245-252 (1998).
3. Underhill, D.M. & Ozinsky, A. Toll-like receptors: key mediators of microbe detection. *Curr. Opin. Immunol.* **14**, 103-110 (2002).
4. Weis, W.I., Taylor, M.E. & Drickamer, K. The C-type lectin superfamily in the immune system. *Immunol. Rev.* **163**, 19-34 (1998).
5. Steinman, R.M. & Inaba, K. Myeloid dendritic cells. *J. Leukocyte Biol.* **66**, 205-208 (1999).
6. Mellman, I., Turley, S.J. & Steinman, R.M. Antigen processing for amateurs and professionals. *Trends Cell. Biol.* **8**, 231-237 (1998).
7. Steinman, R.M. DC-SIGN: a guide to some mysteries of dendritic cells. *Cell* **100**, 491-494 (2000).
8. Gringhuis, S.I. & Geijtenbeek, T.B.H. Carbohydrate Signaling by C-Type Lectin DC-SIGN Affects NF-kappaB Activity. *Methods Enzymol.*, **480**, 151-164 (2010).
9. van Kooyk, Y. & Geijtenbeek, T.B.H. DC-SIGN: Escape mechanism for pathogens. *Nat. Rev. Immunol.* **3**, 697-709 (2003).
10. Engering, A., Geijtenbeek, T.B. & van Kooyk, Y. Immune escape through C-type lectins on dendritic cells. *Trends Immunol.* **23**, 480-485 (2002).
11. Weis, W.I., Taylor, M.E. & Drickamer, K. The C-type lectin superfamily in the immune system. *Immunological Reviews* **163**, 19-34 (1998).
12. Kawasaki, N., Kawasaki, T. & Yamashina, I. Isolation and Characterization of a Mannan-Binding Protein from Human-Serum. *J. Biochem. (Tokyo)* **94**, 937-947 (1983).
13. Aspberg, A., Miura, R., Bourdoulous, S., Shimonaka, M., Heinegard, D., Schachner, M., Ruoslahti, E. & Yamaguchi, Y. The C-type lectin domains of lecticans, a family of aggregating chondroitin sulfate proteoglycans, bind tenascin-R by protein-protein interactions independent of carbohydrate moiety. *Proc. Natl. Acad. Sci. U. S. A.* **94**, 10116-10121 (1997).
14. Soilleux, E.J., Barten, R. & Trowsdale, J. DC-SIGN; a related gene, DC-SIGNR; and CD23 form a cluster on 19p13. *J. Immunol.* **165**, 2937-42 (2000).
15. van Kooyk, Y., van Vliet, S., Engering, A., Appelmelk, B., van Die, I. & Geijtenbeek, T. Immune function of C-type lectins on dendritic cells. *Glycobiology*, 641-641 (2002).
16. Curtis, B.M., Scharnrowske, S. & Watson, A.J. Sequence and expression of a membrane-associated C-type lectin that exhibits CD4-independent binding of human

- immunodeficiency virus envelope glycoprotein gp120. *Proc. Natl Acad. Sci. USA* **89**, 8356-8360 (1992).
17. Geijtenbeek, T.B.H. Identification of DC-SIGN, a novel dendritic cell-specific ICAM-3 receptor that supports primary immune responses. *Cell* **100**, 575-585 (2000).
 18. Geijtenbeek, T.B.H. et al. DC-SIGN, a dendritic cell-specific HIV-1-binding protein that enhances trans-infection of T cells. *Cell* **100**, 587-597 (2000).
 19. Gringhuis, S.I., den Dunnen, J., Litjens, M., Hof, B.V., van Kooyk, Y. & Geijtenbeek, T.B.H. C-type lectin DC-SIGN modulates toll-like receptor signaling via Raf-1 kinase-dependent acetylation of transcription factor NF-kappa B. *Immunity* **26**, 605-616 (2007).
 20. Svajger, U., Anderluh, M., Jeras, M. & Obermajer, N. C-type lectin DC-SIGN: An adhesion, signalling and antigen-uptake molecule that guides dendritic cells in immunity. *Cell. Signal.* **22**, 1397-1405 (2010).
 21. Engering, A., Van Vliet, S.J., Geijtenbeek, T.B. & van Kooyk, Y. Subset of DC-SIGN+ dendritic cells in human blood transmits HIV-1 to T lymphocytes. *Blood* **100**, 1780-1786 (2002).
 22. Geijtenbeek, T.B.H., Krooshoop, D., Bleijs, D.A., van Vliet, S.J., van Duijnhoven, G.C.F., Grabovsky, V., Alon, R., Figdor, C.G. & van Kooyk, Y. DC-SIGN-ICAM-2 interaction mediates dendritic cell trafficking. *Nat. Immunol.* **1**, 353-357 (2000).
 23. Geijtenbeek, T.B.H. DC-SIGN, a dendritic cell-specific HIV-1-binding protein that enhances trans-infection of T cells. *Cell* **100**, 587-597 (2000).
 24. Garcia-Vallejo, J.J. et al. DC-SIGN mediates adhesion and rolling of dendritic cells on primary human umbilical vein endothelial cells through Lewis(Y) antigen expressed on ICAM-2. *Mol. Immunol.* **45**, 2359-2369 (2008).
 25. Geijtenbeek, T.B.H., Torensma, R., van Vliet, S.J., van Duijnhoven, G.C.F., Adema, G.J., van Kooyk, Y. & Figdor, C.G. Identification of DC-SIGN, a novel dendritic cell-specific ICAM-3 receptor that supports primary immune responses. *Cell* **100**, 575-585 (2000).
 26. Geijtenbeek, T. et al. DC-SIGN, a novel dendritic cell-specific adhesion receptor for ICAM-3 mediates DC-T cell interactions and HIV-1 infection of DC. *Blood* **94**, 434A-434A (1999).
 27. Scharenberg, M. Biological Characterization of the Lectins DC-SIGN and FimH: Putative Targets for novel Anti-Infectives, University of Basel (2011).
 28. Feinberg, H., Guo, Y., Mitchell, D.A., Drickamer, K. & Weis, W.I. Extended neck regions stabilize tetramers of the receptors DC-SIGN and DC-SIGNR. *J. Biol. Chem.* **280**, 1327-1335 (2005).
 29. Tabarani, G., Thepaut, M., Stroebel, D., Ebel, C., Vives, C., Vachette, P., Durand, D. & Fieschi, F. DC-SIGN neck domain is a pH-sensor controlling oligomerization: SAXS and hydrodynamic studies of extracellular domain. *J. Biol. Chem.* **284**, 21229-21240 (2009).
 30. Kwon, D.S., Gregorio, G., Bitton, N., Hendrickson, W.A. & Littman, D.R. DC-SIGN-mediated internalization of HIV is required for trans-enhancement of T cell infection. *Immunity* **16**, 135-144 (2002).
 31. Frison, N. Oligolysine-based oligosaccharide clusters: selective recognition and endocytosis by the mannose receptor and dendritic cell-specific intercellular adhesion molecule 3 (ICAM-3)-grabbing nonintegrin. *J. Biol. Chem.* **278**, 23922-23929 (2003).
 32. Cambi, A. et al. Microdomains of the C-type lectin DC-SIGN are portals for virus entry into dendritic cells. *J. Cell Biol.* **164**, 145-155 (2004).
 33. Koopman, M., Cambi, A., Joosten, B., Garcia-Parajo, M.F., Figdor, C.G. & van Hulst, N.F. Cell plasma membrane organization at nanometer scale studied with single molecule sensitive fluorescence microscopy. *Biophys. J.* **86**, 363A-364A (2004).

34. Feinberg, H., Mitchell, D.A., Drickamer, K. & Weis, W.I. Structural basis for selective recognition of oligosaccharides by DC-SIGN and DC-SIGNR. *Science* **294**, 2163-2166 (2001).
35. Mitchell, D.A., Fadden, A.J. & Drickamer, K. A Novel Mechanism of Carbohydrate Recognition by the C-type Lectins DC-SIGN and DC-SIGNR. *J. Biol. Chem.* **276**, 28939-28945 (2001).
36. Appelmelk, B., van Die, I., van Vliet, S., Vandenbroucke-Grauls, C., Geijtenbeek, T. & van Kooyk, Y. Cutting edge: Carbohydrate profiling identifies new pathogens that interact with dendritic cell-specific ICAM-3-grabbing nonintegrin on dendritic cells. *J. Immunol.*, 1635-1639 (2003).
37. Naarding, M.A., Ludwig, I.S., Groot, F., Berkhout, B., Geijtenbeek, T.B.H., Pollakis, G. & Paxton, W.A. Lewis X component in human milk binds DC-SIGN and inhibits HIV-1 transfer to CD4(+) T lymphocytes. *J. Clin. Invest.* **115**, 3256-3264 (2005).
38. Khoo Us Fau - Chan, K.Y.K., Chan Ky Fau - Chan, V.S.F., Chan Vs Fau - Lin, C.L.S. & Lin, C.L. DC-SIGN and L-SIGN: the SIGNs for infection.
39. Pöhlmann, S., Soilleux, E.J., Baribaud, F., Leslie, G.J., Morris, L.S., Trowsdale, J., Lee, B., Coleman, N. & Doms, R.W. DC-SIGNR, a DC-SIGN homologue expressed in endothelial cells, binds to human and simian immunodeficiency viruses and activates infection in trans. *Proc. Natl. Acad. Sci. U. S. A.* **98**, 2670-2675 (2001).
40. Guo, Y., Feinberg, H., Conroy, E., Mitchell, D., Alvarez, R., Blixt, O., Taylor, M., Weis, W. & Drickamer, K. Structural basis for distinct ligand-binding and targeting properties of the receptors DC-SIGN and DC-SIGNR. *Nat. Struct. Mol. Biol.* **11**, 591-598 (2004).
41. Stambach, N.S. & Taylor, M.E. Characterization of carbohydrate recognition by langerin, a C-type lectin of Langerhans cells. *Glycobiology* **13**, 401-410 (2003).
42. de Witte, L., Nabatov, A. & Geijtenbeek, T.B.H. Distinct roles for DC-SIGN+-dendritic cells and Langerhans cells in HIV-1 transmission. *Trends Mol. Med.* **14**, 12-19 (2008).
43. Turville, S.G. Diversity of receptors binding HIV on dendritic cell subsets. *Nature Immunol.* **3**, 975-983 (2002).
44. de Witte, L., Nabatov, A., Pion, M., Fluitsma, D., de Jong, M.A.W.P., de Gruijl, T., Piguet, V., van Kooyk, Y. & Geijtenbeek, T.B.H. Langerin is a natural barrier to HIV-1 transmission by Langerhans cells. *Nat. Med.* **13**, 367-371 (2007).
45. den Dunnen, J., Gringhuis, S.I. & Geijtenbeek, T.B.H. Dusting the sugar fingerprint: C-type lectin signaling in adaptive immunity. *Immunol. Lett.* **128**, 12-16 (2010).
46. Alvarez, C.P., Lasala, F., Carrillo, J., Muniz, O., Corbi, A.L. & Delgado, R. C-Type Lectins DC-SIGN and L-SIGN Mediate Cellular Entry by Ebola Virus in cis and in trans. *J. Virol.* **76**, 6841-6844 (2002).
47. Lasala, F., Arce, E., Otero, J.R., Rojo, J. & Delgado, R. Mannosyl Glycodendritic Structure Inhibits DC-SIGN-Mediated Ebola Virus Infection in cis and in trans. *Antimicrob. Agents Chemother.* **47**, 3970-3972 (2003).
48. Lozach, P.Y. et al. DC-SIGN and L-SIGN are high affinity binding receptors for hepatitis C virus glycoprotein E2. *J. Biol. Chem.* **278**, 20358-20366 (2003).
49. Ludwig, I.S., Lekkerkerker, A.N., Depla, E., Bosman, F., Musters, R.J.P., Depraetere, S., van Kooyk, Y. & Geijtenbeek, T.B.H. Hepatitis C Virus Targets DC-SIGN and L-SIGN To Escape Lysosomal Degradation. *J. Virol.* **78**, 8322-8332 (2004).
50. Tassaneeritthep, B. DC-SIGN (CD209) mediates dengue virus infection of human dendritic cells. *J. Exp. Med.* **197**, 823-829 (2003).
51. de Jong, M.A.W.P., de Witte, L., Bolmstedt, A., van Kooyk, Y. & Geijtenbeek, T.B.H. Dendritic cells mediate herpes simplex virus infection and transmission through the C-type lectin DC-SIGN. *J. Gen. Virol.* **89**, 2398-2409 (2008).

52. Han, D.P., Lohani, M. & Cho, M.W. Specific asparagine-linked glycosylation sites are critical for DC-SIGN- and L-SIGN-Mediated severe acute respiratory syndrome coronavirus entry. *J. Virol.* **81**, 12029-12039 (2007).
53. Geijtenbeek, T., van Vliet, S., Koppel, E., Sanchez-Hernandez, M., Vandenbroucke-Grauls, C., Appelmelk, B. & van Kooyk, Y. Mycobacteria target DC-SIGN to suppress dendritic cell function. *J. Exp. Med.*, 7-17 (2003).
54. Tailleux, L. DC-SIGN is the major Mycobacterium tuberculosis receptor on human dendritic cells. *J. Exp. Med.* **197**, 121-127 (2003).
55. Cambi, A. The C-type lectin DC-SIGN (CD209) is an antigen-uptake receptor for *Candida albicans* on dendritic cells. *Eur. J. Immunol.* **33**, 532-538 (2003).
56. Colmenares, M., Puig-Kroger, A., Pello, O.M., Corbi, A.L. & Rivas, L. Dendritic cell (DC)-specific intercellular adhesion molecule 3 (ICAM-3)-grabbing nonintegrin (DC-SIGN, CD209), a C-type surface lectin in human DCs, is a receptor for *Leishmania amastigotes*. *J. Biol. Chem.* **277**, 36766-36769 (2002).
57. Gringhuis, S.I., den Dunnen, J., Litjens, M., van der Vlist, M. & Geijtenbeek, T.B.H. Carbohydrate-specific signaling through the DC-SIGN signalosome tailors immunity to *Mycobacterium tuberculosis*, HIV-1 and *Helicobacter pylori*. *Nat. Immunol.* **10**, 1081-U58 (2009).
58. Van Die, I., Van Vliet, S.J., Schiphorst, W., Bank, C.M.C., Appelmelk, B., Nyame, A.K., Cummings, R.D., Geijtenbeek, T.B.H. & Van Kooyk, Y. The dendritic cell specific C-type lectin DC-SIGN recognizes Lewis x, a major glycan epitope of *Schistosoma mansoni* egg antigen. *Glycobiology* **12**, 3 (2002).
59. van Die, I., van Vliet, S.J., Nyame, A.K., Cummings, R.D., Bank, C.M.C., Appelmelk, B., Geijtenbeek, T.B.H. & van Kooyk, Y. The dendritic cell-specific C-type lectin DC-SIGN is a receptor for *Schistosoma mansoni* egg antigens and recognizes the glycan antigen Lewis x. *Glycobiology* **13**, 471-478 (2003).
60. Geijtenbeek, T.B.H., van Vliet, S.J., Koppel, E.A., Sanchez-Hernandez, M., Vandenbroucke-Grauls, C., Appelmelk, B. & van Kooyk, Y. Mycobacteria target DC-SIGN to suppress dendritic cell function. *J. Exp. Med.* **197**, 7-17 (2003).
61. Koppel, E.A. et al. Identification of the mycobacterial carbohydrate structure that binds the C-type lectins DC-SIGN, L-SIGN and SIGNR1. *Immunobiology* **209**, 117-127 (2004).
62. Robinson, M.J., Sancho, D., Slack, E.C., LeibundGut-Landmann, S. & Sousa, C.R.E. Myeloid C-type lectins in innate immunity. *Nat. Immunol.* **7**, 1258-1265 (2006).
63. Ouaz, F., Arron, J., Zheng, Y., Choi, Y.W. & Beg, A.A. Dendritic cell development and survival require distinct NF-kappa B subunits. *Immunity* **16**, 257-270 (2002).
64. van Vliet, S.J., den Dunnen, J., Gringhuis, S.I., Geijtenbeek, T.B.H. & van Kooyk, Y. Innate signaling and regulation of dendritic cell immunity. *Curr. Opin. Immunol.* **19**, 435-440 (2007).
65. McDonald, D., Wu, L., Bohks, S.M., KewalRamani, V.N., Unutmaz, D. & Hope, T.J. Recruitment of HIV and Its Receptors to Dendritic Cell-T Cell Junctions. *Science* **300**, 1295-1297 (2003).
66. Smed-Sorensen, A., Lore, K., Vasudevan, J., Louder, M.K., Andersson, J., Mascola, J.R., Spetz, A.L. & Koup, R.A. Differential susceptibility to human immunodeficiency virus type 1 infection of myeloid and plasmacytoid dendritic cells. *J. Virol.* **79**(2005).
67. Okano, M., Satoskar, A.R., Nishizaki, K., Abe, M. & Harn, D.A. Induction of TH2 responses and IgE is largely due to carbohydrates functioning as adjuvants on *Schistosoma mansoni* egg antigens. *J. Immunol.* **163**, 6712-6717 (1999).

68. Bergman, M.P. et al. Helicobacter pylori modulates the T helper cell 1/T helper cell 2 balance through phase-variable interaction between lipopolysaccharide and DC-SIGN. *J. Exp. Med.* **200**(2004).
69. Feinberg, H., Castelli, R., Drickamer, K., Seeberger, P.H. & Weis, W.I. Multiple modes of binding enhance the affinity of DC-SIGN for high mannose N-linked glycans found on viral glycoproteins. *J. Biol. Chem.* **282**, 4202-4209 (2007).
70. Anderluh, M., Jug, G., Svajger, U. & Obermajer, N. DC-SIGN Antagonists, a Potential New Class of Anti-Infectives. *Curr. Med. Chem.* **19**, 992-1007 (2012).
71. Ernst, B. & Magnani, J.L. From carbohydrate leads to glycomimetic drugs. *Nat. Rev. Drug Discovery* **8**, 661-677 (2009).
72. Sanchez-Navarro, M., Rojo, J., Bernardi, A., Sattin, S., Fieschi, F., Thepaut, M., Clerici, M. & Berzi, A. Dc-Sign: A Target for the Design of New Antiviral Drugs. *Drugs Future* **34**, 52-52 (2009).
73. Sattin, S. et al. Inhibition of DC-SIGN-Mediated HIV Infection by a Linear Trimannoside Mimic in a Tetravalent Presentation. *ACS Chem. Biol.* **5**, 301-312 (2010).
74. van Liempt, E. et al. Specificity of DC-SIGN for mannose- and fucose-containing glycans. *FEBS Lett.* **580**, 6123-6131 (2006).
75. Wang, S.K., Liang, P.H., Astronomo, R.D., Hsu, T.L., Hsieh, S.L., Burton, D.R. & Wong, C.H. Targeting the carbohydrates on HIV-1: Interaction of oligomannose dendrons with human monoclonal antibody 2G12 and DC-SIGN. *Proc. Natl. Acad. Sci. U. S. A.* **105**, 3690-3695 (2008).
76. Martinez-Avila, O., Bedoya, L.M., Marradi, M., Clavel, C., Alcami, J. & Penades, S. Multivalent Manno-Glyconanoparticles Inhibit DC-SIGN-Mediated HIV-1 Transinfection of Human T Cells. *ChemBioChem* **10**, 1806-1809 (2009).
77. Berzi, A., Sattin, S., Sanchez-Navarro, M., Rojo, J.F., Bernardi, A. & Clerici, M. A Linear Trimannoside Mimic Inhibits DC-SIGN Mediated HIV Infection by Polyvalent Presentation. *Infection* **38**, 17-17 (2010).
78. Garber, K.C.A., Wangkanont, K., Carlson, E.E. & Kiessling, L.L. A general glycomimetic strategy yields non-carbohydrate inhibitors of DC-SIGN. *Chem. Commun. (Camb.)* **46**, 6747-9 (2010).
79. Kabanova, A., Adamo, R., Proietti, D., Berti, F., Tontini, M., Rappuoli, R. & Costantino, P. Preparation, characterization and immunogenicity of HIV-1 related high-mannose oligosaccharides-CRM197 glycoconjugates. *Glycoconjugate J.* **27**, 501-513 (2010).
80. Lederman, M.M., Offord, R.E. & Hartley, O. Microbicides and other topical strategies to prevent vaginal transmission of HIV. *Nat. Rev. Immunol.* **6**, 371-382 (2006).
81. Obermajer, N., Sattin, S., Colombo, C., Bruno, M., Švajger, U., Anderluh, M. & Bernardi, A. Design, synthesis and activity evaluation of mannose-based DC-SIGN antagonists. *Mol. Diversity*, 1-14 (2010).
82. Timpano, G. et al. Synthesis of novel DC-SIGN ligands with an alpha-fucosylamide anchor. *ChemBioChem* **9**, 1921-1930 (2008).
83. Reina, J.J. et al. 1,2-mannobioside mimic: Synthesis, DC-SIGN interaction by NMR and docking, and antiviral activity. *ChemMedChem* **2**, 1030-1036 (2007).
84. Maria, S., Sanchez-Medina, I., Mereghetti, P., Belvisi, L., Jimenez-Barbero, J. & Bernardi, A. Synthesis and conformational analysis of an alpha-D-mannopyranosyl(1 -> 2)-alpha-D-mannopyranosyl-(1 -> 6)-alpha-D-mannopyranose mimic. *Carbohydr. Res.* **342**, 1859-1868 (2007).
85. Bogoevska, V., Nollau, P., Lucka, L., Grunow, D., Klampe, B., Uotila, L.M., Samsen, A., Gahmberg, C.G. & Wagener, C. DC-SIGN binds ICAM-3 isolated from

- peripheral human leukocytes through Lewis x residues. *Glycobiology* **17**, 324-333 (2007).
86. Andreini, M. et al. Second generation of fucose-based DC-SIGN ligands: affinity improvement and specificity versus Langerin. *Org. Biomol. Chem.* **9**, 5778-5786 (2011).
87. Timpano, G. et al. Synthesis of Novel DC-SIGN Ligands with an α -Fucosylamide Anchor. *ChemBioChem* **9**, 1921-1930 (2008).
88. Guzzi, C., Angulo, J., Doro, F., Reina, J.J., Thepaut, M., Fieschi, F., Bernardi, A., Rojo, J. & Nieto, P.M. Insights into molecular recognition of LewisX mimics by DC-SIGN using NMR and molecular modelling. *Org. Biomol. Chem.* **9**, 7705-7712 (2011).
89. Borrok, M.J. & Kiessling, L.L. Non-carbohydrate inhibitors of the lectin DC-SIGN. *J. Am. Chem. Soc.* **129**, 12780-5 (2007).

2.2 STD NMR with DC-SIGN

2.2.1 *Manuscript 1: Binding of Lewis^{a/x} to DC-SIGN – Nature of Aglycone Determines Binding Mode*

Author contributions:

Katharina Mayer: STD NMR experiments, data collection, coordination, and preparation of manuscript.

Dr. Meike Scharenberg: Protein expression, biological evaluation of antagonists, and contribution to manuscript.

Sameh Eid: Molecular modeling studies, molecular dynamics simulations, and contribution to manuscript.

Dr. Katrin Lemme: ITC experiments.

Dr. Arjan Odedra: Synthesis of antagonist **4**.

Manuscript in preparation for **ChemBioChem**

BINDING OF LEWIS^{a/x} TO DC-SIGN – NATURE OF AGLYCON DETERMINES BINDING MODE

Katharina Mayer,^{‡ a} Meike Scharenberg,^{‡ a} Sameh Eid,^{‡ a} Katrin Lemme,^a Arjan Odedra,^a
Brian Cutting,^a Said Rabbani,^a Angelo Vedani,^a Beat Ernst*^a

^a *Institute of Molecular Pharmacy, Pharmacenter, University of Basel, Klingelbergstr.50, 4056 Basel, Switzerland*

* Corresponding author: Prof. Dr. Beat Ernst, Institute of Molecular Pharmacy, Pharmacenter, University of Basel, Klingelbergstrasse 50, CH-4056 Basel, Switzerland, Tel: +41 61 2671551, Fax: +41 61 2671552; e-mail: beat.ernst@unibas.ch

[‡] These authors contributed equally to this work

Keywords: DC-SIGN · carbohydrate-lectin interaction · Lewis antigens · binding mode · STD NMR · F313A mutant

Abbreviations: CRD, carbohydrate recognition domain; DCs, dendritic cells; DC-SIGN, dendritic cell-specific intercellular adhesion molecule-3 grabbing nonintegrin; Fuc, fucose; Gal, galactose; ITC, isothermal titration calorimetry; Le, Lewis; LNFP III, lacto-*N*-fucopentaose III; Man, mannose; MHC, major histocompatibility complex; MD, molecular dynamics; NMR, nuclear magnetic resonance; PAA, polyacrylamide; PDB, protein data bank; PRR, pathogen recognition receptor; STD, saturation transfer difference

ABSTRACT

Dendritic cells (DCs) are antigen presenting cells and are essential bridges between innate and adaptive immune system. In particular, they activate T-cells during the course of infection with various pathogens. DC-SIGN (DC-specific intercellular adhesion molecule-3-grabbing non-integrin) is one of the major receptors on DCs involved in the uptake of pathogens and has gained increasing interest over the last decade. It is crucially involved in infections caused by HIV-1, Ebola virus, *Mycobacterium tuberculosis*, and a variety of other pathogens. High-mannosylated *N*-glycans or L-Fuc-containing trisaccharide motifs such as the Lewis (Le) blood group antigens Le^a and Le^x, which are surface components of these microorganisms, mediate binding to DC-SIGN.

Crystallographic data for DC-SIGN in complex with a Le^x-containing pentasaccharide suggest that the terminal sugar residues, L-Fuc and D-Gal, are predominantly involved in binding. We elucidated the interaction of DC-SIGN with Le^a and Le^x bearing two different aglycones. Binding assays together with STD NMR analysis, molecular modeling and mutagenesis studies revealed distinct binding modes dependent on the nature of the aglycone. Introduction of phenyl aglycones at the Le trisaccharides offers the establishment of an additional hydrophobic contact with Phe313 in the binding site of DC-SIGN, which entails a switch of the binding mode. Based on this information a new series of DC-SIGN antagonists can be designed.

1. INTRODUCTION

Immature dendritic cells (DCs), found in peripheral tissues throughout the body, play an essential role in triggering the immune response as they are antigen-presenting cells.^{1,2} DCs recognize and capture a broad variety of pathogens including viruses,³ bacteria,⁴ and yeasts⁵ by pathogen recognition receptors (PRRs). Pathogen uptake by PRRs as well as inflammatory cytokines and chemokines (*e.g.* IL-4) trigger DC differentiation and migration to the lymphoid organs where the mature DCs present pathogenic peptides on the major histocompatibility complex (MHC) to resting T cells.

Dendritic cell-specific intercellular adhesion molecule-3 grabbing nonintegrin (DC-SIGN) is one of the main receptors on DCs for recognition and uptake of pathogens. Since its first discovery by Geijtenbeek *et al.* in 2000³ DC-SIGN gained popularity, particularly because a variety of pathogens exploit DC-SIGN to infect their host, including HIV, Ebola virus or

SARS.^{6,7,8} The fact that different pathogens have capitalized on this infection strategy makes DC-SIGN an interesting target for a new class of anti-infectives.⁹ In a study on the binding and transfer of HIV in human rectal mucosa cells, DC-SIGN⁺ cells accounted for more than 90% of bound viruses although they represented only 1–5% of the total mucosal mononuclear cells. Furthermore, anti-DC-SIGN antibodies blocked more than 90% of HIV binding.¹⁰

DC-SIGN is a type II transmembrane protein with a C-terminal carbohydrate recognition domain (CRD). It is part of the C-type lectin family and ligand binding is Ca²⁺-dependent. The majority of pathogens bind with *N*-linked high-mannose oligosaccharides to DC-SIGN^{11,12}, e.g. mannan structures on the gp120 envelope protein of HIV-1.^{6,13} Besides oligomannosides, L-Fuc-containing blood group antigens, such as Lewis^x (Le^x, Galβ(1-4)[Fucα(1-3)]GlcNAc) and Lewis^a (Le^a, Galβ(1-3)[Fucα(1-4)]GlcNAc) that are also commonly found on pathogens, are recognized by DC-SIGN.¹⁴⁻¹⁷ Le^x and Le^a bind to DC-SIGN in the low millimolar range, with Le^a exhibiting a slightly higher binding affinity than Le^x.^{18,19} Since pathogens present these rather low-affinity sugar motives in a multimeric form to the DC-SIGN tetramers, high binding avidities are observed.^{20,21}

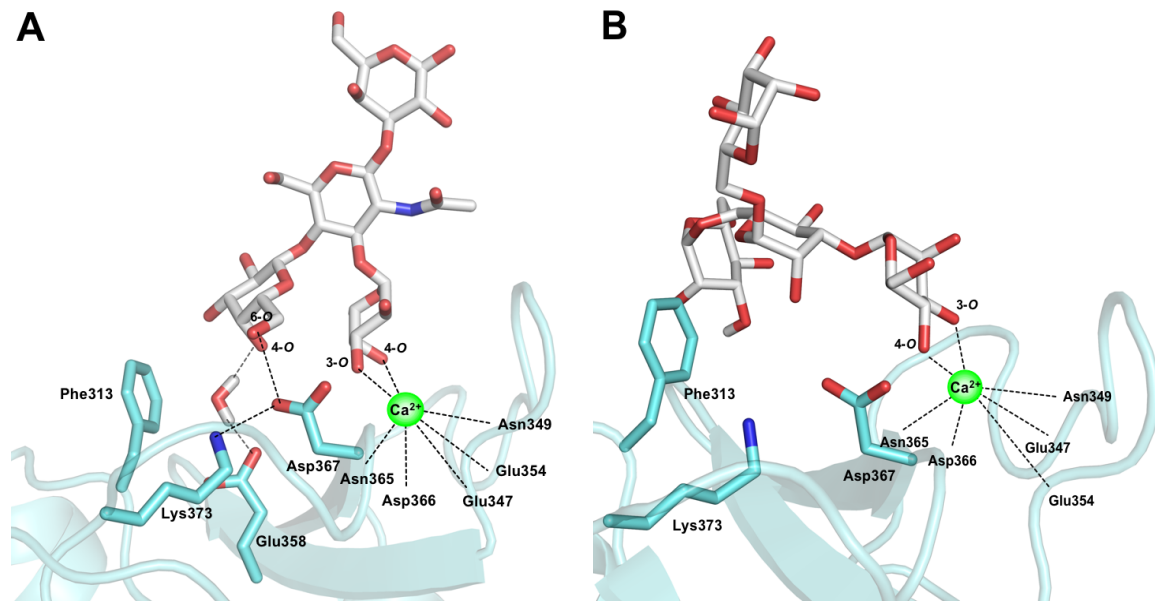


Figure 1. A) X-ray of LNFP III/CRD of DC-SIGN (PDB 1SL5).²² The equatorial 3-OH and the axial 4-OH of L-Fuc coordinate the calcium ion. The interaction of 4-OH with Glu358 is mediated by a water molecule. The 6-OH of D-galactose forms a H-bond with Asp367 which on its part is stabilized by an interaction with Lys373. B) X-ray of Man₄ {Manα(1-6)[Manα(1-3)]Manα(1-6)Man}/CRD of DC-SIGN (PDB 1SL4).^{11,22} The calcium ion is coordinated by the equatorial 3-OH and the equatorial 4-OH of the terminal α(1-3)-linked D-Man. In addition, a hydrophobic contact of the terminal α(1-6)-linked D-Man further stabilizes the interaction.

Crystallographic data (PDB: 1SL5)²² obtained from the CRD of DC-SIGN co-crystallized with lacto-*N*-fucopentaose III (LNFP III, Gal β (1-4)[Fuc α (1-3)]GlcNAc β (1-3)Gal β (1-4)Glc) suggest that the equatorial 3-OH and axial 4-OH of the L-Fuc moiety coordinate the calcium ion (Figure 1A). For the 4-OH of the D-Gal moiety a water-bridged H-bond with Glu358 is proposed. In addition, a H-bond of 6-OH of D-Gal to Lys373, bridged by Asp367 is assumed.²² For the CRD of DC-SIGN co-crystallized with oligomannosides (Man₄ and GlcNAc₂Man₃) a comparable binding mode was obtained where the equatorial 3- and 4-OH of the α (1-3)-linked D-Man moiety complex the calcium ion (Figure 1B). In addition, Man₄ (PDB 1SL4) addresses a second binding site lined by Phe313, contributing to selectivity as well as affinity.^{11,22} Only recently, Bernardi *et al.* took advantage of this additional hydrophobic contact for their design of glycomimetic DC-SIGN antagonists.^{23,24}

In our program directed to the identification of high-affinity DC-SIGN antagonists, a large library of carbohydrates and mimetics thereof was screened. One interesting finding was the unexpectedly improved affinity discovered for Le^x and Le^a antigens with aromatic aglycones (\rightarrow 3,4) compared to the corresponding methyl glycosides (\rightarrow 1,2). When these derivatives adopt a binding mode similar to LNFP III,²² the aglycones should point to the solvent and therefore not contribute directly to binding. To clarify whether a modified binding mode is responsible for the increased affinity, the binding epitopes of the Le^a and Le^x derivatives **1-4** were analyzed by STD NMR and docking studies.

2. RESULTS AND DISCUSSION

2.1. Binding Affinities for Lewis Structures. For the determination of the affinities of methyl Le^x (**1**), methyl Le^a (**2**), phenyl Le^x (**3**) and phenyl Le^a (**4**) (Table 1) a cell-free competitive binding assay was developed. It is based on the competition of a biotinylated polyacrylamide glycopolymer (Gal β (1-3)[Fuc α (1-4)]GlcNAc β -polyacrylamide, Le^a-PAA) and the ligand of interest for the CRD of DC-SIGN. A soluble recombinant protein consisting of the DC-SIGN CRD-Fc (amino acid residues 250-404) was expressed in CHO-K1 cells and purified by affinity chromatography (protein A- and L-Fuc-sepharose column). For the determination of IC₅₀ values, a microtiter plate coated with DC-SIGN CRD-Fc was incubated with biotinylated Le^a-PAA polymer conjugated to streptavidin-horseradish peroxidase and the DC-SIGN antagonist in a serial dilution. The assay was performed in duplicates and

repeated three times for each compound. To ensure comparability of different ligands, the reference compound L-Fuc was tested in parallel on each individual microtiter plate.

L-Fuc and D-Man were used as reference compounds showing IC_{50} values of 7.6 mM and 9.1 mM, respectively. These affinities correlate well with published data.²⁰ Phenyl Le^x (**3**) (IC_{50} 1.2 mM) and phenyl Le^a (**4**) (IC_{50} 0.9 mM) showed a two- to threefold increase in affinity compared to corresponding methyl derivatives [IC_{50} 2.3 mM for methyl Le^x (**1**) and 2.9 mM for methyl Le^a (**2**)]. For phenyl Le^a (**4**), the best antagonist in this series, we also performed isothermal titration calorimetry (ITC) experiments. The K_D of 582 μ M for phenyl Le^a (**4**) confirms the results of the competitive binding assay (see experimental section) with affinity in the high micromolar range. As observed for the majority of carbohydrate–lectin interactions,²⁵⁻²⁷ the binding is enthalpy driven ($\Delta H = -28.0 \pm 2.0$ kJ/mol, $T\Delta S = -9.5 \pm 2.1$ kJ/mol).

If the Le^x- and Le^a-motifs bind comparable to LNFP III,²² only the L-Fuc and D-Gal moiety participate in binding, whereas the D-GlcNAc moiety as well as the aglycone point to the solvent. Therefore, the observed beneficial effect of the aromatic aglycone was unexpected.

Table 1. The cell-free competitive binding assay is based on the competition of a biotinylated Le^a-PAA with the antagonist of interest for the CRD of DC-SIGN. The assay was performed in duplicates and repeated three times for each compound. To ensure comparability of different ligands, the reference compound L-Fuc was tested in parallel on each individual microtiter plate. ITC experiments were performed at 25 °C. Thermodynamic parameters were calculated according to the equation $\Delta G^\circ = \Delta H^\circ - T\Delta S^\circ = -RT\ln K_D$; n.d. not determined.

Ligand	Competitive binding assay, IC_{50}	Isothermal titration calorimetry, K_D
D-Man	9.1 \pm 1.3 mM	n.d.
L-Fuc	7.6 \pm 2.6 mM	n.d.
Methyl Le ^x (methyl Gal β (1-4)[Fuc α (1-3)] β GlcNAc) (1)	2.3 \pm 0.1 mM	n.d.
Methyl Le ^a (methyl Gal β (1-3)[Fuc α (1-4)] β GlcNAc) (2)	2.9 \pm 0.5 mM	n.d.
Phenyl Le ^x (phenyl Gal β (1-4)[Fuc α (1-3)] β GlcNAc) (3)	1.2 \pm 0.5 mM	n.d.
Phenyl Le ^a (phenyl Gal β (1-3)[Fuc α (1-4)] β GlcNAc) (4)	0.9 \pm 0.3 mM	582 \pm 40 μ M
		ΔG° : -18.5 \pm 1.0 kJ/mol
		ΔH° : -28.0 \pm 2.0 kJ/mol
		$T\Delta S^\circ$: -9.5 \pm 2.1 kJ/mol

2.2. Saturation Transfer Difference (STD) NMR Analysis. For the interpretation of the unexpected higher affinities correlated with the phenyl aglycone of antagonists **3** and **4**, the binding epitopes of the Le^a and Le^x derivatives were characterized by STD NMR (Figure 2A-D), which is particularly suited for epitope mapping of ligand receptor couples with weak interactions.²⁸⁻³¹ STD NMR experiments are based on spin magnetization transfer from a macromolecule, the protein, to a smaller binding molecule, the ligand. The saturation transfer proceeds through space via dipolar coupling and is therewith dependent on the distance (r^{-6}) of ligand hydrogens to the protein surface.

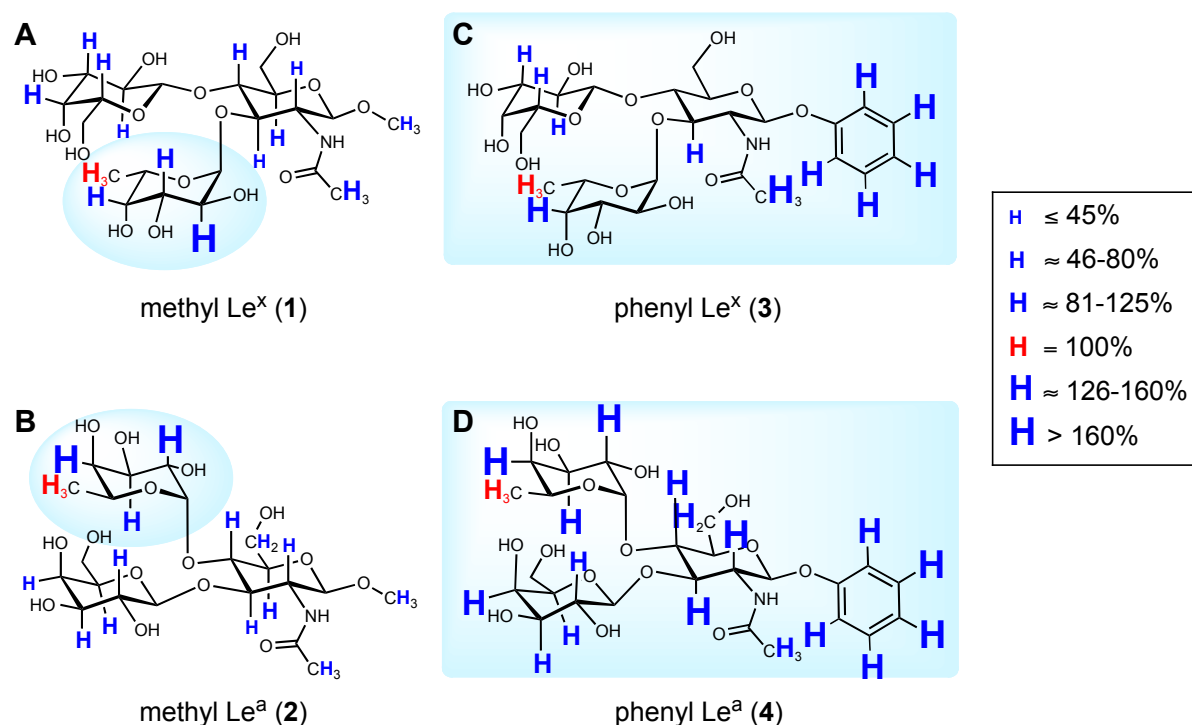


Figure 2. Binding epitopes of the Lewis antigens **1** - **4** interacting with DC-SIGN CRD-Fc determined by STD NMR. The contribution of each hydrogen to the STD epitope is quantified by forming the ratio of the signal intensities in the STD to those in the reference spectrum. These values are normalized to H-6 of L-Fuc (in red, 100%) to give the percentage epitope. STD values greater than 100% represent proximity to DC-SIGN CRD-Fc closer than that of the H-6 of L-Fuc. The letter size used for the hydrogens expresses the proximity to the protein, *i.e.* the relative amount of saturation transfer. The STD epitope for methyl Le^x (**1**) is consistent with recently published data with respect to experimental accuracy.³² Further details regarding the percentage epitope, sample preparation and parameters for the STD NMR measurement are available in the experimental section.

In the STD NMR analysis significantly higher STD values for the aromatic hydrogens (**3** and **4**, Figure 2C&D) compared to the methyl groups (in **1** and **2**, Figure 2A&B) were found. This data fits better to a model with spatial proximity of the aromatic aglycones to DC-SIGN.

However, a comparison of the binding epitopes reveals further differences going beyond aglycones. For the D-GlcNAc moieties of methyl Le^x (**1**) and Le^a (**2**) the maximal STD values for ring hydrogens are smaller than for H-6 of L-Fuc (up to 75%), whereas for the phenyl derivatives **3** and **4** the values reach up to 165%. Especially for phenyl Le^a (**4**), and to a lesser extent for phenyl Le^x (**3**), high STD values (80-220%) are equally distributed over the entire structure. In contrast, for methyl Le^x (**1**), methyl Le^a (**2**) high STD values are predominantly located on the L-Fuc moiety. The latter finding corresponds with X-ray data when the Le^x-containing LNFP III is co-crystallized with DC-SIGN,²² indicating the dominant role of the L-Fuc moiety in these binding epitopes.

2.3. Molecular Modeling Studies. Overall, the correlation of increased affinity with the presence of aromatic aglycones as well as the STD NMR data suggest a spatial proximity of the phenyl substituent to DC-SIGN. This is in contrast to the structural information deduced from the co-crystallization of LNFP III with the CRD of DC-SIGN.²² For a possible solution of this riddle, docking studies were initiated. The crystal structure 1SL5²² was used as starting point for the docking studies. The replacement of the internal D-Gal moiety in LNFP III by a methyl aglycone [LNFP III → methyl Le^x (**1**)] is not expected to have a significant influence on its binding mode as indicated by the small STD value of the aglycone in **1** (Figure 2A). In addition, the proximity of the *N*-acetyl of the D-GlcNAc moiety to Val351 as proposed by the crystal structure (inter-proton distance of 2.5 Å)²² is reflected by the increased STD value.

Automated docking of methyl Le^x (**1**) positions the Le^x subunit in close agreement (RMSD 0.7 Å) with its orientation in the crystal structure²² as shown in Figure 3A. In the docking pose of methyl Le^a (**2**), on the other hand, the D-GlcNAc residue is flipped along its C1-O5 axis, thereby positioning L-Fuc moiety similar to the LNFP III crystal structure. Calcium coordination and H-bond network to L-Fuc are thus maintained (Figure 3B). In this new orientation D-Gal can establish the same characteristic H-bond to Asp367 as well. However, *N*-acetyl group of D-GlcNAc no longer forms a hydrophobic contact with Val351 but with Phe313 instead, with a much longer inter-proton distance of ~ 4.5 Å. This is in good agreement with the lower intensity of the STD NMR signal of the *N*-acetyl group of GlcNAc in methyl Le^a (**2**, Figure 2B).

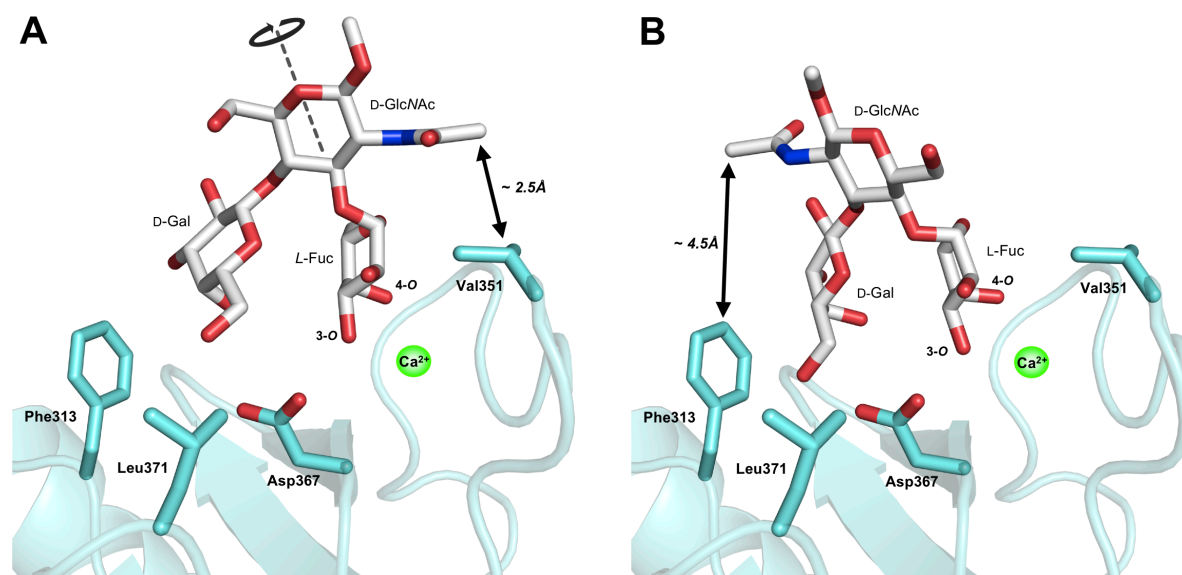


Figure 3. A) Docking modes of methyl Le^x (1) and B) methyl Le^a (2). Contacts between the *N*-acetyl groups and closest protein residues are highlighted with double-headed arrows.

A binding mode for phenyl Le^x (3) where the Le^x subunit adopts an analogous orientation to LNFP III (Figure 1A) is inconsistent with the significant saturation transfer observed for the aromatic protons, since the aglycone would point to the solvent with no close contacts to the protein (Figure 4A). The top-ranked pose from Glide XP³³ induced-fit docking presents an alternative pose where the ligand lies “flat” on the receptor and the phenyl aglycone makes a close contact with a hydrophobic cavity formed by the side chains of Phe313 and Leu371 (Figure 4B). This docking pose perfectly explains the large STD values of the aromatic protons of phenyl Le^x (3, Figure 2C), indicating a close proximity to DC-SIGN.

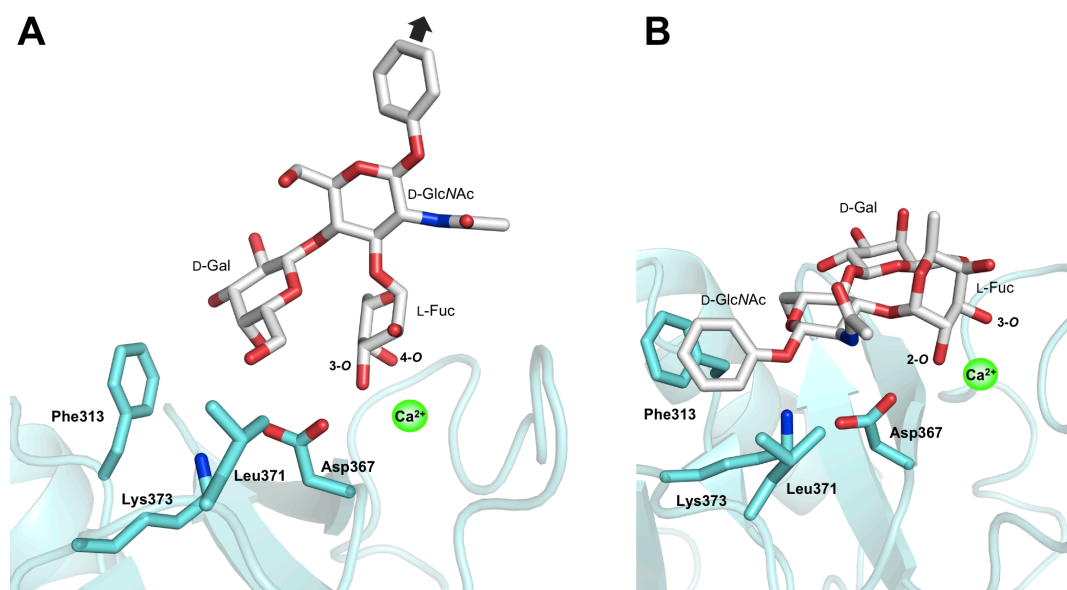


Figure 4. A) When phenyl Le^x (**3**) binds to DC-SIGN in a manner comparable to methyl Le^x (**2**) (Figure 3A) and LNFP III (Figure 1A), the phenyl aglycone points to the solvent (black arrow), not exhibiting an apparent protein contact. B) The induced-fit docking pose for phenyl Le^x (**3**) shows an interaction of the phenyl aglycone with the hydrophobic cleft formed by Phe313 and Leu371, rationalizing the strong aromatic proton signals in STD NMR.

Because of smaller overlaps of the resonances in the ¹H-NMR spectrum of phenyl Le^a (**4**), its STD NMR analysis is more detailed. The automated docking pose of phenyl Le^a (Figure 5) is similar to phenyl Le^x (**3**) where L-Fuc coordinates to Ca²⁺ via the two equatorial hydroxyl groups at the 2- and 3-position. In addition, H-bonds from 2-OH to both Glu354 and Asn365 and between 3-OH and Glu347 are formed. The D-Gal moiety lies close to the primary binding site forming two H-bonds from 6-OH to Glu347 and from 2-OH to Ser360 (not shown). The phenyl aglycone occupies the same hydrophobic pocket (Phe313 and Leu371) as phenyl Le^x (**3**) (Figure 4B), rationalizing the large STD values for the aromatic protons (Figure 2D). Moreover, D-GlcNAc also interacts via a H-bond between its 6-OH and Asp367, which in turn bridges this H-bond to Lys373. In the proposed orientation, the D-GlcNAc moiety of phenyl Le^a (**4**) is in closer contact with the receptor compared to methyl Le^a (**2**) (Figure 3B), which explains the observed larger STD values for the D-GlcNAc protons.

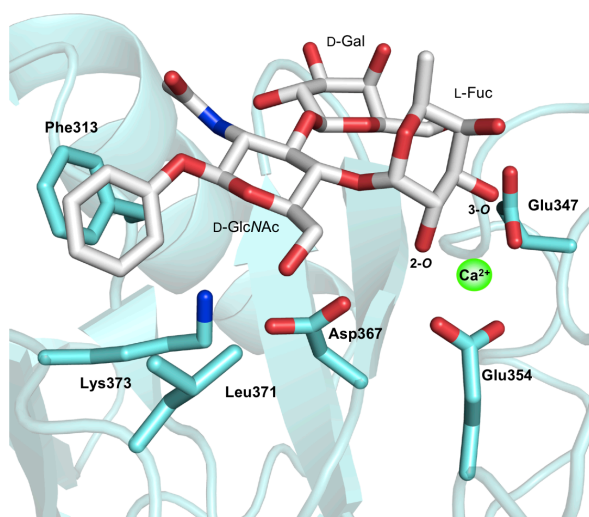


Figure 5. Binding mode of phenyl Le^a (**4**) to DC-SIGN. Binding of the phenyl aglycone in the hydrophobic cleft formed by Phe313 and Leu371 and proximity of the D-GlcNAc moiety to protein surface coincides with the measured STD NMR values (Figure 2D).

Dynamic stability of this novel binding mode was confirmed by molecular dynamics (MD) simulation. Analysis of MD trajectories revealed that the interactions of phenyl Le^a (**4**) with key residues in the DC-SIGN binding site were maintained throughout the simulation (Figure 6A). Particularly, the favorable interaction of phenyl Le^a with Phe313 was stable during the simulated time span (Figure 6B). Despite the alteration in binding mode in comparison to the crystal structure of LNFP III, the Ca²⁺ coordination via Fuc-O2 and Fuc-O3 of phenyl Le^a (**4**) is of comparable stability as reflected by the variation in the distance between Ca²⁺ and its two coordinating oxygens (Figure 6C&6D). Additionally, throughout the MD simulation all protons of the phenyl moiety of phenyl Le^a exhibited one or more contacts with a proton from a nearby protein residue, consistent with the observed STD signals for these protons (Supporting Information, Figure S4).

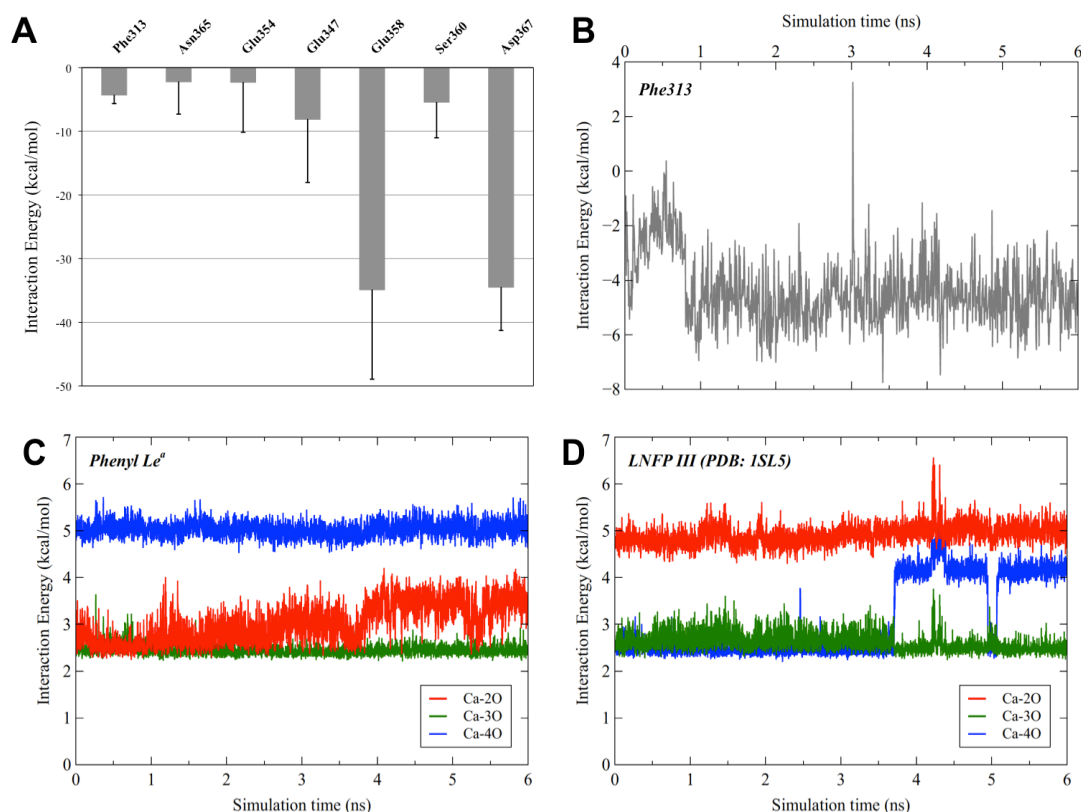


Figure 6. Results of molecular dynamics simulations. A) average interaction energies between phenyl Le^a (4) and some binding site residues during a 6 ns MD simulation, standard deviations are indicated by error bars. B) time evolution of interaction energy between phenyl Le^a and Phe313 residue throughout the MD simulation. C) and D) time evolution of the distances between Ca²⁺ and L-Fuc oxygens (2O, 3O, 4O) along MD simulations starting from LNFP III (in 1SL5 crystal structure) and the docking mode of phenyl Le^a, respectively. The third (non-Ca²⁺-coordinating) oxygen is shown for comparison.

2.4. Mutagenesis Studies. To further confirm the proposed hydrophobic interaction between Phe313 and the aromatic aglycone, the previously described DC-SIGN CRD F313A²² was expressed and the binding affinities for methyl Le^a (2) and phenyl Le^a (4) were determined. Table 2 summarizes the results of the competitive binding assay with wild type and mutant DC-SIGN CRD. L-Fuc was included as reference compound. The F313A mutation should not have an impact on binding affinity of L-Fuc since the monosaccharide is assumed to bind exclusively in the primary binding site.²² However, L-Fuc showed a lower IC₅₀ value for the mutant protein (IC₅₀ 3.9 mM) than for the wild type (IC₅₀ 7.6 mM). This can be explained by the lower affinity of Le^a-PAA for the F313A mutant, reflected by the EC₅₀ value (Table 2). For a better comparison we state relative IC₅₀ values (rIC₅₀) with L-Fuc as reference (Table 2).

Table 2. Results of the competitive binding assay for L-Fuc, methyl Le^a (**2**), and phenyl Le^a (**4**) with wild type and mutant DC-SIGN. The observed differences in the absolute inhibitory potencies between wild type and mutant are due to different binding affinities to Le^a-PAA reflected by a higher EC₅₀ value (half maximal effective concentration) in case of the mutant protein. The rIC₅₀ values of methyl Le^a (**2**) and phenyl Le^a (**4**) with L-Fuc as reference were determined by dividing the respective IC₅₀ values by the IC₅₀ of L-Fuc; a value below 1 resembles higher affinity than L-Fuc. Detailed information on protein expression and competitive binding assay is given in the experimental section.

Ligand	DC-SIGN wild type	DC-SIGN F313A mutant
EC ₅₀ Le ^a -PAA	66.9 ± 0.3 ng/ml	111.2 ± 0.2 ng/ml
rIC ₅₀ L-Fuc	1	1
rIC ₅₀ methyl Le ^a (2)	0.38	0.46
rIC ₅₀ phenyl Le ^a (4)	0.12	0.43
Factor of 2 to 4	3.2	1.1

In Figure 7, inhibition curves for methyl Le^a (**2**) and phenyl Le^a (**4**) with wild type and mutant DC-SIGN CRD-Fc are shown. Graph A visualizes the aforementioned difference in binding affinity of methyl Le^a (**2**) and phenyl Le^a (**4**) to wild type DC-SIGN (factor 3.2). In contrast, both compounds exhibited near identical binding affinities (factor 1.1, Figure 6B) for the F313A mutant, which indicates the omission of the beneficial hydrophobic contact of Phe313 with the phenyl aglycone.

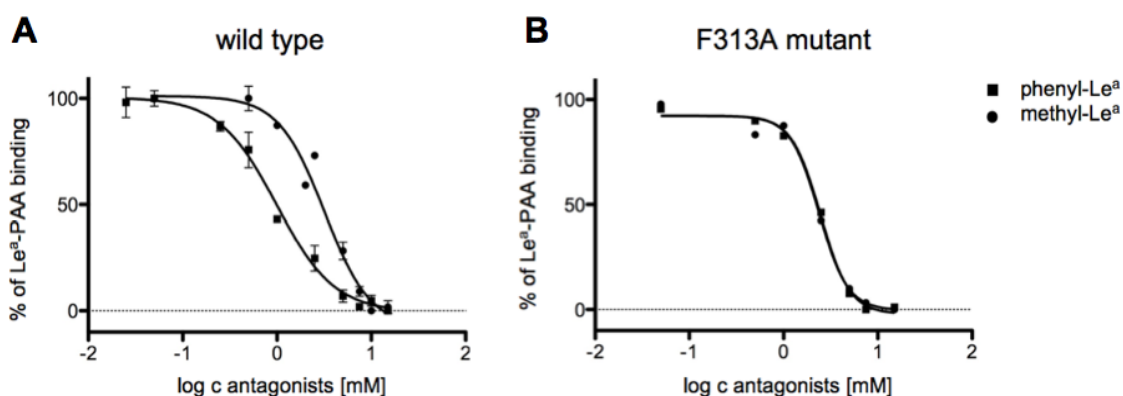


Figure 7. Inhibition curves for methyl Le^a (**2**) and phenyl Le^a (**4**) obtained from the competitive binding assay, with (A) wild type DC-SIGN and (B) F313A mutant.

3. CONCLUSIONS

STD NMR spectroscopy and molecular modeling supplemented with a protein mutation study were used to rationalize diverging binding modes of Le^a and Le^x antigens to DC-SIGN induced by the nature of the aglycone. The originally found improved binding affinity of phenyl Le^x (**3**) and phenyl Le^a (**4**) indicated a contribution of the phenyl aglycone to binding, presumably by a hydrophobic contact with the protein. Strong STD NMR values further confirmed this assumption. Docking and MD studies finally revealed a favorable interaction of the phenyl aglycone with a hydrophobic pocket formed by Phe313 and Leu371. With a single-point mutation of the DC-SIGN CRD the proposed interactions of the phenyl aglycone of **4** with Phe313 could be verified.

Here, we report an interesting example, illustrating how flexible binding modes on shallow protein surfaces can be, especially when the starting affinity is low, a situation often present in carbohydrate-lectin interactions. Therefore, improved affinities induced by structural modifications should be carefully analyzed regarding possible reorientations of binding modes. STD NMR experiments^{28,29} represent an excellent tool for this endeavor.

Based on the new binding mode of phenyl Le^x (**3**) and phenyl Le^a (**4**), the interaction within the hydrophobic pocket formed by Phe313 and Leu371 provides a promising rationale for the design of more potent DC-SIGN antagonists. Therewith, our findings support recent approaches from other researchers with the objective of using this interaction for the design of glycomimetic DC-SIGN ligands.²⁴

Our findings that introduction of a hydrophobic moiety at Lewis trisaccharides induces a switch in the binding mode in order to establish an additional contact with the protein demonstrates the value of this interaction. In fact, recently Bernardi *et al.* made use of this interaction for the design of glycomimetic DC-SIGN antagonists.²⁴

4. EXPERIMENTAL SECTION

4.1. Ligands. Methyl Le^x (**1**) and methyl Le^a (**2**) were purchased from Toronto Research Chemicals Inc. Phenyl Le^x (**3**) was prepared according to ref³⁴ and phenyl Le^a (**4**) was prepared as described in the supporting information.

4.2. Cloning of DC-SIGN CRD-IgG(Fc). Plasmids containing the full-length cDNA of DC-SIGN were kindly provided by Daniel A. Mitchell (Glycobiology Institute, Department of Biochemistry, University of Oxford). Standard molecular techniques³⁵ were used for the cloning of the carbohydrate recognition domain of DC-SIGN (DC-SIGN CRD; aa residues 250-404, GenBank accession no. M98457). The DC-SIGN CRD encoding insert was amplified by PCR using specific forward and reverse primers containing the restriction sites *EcoRI* and *NcoI* (New England BioLabs, Allschwil, Switzerland), respectively. The insert was ligated into the corresponding cloning site of the pFUSE-hIgG2-Fc2 expression vector (Invivogen, Toulouse, France). The construct was amplified in chemocompetent DH5 α *E. coli* (Novagen, Lucerne, Switzerland). After plasmid minipreparation and restriction control, the construct correctness was confirmed by DNA sequencing.

4.3. Expression and purification of DC-SIGN CRD-Fc. CHO-K1 cells (American Type Culture Collection No. CCL-61TM) were cultivated in Ham's Nutrient Mixture F-12 (Invitrogen, Paisley, UK) supplemented with 2 mM L-glutamate, 10% fetal calf serum (FCS, Invitrogen, Paisley, UK), 100 U/mL penicillin, and 100 μ g/mL streptomycin (Sigma-Aldrich, Basel, Switzerland). The cells were cultivated as monolayers in tissue culture flasks (Nunc, Roskilde, Denmark). The CHO-K1 cells were transfected with the DC-SIGN CRD expression vector using the FuGENE[®] HD transfection reagent (Roche Applied Science, Rotkreuz, Switzerland) following to the instructions of the supplier. Stably transfected CHO-K1 cells were selected by treatment with ZeocinTM (0.5 μ g/ml, Invitrogen, Paisley, UK) and single clones were obtained by limiting dilution. For DC-SIGN CRD-Fc production the cells were cultivated as described above and the culture medium, containing the secreted DC-SIGN CRD-Fc chimera was harvested weekly, adjusted to pH 7.6 and sterile filtrated (conditioned medium).

The purification of the recombinant protein was achieved by applying conditioned medium on a protein A-sepharose column (BioVision, Mountain View, CA, USA) attached to a fast

protein liquid chromatography apparatus (BioLogic (FPLC) system, BioRad, Reinach BL, Switzerland), which was previously equilibrated with loading buffer I (20 mM Tris/HCl, pH 7.6, 150 mM NaCl, 0.05% (v/v) Tween-20TM). The protein was eluted with elution buffer I (0.5 M acetic acid/ammonium acetate, pH 3.4). The collected protein was further purified on a L-Fuc-sepharose column (prepared in house) using loading buffer II (20 mM Tris/HCl, pH 7.8, 0.5 M NaCl, 25 mM CaCl₂) and elution buffer II (20 mM Tris/HCl, pH 7.8, 0.5 M NaCl, 2 mM EDTA). For long-term storage, the protein was frozen at -80 °C.

4.4. Cloning of the F313A DC-SIGN CRD mutant. The PCR overlap extension method³⁶ was used for the substitution of the codon TTC against CGC at cDNA bp 968-970, resulting in the mutation of phenyl alanine 313 to an alanine. In a first step, two overlapping DNA fragments were generated separately, both using wild type DC-SIGN cDNA as template (PCR 1: primer fw: 5` g gaa ttc cat atg gaa cgc ctg tgc cac ccc 3` and primer F313A rv: 5`tcc aga agt aac cgc **gcg** acc tgg atg gga 3`; PCR 2: primer F313A fw: 5`aag tcc cat cca ggt **cgc** gcg gtt act tct 3` and primer rv: 5` cgc gga tcc tta cta cgc agg agg ggg gtt tgg g 3`). The two internal primers contained a mismatch for the site-directed base substitution (bold). In a second step, both overlapping DNA fragments were elongated to the full-length gene, containing the single point mutation. The *NdeI* and *BamHI* (New England BioLabs, Allschwil, Switzerland) treated insert was ligated into the corresponding cloning site of the expression vector pET-3a. After *E.coli* DH5 α transformation, plasmid miniprep, the mutation was confirmed by DNA sequencing. Finally, for protein expression the construct was transformed into BL21 *E.coli* (Novagen, Lucerne, Switzerland).

4.5. Expression and purification of F313A DC-SIGN CRD mutant. Protein expression was carried out in TB medium (terrific broth) containing 100 μ g/mL ampicillin (Applichem, Darmstadt, Germany). The bacteria were cultured at 37 °C until an OD₆₀₀ of 1.0 was reached. The expression was induced by the addition of isopropyl- β -D-thiogalactoside (IPTG, Applichem, Darmstadt, Germany) at the final concentration of 0.4 mM. The cells were further cultivated for 12 h, prior to harvesting by centrifugation at 4000 rpm for 20 min at 4 °C. For bacterial lysis, the pellet was dissolved in 20 mM Tris-HCl buffer, pH 7.8, 0.5 M NaCl, containing 1 mg/mL lysozym (Sigma, Buchs, Switzerland) and incubated for 30 min at 4 °C under shaking. The inclusion bodies were solubilized by addition of β -mercaptoethanol (0.01 % v/v), urea (8 M), and brief sonication followed by gentle rotation for 30 min at 4 °C. The mixture was centrifuged at 22000 rpm for 1 h at 4°C and the supernatant was diluted by

slow addition of the fivefold volume loading buffer II. The mixture was dialyzed against 6 volumes of loading buffer II with 6 buffer exchanges. After dialysis, insoluble precipitate was removed by centrifugation at 22000 rpm for 1 h at 4 °C. The protein was purified using a L-Fuc-sepharose column as described above.

Protein purity was confirmed by standard SDS-PAGE analysis³⁷ followed by Coomassie Brilliant Blue G-250 staining (Bio-Rad laboratories, Hercules, CA, USA). Protein concentration was determined either by the Bradford method (Bio-Rad laboratories, Hercules, CA, USA) or with HPLC³⁸.

4.6. Competitive binding assay. Biotinylated Le^a-PAA polymer (20 µL, 1 mg/mL, GlycoTech, Gaithersburg, MD, USA) was mixed with 80 µL assay buffer (20 mM HEPES, 150 mM NaCl, 10 mM CaCl₂, pH 7.4), 20 µL FCS and 80 µL streptavidin-horseradish peroxidase-conjugate (500 U/mL, Roche, Mannheim, Germany) and incubated for 2 h at 37 °C. The complex was stable for several weeks when stored at 4 °C.

Flat-bottom 96-well microtiter plates (F96 MaxiSorp, Nunc) were coated with 100 µL/well of a 2.5 µg/mL solution of DC-SIGN CRD-Fc protein in assay buffer overnight at 4 °C in a humidified chamber. The coating solution was discarded and the wells were blocked with 200 µL/well of 3% bovine serum albumin (BSA, Sigma-Aldrich, Buchs, Germany) in assay buffer for 2 h at 4 °C. After three washing steps with assay buffer (150 µL/well), a serial dilution of the test compound (25 µL/well) in assay buffer and streptavidin-peroxidase coupled Le^a-PAA (25 µL/well, 0.25 µg/mL final concentration) were added. Subsequent to an incubation of 3 h at room temperature and 350 rpm the plate was carefully washed four times with 200 µL/well assay buffer. Le^a-PAA binding was detected by addition of 100 µL/well of ABTS-substrate (2,2'-azino-bis-(3-ethylbenzthiazoline-6-sulfonic acid, Invitrogen, Paisley, UK). The colorimetric reaction was allowed to develop for 2 min, then stopped by the addition of 2% aqueous oxalic acid before the optical density (OD) was measured at 415 nm on a microplate-reader (Spectramax 190, Molecular Devices, Ca, USA). The IC₅₀-values were calculated using the Prism software (GraphPad Software, Inc, La Jolla, USA). The IC₅₀ (half maximal inhibitory concentration) defines the molar concentration of the test compound that reduces the maximal specific binding of carbohydrate-polymer to DC-SIGN-CRD-Fc by 50%.

For EC₅₀ determination (half maximal effective concentration) of the Le^a-PAA, the assay was performed as described above with a serial dilution of Le^a-PAA (0-3 µg/mL) in absence of antagonist.

4.7. Isothermal titration calorimetry. ITC experiments were performed at 298 K and a reference power of 10 µcal/sec under constant stirring speed of 307 rpm using a MicroCal VP-ITC instrument (MicroCal, Northampton, MA). The concentration of DC-SIGN CRD-Fc was determined by HPLC-UV against a standard curve of BSA at 210 nm³⁸ after extensive dialysis against 10 mM HEPES, 150 mM NaCl, 10 mM CaCl₂, pH 7.4. The ligand was diluted in the dialysat. Injections of 3-5 µl ligand solutions were added from a syringe at an interval of 5 min into the sample cell solution containing DC-SIGN CRD-Fc (cell volume 1.4523 ml). Control experiments were performed, where identical ligand solutions were injected into buffer without protein, and showed insignificant heat of dilution. The experimental data were fitted to a theoretical titration curve (one site binding model) using Origin software (version 7, MicroCal). The quantity $c = Mt(0)/K_D$ with $Mt(0)$ as initial macromolecule concentration, is of importance in titration microcalorimetry.³⁹ The experiments were performed with c values below 1. The stoichiometry was fixed to 1 (concentration expressed in terms of binding site) to allow reliable determination of K_D and ΔH .^{40, 41} Thermodynamic parameters were calculated from the equation 1,

$$\Delta G^\circ = \Delta H^\circ - T\Delta S^\circ = -RT\ln K_A = RT\ln K_D \quad (\text{eq. 1})$$

where ΔG° , ΔH° , and ΔS° are the changes in free energy, enthalpy, and entropy of binding, respectively. T is the absolute temperature, and $R = 8.314 \text{ J/mol/K}$.

4.8. STD NMR. Experiments were performed on a Bruker 11.7 T spectrometer with an Avance III console at a temperature of 298 K. Shigemi NMR tubes with a sample volume of 250 µL were used for the measurements. Each sample contained 20-30 µM DC-SIGN CRD-Fc (dimer) and 1-2 mM ligand. A d-Tris buffer was used as solvent containing 20 mM d-TRIS (98% Cambridge Isotope Libraries), 4 mM CaCl₂ and 150 mM NaCl in D₂O (99.8% Sigma-Aldrich) adjusted to a pH of 8.1 with HCl.

Using a pulse sequence modified from Mayer and Meyer²⁸ allows simultaneous saturation of the protein at two frequencies, which leads to a more intense STD epitope. The cosine modulated E-Burp-1 pulse⁴² for the on-resonance spectrum was centered at 1555 Hz and resulted in two sidebands at 0 and 3110 Hz with a power of 53 dB.⁴³ The duration of each of

the 40 E-Burp-1 pulses used to saturate the protein was 50 ms with a 1 ms recovery between the pulses.

Off-resonance excitation was set to 26000 Hz. STD NMR experiments were performed applying a Watergate solvent suppression. Specific parameters were determined via preliminary experiments including negative control experiments with only ligand-containing sample to avoid artifacts from direct excitation. Scaling each STD signal on an off-resonance reference spectrum resulted in a relative binding epitope (approximate values, see supporting information).³⁰ Ligand resonances were assigned by using 2D NMR and 1D selective TOCSY experiments. Not all protons could be assigned doubtlessly, due to solvent suppression and partial signal overlap.

Detailed conditions: STD NMR of methyl-bearing compounds: 2 mM ligand with 20 μ M DC-SIGN CRD-Fc, STD NMR of phenyl Le^a: 1 mM ligand with 20 μ M DC-SIGN CRD-Fc, STD NMR of phenyl Le^x: 1 mM with 30 μ M DC-SIGN CRD-Fc; number of scans was typically 14k for on-resonance spectra and 512 for off-resonance spectra.

Experiments with different saturation times were performed for phenyl Le^a. These data indicate an overall consistent epitope at either saturation times of 0.7, 1, 2, and 3 s and exclude misinterpretation due to T1 bias for different proton species (see supporting information).

4.9. Molecular Modeling. All ligands were manually built using Maestro, and optimized using standard procedures. Model for DC-SIGN in complex with LNFP III was downloaded from the Protein Data Bank (code: 1SL5). Hydrogens were added and water molecules were removed using Maestro Protein Preparation Wizard. Partial charges were calculated from OPLS2005 force field while protonation states and oxidation states for metals were assigned by Epik⁴⁴ Orientation of added hydrogens was sampled for optimal H-bond formation and the model was then refined by minimization within RMSD of 0.3Å.

GlideXP³³ was used for docking of novel ligands to DC-SIGN. To account for the possibility of side chain re-organization upon ligand binding the Induced-Fit Docking (IFD) methodology was employed⁴⁵. The binding site was defined to include residues within 5 Å radius around the co-crystallized ligand LNFP III in the prepared complex. In the initial stages of IFD protocol amino acids within 5 Å radius around any found pose were considered as flexible, and their side chain conformations were optimized. Up to 50 poses were retained for each calculation within an energy window of 40 kcal/mol to allow for larger diversity in

output poses. Prioritization was done by Standard Precision (SP)⁴⁶ scoring function in the initial soft-docking stage followed by more rigorous Extra Precision (XP)⁴⁷ scoring in the redocking stage. Output poses were then visually inspected for agreement with STD NMR experiment, and those showing considerable discrepancy were disregarded.

Stability of the proposed modes was assessed using molecular dynamics. Docking poses and crystal structure (PDB 1SL5) were used as a starting point for 6 ns MD simulations using Desmond package⁴⁸ from D. E. Shaw Research lab. The protein-ligand complex was soaked in an orthorhombic TIP3P water box extending 10 Å away from the complex. Counter-ions were added to make it neutral and 0.15 M sodium and chloride ions were added to approximate physiological conditions. The complex was then minimized to a convergence threshold of 1.0 kcal/mol/Å. MD experiments were carried out using the OPLS2005 force field and the NPT ensemble (constant number of particles, pressure and temperature) at 300 K with periodic boundary conditions. Default parameters were used and snapshots recorded every 1.2 ps. Output files were analyzed using component-interactions script in Maestro (Maestro, version 9.2, Schrödinger, LLC, New York, NY, 2011) to compute interaction energies between the ligand and individual amino acids defining the binding site as well as the conserved calcium along the MD simulations. Interaction energies were computed as the sum of OPLS2005 Van der Waals and electrostatic terms.

ASSOCIATED CONTENT

Detailed protocols concerning the synthesis of phenyl Le^a (**4**), ITC experiments, STD NMR experiments, and molecular dynamics simulations are given in the “Supporting Information”.

ACKNOWLEDGEMENT

The authors gratefully acknowledge the financial support by the Swiss National Science Foundation (grant no. 200020_129935).

REFERENCES

- (1) Hart, D. N. J.; Clark, G. J.; Dekker, J. W.; Fearnley, D. B.; Kato, M.; Hock, B. D., McLellan, A. D.; Neil, T.; Sorg, R. V., Sorg, U.; Summers, K. L.; Vuckovic, S. *Dendritic Cells in Fundamental and Clinical Immunology, Vol 3* **1997**, 417, 439-442.
- (2) Banchereau, J.; Steinman, R. M.; *Nature* **1998**, 392, 245-252.
- (3) Geijtenbeek, T. B. H.; Torensma, R.; van Vliet, S. J.; van Duijnhoven, G. C. F.; Adema, G. J.; van Kooyk, Y.; Figdor, C. G.; *Cell* **2000**, 100, 575-585.
- (4) Geijtenbeek, T. B. H.; van Vliet, S. J.; Koppel, E. A.; Sanchez-Hernandez, M.; Vandenbroucke-Grauls, C.; Appelmelk, B.; van Kooyk, Y. *J. Exp. Med.* **2003**, 197, 7-17.
- (5) Cambi, A.; Gijzen, K.; de Vries, J. M.; Torensma, R.; Joosten, B.; Adema, G. J.; Netea, M. G.; Kullberg, B. J.; Romani, L.; Figdor, C. G. *Eur. J. Immunol.* **2003**, 33, 532-538.
- (6) Geijtenbeek, T. B. H.; Kwon, D. S.; Torensma, R.; van Vliet, S. J.; van Duijnhoven, G. C. F.; Middel, J.; Cornelissen, I.; Nottet, H.; KewalRamani, V. N.; Littman, D. R.; Figdor, C. G.; van Kooyk, Y. *Cell* **2000**, 100, 587-597.
- (7) Alvarez, C. P. *J. Virol.* **2002**, 76, 6841-6844.
- (8) Marzi, A.; Gramberg, T.; Simmons, G.; Moller, P.; Rennekamp, A. J.; Krumbiegel, M.; Geier, M.; Eisemann, J.; Turza, N.; Saunier, B.; Steinkasserer, A.; Becker, S.; Bates, P.; Hofmann, H.; Pohlmann, S. *J. Virol.* **2004**, 78, 12090-12095.
- (9) Anderluh, M.; Jug, G.; Svajger, U.; Obermajer, N. *Curr. Med. Chem.* **2012**, 19, 992-1007.
- (10) Gurney, K. B.; Elliott, J.; Nassanian, H.; Song, C.; Soilleux, E.; McGowan, I.; Anton, P. A.; Lee, B. *J. Virol.* **2005**, 79, 5762-5773.
- (11) Feinberg, H.; Mitchell, D. A.; Drickamer, K.; Weis, W. I. *Science* **2001**, 294, 2163-2166.
- (12) van Kooyk, Y.; Geijtenbeek, T. B. H. *Nat. Rev. Immunol.* **2003**, 3, 697-709.
- (13) Hong, P. W.; Flummerfelt, K. B.; de Parseval, A.; Gurney, K.; Elder, J. H.; Lee, B. *J. Virol.* **2002**, 76, 12855-12865.
- (14) Van Die, I.; Van Vliet, S. J.; Schiphorst, W.; Bank, C. M. C.; Appelmelk, B.; Nyame, A. K.; Cummings, R. D.; Geijtenbeek, T. B. H.; Van Kooyk, Y. *Glycobiology* **2002**, 12, 3.
- (15) Van Die, I.; van Vliet, S. J.; Nyame, A. K.; Cummings, R. D.; Bank, C. M. C.; Appelmelk, B.; Geijtenbeek, T. B. H.; van Kooyk, Y. *Glycobiology* **2003**, 13, 471-478.
- (16) Appelmelk, B. J.; van Die, I.; van Vliet, S.; Vandenbroucke-Grauls, C.; Geijtenbeek, T.; van Kooyk, Y. *J. Immunol.* **2003**, 170, 1635-1639.

- (17) Naarding, M. A.; Ludwig, I. S.; Groot, F.; Berkhout, B.; Geijtenbeek, T. B. H.; Pollakis, G.; Paxton, W. A. *J. Clin. Invest.* **2005**, *115*, 3256-3264.
- (18) Timpano, G.; Tabarani, G.; Anderluh, M.; Invernizzi, D.; Vasile, F.; Potenza, D.; Nieto, P. M.; Rojo, J.; Fieschi, F.; Bernardi, A. *ChemBioChem* **2008**, *9*, 1921-1930.
- (19) van Liempt, E.; Bank, C. M. C.; Mehta, P.; Garcia-Vallejo, J. J.; Kawar, Z. S.; Geyer, R.; Alvarez, R. A.; Cummings, R. D.; van Kooyk, Y.; van Die, I. *FEBS Lett.* **2006**, *580*, 6123-6131.
- (20) Mitchell, D. A.; Fadden, A. J.; Drickamer, K. *J. Biol. Chem.* **2001**, *276*, 28939-28945.
- (21) Feinberg, H.; Guo, Y.; Mitchell, D. A.; Drickamer, K.; Weis, W. I.; *J. Biol. Chem.* **2005**, *280*, 1327-1335.
- (22) Guo, Y.; Feinberg, H.; Conroy, E.; Mitchell, D.; Alvarez, R.; Blixt, O.; Taylor, M.; Weis, W. I.; Drickamer, K. *Nat. Struct. Mol. Biol.* **2004**, *11*, 591-598.
- (23) Obermajer, N.; Sattin, S.; Colombo, C.; Bruno, M.; Švajger, U.; Anderluh, M.; Bernardi, A. *Mol. Diversity* **2010**, 1-14.
- (24) Andreini, M.; Doknic, D.; Sutkeviciute, I.; Reina, J. J.; Duan, J.; Chabrol, E.; Thepaut, M.; Moroni, E.; Doro, F.; Belvisi, L.; Weiser, J.; Rojo, J.; Fieschi, F.; Bernardi, A. *Org. Biomol. Chem.* **2011**, *9*, 5778-5786.
- (25) Toone, E. J. *Curr. Opin. Struct. Biol.* **1994**, *4*, 719-728.
- (26) Ambrosi, M.; Cameron, N. R.; Davis, B. G. *Org. Biomol. Chem.* **2005**, *3*, 1593-1608.
- (27) Dam, T. K.; Brewer, C. F. *Chem. Rev.* **2002**, *102*, 387-429.
- (28) Mayer, M.; Meyer, B. *Angew. Chem., Int. Ed.* **1999**, *38*, 1784-1788.
- (29) Meyer, B.; Peters, T. *Angew. Chem., Int. Ed.* **2003**, *42*, 864-890.
- (30) Mayer, M.; Meyer, B. *J. Am. Chem. Soc.* **2001**, *123*(25), 6108-6117.
- (31) Haselhorst, T.; Lamerz, A.-C.; von Itzstein, M. *Methods Mol Biol* **2009**, *534*, 375-387.
- (32) Guzzi, C.; Angulo, J.; Doro, F.; Reina, J. J.; Thepaut, M.; Fieschi, F.; Bernardi, A.; Rojo, J.; Nieto, P. M. *Org. Biomol. Chem.* **2011**, *9*, 7705-7712.
- (33) Glide, version 5.7, Schrödinger, LLC, New York, NY, 2011.
- (34) Su, Z.; Wagner, B.; Cocinero, E. J.; Ernst, B.; Simons, J. P. *Chem. Phys. Lett.* **2009**, *477*, 365-368.
- (35) Sambrook, J.; Fritsch, E. F.; Maniatis, T. Cold Spring Harbor Laboratory Press, NY, **1989**.
- (36) Ho, S. N.; Hunt, H. D.; Horton, R. M.; Pullen, J. K.; Bell, M. P.; McKean, D. J.; Pease, L. R. *FASEB J.* **1989**, *3*, A519.
- (37) Laemmli, U. K. *Nature* **1970**, *227*, 680-685.

- (38) Bitsch, F.; Aichholz, R.; Kallen, J.; Geisse, S.; Fournier, B.; Schlaeppli, J.-M. *Anal. Biochem.* **2003**, *323*, 139-149.
- (39) Wiseman, T.; Williston, S.; Brandts, J. F.; Lin, L. N. *Anal. Biochem.* **1989**, *179*, 131-137.
- (40) Turnbull, W. B.; Daranas, A. H. *J. Am. Chem. Soc.* **2003**, *125*, 14859-14866.
- (41) Tellinghuisen, J. *Anal. Biochem.* **2008**, *373*, 395-397.
- (42) Geen, H.; Wimperis, S.; Freeman, R. *J. of Magn. Reson.* **1989**, *85*, 620-627.
- (43) Cutting, B.; Shelke, S. V.; Dragic, Z.; Wagner, B.; Gathje, H.; Kelm, S.; Ernst, B. *Magn. Reson. Chem.* **2007**, *45*, 720-724.
- (44) Shelley, J. C.; Cholleti, A.; Frye, L. L.; Greenwood, J. R.; Timlin, M. R.; Uchimaya, M. *J. Comput.-Aided Mol. Des.* **2007**, *21*, 681-691.
- (45) Sherman, W.; Day, T.; Jacobson, M. P.; Friesner, R. A.; Farid, R. *J. Med. Chem.* **2006**, *49*, 534-553.
- (46) Friesner, R. A.; Banks, J. L.; Murphy, R. B.; Halgren, T. A.; Klicic, J. J.; Mainz, D. T.; Repasky, M. P.; Knoll, E. H.; Shelley, M.; Perry, J. K.; Shaw, D. E.; Francis, P.; Shenkin, P. S. *J. Med. Chem.* **2004**, *47*, 1739-1749.
- (47) Friesner, R. A.; Murphy, R. B.; Repasky, M. P.; Frye, L. L.; Greenwood, J. R.; Halgren, T. A.; Sanschagrin, P. C.; Mainz, D. T. *J. Med. Chem.* **2006**, *49*, 6177-6196.
- (48) K. J. Bowers, E. Chow, H. Xu, R. O. Dror, M. P. Eastwood, B. A. Gregersen, J. L. Klepeis, I. Kolossvary, M. A. Moraes, F. D. Sacerdoti, J. K. Salmon, Y. Shan, D. E. Shaw, Scalable algorithms for molecular dynamics simulations on commodity clusters, in Proceedings of the 2006 ACM/IEEE conference on Supercomputing, ACM, Tampa, Florida, **2006**, p. 84.

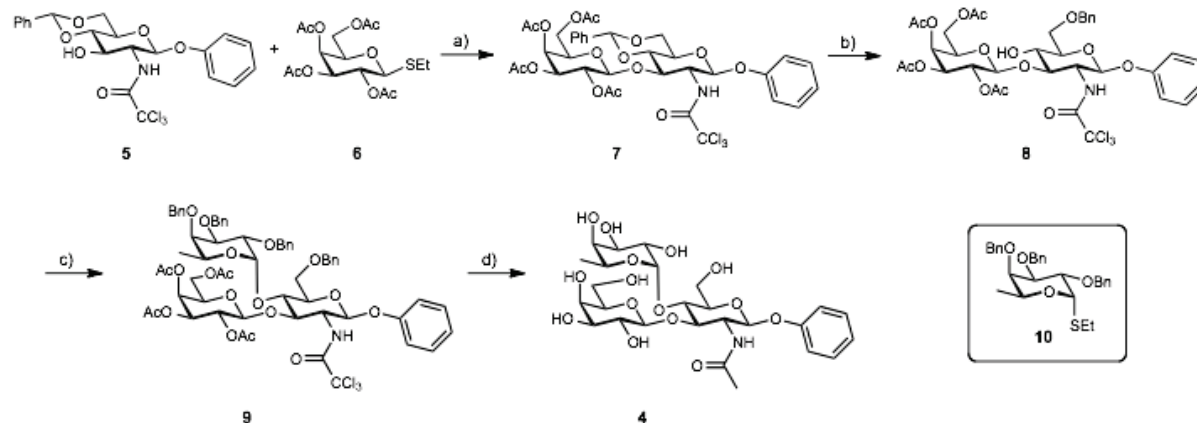
2.2.1.1 Supporting Information

Binding of Lewis^{a/x} to DC-SIGN – Nature of Aglycone Determines Binding Mode

Content

1. Synthesis of phenyl Le^a	52
2. Isothermal Titration Calorimetry	56
3. Saturation Transfer Difference NMR	57
4. Molecular Dynamics	60

1. Synthesis of phenyl Le^a (4)



Scheme S1. a) **4**, NIS, TfOH, DCM, -20 °C, 4 h, 81%; b) Me₃NBH₃, AlCl₃, THF, rt, overnight, 77%; c) **10**, Br₂, Et₄NBr, DCM/DMF (1:1), rt, overnight, 49%; d) i. NaOMe, MeOH, rt, 1 h, 90%, ii. Pd(OH)₂, H₂ (4 atm), NEt₃, dioxane/water (4:1), 12 h, iii. Pd(OH)₂, H₂ (4 atm), dioxane/water (4:1) 12 h, 92% over two steps.

The phenyl Le^a (**4**) was prepared from the known building block **5** in six steps. The glucosamine acceptor **5** was glycosylated with thiogalactoside **6** using NIS/TfOH in good yield. Regioselective opening of acetal **7** was performed with AlCl₃/ Me₃NBH₃ to afford **8** ready for the fucosylation. The acceptor **8** was fucosylated using bromofucose prepared from thiofucose under in situ anomerization condition to give **9**. Finally, removal of *O*-acetyl group by mild transesterification with catalytic NaOMe, reduction of trichloroacetamide group to *N*-Ac and removal of benzyl protecting groups under hydrogenolytic condition afforded the Ph-*O*-Le^a **4** in very good yield.

Experimental procedure

General Methods

NMR spectra were recorded on a Bruker Avance DMX-500 (500 MHz) spectrometer. Assignment of ¹H and ¹³C NMR spectra was achieved using 2D methods (COSY, HSQC, TOCSY). Chemical shifts are expressed in ppm using residual CHCl₃, CHD₂OD, and HDO as references. Optical rotations were measured using Perkin-Elmer polarimeter 341. Electron spray ionization mass spectra (ESI-MS) were obtained on a Waters micromass ZQ. LC/HRMS analysis was carried out using a Agilent 1100 LC equipped with a photodiode array detector and a Micromass QTOF I equipped with a 4 GHz digital-time converter.

Microanalyses were performed at the Department of Chemistry, University of Basel, Switzerland. Reactions were monitored by TLC using glass plates coated with silica gel 60

F₂₅₄ (Merck) and visualized by using UV light and/or by heating to 140°C for 5 min with a molybdate solution (a 0.02 M solution of ammonium cerium sulfate dihydrate and ammonium molybdate tetrahydrate in aqueous 10% H₂SO₄). Column chromatography was performed on a CombiFlash Companion (Teledyne-ISCO, Inc.) using RediSep normal phase disposable flash columns (silica gel). Reversed phase chromatography was performed on LiChroprepRP-18 (Merck, 40-63 μm). LC-MS separation was done on a Waters system equipped with sample manager 2767, pump 2525, PDA 2525 and micromass ZQ. Commercially available reagents were purchased from Fluka, Aldrich, Merck, AKSci, ASDI, or Alfa Aesar. Methanol (MeOH) was dried by refluxing with sodium methoxide and distilled immediately before use. Toluene and dichloromethane were dried by filtration over Al₂O₃ (Fluka, type 5016 A basic). Tetrahydrofuran was dried by distillation from sodium/benzophenone. Molecular sieves 4Å were activated under vacuum at 500°C for 2 h immediately before use.

Phenyl (2,3,4,6-tetra-*O*-acetyl-β-D-galactopyranosyl)-(1→3)-4,6-*O*-benzylidene-2-deoxy-2-trichloroacetamido-β-D-glucopyranoside (7). A mixture of **5** (500 mg, 1.02 mmol), **6** (602 mg, 1.53 mmol) and powdered molecular sieves 4Å in DCM (20 mL) was stirred at rt for 1 h. Then *N*-iodosuccinimide (690 mg, 3.07 mmol) was added, the solution was cooled to -20°C and treated with trifluoromethanesulfonic acid (27 μL, 0.31 mmol). After stirring for 2 h at -20°C the reaction mixture was filtered, diluted with DCM (30 mL) and washed successively with aq. NaHCO₃ (20 mL), aq. Na₂S₂O₈ (20 mL) and brine (20 mL). The DCM layer was dried with Na₂SO₄ and concentrated under reduced pressure. The residue was purified by chromatography on silica (petrol ether/EtOAc, 4:1 to 2:1) to yield **7** (800 mg, 81%).

[α]_D²⁰ -17.9 (*c* 1.00, CHCl₃); ¹H NMR (500 MHz, CDCl₃): δ 7.44-7.39 (m, 2H, Ar-H), 7.33-7.28 (m, 3H, Ar-H), 7.27 (d, *J* = 7.6 Hz, 1H, NH), 7.21-7.17 (m, 2H, Ar-H), 6.98 (t, *J* = 7.4 Hz, 1H, Ar-H), 6.92 (d, *J* = 8.7 Hz, 2H, Ar-H), 5.51 (d, *J* = 8.2 Hz, 1H, Glc-H1), 5.48 (s, 1H, CHPh), 5.25 (dd, *J* = 0.8, 3.5 Hz, 1H, Gal-H4), 5.14 (dd, *J* = 8.0, 10.4 Hz, 1H, Gal-H2), 4.87 (dd, *J* = 3.4, 10.4 Hz, 1H, Gal-H3), 4.73 (d, *J* = 8.0 Hz, 1H, Gal-H1), 4.55 (t, *J* = 9.6 Hz, 1H, Glc-H3), 4.29 (dd, *J* = 4.9, 10.5 Hz, 1H, Glc-H6a), 4.05 (dd, *J* = 6.9, 11.3 Hz, 1H, Gal-H6a), 3.91 (dd, *J* = 6.6, 11.2 Hz, 1H, Gal-H6b), 3.79-3.72 (m, 3H, Glc-H2, -H4, -H6b), 3.68 (t, *J* = 7.1 Hz, 1H, Gal-H5), 3.56 (td, *J* = 4.9, 9.8 Hz, 1H, Glc-H5), 2.03, 1.93, 1.88, 1.82 (4 s, 12H, 4 COCH₃); ¹³C NMR (125 MHz, CDCl₃): δ 170.3, 170.2, 170.1, 169.6 (4 COCH₃), 162.2 (COCCl₃), 156.8, 136.9, 129.7, 129.3, 128.3, 126.2, 123.6, 117.3, (12C, 2 C₆H₅), 101.5

(CHPh), 99.3 (Glc-C1), 98.4 (Gal-C1), 92.4 (CCl₃), 78.7 (Glc-C4), 75.9 (Glc-C3), 71.0 (Gal-C3), 70.7 (Gal-C5), 68.9 (Gal-C2), 68.5 (Glc-C6), 66.9 (Gal-C4), 66.4 (Glc-C5), 61.3 (Gal-C6), 58.5 (Glc-C2), 20.7, 20.6, 20.6, 20.5 (4 COCH₃); ESI-MS: *m/z* calcd for C₃₅H₃₈Cl₃NO₁₅ [M+Na]⁺: 840.12, found: 840.36; Anal. calcd: C, 51.33; H, 4.68; N, 1.71; found: C, 51.13; H, 4.68; N, 1.54.

Phenyl (2,3,4,6-tetra-*O*-acetyl-β-D-galactopyranosyl)-(1→3)-6-*O*-benzyl-2-deoxy-2-trichloroacetamido-β-D-glucopyranoside (8). To a solution of **7** (800 mg, 0.98 mmol) in dry THF (20 mL) were added successively borane-trimethylamine complex (285 mg, 3.90 mmol) and AlCl₃ (780 mg, 5.85 mmol) at rt. After 15 h water (20 mL) was carefully added followed by 1 N HCl (10 mL). The mixture was extracted with EtOAc (3 × 30 mL), and the combined organic layers were washed with water (20 mL) and brine (15 mL), dried with Na₂SO₄, and concentrated. Column chromatography of the residue on silica (petrol ether/EtOAc, 2:1) gave **8** (615 mg, 77%).

[α]_D²⁰ -15.8 (*c* 1.00, CHCl₃); ¹H NMR (500 MHz, CDCl₃): δ 7.30-7.14 (m, 8H, Ar-H, NH), 6.97-6.90 (m, 3H, Ar-H), 5.30 (s, 1H, Gal-H4), 5.25 (dd, *J* = 3.2, 8.2 Hz, 1H, Glc-H1), 5.19 (dd, *J* = 8.8, 10.4, 1H, Gal-H2), 4.87 (dd, *J* = 3.4, 10.5 Hz, 1H, Gal-H3), 4.54 (d, *J* = 7.5 Hz, 1H, Gal-H1), 4.51 (s, 2H, CH₂Ph), 4.22 (m, 1H, Glc-H3), 4.04 (m, 1H, Glc-H6a), 3.94 (t, *J* = 6.5 Hz, 1H, Gal-H5), 3.85 (d, *J* = 10.3 Hz, 1H, Glc-H6a), 3.72 (m, 1H, Glc-H2), 3.66-3.53 (m, 3H, Glc-H4, -H5, -H6b), 2.07, 2.02, 1.95, 1.89 (4 s, 12H, 4 COCH₃); ¹³C NMR (125 MHz, CDCl₃): δ 170.5, 170.2, 170.1, 169.6 (4 COCH₃), 162.3 (COCCl₃), 157.1, 138.2, 129.6, 128.3, 127.6, 127.5, 123.3, 117.2 (12C, 2 C₆H₅), 100.8 (Gal-C1), 97.9 (Glc-C1), 92.4 (CCl₃), 82.5 (Glc-C3), 75.7 (Glc-C5), 73.5 (CH₂Ph), 71.1 (Gal-C5), 70.9 (Gal-C3), 69.4 (Glc-C6), 69.3 (Glc-C4), 68.5 (Gal-C2), 66.9 (Gal-C4), 61.2 (Gal-C6), 57.8 (Glc-C2), 21.0, 20.6, 20.6, 20.5 (4 COCH₃); ESI-MS: *m/z* calcd for C₃₅H₄₀Cl₃NO₁₅ [M+Na]⁺: 842.14, found: 842.28; Anal. calcd: C, 51.20; H, 4.91; N, 1.71; found: C, 51.13; H, 4.90; N, 1.51.

Phenyl (2,3,4,6-tetra-*O*-acetyl-β-D-galactopyranosyl)-(1→3)-[(2,3,4-tri-*O*-benyl-6-deoxy-α-L-galactopyranosyl-(1→4)]-6-*O*-benzyl-2-deoxy-2-trichloroacetamido-β-D-glucopyranoside (9). To a solution of **10** (525 mg, 1.10 mmol) in DCM (5 mL) was added bromine (60 μL, 1.21 mmol) at 0°C under argon. After 5 min, the cooling bath was removed and the reaction mixture was stirred for 30 min at rt. Then cyclohexene (100 μL) was added to destroy the excess bromine. The reaction mixture was added to a pre-stirred suspension

(2 h, rt) of **8** (300 mg, 0.37 mmol), Et₄NBr (160 mg, 0.76 mmol) and powdered molecular sieves 4Å in DCM (2.5 mL) and DMF (10 mL). After stirring overnight, the reaction mixture was filtered, diluted with DCM (30 mL) and washed with aq. NaHCO₃ (20 mL) and brine (20 mL). The organic layer was dried (Na₂SO₄), filtered, and evaporated to dryness. The residue was purified by chromatography on silica (petrol ether/EtOAc/MeOH, 8:1.8:0.2) to yield **9** (225 mg, 0.18 mmol, 49 %).

$[\alpha]_D^{20}$ -29.6 (*c* 1.00, CHCl₃); ¹H NMR (500 MHz, CDCl₃): δ 7.32 (d, *J* = 7.2 Hz, 2H, Ar-H), 7.30-7.11 (m, 20H, Ar-H), 7.07 (d, *J* = 8.2 Hz, 1H, NH), 6.96 (d, *J* = 7.4 Hz, 1H, Ar-H), 6.95-6.90 (m, 2H, Ar-H), 5.30 (d, *J* = 3.1 Hz, 1H, Gal-H4), 5.21 (d, *J* = 6.1 Hz, 1H, Glc-H1), 5.13 (dd, *J* = 8.1, 10.5 Hz, 1H, Gal-H2), 5.04 (d, *J* = 3.9 Hz, 1H, Fuc-H1), 4.93-4.86 (m, 2H, Gal-H3, CH₂Ph), 4.81 (d, *J* = 8.1 Hz, 1H, Gal-H1), 4.75-4.67 (m, 3H, 3H of CH₂Ph), 4.63 (d, *J* = 11.8 Hz, 1H, CH₂Ph), 4.57 (d, *J* = 11.4 Hz, 1H, CH₂Ph), 4.34 (s, 2H, CH₂Ph), 4.25 (q, *J* = 6.3 Hz, 1H, Fuc-H5), 4.11-4.01 (m, 5H, Fuc-H2, -H3, Glc-H2, -H3, Gal-H6a), 3.98 (dd, *J* = 5.9, 11.0 Hz, 1H, Gal-H6b), 3.86-3.81 (m, 3H, Gal-H5, Glc-H4, -H5), 3.72 (dd, *J* = 4.7, 10.6 Hz, 1H, Glc-H6a), 3.67-3.62 (m, 2H, Fuc-H4, Glc-H6b), 1.98, 1.93, 1.88, 1.87 (4 s, 12H, 4 COCH₃), 1.18 (d, *J* = 6.5 Hz, 3H, Fuc-H6); ¹³C NMR (125 MHz, CDCl₃): δ 170.2, 170.0, 170.0, 169.5 (4 COCH₃), 161.8 (COCCl₃), 156.9, 138.6, 138.5, 138.2, 138.1, 129.6, 128.5, 128.4, 128.4, 128.3, 128.3, 127.9, 127.7, 127.6, 127.5, 127.1, 123.0, 117.0 (30C, 5 C₆H₅), 100.0 (Gal-C1), 97.8 (Glc-C1), 96.5 (Fuc-C1), 92.3 (CCl₃), 80.2 (Glc-C4), 76.8 (Fuc-C4), 76.5 (Glc-C3), 75.7 (Fuc-C3), 74.8 (Gal-C5), 74.6, 74.5, 73.2, 72.4 (4 CH₂Ph), 71.2 (Fuc-C2), 70.9 (Glc-C5), 70.8 (Gal-C3), 68.6 (Glc-C6), 68.3 (Gal-C2), 66.9 (2C, Fuc-C5, Gal-C4), 60.5 (Gal-C6), 55.9 (Glc-C2), 20.8, 20.7, 20.6, 20.5 (4 COCH₃), 16.9 (Fuc-C6); ESI-MS: *m/z* calcd for C₆₂H₆₈Cl₃NO₁₉ [M+Na]⁺: 1258.33; found: 1258.29; Anal. calcd: C, 60.17; H, 5.54; N, 1.13; found: C, 59.95; H, 5.58; N, 0.90.

Phenyl β-D-galactopyranosyl-(1→3)-[α-L-fucopyranosyl-(1→4)]-2-acetamido-2-deoxy-β-D-glucopyranoside (4). To a solution of **9** (225 mg, 0.18 mmol) in MeOH (10 mL) was added a catalytic amount of NaOMe at rt. After stirring for 30 min the mixture was neutralized with AcOH and evaporated to dryness. Column chromatography on silica (petrol ether/EtOAc/MeOH, 6:3.6:0.4) afforded the benzylated intermediate (185 mg, 94%). A mixture of the intermediate (185 mg, 0.17 mmol), Pd(OH)₂/C (50 mg) and NEt₃ (100 μL) in dioxane/water (4:1, 10 mL) was hydrogenated (4 bar H₂) in a Parr shaker for 5 h. ESI-MS analysis indicated complete reduction of the trichloroacetamide group to the acetamide. The mixture was filtered over celite and the filtrate was concentrated. The residue was dissolved

in dioxane/water (4:1, 10 mL), Pd(OH)₂/C (50 mg) was added and the mixture was hydrogenated (4 bar H₂) for 24 h. The catalyst was filtered off and the solution was concentrated under reduced pressure. The residue was purified by preparative LCMS to afford **4** (100 mg, 92%).

$[\alpha]_D^{20}$ -56.1 (*c* 1.00, MeOH); ¹H NMR (500 MHz, D₂O): δ 7.35-7.30 (m, 2H, Ar-H), 7.08 (t, *J* = 7.4 Hz, 1H, Ar-H), 7.02 (d, *J* = 7.8 Hz, 2H, Ar-H), 5.10 (d, *J* = 8.1 Hz, 1H, Glc-H1), 4.99 (d, *J* = 3.9 Hz, 1H, Fuc-H1), 4.83 (q, *J* = 6.6 Hz, 1H, Fuc-H5), 4.46 (d, *J* = 7.7 Hz, 1H, Gal-H1), 4.15-4.08 (m, 2H, Glc-H2, -H3), 3.94 (dd, *J* = 2.0, 12.5 Hz, 1H, Glc-H6a), 3.86-3.80 (m, 3H, Fuc-H3, Glc-H6b, Gal-H4), 3.80-3.73 (m, 3H, Glc-H4, Fuc-H2, -H4), 3.70-3.63 (m, 3H, Gal-H6, Glc-H5), 3.56 (dd, *J* = 3.4, 9.8 Hz, 1H, Gal-H3), 3.51 (dd, *J* = 4.9, 7.0 Hz, 1H, Gal-H5), 3.45 (dd, *J* = 7.7, 9.8 Hz, 1H, Gal-H2), 1.95 (s, 3H, COCH₃), 1.14 (d, *J* = 6.6 Hz, 3H, Fuc-H6); ¹³C NMR (125 MHz, D₂O): δ 174.7 (CO), 156.8, 130.0, 123.5, 116.7 (6C, C₆H₅), 102.9 (Gal-C1), 99.5 (Glc-C1), 98.1 (Fuc-C1), 75.9 (Glc-C3), 75.6 (Glc-C5), 74.8 (Gal-C5), 72.3 (Gal-C3), 72.2 (Fuc-C4), 72.0 (Fuc-C2), 70.5 (Gal-C2), 69.2 (Fuc-C3), 68.4 (Gal-C4), 67.8 (Glc-C4), 66.9 (Fuc-C5), 61.7 (Gal-C6), 59.6 (Glc-C6), 55.7 (Glc-C2), 22.2 (CH₃), 15.4 (Fuc-C6); HRMS: *m/z* calcd for C₂₆H₃₉NO₁₅ [M+Na]⁺: 628.2212, found: 628.2211.

Compound purity: 99.0 % (R_t 7.73 min, λ 168-216 nm; HPLC system: Beckmann Gold; Column: Waters Atlantis dC18, 3 μ m, 4.6 \times 75mm; Mobile phase: A: H₂O + 0.1% HCO₂H; B: MeCN + 0.1% HCO₂H; Gradient: 5% B \rightarrow 50% B over 20 min; Flow rate: 0.5 ml/min).

2. Isothermal Titration Calorimetry (ITC)

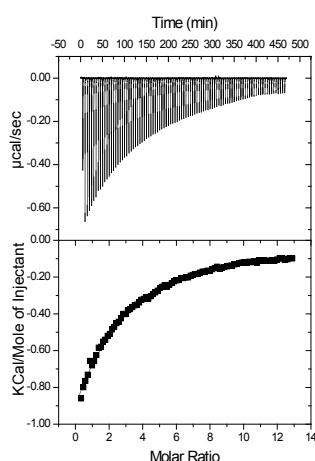


Figure S1. ITC profile of phenyl Le^a (**4**) titrated into DC-SIGN CRD-Fc.

Table S1. Thermodynamics of phenyl Le^a binding to DC-SIGN CRD-Fc. Confidence intervals (95%) of the fit were within the standard deviations. ^a Stoichiometry fixed at 1; concentration expressed in terms of binding site.

Compound	N	K _D [μM]	ΔG° [kJ/mol]	ΔH° [kJ/mol]	TΔS° [kJ/mol]
Phenyl Le ^a (4)	1 ^a	582 ± 40	-18.5 ± 0.1	-28.0 ± 2.0	-9.5 ± 2.1

3. Saturation Transfer Difference (STD) NMR

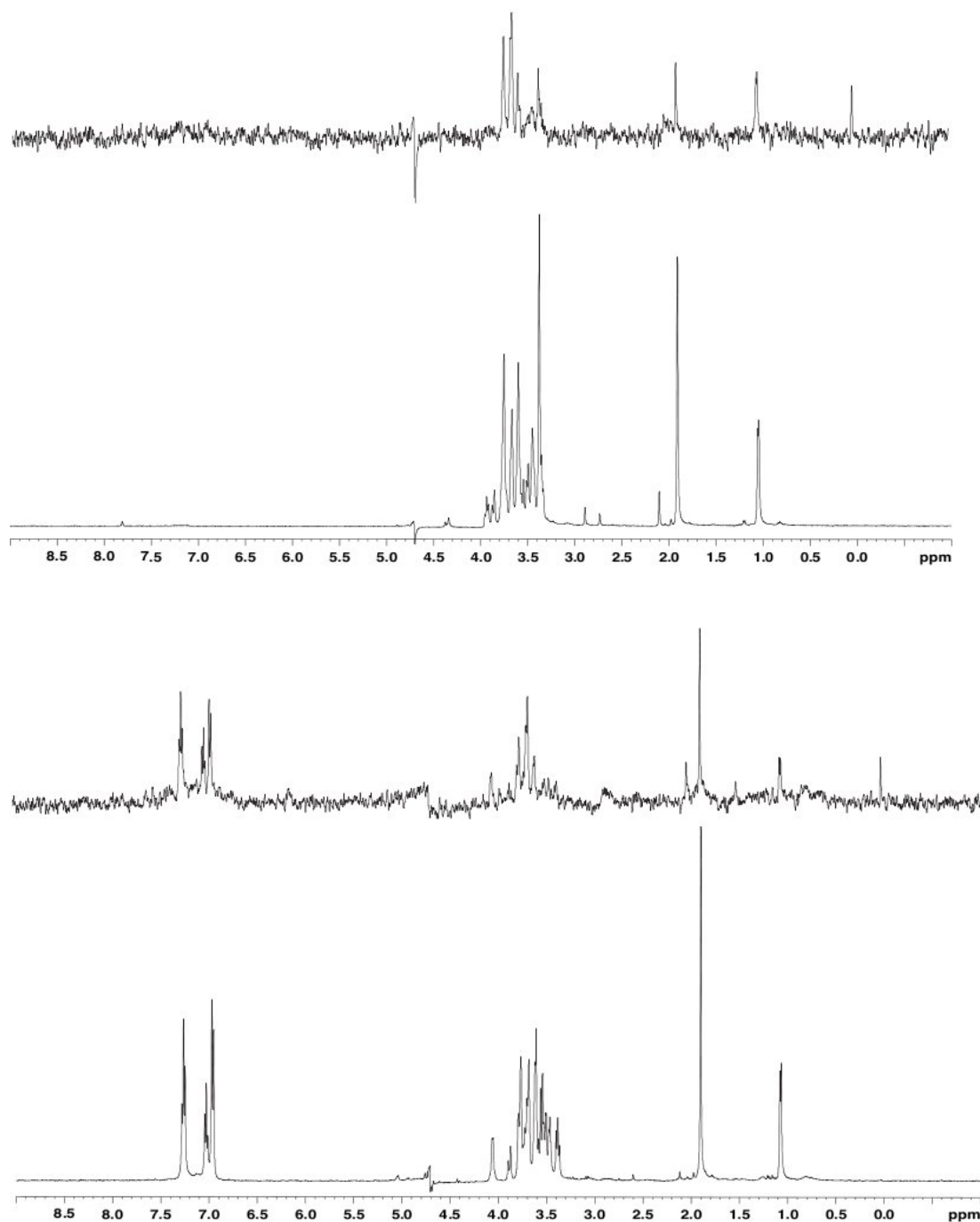


Figure S2. STD and reference NMR spectra of methyl Le^a (2) (top) and phenyl Le^a (4) (bottom) in presence of DC-SIGN CRD-Fc.

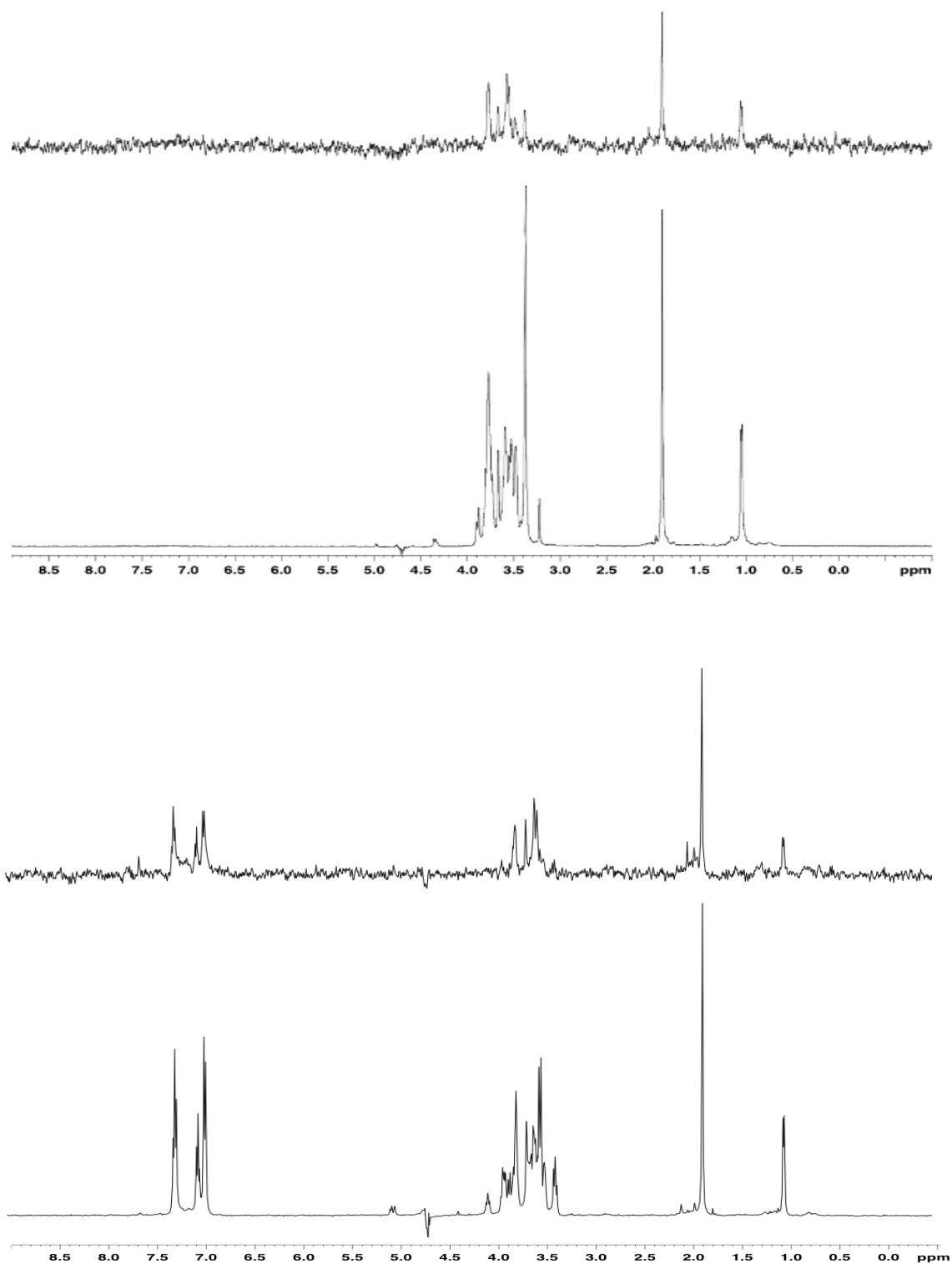


Figure S3. STD and reference NMR spectra of methyl Le^x (**1**) (top) and phenyl Le^x (**3**) (bottom) in presence of DC-SIGN CRD-Fc.

Table S2. Approximate percentage values determined from STD NMR spectra in presence of DC-SIGN CRD-Fc; “-“ protons show potentially STD signals, however, no quantification could be unambiguously achieved due to signal overlap or interference with water suppression.

	Aglycones		D-GlcNAc						
	Methyl	Phenyl	H1	H2	H3	H4	H5	H6	NAc
Methyl Le ^a (2)	40%		-	<40%	<40%	65%	74%	<45%	40%
Methyl Le ^x (1)	30%		-	<40%	<40%	70-75%	70%	-	123%
Phenyl Le ^a (4)		140-205%	-	164%	164%	<127%	-	<148%	122%
Phenyl Le ^x (3)		130-160%	-	-	100%	-	-	-	190%

	L-Fuc					
	H1	H2	H3	H4	H5	H6
Methyl Le ^a (2)	-	187%	106%	121%	-	100%
Methyl Le ^x (1)	-	175%	95%	175%	-	100%
Phenyl Le ^a (4)	-	218%	136%	218%	-	100%
Phenyl Le ^x (3)	-	-	-	160%	-	100%

	D-Gal					
	H1	H2	H3	H4	H5	H6
Methyl Le ^a (2)	-	75%	60%	<40%	75%	-
Methyl Le ^x (1)	-	43%	67%	100%	71%	-
Phenyl Le ^a (4)	-	82%	91%	133%	100%	-
Phenyl Le ^x (3)	-	80%	80%	-	80%	-

Experiments at different saturation times with phenyl Le^a (4)

The total recycle delay time was kept constant and the saturation time set to 0.7, 1, 2, and 3s. We determined relative STD intensities for specific protons of phenyl Le^a (4) and compared the values to exclude T1 bias of different proton types (Table S4). In conclusion, different saturation times do not affect the intensity of aromatic protons and the overall binding epitope significantly.

Table S3. Ratio (STD/reference signal) determined from STD NMR spectra in presence of DC-SIGN CRD. The signals were normalized to the para aryl proton. For short saturation times STD effect is weak and signal of carbohydrate protons could not be determined doubtlessly.

saturation time [s]	0.7	1	2	3
Aryl H (meta)	0.8	0.9	0.8	0.9
Aryl H (para)	1.0	1.0	1.0	1.0
Aryl H (ortho)	0.7	0.7	0.7	0.8
Gal-H2	-	-	0.6	0.6
NAc (CH ₃)	0.6	0.8	0.6	0.6
Fuc-H6	0.7	0.6	0.5	0.5

4. Molecular Dynamics

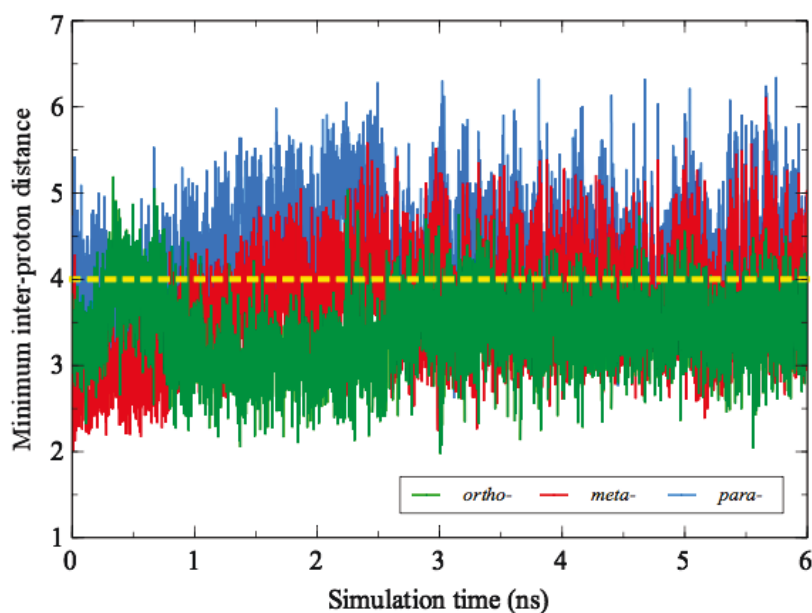


Figure S4. Time evolution of inter-proton distance between each of the phenyl protons of phenyl Lewis^a (4) and the closest proton of neighboring protein side chains in a 6 ns molecular dynamics simulation.

2.3 Synthesis of Glycomimetic Antagonists for DC-SIGN

2.3.1 *Manuscript 2: Le^x Mimics: The Role of N-Acetylglucosamine and D-Galactose in Binding to DC-SIGN*

Author contributions:

Katharina Mayer: synthesis of Le^x mimics, data collection and coordination, preparation of manuscript.

Sameh Eid: molecular modeling studies, contribution to manuscript.

Dr. Meike Scharenberg: protein expression, IC₅₀ determination in competitive polymer binding assay.

Dr. Katrin Lemme and Roland Preston: ITC experiments.

Manuscript in preparation for **Bioorganic & Medicinal Chemistry**

Le^x Mimics: The Role of *N*-Acetylglucosamine and *D*-Galactose in Binding to DC-SIGN

Katharina Mayer,^a Sameh Eid,^a Meike Scharenberg,^a Katrin Lemme,^a Roland Preston,^a Beat Ernst^{*a}

^a *Institute of Molecular Pharmacy, Pharmacenter, University of Basel, Klingelbergstr.50, 4056 Basel, Switzerland*

* Corresponding author: Prof. Dr. Beat Ernst, Institute of Molecular Pharmacy, Pharmacenter, University of Basel, Klingelbergstrasse 50, CH-4056 Basel, Switzerland, Tel: +41 61 2671551, Fax: +41 61 2671552; e-mail: beat.ernst@unibas.ch

Keywords: DC-SIGN · Lewis antigens · glycomimetics · ITC

Abbreviations: AIBN, Azodiisobutyronitrile; CAN, ceric ammonium nitrate; Cy, Cyclohexyl; DC, dendritic cells; DCE, 1,2-dichloroethane; DC-SIGN, DC-specific ICAM-3-grabbing nonintegrin; DMF, *N,N*-dimethylformamide; DMTST, dimethyl(methylthio)sulfonium triflate; Fuc, fucose; LNFP III, lacto-*N*-fucopentaose III; Gal, galactose; GlcNAc, *N*-acetylglucosamine; HPLC, high-performance liquid chromatography; IC₅₀, halfmaximal inhibitory concentration; ICAM, intercellular adhesion molecule; ITC, isothermal titration calorimetry; Le^x, Lewis^x; MHC, major histocompatibility complex; MS, molecular sieves; NMR, nuclear magnetic resonance; TES, triethylsilane; TBAB, tetrabutylammonium bromide; TCDI, *N,N*-thiocarbonyl diimidazole; TLC, thin layer chromatography; TMSE, 2-(trimethylsilyl)ethyl; TMSOTf, trimethylsilyl triflate; Ts, tosyl.

ABSTRACT

As part of the innate immune system, dendritic cells (DCs) have the function of presenting antigens to other processing cells of the immune system, in particular T-cells. DC-specific ICAM-3-grabbing nonintegrin (DC-SIGN), one of the transmembrane receptors in DCs, is a C-type lectin and recognizes oligomannosides and fucose-containing Lewis blood group antigens, such as Lewis^x (Le^x), in a Ca²⁺ dependent manner. These structures are present in a series of pathogens, including viruses, bacteria, and yeasts. Many microorganisms evade the normal degradation mechanisms by binding to DC-SIGN and furthermore, exploit this interaction to efficiently infect the host. A blockage of this first interaction with appropriate DC-SIGN antagonists is therefore a promising therapeutic approach towards prevention of infectious diseases.

Co-crystallization of DC-SIGN with Le^x as part of lacto-*N*-fucopentaose III indicates that the terminal sugar residues D-Gal and L-Fuc are involved in binding, whereas the linking sugar D-GlcNAc is directed towards the solvent. L-Fuc is crucial for coordination of the Ca²⁺ ion in the binding site. In this study, we investigated the role Gal and D-GlcNAc in Le^x-type structures for binding to DC-SIGN.

We synthesized a series of trisaccharide mimics of Le^x in which D-GlcNAc is replaced by a (1*R*,2*R*,3*S*)-3-methyl-cyclohexane-1,2-diol moiety. Variations of the D-Gal moiety include deoxy D-Gal derivatives as well as the D-Glc (epimer to D-Gal in the 4-position). Additionally, a disaccharide mimic without the respective D-Gal moiety was synthesized. Binding affinities obtained in a static cell-free competition assay and ITC data indicate a minor influence of 4- and 6-OH of Gal in Le^x mimics binding to DC-SIGN. Furthermore, the affinity was improved by replacing the D-GlcNAc mimic with a methylcyclohexyl based mimic. ITC data of Le^x and mimics indicated affinity in the low millimolar range and elucidated the thermodynamic properties of this interaction. Based on this information DC-SIGN ligands with improved binding affinity and reduced structural complexity can be designed.

INTRODUCTION

Immature dendritic cells (DCs), located in mucosal tissue, play an essential role in immune response as they are antigen-presenting cells.¹ In general, pathogen-uptake initiates maturation and migration of the DC to the lymphatic system where the antigen is presented on the major histocompatibility complex (MHC) to resting T-cells.

DC-specific ICAM-3-grabbing nonintegrin (DC-SIGN), located on the surface of DCs, was discovered to be one of the main receptors for recognition and internalization of pathogens.² DC-SIGN is a type II transmembrane protein with a C-terminal carbohydrate recognition domain (CRD). As member of the C-type lectin family, binding to DC-SIGN occurs in a Ca^{2+} -dependent manner. Besides its function as a cell-adhesion receptor for the control of DC migration via intercellular adhesion molecule-2 (ICAM-2), DC-SIGN regulates the DC–T-cell interactions via ICAM-3 which is located on the surface of T-cells.^{2,3} The latter fact indicates the significant role of DC-SIGN in development of an immune response. A broad variety of pathogens including viruses (e.g. HIV, Ebola virus)^{4,5}, bacteria (e.g. *Mycobacterium tuberculosis*, *Helicobacter pylori*)^{6,7}, and yeasts (e.g. *Candida albicans*)⁸ evolved mechanisms to evade the immune response. One major measure is making beneficial use of the interaction with DC-SIGN for an efficient establishment of infection.^{9,10} The mechanisms cover a multitude of simultaneous and ligand-specific processes including alteration of Toll-like receptor-mediated signaling cascades.¹¹⁻¹³ The design of DC-SIGN ligands that can block the initial interaction with pathogens is a promising therapeutic approach towards prevention of infectious diseases.¹⁴

The majority of pathogens bind with *N*-linked high-mannose oligosaccharides to DC-SIGN.¹⁵ An established example for this is HIV that contains this mannan structure on its gp120 envelope protein.^{16,17} HIV and Ebola were shown to escape the DC-mediated degradation mechanism.^{9,18-25} In fact, binding of these viruses to DC-SIGN rather triggers the effective *trans*-infection of T-cells via viral synapses.^{5,15,26}

Besides mannosylated structures, the L-Fuc embodying Lewis blood group antigens such as Lewis^x (Le^x, Gal β (1-4)[Fuc α (1-3)]GlcNAc) **1**, prevalent on *Schistosoma mansoni* or *Helicobacter pylori*, are recognized by DC-SIGN.²⁷ Naarding and Geijtenbeek showed that human milk containing Le^x (**1**) in a multimeric manner inhibits HIV-1 gp120 binding to the CRD of DC-SIGN and the subsequent *trans*-infection of CD4⁺ T-cells.²⁸ The minimal binding epitope for DC-SIGN is the Le^x trisaccharide (**1**).²⁸⁻³¹ Crystallographic data obtained

from DC-SIGN co-crystallized with lacto-*N*-fucopentaose III (LNFP III, Le^x-D-Gal-D-Glc) that contains the Le^x motif, revealed the α 1-3-linked L-Fuc coordinating the Ca²⁺ ion via its equatorial 3- and axial 4-OH group.²⁹ The 2-OH of L-Fuc is positioned close to Val351 allowing a van der Waals contact. Likewise, the *NAc* group in D-GlcNAc moiety of Le^x forms a hydrophobic contact with Val351, which represents the only interaction with the protein mediated by this moiety. D-Gal is involved in a water-bridged H-bond of the 4-OH to Glu358 and direct H-bond of 6-OH with Asp367.²⁹ Asp367 on its part is involved in a H-bond network with Glu358 and Lys373 (Figure 1).

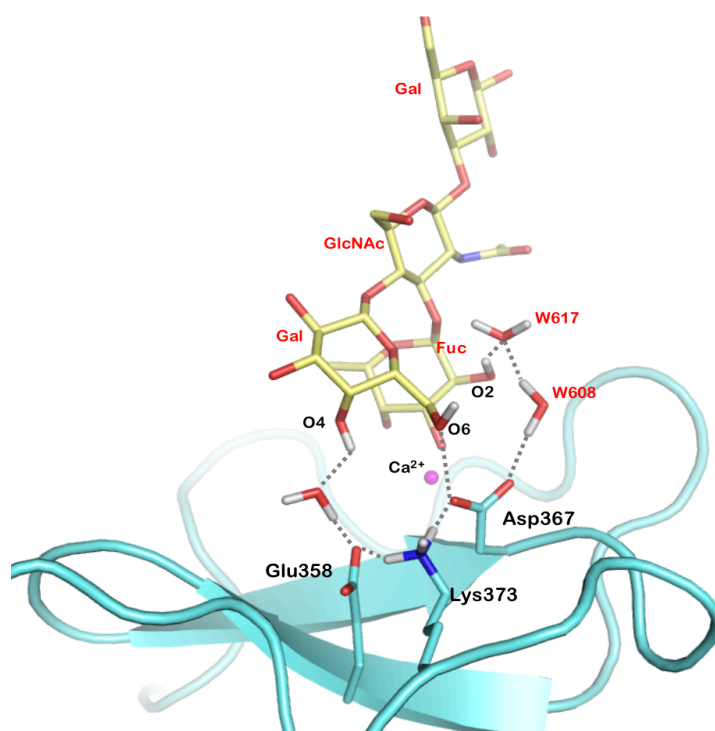


Figure 1. Binding mode of the resolved part of LNFP III derived from co-crystallization with DC-SIGN (PDB 1SL5²⁹). The Asp367-Lys373-Glu358 H-bonding network involved in D-Gal binding is highlighted. L-Fuc complexes the Ca²⁺ ion via its 3- and 4-OH, 2-OH of L-Fuc establishes a water bridged H-bond to Asp367 and makes van der Waals contact with Val351 (not shown).

Carbohydrates are highly polar, known to have unfavorable properties for drug development with respect to their pharmacokinetic and pharmacodynamic properties. Therefore, glycomimetics with reduced polarity but retained biological function are developed.³² In this study, we mimic one of the sugar moieties in Le^x to improve the drug-like properties and affinity. We have previously shown that in case of E-selectin, replacement of the D-GlcNAc part of sialyl Le^x with different cyclohexanediol derivatives improves the affinity in a static competitive binding assay up to a factor of 20.^{33,34} The D-GlcNAc motif mainly has the role

of a spacer that keeps the two residues at its 3- and 4-position (namely L-Fuc and D-Gal) in the correct spatial orientation, i.e. a conformation close to the bioactive conformation.^{35,36} (1*R*,2*R*,3*S*)-3-methyl-cyclohexane-1,2-diol showed better preorganization of the core structure than a cyclohexanediol unit and hence higher affinity.^{33,37}

In a first approach, we attempted to apply these findings to the Le^x-DC-SIGN interaction by replacing the D-GlcNAc part of the Le^x trisaccharide by a (1*R*,2*R*,3*S*)-3-methyl-cyclohexane-1,2-diol (Figure 2).

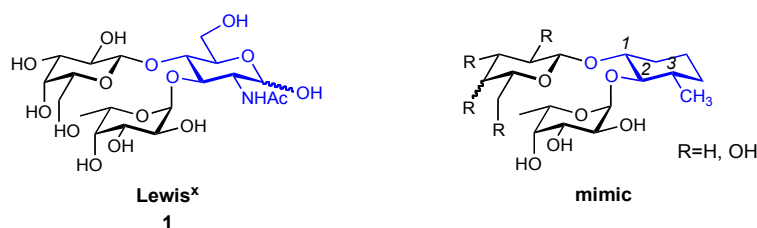


Figure 2. Le^x trisaccharide and general trisaccharide mimic.

Moreover, to investigate the role of D-Gal in binding to DC-SIGN, we synthesized Le^x mimics containing 2-, 3-, 4-, and 6-deoxygenated D-Gal moieties, the 4-OH epimeric compound (\rightarrow D-Glc), as well as the respective disaccharide mimic lacking the D-Gal moiety entirely. These mimics were evaluated by means of a static competitive binding assay for affinity to DC-SIGN CRD. Selected compounds were additionally tested with isothermal titration calorimetry (ITC) to determine K_D values and the thermodynamic profile of this interaction. With molecular modeling studies the experimental results were structurally interpreted.

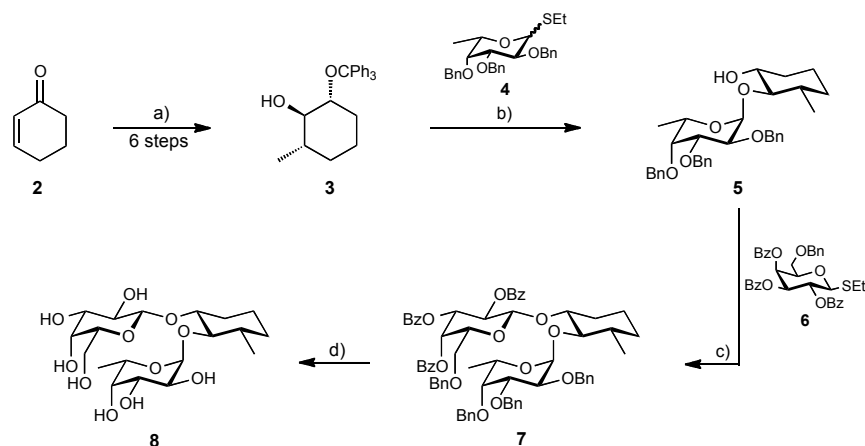
Information on the interactions between ligand and protein is essential for further development of high-affinity low molecular weight compounds, which can serve as starting point for a lead optimization program.

RESULTS & DISCUSSION

Synthesis of Le^x mimics

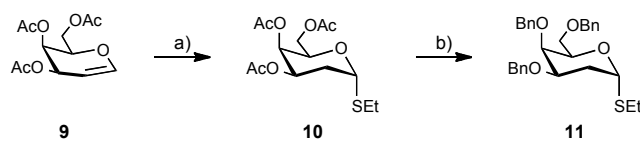
Retrosynthetically, the trisaccharide mimic **8** can be disconnected into the D-Gal derivative **6**^{36,38} and the pseudo-disaccharide **5**³³. Following an established route, the D-GlcNAc mimic **3** is obtained in a 6-step synthesis starting from 2-cyclohexen-1-one (**2**).³³ Fucosylation by *in situ* bromination of the thiofucoside **4** yielded the α -fucoside **5** which was glycosylated with

galactosyl donor **6** using dimethyl-(methylthio)sulfonium triflate (DMTST) as promoter. Subsequent deprotection yielded the trisaccharide mimic **8** (Scheme 1).



Scheme 1. a) Prepared according to reference³³; b) *i*) TBAB, 2,6-di-*tert*-butyl-4-methylpyridine, MS 4Å, CuBr₂, DMF, CH₂Cl₂, r.t., 20 h, 43%; *ii*) ZnBr₂, TES, CH₂Cl₂, r.t., 10 h, 63%; c) DMTST, MS 4Å, CH₂Cl₂, r.t., 16 h, 49%; d) Pd(OH)₂/C, dioxane/water, ii) NaOMe, MeOH, 70%.

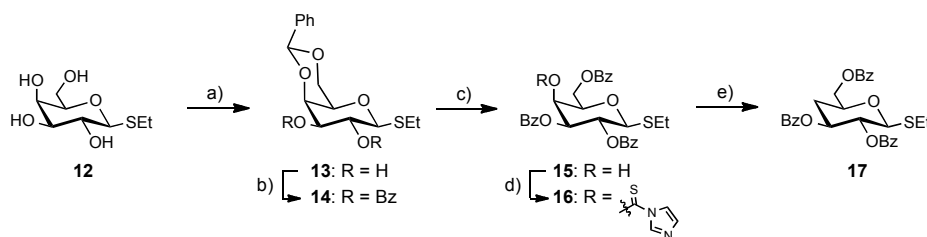
A similar approach can be applied for the synthesis of the deoxy trisaccharide mimics. The synthesis of the respective 2-, 3-, 4-, and 6-deoxy D-Gal thioglycosides is described in the following. The 2-deoxy D-Gal derivative was prepared by reacting the peracetylated D-galactal (**9**) with thioethanol in the presence of ceric ammonium nitrate, following a published procedure³⁹ (Scheme 2). In order to increase the yield in the later glycosylation step compound **10** was transformed into the armed perbenzylated derivative **11**.



Scheme 2. a) CAN, EtSH, CH₂Cl₂, 0°C to r.t., 1h, 58%; b) *i*) NaOMe, MeOH, r.t., 98%; *ii*) BnBr, DMF, 0°C to r.t., 72%.

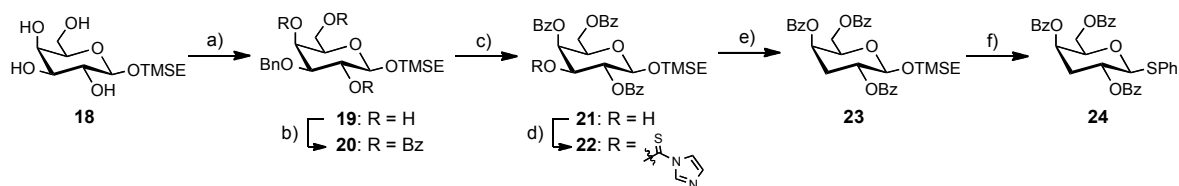
For all other D-Gal derivatives, participating neighboring groups in 2-position were introduced in order to favor β -glycosylation. For the synthesis of the 4-deoxy derivative **17**, ethyl thiogalactoside **12** served as starting material. Following a published procedure the 4,6-benzylidene acetal was formed and the 2- and 3-OH groups were benzoylated. After subsequent acetal cleavage and benzoylation in the 6-position, the 4-*O*-unprotected D-Gal derivative **15** was obtained.⁴⁰ Application of standard Barton McCombie deoxygenation

condition, namely derivatization to the imidazolyl thiocarbamate (**16**) by use of *N,N*-thiocarbonyl diimidazole (TCDI) and subsequent deoxygenation with tributyltin hydride, afforded the 4-deoxy compound **17** in good yield (Scheme 3).



Scheme 3. a) α,α -Dimethoxytoluene, TsOH, CH_3CN , 80%; b) BzCl, pyridine, 80%; c) *i*) ethylene glycol, $\text{CH}_2\text{Cl}_2/\text{TFA}$ (5:1), *ii*) BzCl, pyridine, 79%; d) TCDI, dichloroethane, 4h, Δ , 90%; e) Bu_3SnH , AIBN, PhCH_3 , 4h, Δ , 93%;

The 3- and 6-deoxy D-Gal derivatives were synthesized from the 2-(trimethylsilyl)ethyl (TMSE) galactoside **18**⁴¹. For the deoxygenation leading to the 3-deoxy derivative **24**, Barton McCombieconditions were applied. Therefore, compound **20** was synthesized using a sequence of 3-selective benzylation via tin acetal formation (\rightarrow **19**), followed by benzylation of the residual OH-groups. Removal of benzyl in 3-position gave access to compound **21** that was deoxygenated as described above to give 3-deoxy derivative **23**. Transformation of the TMSE aglycone into the thioglycoside was performed using boron trifluoride etherate for the transformation into the acetate and subsequently the thiophenyl derivative **24** (Scheme 4).



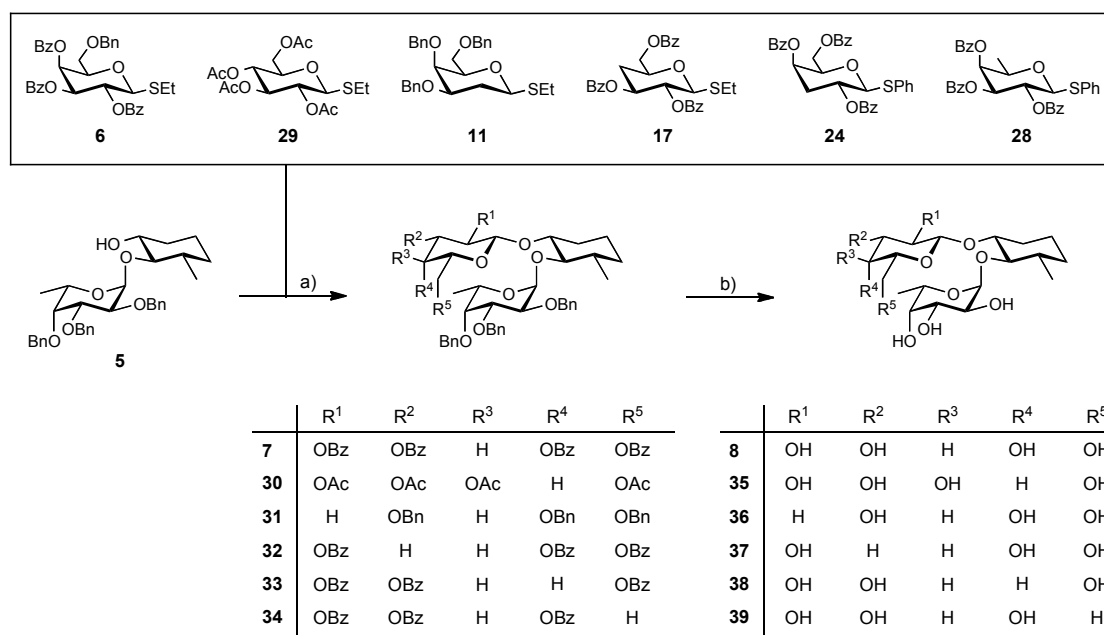
Scheme 4. a) Bu_2SnO , BnBr, Bu_4NBr , PhCH_3 , Δ , 62%; b) BzCl, pyridine, CH_2Cl_2 , 3h, 92%; c) NaBrO_3 , $\text{Na}_2\text{S}_2\text{O}_4$, $\text{EtOAc}/\text{H}_2\text{O}$, r.t., 2h, 89%, or $\text{Pd}(\text{OH})_2/\text{C}$, dioxane/ H_2O , 1d, 95%; d) TCDI, DCE, Δ , 4-6h, 92%; e) Bu_3SnH , AIBN, PhCH_3 , Δ , 4h, 86%; f) *i*) Ac_2O , $\text{BF}_3 \cdot \text{Et}_2\text{O}$, PhCH_3 , 80% (α/β , 4:3), *ii*) PhSH , $\text{BF}_3 \cdot \text{Et}_2\text{O}$, CH_2Cl_2 , 68% (α/β , 1:1).

The synthetic approach towards the 6-deoxy derivative **28** is shown in Scheme 5. 6-*O*-selective tosylation (\rightarrow **25**) with subsequent reduction of the tosyl group by means of lithium aluminium hydride afforded the fucoside **26**. Benzylation (\rightarrow **27**) and transformation of the TMSE aglycon into thiophenyl afforded the 6-deoxy derivative **28**.



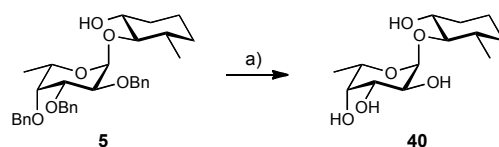
Scheme 5. a) TsCl, pyridine, 0°C, 87%; b) LiAlH₄, THF, Δ, 72%; c) BzCl, pyridine, 96%; d) i) Ac₂O, BF₃·Et₂O, pyridine, 99%, ii) PhSH, BF₃·Et₂O, CH₂Cl₂, 47%.

The pseudo-disaccharide **5** was glycosylated with the deoxy D-Gal donors **17**, **24**, **28** and the D-Glc derivative **29**⁴² using DMTST as promoter yielding predominantly the β-glycosides (Scheme 6). For the 2-deoxy D-Gal derivative **11** missing a participating neighboring group in the 2-position, low temperature and low concentration with acetonitrile as assisting solvent⁴³ were applied to obtain the protected β-glycosylated trisaccharide mimic **31** although in moderate yield. The final deprotection of the trisaccharide mimics **30-34** was performed using standard *Zemplén* conditions and hydrogenolysis with Pd(OH)₂/C as catalyst to afford compounds **35-39** (Scheme 6).



Scheme 6. Typical procedure for glycosylation and deprotection: glycosyl acceptor **5**, donors **6**, **17**, **24**, **28**, and **29**, DMTST, MS 4Å, CH₂Cl₂, r.t., 16-24 h, 48-75% i) Pd(OH)₂/C, dioxane/water, ii) NaOMe, MeOH 68-81%; conditions for donor **11**: NIS, TMSOTf, MS 3Å, -65°C, 1h, 14% (over two steps).

The pseudo disaccharide **5** was accordingly treated with hydrogenolytic conditions to give the respective pseudo-disaccharide **40** (Scheme 7).



Scheme 7. Deprotection of pseudodisaccharide **5**. a) Pd(OH)₂/C, dioxane/water, 1h, 91%.

Docking of compounds and FEP calculations

Automated docking (Glide⁴⁴) of the Le^x trisaccharide (**1**) and compound **8** (Figure 3) resulted in a binding mode similar to that of the Le^x subunit in LNFP III in complex with DC-SIGN (see Figure 1). Mimicking the D-GlcNAc moiety, as expected, does not affect the binding mode since this part points to the solvent. The calcium ion is coordinated via the 3- and 4-OH group of L-Fuc, D-Gal participates in (water assisted) H-bonds. The NAc group in D-GlcNAc establishes a van der Waals contact with Val351. The same interaction is seen for the methyl group in **8** causing a minor reorientation of this amino acid side chain.

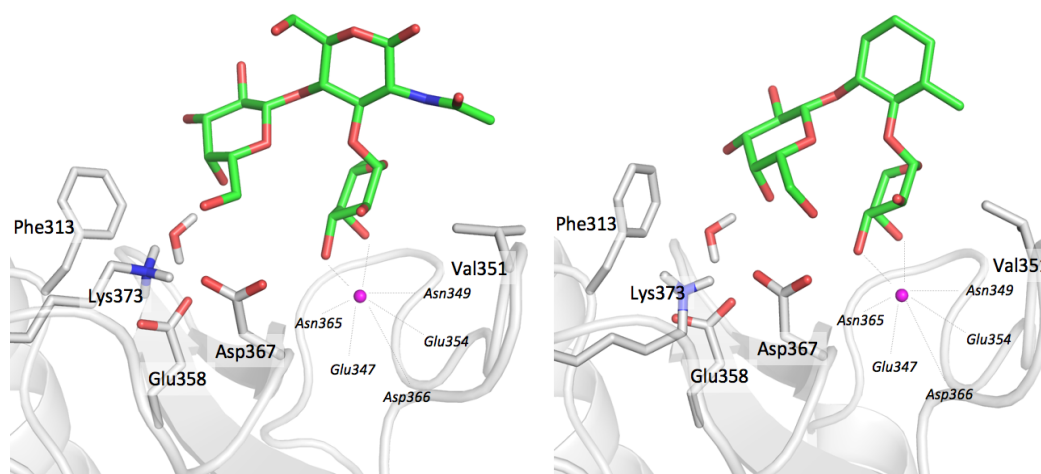


Figure 3. Le^x (**1**) and Le^x mimic (**8**) docked in 1SL5 maintain the orientation and interaction as the Le^x subunit in LNFP III (compare Figure 1).²⁹

Likewise, the top-ranked binding pose of the pseudo-disaccharide **40** resembles the discussed binding mode for **1** and **8**, i.e. L-Fuc coordinates the Ca²⁺ via its 3- and 4-OH (Figure 4). Due to the upright orientation no further contacts with the protein are established.

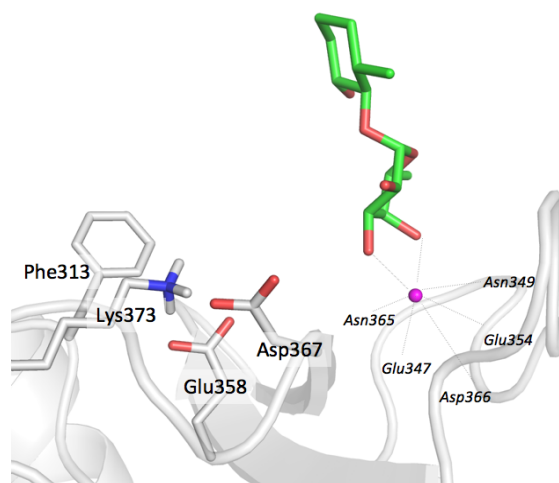


Figure 4. The pseudo-disaccharide **40** docked to the crystal structure of DC-SIGN (PDB 1SL5). Top-ranked pose resembles the orientation of the Le^x subunit in LNFP III (see Figure 1).²⁹

We further performed free energy perturbation (FEP) calculations that show the influence of small structural changes on free binding energy. Therefore, mimic **8** was compared with its respective 3-, 4-, and 6-deoxy analogues (**37**, **38**, **39**). Two-nanosecond FEP simulations were performed starting from the docking pose found for **8**. Results for $\Delta\Delta G$ are shown in Table 1. Whereas 3-deoxygenation is predicted to marginally increase affinity, lacking of the OH-group in the 4- or 6-position is considered to decrease affinity by a factor of 3.5 and 2, respectively. The predicted influence of the 4- and 6-OH group in binding to DC-SIGN correlates with crystallographic data.

Table 1. 2.0 ns FEP simulation were performed to quantify the theoretical effect of deoxygenation, calculated $\Delta\Delta G$ values are presented.

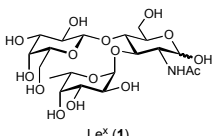
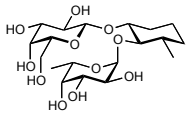
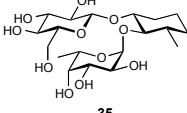
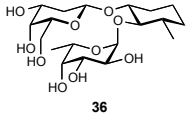
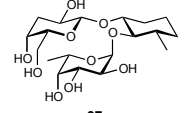
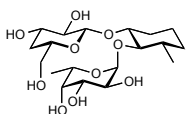
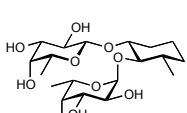
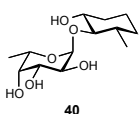
Compound	Estimated $\Delta\Delta G$ vs. mimic 29 [kcal/mol]
29 direct Lewis ^x mimic	—
32 3-deoxy	-0.13 ± 0.27 (<i><1.3x increase in affinity</i>)
33 4-deoxy	0.77 ± 0.22 (<i>~3.5x drop in affinity</i>)
34 6-deoxy	0.49 ± 0.26 (<i>~2.2x drop in affinity</i>)

Binding Affinity

Compounds **1**, **8** and **35-40** were tested in a static competitive polymer binding assay with biotinylated polyacrylamide glycopolymer (Gal β (1-3)[Fuc α (1-4)]GlcNAc β -polyacrylamide,

Le^a-PAA) as competitor for binding to DC-SIGN CRD-Fc. The affinities (IC₅₀) listed in Table 2 were measured three times as duplicates. To ensure comparability of the experiments, the reference compound L-Fuc was tested in parallel on each individual microtiter plate. Despite the rather high deviation, the relative values from one experiment to another were consistent (data not shown).

Table 2. IC₅₀ values for binding to DC-SIGN CRD-Fc were determined in a target-based polymer binding assay for Le^x (**1**) and the mimics **8** and **35-40** vs. biotinylated Le^a-polyacrylamide polymer (Le^a-PAA). ITC experiments were performed as single determination for **8**, **39**, **40** and duplicate for **1** indicating a good reproducibility of the calorimetric experiment (entry 1); “n.d.” = not determined.

Entry	Structure	IC ₅₀ [mM]	K _D [μM]	ΔG° [kJ/mol]	ΔH° [kJ/mol]	-TΔS° [kJ/mol]
1	 Le ^x (1)	3.8 (n=1)	1068 ± 13 (n=2)	-17.0 ± 0.0	-23.8 ± 0.3	+6.9 ± 0.3
2	 8	1.9 ± 0.4	645	-18.2 ± 0.5	-31.4	+13.2
3	 35	1.8 ± 0.5	n.d.	n.d.	n.d.	n.d.
4	 36	2.5 ± 0.3	n.d.	n.d.	n.d.	n.d.
5	 37	2.1 ± 0.5	n.d.	n.d.	n.d.	n.d.
6	 38	2.9 ± 0.7	n.d.	n.d.	n.d.	n.d.
7	 39	4.7 ± 0.9	1277	-16.5	-29.7	+13.2
8	 40	3.2 ± 0.8	1073	-16.9	-34.4	+17.5

All compounds bind in the low millimolar range with the highest affinities in this series for **8** and **35** (Table 2, entry 2 and 3) and the lowest for **39** (Table 2, entry 7). Compared to Le^x (**1**), the substitution of D-GlcNAc for a cyclohexanediol moiety (**1**→**8**) results in an affinity improvement by a factor of 2. Moreover, our data indicate that deoxygenation in 2- or 3-position of D-Gal (→**36**, →**37**) does not affect binding affinity significantly. Also changing D-Gal to D-Glc (→**35**) does not impair binding affinity. A slight drop in affinity is observed for the 4-deoxygenated compound (→**38**), and a more apparent drop when deoxygenated in the 6-position (→**39**). These results are in accordance with crystallographic data that imply these two hydroxyl groups being involved in a hydrogen bond network.²⁹ Our FEP calculations agree with these results within experimental accuracy. Hence, this provides further evidence that this group of deoxy Le^x mimics binds DC-SIGN in the same orientation as observed in the LNFP III complex (1SL5). Nevertheless, the interaction of 4- and 6-OH of D-Gal with the protein is presumably rather weak, since a drop by a factor of only 2.5 is observed. To confirm this hypothesis we tested as well the disaccharide mimic **40** lacking the D-Gal moiety. In fact, binding is not abolished but comparable to Le^x (**1**). A comparison with the 6-deoxy compound shows that affinity is regained. Bernardi *et al.* arrived at a similar conclusion with a series of α -fucosylamides. The compounds lacking a D-Gal-like residue but still containing the L-Fuc moiety still show selective inhibition of DC-SIGN.^{45,46}

To get a deeper insight into the binding thermodynamics of Le^x (**1**), **8**, **39**, and **40** to DC-SIGN, ITC experiments were performed. In Table 2, K_D values and the thermodynamic fingerprints are summarized (entry 1, 2, 7, and 8). Overall, the above discussed trend in affinity is supported by the K_D values. Le^x (**1**) showed binding affinity around 3.8 mM in our polymer binding assay and a K_D of 1.1 mM in the ITC experiment. In both assay formats a gain in affinity by a factor of 2 was observed when the D-GlcNAc moiety is mimicked by (1*R*,2*R*,3*S*)-3-methyl-cyclohexane-1,2-diol (→**8**, K_D =0.6 mM). This gain in affinity is lost again when the 6-position is deoxygenated (→**39**, K_D =1.3 mM). Finally, the pseudo-disaccharide **40** binds with near identical affinity as Le^x (**1**) to DC-SIGN (K_D =1.1 mM).

All compounds reveal an enthalpy-driven binding, which is typical for carbohydrate–lectin interactions.⁴⁷⁻⁴⁹ The range of deviation concerning enthalpy and entropy contributions throughout the mimic series (**8**, **39**, **40**) is close to experimental precision limit. The 6-deoxy derivative **39** shows a smaller enthalpic contribution to binding than **8** (-29.7 vs. -31.4 kJ/mol). Even though the results have to be regarded with caution, the observed trend in enthalpy is in accordance with the assumption that the 6-OH group of D-Gal is involved in

binding. However, when losing a substantial H-bond a drop in affinity in the range of one order of magnitude would be expected.⁵⁰ Although, the desolvation of the deoxygenated compound is favorable in terms of enthalpy, which can partly compensate the lost interaction with the protein.

The pseudo-disaccharide **40** (entry 8) shows an improved enthalpy term compared to **8** (entry 2). We reason that the absence of the entire D-Gal moiety results in a smaller polar surface area and therefore in a reduced desolvation penalty. This entails, despite the fact that no interaction with the protein can be established, a more favorable enthalpy term. The gain in enthalpy is accompanied and nearly compensated by unfavorable entropy. However, this is no classical enthalpy-entropy compensation. The unfavorable entropy term can rather be explained by different sizes of the binding interface (comparing **40** with **8**) resulting in the release of fewer water molecules to bulk.

Significant differences in the thermodynamic profile resulted for the modification of D-GlcNAc to methylcyclohexanediol (**1**→**8**). **8** revealed an improved enthalpy term, partly outweighed by an unfavorable entropic contribution. Basically, the exchange of D-GlcNAc is associated with two effects: 1) preorganization which should minimize entropic costs upon binding and 2) reduction of desolvation costs which is supposed to improve the enthalpy term. Interestingly, the ITC experiments revealed an ambiguous effect. Regarding the observed favorable enthalpic term, this is in accordance with a reduced desolvation energy that has to be paid upon introduction of a lipophilic moiety. Desolvation of polar surfaces is energetically more cost intensive than desolvation of lipophilic surfaces.⁵¹ The more unfavorable entropy term for **8** compared to **1** indicates that the effect of preorganization is not efficient in the present case. We are convinced that **1** and **8** bind in the same orientation to DC-SIGN, hence, the significant entropic costs can not result from different binding modes nor from conformational changes of the protein. Differences of the ligands polar and non-polar surface areas affecting solvation and desolvation properties can more likely explain the different entropy terms.

To the best of our knowledge, the only ITC data available on DC-SIGN up to now, have been reported by Holla and Skerra. They present K_D values for mannose and a dimannoside with K_D of 3.5 and 0.9 mM, respectively. The thermodynamic profile of these compounds is in accordance with our findings of an enthalpy-driven binding with an unfavourable entropy term.⁵²

Molecular Dynamics Simulations

The exchange of D-GlcNAc in Le^x (**1**) by a methylcyclohexanediol moiety (\rightarrow **8**) was expected to have an advantageous effect on affinity due to reduced desolvation costs and better preorganization.^{33,37,53} Although, an overall improved affinity was achieved, the entropic disadvantage of the mimic (throughout the series) compared to Le^x (**1**) was unexpected. To prove our assumptions of preorganization, an exhaustive conformational search was done for both Le^x (**1**) and **8**. Comparing the energy of the global minimum with the energy of its bound conformation reflects the internal strain penalty paid by each ligand to reach its bound conformation. The results support our assumption of a pre-organized conformation of mimic **8** (reflected by the number of conformations obtained for both) leading to reduction of the strain penalty by 3.3 kcal/mol compared to Le^x (**1**). Thus, binding of **8** to DC-SIGN would incur a lower enthalpic and entropic penalty compared to Le^x (**1**).

Concerning desolvation costs, less energy has to be paid to break the H-bond network of water molecules on non-polar surfaces, i.e. replacement of polar groups by lipophilic groups entails a favorable enthalpic contribution. Despite the fact, that a dominant part of the D-GlcNAc portion is solvent-exposed, the enthalpic gain in case of **8** can be explained by a partial desolvation of the cyclohexyl moiety as well as a reduced internal strain penalty.

The higher entropic cost ($-T\Delta\Delta S > 6$ kJ/mol) for **8** binding to DC-SIGN compared to **1** is controversial. The conformational search indicates that mimic **8** is more rigid than **1**, which would result in less entropic costs upon binding.

To investigate whether differences in solvation can account for the significant entropic costs the solvent-accessible surface area (SASA) was calculated and 10 ns molecular dynamics (MD) simulations were initiated. These data indicate a significant difference in the average solvent-exposed surface areas in the free state. **1** shows a larger SASA ($675 \pm 9 \text{ \AA}^2$) than **8** ($620 \pm 8 \text{ \AA}^2$) resulting in the assembly of more water molecules on the surface of **1**. In this respect, even only a partial desolvation of the D-GlcNAc moiety is assumed to result in the release of more water molecules with respect to **8** and can rationalize the differences in the entropy term (Figure 4).

In case of Le^x the preorganization of the core structure, which was substantial for high-affinity ligands in case of the selectins³⁷, is therewith not as critical for binding as previously assumed. The impact of desolvation effects accompanying the solvent-exposed binding site in DC-SIGN predominates.

CONCLUSION

We synthesized and evaluated a series of Le^x mimics for their binding affinity to DC-SIGN and therewith their potential as DC-SIGN ligands. An exchange of the central D-GlcNAc moiety in Le^x is associated with a gain in affinity. The contribution of D-Gal was investigated by a series of deoxy Le^x derivatives. Mono-deoxygenation of D-Gal in positions 2, 3, 4, and 6 proved that mainly the 4- and 6-OH contribute to binding. However, our results indicate that this interaction with the protein is not critical for binding. A mimic lacking the entire D-Gal moiety still showed affinity comparable to that of Le^x.

It is still a challenging task to design glycomimetic compounds with an improved interaction profile for this solvent-exposed binding site. Our study gives an insight into the thermodynamic properties of Le^x and mimics thereof binding to DC-SIGN. It also shows that small changes in affinity can result from significant changes in the thermodynamic profile. Solvation effects have a remarkable impact on this binding interaction. Ultimately, we provided evidence that ligands with a reduced and more drug-like structure bind to DC-SIGN. This is valuable information for the design of more potent, structurally simplified glycomimetic DC-SIGN ligands.

EXPERIMENTAL SECTION

Synthesis

General Methods. NMR spectra were recorded on a Bruker Avance DMX-500 (500 MHz) spectrometer. Assignment of ¹H and ¹³C NMR spectra was achieved using 2D methods (COSY, HSQC, HMBC, TOCSY). Chemical shifts are expressed in ppm in relation to the residual solvent signals (CHCl₃, CHD₂OD, and HDO) on the δ-scale. Coupling constants *J* are given in Hertz (Hz). Multiplicities were specified as follows: s (singlet), d (doublet), dd (doublet of a doublet), t (triplet), q (quartet), m (multiplet). For assignment of resonance signals to the appropriate nuclei the following abbreviations were used: Fuc (fucose), Gal (galactose), MeCy (3-methylcyclohexane-1,2-diol), Imi (imidazole). Commercially available reagents were purchased from Fluka, Aldrich, Merck, and Abcr. Solvents were dried prior to use as indicated. Dichloromethane (CH₂Cl₂), 1,2-dichloroethane (DCE), and acetonitrile (CH₃CN) were dried by filtration over Al₂O₃ (Fluka, type 5016 A basic). Dimethylformamide (DMF), pyridine, and toluene were dried by distillation from calcium hydride. Tetrahydrofuran (THF) was dried by distillation from sodium/benzophenone. Methanol

(MeOH) was dried by refluxing with sodium methoxide and distilled immediately before use. Molecular sieves (3Å, 4Å) were activated under vacuum at 500°C for 1 h immediately before use. Reactions were monitored by TLC using glass plates coated with silica gel 60 F₂₅₄ (Merck) and visualized by using UV light and/or by charring with a molybdate solution (a 0.02 M solution of ammonium cerium sulfate dihydrate and ammonium molybdate tetrahydrate in aqueous 10% H₂SO₄). Column chromatography was performed on a CombiFlash Companion (Teledyne-ISCO, Inc.) using RediSep normal phase disposable flash columns (silica gel, 40-63 μm). Reversed phase chromatography was performed on LiChroprepRP-18 (Merck, 40-63 μm). LC-MS separations were carried out using Sunfire C₁₈ columns (19 x 150 mm, 5.0 μm) on a Waters 2525 LC, equipped with Waters 2996 photodiode array and Waters micromass ZQ MS for detection. Electron spray ionization mass spectra (ESI-MS) were obtained on a Waters micromass ZQ. HR-MS analysis were carried out using a Agilent 1100 LC equipped with a photodiode array detector and a Micromass QTOF I equipped with a 4 GHz digital-time converter. Optical rotations were measured using Perkin-Elmer polarimeter 341. Microanalysis was performed at the Institute of Organic Chemistry at the University of Basel, Switzerland. Compound purity was determined on an Agilent 1200 HPLC; ELS detector, Waters 2420; column: Waters Atlantis dC18, 3 μm, 4.6 x 75 mm; eluents: A: water + 0.1% TFA; B: 90% acetonitrile + 10% water + 0.1% TFA. Linear gradient was applied: 0 - 1 min 5% B; 1 - 15 min 5 to 70% B; 16 - 20 min 70 to 5% B flow: 0.5 mL/min.

Ethyl 3,4,6-tri-*O*-acetyl-2-deoxy-1-thio- α -D-xylo-galactopyranoside (10)

3,4,6-Tri-*O*-acetyl-1,5-anhydro-2-deoxy-D-*lyxo*-hex-1-enitol (300 mg, 1.1 mmol) and ceric ammonium nitrate (60 mg, 0.11 mmol, 0.1 eq) were stirred in dry CH₃CN (2 ml) at 0°C under argon atmosphere. EtSH (0.41 ml, 5 eq, 5.5 mmol) in dry CH₃CN (1 ml) was added dropwise and the reaction mixture was stirred for 2 d. The mixture was concentrated and purified by flash column chromatography (PE/EtOAc, 1:0→7:3). The product was obtained as α/β mixture in 66 % yield ($\alpha:\beta \approx 7:1$).

NMR data of the α -anomer are in accordance with literature data.³⁹

¹H NMR (500 MHz, CDCl₃): δ 5.53 (d, $J = 5.6$ Hz, 1H, H-1), 5.33 (s, 1H, H-4), 5.21 (d, $J = 12.0$ Hz, 1H, H-3), 4.54 (t, $J = 6.2$ Hz, 1H, H-5), 4.11 (d, $J = 6.2$ Hz, 2H, H-6_{a/b}), 2.64 (dq, $J = 14.4, 7.3$ Hz, 1H, CH_{2a}), 2.54 (dq, $J = 14.2, 7.3$ Hz, 1H, CH_{2b}), 2.42 (td, $J = 12.8, 5.8$ Hz, 1H, H-2_b), 2.19 – 1.95 (m, 9H, CH₃), 1.87 (d, $J = 9.2$, 1H, H-2_a), 1.28 (t, $J = 7.4$ Hz, 3H,

CH₂-CH₃); ¹³C NMR (125 MHz, CDCl₃): δ 170.64, 170.41, 170.06 (3C, CO) 80.12 (C-1), 66.98, 66.90 (3C, C-3, C-4, C-5), 62.56 (C-6), 30.46 (C-2), 24.96 (S-CH₂), 20.98, 20.86 (3C, CH₃), 14.90 (CH₂-CH₃); ESI-MS: *m/z* calcd for C₁₄H₂₂O₇S [M+Na]⁺: 357.10, found: 357.03.

Ethyl 3,4,6-tri-*O*-benzyl-2-deoxy-1-thio- α -D-xylo-galactopyranoside (11**)³⁹**

Compound **10** (200 mg, 0.6 mmol) was dissolved in dry MeOH (2 ml) under argon atmosphere. A catalytic amount of freshly prepared methanolic NaOMe solution (1 M) was added. After completion of the reaction (TLC and ESI-MS control), AcOH was added to neutralize the mixture. After removal of the solvent under reduced pressure, the crude product was purified by flash column chromatography on silica gel (CH₂Cl₂/MeOH, 1:0→10:4) and yield ethyl 2-deoxy-1-thio- α -D-xylo-galactopyranoside^{39,54,55} (122 mg, 98%).

The product was used for the next step without further characterization.

Sodium hydride (53 mg, 4 eq, 1.32 mmol, 60 % suspension in oil) was suspended in dry DMF (0.8 ml) under argon atmosphere. The stirred suspension was cooled to 0 °C and a solution of ethyl 2-deoxy-1-thio- α -D-xylo-galactopyranoside (68 mg, 0.33 mmol) in dry DMF (1.2 ml) was added followed by addition of BnBr (157 μ l, 4 eq, 1.32 mmol). The mixture was stirred at room temperature for 1 h. After cooling to 0 °C, the reaction was quenched by slow addition of MeOH and stirred for 20 min. The solvent was removed under reduced pressure and the crude product purified by flash column chromatography on silica gel (PE/EtOAc, 1:0→1:1) to give **11** (113 mg, 72%).

Spectroscopic data were in accordance with literature.³⁹

$[\alpha]_D^{20} = +174$ (*c* = 0.102, CHCl₃); ¹H NMR (500 MHz, CD₃OD): δ 7.40 – 7.21 (m, 15H, Ar-H), 5.47 (d, *J* = 5.7 Hz, 1H, H-1), 4.84 (m, 1H, CH₂), 4.63 – 4.41 (m, 5H, CH₂), 4.26 (t, *J* = 6.3 Hz, 1H, H-5), 3.91 (s, 1H, H-4), 3.85 (m, 1H, H-3), 3.63 – 3.51 (m, 2H, H-6), 2.62 (m, 1H, S-CH_{2a}), 2.55 – 2.38 (m, 2H, S-CH_{2b}, H-2a), 1.92 (dd, *J* = 13.0, 4.5 Hz, 1H, H-2b), 1.23 (t, *J* = 7.4 Hz, 3H, CH₃); ¹³C NMR (126 MHz, CD₃OD): δ 140.15, 139.83, 139.57 (3 quart. Ar-C), 129.43, 129.40, 129.30, 129.26, 128.93, 128.78, 128.74, 128.70, 128.65 (15C, 15 Ar-C), 81.55 (C-1), 76.41 (C-3), 75.62 (CH₂), 75.10 (C-4), 74.35 (CH₂), 71.47 (CH₂), 71.24 (C-5), 70.73 (C-6), 32.56 (S-CH₂), 25.58 (C-2), 15.24 (CH₃); ESI-MS: *m/z* calcd for C₂₉H₃₄O₄S [M+Na]⁺: 501.21, found: 501.23.

Ethyl 2,3,6-tri-*O*-benzoyl-1-thio- β -D-galactopyranoside (15)

Compound **15** was synthesized in three steps from ethyl 1-thio- β -D-galactopyranoside **12** following a published procedure.⁴⁰

Ethyl 2,3,6-tri-*O*-benzoyl-4-*O*-(imidazol-1-ylthiocarbonyl)-1-thio- β -D-galacto-pyranoside (16)

Compound **15** (161 mg, 0.3 mmol) was dissolved in dry DCE (1.5 ml) in a dry, argon-flushed flask. 1,1'-Thiocarbonyldiimidazole (96 mg, 1.5 eq, 0.5 mmol) was added and the sealed flask was refluxed until TLC showed complete consumption of starting material (approx. 5 h). The solvent was evaporated and the crude product purified by flash column chromatography (PE/EtOAc, 1:0→2:1). Compound **16** was obtained as colorless foam (176 mg, 90%).

¹H NMR (500 MHz, CDCl₃): δ 8.40 (s, 1H, Imi-H), 7.98 (dd, J = 24.6, 7.4 Hz, 4H, Ar-H), 7.77 (d, J = 7.5, 2H, Ar-H), 7.68 (s, 1H, Imi-H), 7.62 – 7.22 (m, 11H, Ar-H), 7.14 (s, 1H, Imi-H), 6.62 (s, 1H, H-3), 5.80 – 5.64 (m, 2H, H-2, H-3), 4.90 (d, J = 9.4 Hz, 1H, H-1), 4.64 (d, J = 6.2 Hz, 1H, H-6b), 4.37 (m, 2H, H-4, H-6a), 2.83 (dd, J = 13.0, 6.6 Hz, 2H, SCH₂), 1.31 (t, J = 7.3 Hz, 3H, CH₃); ¹³C NMR (126 MHz, CDCl₃): δ 183.78 (C=S), 166.30, 165.95, 165.58 (4C, 4CO), 139.16, 137.86, 134.10, 133.91, 131.92, 130.24, 130.13, 128.86, 118.12 (18C, 3Imi-C, 15Ar-C), 84.73 (C-1), 76.81 (C-3), 75.14 (C-2), 72.75 (C-4), 68.32 (C-2); 61.95 (C-5), 24.74 (CH₂), 15.28 (CH₃).

Ethyl 2,3,6-tri-*O*-benzoyl-4-deoxy-1-thio- β -D-xylo-hexopyranose (17)⁵⁶

A solution of the imidazolylthiocarbonyl derivative (160 mg, 0.25 mmol) in dry toluene (2 ml) and added dropwise to a refluxing solution of Bu₃SnH (100 μ l, 1.5 eq, 0.4 mmol) and a catalytic amount of AIBN in dry toluene (5 ml). After 5h, supplemental Bu₃SnH (66 μ l, 1 eq, 0.25 mmol) was added to complete the conversion of the starting material. The reaction mixture was cooled to r.t. and the solvent was evaporated under reduced pressure. Purification by flash column chromatography (PE/EtOAc) afforded **17** (120 mg, 93%).

Spectroscopic data were in accordance with literature data⁵⁶

¹H NMR (500 MHz, CDCl₃): δ 8.07 (dd, J = 8.3, 1.2 Hz, 2H, Ar-H), 8.01 – 7.97 (m, 2H, Ar-H), 7.95 (dd, J = 8.3, 1.2 Hz, 2H, Ar-H), 7.58 (m, 1H, Ar-H), 7.53 – 7.41 (m, 4H, Ar-H), 7.37 (dd, J = 15.9, 8.1 Hz, 4H, Ar-H), 5.51 – 5.42 (m, 2H, H-2, H-3), 4.74 (m, 1H, H-1), 4.47 (qd, J = 11.7, 5.1 Hz, 2H, H-6), 4.10 (m, 1H, H-5), 2.89 – 2.68 (m, 2H, SCH₂), 2.51 (m, 1H, H-

4a), 1.92 (m, 1H, H-4b), 1.35 – 1.18 (m, 3H, CH₃); ¹³C NMR (125 MHz, CDCl₃): δ 166.28, 165.92, 165.62 (3CO), 133.38, 133.34, 133.31, 129.89, 129.80, 129.74, 129.50, 129.38, 128.53, 128.50, 128.45 (18C, 18Ar-C), 83.92 (C-1), 73.73 (C-5), 72.66, 71.16 (C-2, C-3), 66.03 (C-6), 33.27 (C-4), 24.41 (SCH₂), 15.09 (CH₃); ESI-MS: *m/z* calcd for C₂₉H₂₈O₇S [M+Na]⁺: 543.14, found: 543.16.

2-(Trimethylsilyl)ethyl 3-*O*-benzyl-β-D-galactopyranoside (19)

A mixture of 2-(trimethylsilyl)ethyl β-D-galactopyranoside **18**⁴¹ (202 mg, 0.72 mmol) and Bu₂SnO (179 mg, 1 eq, 0.72 mmol) was suspended in dry toluene (15 ml) under argon and refluxed for 16 h. Bu₄Ni (266 mg, 1 eq, 0.72 mmol) and benzyl bromide (0.18 ml, 2.1 eq, 1.51 mmol) were added and the mixture was refluxed for 6 h. Evaporation to dryness gave a residue which was purified by column chromatography on silica gel (EtOAc/MeOH, 1:0→10:1) to give 2-(trimethylsilyl)ethyl 3-*O*-benzyl-β-D-galactopyranoside **19** (166 mg, 62%).

Spectroscopic data were in accordance with literature values.⁵⁷

¹H NMR (500 MHz, CD₃OD): δ 7.53 – 7.17 (m, 5H, Ar-H), 4.81 – 4.60 (m, 2H, CH₂), 4.24 (d, *J* = 7.8 Hz, 1H, H-1), 4.09 – 3.95 (m, 2H, OCH_{2a}, H-4), 3.80 – 3.70 (m, 2H, H-6), 3.69 – 3.57 (m, 2H, OCH_{2b}, H-2), 3.44 (t, *J* = 6.1 Hz, 1H, H-5), 3.36 (dd, *J* = 9.6, 3.3 Hz, 1H, H-3), 1.09 – 0.89 (m, 2H, CH₂Si), 0.03 (s, 9H, Si(CH₃)₃); ¹³C NMR (126 MHz, CD₃OD): δ 139.87, 129.28, 129.08, 128.62 (Ar-C), 104.42 (C-1), 82.53 (C-3), 76.47 (C-5), 72.52 (PhCH₂), 71.80 (C-2), 68.03 (OCH₂), 67.10 (C-4), 62.48 (C-6), 19.13 (CH₂Si), -1.41 (Si(CH₃)₃); ESI-MS: *m/z* calcd for C₁₈H₃₀O₆S [M+Na]⁺: 393.17, found: 392.96.

2-(Trimethylsilyl)ethyl 2,4,6-tri-*O*-benzoyl-3-*O*-benzyl-β-D-galactopyranoside (20)^{58,59}

Compound **19** (500 mg, 1.35 mmol) was dissolved in anhydrous pyridine (5 ml) and cooled to 0°C under argon. BzCl (4.7 mmol, 3.5 eq, 0.54 ml) was added and the mixture was stirred and allowed to reach r.t. until TLC showed complete conversion of the starting material. Pyridine was removed by co-evaporation with toluene. The resulting residue was dissolved in CH₂Cl₂ (100 ml) and washed with satd. aq. NaHCO₃ solution (100 ml) and brine (50 ml). The aq. phase was extracted with CH₂Cl₂ (2x 100 ml). The organic phase was dried over Na₂SO₄, filtered and concentrated under reduced pressure. The crude product was purified by flash column chromatography on silica gel (PE/EtOAc, 1:0→1:1) to yield **20** as resin in (850 mg, 92%).

Spectroscopic data were in accordance with literature values.^{58,59}

¹H NMR (500 MHz, CDCl₃): δ 8.22 – 8.15 (m, 2H, Ar-H), 8.08 – 8.03 (m, 2H, Ar-H), 8.01 – 7.96 (m, 2H, Ar-H), 7.59 (dt, *J* = 9.9, 7.4 Hz, 3H, Ar-H), 7.54 – 7.40 (m, 6H, Ar-H), 7.19 – 7.03 (m, 5H, Ar-H), 5.91 (d, *J* = 2.7 Hz, 1H, H-4), 5.53 (dd, *J* = 9.9, 8.1 Hz, 1H, H-2), 4.70 (d, *J* = 12.9 Hz, 1H, PhCH_{2a}), 4.65 – 4.58 (m, 2H, H-1, H-6a), 4.50 (d, *J* = 12.8 Hz, 1H, PhCH_{2b}), 4.44 (dd, *J* = 11.4, 6.1 Hz, 1H, H-6b), 4.08 (t, *J* = 6.9 Hz, 1H, H-5), 4.00 (m, 1H, O-CH_{2a}), 3.79 (dd, *J* = 10.0, 3.4 Hz, 1H, H-3), 3.56 (td, *J* = 10.4, 6.5 Hz, 1H, O-CH_{2b}), -0.09 (s, 9H, Si(CH₃)₃); ¹³C NMR (126 MHz, CDCl₃): δ 166.33, 166.07, 165.29 (3CO), 137.39, 133.55, 133.40, 133.12, 130.31, 130.21, 130.03, 129.89, 129.77, 129.51, 128.65, 128.62, 128.38, 128.08, 127.79 (Ar-C), 101.09 (C-1), 76.46 (C-3), 71.44, 71.41, 71.03 (C-2, C-5, PhCH₂) 67.57 (OCH₂), 66.79 (C-4), 62.79 (C-6), 18.07 (CH₂Si), -1.40 (Si(CH₃)₃).

2-(Trimethylsilyl)ethyl 2,4,6-tri-*O*-benzoyl-β-D-galactopyranoside (**21**)

a) Compound **20** (205 mg, 0.30 mmol) was dissolved in dioxane/water (4:1, v/v, 4 ml) and Pd(OH)₂/C (10%) was added under argon atmosphere. The resulting suspension was hydrogenated on a Parr shaker (5 bar) for 20 h, the catalyst was filtered off and fresh Pd(OH)₂/C was added the hydrogenation procedure repeated for 10 h. After complete transformation of the starting material, the catalyst was filtered off and the crude product was purified on silica gel (PE/EtOAc) to give **21** (170 mg, 95%).

b) Compound **20** (204 mg, 0.30 mmol) was dissolved in EtOAc (4 ml) and then a solution of NaBrO₃ (3 eq, 0.9 mmol, 136 mg) in water (3 ml) was added to the well stirred two-phase system. An aq. solution of Na₂S₂O₄ (157 mg, 3 eq, 85% pure in 6 ml H₂O) was added dropwise over 10 min at r.t. The reaction progress was controlled by TLC. After complete conversion of the starting material, the mixture was diluted with EtOAc (25 ml) and washed with an aq. solution of Na₂S₂O₃ (2x 25 ml). The aq. phase was extracted with EtOAc (3x 50ml), the combined organic phases were dried over Na₂SO₄, filtered, and concentrated. Flash column chromatography on silica gel (PE/EtOAc) gave **21** (171 mg, 87%) as a resin.

[α]_D²⁰ -5.6 (*c* 0.33, CHCl₃); ¹H NMR (500 MHz, CD₃OD): δ 8.19 – 7.97 (m, 6H, Ar-H), 7.70 – 7.37 (m, 9H, Ar-H), 5.74 (d, *J* = 3.2 Hz, 1H, H-4), 5.43 (dd, *J* = 10.0, 8.0 Hz, 1H, H-2), 4.82 (d, *J* = 8.0 Hz, 1H, H-1), 4.49 (dd, *J* = 11.3, 7.1 Hz, 1H, H-6a), 4.41 (dd, *J* = 11.3, 5.4 Hz, 1H, H-6b), 4.32 (t, *J* = 6.3 Hz, 1H, H-5), 4.24 (dd, *J* = 10.1, 3.5 Hz, 1H, H-3), 4.01 (td, *J* = 9.9, 5.6 Hz, 1H, CH_{2a}), 3.65 (td, *J* = 9.7, 6.7 Hz, 1H, CH_{2b}), 0.98 – 0.75 (m, 2H, CH₂), 0.13 (s, 9H, (CH₃)₃); ¹³C NMR (126 MHz, CD₃OD): δ 167.61, 167.51, 167.35 (3CO), 134.50,

134.39, 134.31, 131.53, 131.10, 131.02, 131.00, 130.76, 130.66, 129.63, 129.55, 129.49 (15C, Ar-C), 102.26 (C-1), 74.34 (C-2), 72.76, 72.74 (C-4, C-5), 71.58 (C-3), 68.29 (CH₂), 63.99 (C-6), 18.89 (CH₂), -1.40 ((CH₃)₃); HR-MS *m/z* calcd for C₃₂H₃₆O₉Si [M+Na]⁺: 615.2026, found: 615.2029.

2-(Trimethylsilyl)ethyl 2,4,6-tri-*O*-benzoyl-3-*O*-(imidazol-1-ylthiocarbonyl)-β-D-galactopyranoside (22)

Compound **21** (113 mg, 0.19 mmol) was dissolved in dry DCE (1.5 ml) in an dry argon-flushed flask. 1,1'-Thiocarbonyldiimidazole (61 mg, 0.342 mmol, 1.5 eq) was added and the sealed flask was refluxed until TLC control showed complete conversion (5 h). The solvent was evaporated and the crude product was purified by flash column chromatography (PE/EtOAc, 1:0 → 2:1). Compound **22** was obtained as colorless foam (120 mg, 92%).

¹H NMR (500 MHz, CDCl₃): δ 8.11 – 8.08 (m, 2H, Ar-H), 8.02 (dd, *J* = 8.3, 1.2 Hz, 2H, Ar-H), 7.97 (dd, *J* = 8.3, 1.2 Hz, 2H, Ar-H), 7.66- 7.38 (m, 10H, Ar-H, Imi-H), 7.34 (dd, *J* = 4.8, 3.4 Hz, 1H, Imi-H), 6.84 (dd, *J* = 1.6, 0.7 Hz, 1H, Imi-H), 6.10 (d, *J* = 2.6 Hz, 1H, H-4), 6.05 (dd, *J* = 10.3, 3.4 Hz, 1H, H-3), 5.84 (dd, *J* = 10.3, 7.9 Hz, 1H, H-2), 4.88 (t, *J* = 8.9 Hz, 1H, H-1), 4.69 (dd, *J* = 11.4, 6.9 Hz, 1H, H-6_b), 4.45 (dd, *J* = 11.4, 6.4 Hz, 1H, H-6_a), 4.33 (t, *J* = 6.6 Hz, 1H, H-5), 4.15 – 4.02 (m, 1H, CH_{2b}), 3.74 – 3.62 (m, 1H, CH_{2a}), 1.04 – 0.77 (m, 2H, CH₂(CH₃)₃), -0.01 – -0.11 (m, 9H, (CH₃)₃); ESI-MS: *m/z* calcd for C₃₆H₃₈N₂O₉SSi [M+H]⁺: 703.21, found:703.22.

2-(Trimethylsilyl)ethyl 2,4,6-tri-*O*-benzoyl-3-deoxy-β-D-xylo-hexopyranoside (23)

Bu₃SnH (61 μl, 1.5 eq, 0.225 mmol) and a catalytic amount of azobisisobutyronitrile (AIBN) were refluxed in anhydrous toluene (2.5 ml) under argon. The 3-*O*-imidazolylthiocarbonyl derivative **22** (105 mg, 0.15 mmol) was dissolved in anhydrous toluene (1 ml) and added dropwise through a septum to the Bu₃SnH solution. The resulting mixture was refluxed for further 6 h. The solvent was removed under reduced pressure and the crude product was purified by column chromatography on silica gel (PE/EtOAc) to yield **23** (75 mg, 86%) as a foam.

[α]_D²⁰ -23.0 (*c* 0.17, CHCl₃); ¹H NMR (500 MHz, CD₃OD): δ 8.15 – 8.09 (m, 2H, Ar-H), 8.03 – 7.96 (m, 4H, Ar-H), 7.67 – 7.55 (m, 3H, Ar-H), 7.54 – 7.39 (m, 6H, Ar-H), 5.50 (d, *J* = 0.9 Hz, 1H, H-4), 5.24 (ddd, *J* = 11.7, 7.8, 5.2 Hz, 1H, H-2), 4.89 (d, *J* = 7.9 Hz, 1H, H-1), 4.55 (dd, *J* = 11.3, 7.3 Hz, 1H, H-6_a), 4.45 (dd, *J* = 11.3, 5.3 Hz, 1H, H-6_b), 4.40 – 4.34

(m, 1H, H-5), 4.06 (td, $J = 9.9, 5.5$ Hz, 1H, OCH_{2a}), 3.69 (td, $J = 9.6, 6.8$ Hz, 1H, OCH_{2b}), 2.57 (ddd, $J = 14.1, 5.1, 3.4$ Hz, 1H, H-3a), 2.17 (ddd, $J = 14.4, 11.6, 3.1$ Hz, 1H, H-3b), 1.01 – 0.81 (m, 2H, CH₂), -0.07 (s, 9H, Si(CH₃)₃); ¹³C NMR (125 MHz, CD₃OD): δ 167.52, 167.07, 166.97 (3CO), 134.64, 134.46, 134.39, 131.22, 131.05, 131.01, 130.78, 130.66, 130.61, 129.75, 129.58, 129.56 (Ar-C), 103.08 (C-1), 75.48 (C-5), 69.91 (2C, C-2, C-4), 67.93 (CH₂), 64.31 (C-6), 33.77 (C-3), 18.88 (CH₂Si), -1.34 (Si(CH₃)₃); HR-MS: m/z calcd for C₃₂H₃₆O₈Si [M+Na]⁺: 599.2077, found: 599.2078.

Phenyl 2,4,6-tri-*O*-benzoyl-3-deoxy-1-thio- β -*D*-xylo-hexopyranoside (24)

A solution of 2-(trimethylsilyl)ethyl glycoside **23** (115 mg, 0.2 mmol) in dry toluene (1 ml) was treated with acetic acid anhydride (283 μ l, 15 eq, 2 mmol) and BF₃·Et₂O (23 μ l, 0.9 eq, 0.18 mmol) and stirred at r.t. The reaction was monitored by TLC and diluted with dichloromethane (30 ml) after completion (8 h). The mixture was washed with NaHCO₃ solution (30 ml) and water (30 ml). The aq. phase was extracted with CH₂Cl₂ (3x 50 ml). The combined organic phases were dried over Na₂SO₄, filtered and concentrated under reduced pressure. The residue was purified on silica gel to give acetyl 2,4,6-tri-*O*-benzoyl- 3-deoxy- β -*D*-xylo-hexopyranoside (46 mg, 80%, α : β \approx 4:3).

¹H NMR (500 MHz, CDCl₃): δ 8.17 – 8.08 (m, 3H), 8.05 – 7.90 (m, 7H), 7.66 – 7.37 (m, 16H) (15 Ar-H of α and β , ratio 4:3), 6.57 (d, $J = 3.2$ Hz, 1H, H-1 α), 6.05 (d, $J = 8.1$ Hz, 1H, H-1 β), 5.64 (s, 1H, H-4 α), 5.57 (m, 2H, H-2 α , H-4 β), 5.42 (ddd, $J = 11.3, 8.0, 5.1$ Hz, 1H, H-2 β), 4.63 – 4.35 (m, 6H, H-5 α , H-6 α , H- β 5, H-6 β), 2.84 – 2.73 (m, 1H, H-3a β), 2.55 – 2.35 (m, 2H, H-3 α), 2.18 (s, 3H, CH₃ α), 2.14 – 2.04 (m, 4H, H-3b β , CH₃ β). ESI-MS: m/z calcd for C₂₉H₂₆O₉ [M+Na]⁺: 541.15; found: 541.08; Combustion analysis: calcd: C 67.18, H 5.05, found: C 66.66, H 5.21.

The acetyl glycoside (31 mg, 0.06 mmol) was dissolved in dry CH₂Cl₂ (0.5 ml) and PhSH (9 μ l, 1.5 eq, 0.09 mmol) was added followed by BF₃·Et₂O (14 μ l, 1.6 eq, 0.1 mmol). The mixture was stirred overnight, diluted with CH₂Cl₂ (25ml), washed with satd. aq. NaHCO₃ solution (25 ml) and the aq. phase was extracted with CH₂Cl₂ (3x 25 ml). The combined organic phases were dried over Na₂SO₄, filtered, concentrated, and the crude product was purified by flash column chromatography to yield **24** (30 mg, 68%, α : β \approx 1:1).

NMR of β -product ¹H NMR (500 MHz, CDCl₃): δ 8.10 – 7.99 (m, 6H, Ar-H), 7.68 – 7.42 (m, 11H, Ar-H), 7.33 – 7.15 (m, 3H, Ar-H), 5.55 (s, 1H, H-4), 5.31 (m, 1H, H-2), 5.01 (d,

$J = 9.9$ Hz, 1H, H-1), 4.63 – 4.44 (m, 2H, H-6), 4.25 (d, $J = 6.0$ Hz, 1H, H-5), 2.75 (d, $J = 14.1$ Hz, 1H, H-3a), 2.06 (t, $J = 12.6$ Hz, 1H, H-3b); ^{13}C NMR (125 MHz, CDCl_3): δ 166.21, 165.54, 165.22 (3CO), 133.54, 133.36, 133.30, 132.94, 132.39, 129.98, 129.81, 129.80, 129.73, 129.61, 129.33, 128.84, 128.56, 128.51, 128.48, 127.96 (24C, Ar-C), 87.63 (C-1), 77.26 (C-5), 67.87 (C-4), 66.35 (C-2), 63.35 (C-6), 34.75 (C-3); HR-MS: m/z calcd for $\text{C}_{33}\text{H}_{28}\text{O}_7\text{S} [\text{M}+\text{Na}]^+$: 591.1448, found: 591.1448.

2-(Trimethylsilyl)ethyl 6-*O*-tosyl- β -D-galactopyranoside (**25**)⁶⁰

TMSE glycoside **18**⁴¹ (280 mg, 1 mmol) was dissolved in anhydrous pyridine (4 ml) and *p*-toluenesulfonyl chloride (230 mg, 1.2 eq, 1.2 mmol) was added at 0°C. The reaction mixture was stirred at 0°C and warmed to r.t. The reaction was monitored by TLC and was diluted by addition of EtOAc (100 ml) at completion (6 h), then washed with 1N HCl (100 ml), followed by satd. aq. NaHCO_3 solution (100 ml) and brine (100 ml). The aq. phase was extracted repeatedly with EtOAc (3x 100 ml) and the combined organic layers were dried over Na_2SO_4 , filtered, and concentrated under reduced pressure. Purification via flash column chromatography on silica gel ($\text{CH}_2\text{Cl}_2/\text{MeOH}$, 1:0→1:1) gave **25** (380 mg, 87%).

$[\alpha]_{\text{D}}^{20}$ -32.6 (c 0.51, CHCl_3); ^1H NMR (500 MHz, CDCl_3): δ 7.76 (d, $J = 8.2$ Hz, 2H, Ar-H), 7.29 (d, $J = 8.1$ Hz, 2H, Ar-H), 4.32 – 4.07 (m, 3H, H-6, H-3, H-1), 4.02 – 3.82 (m, 2H, H-4, $\text{CH}_{2\text{a}}$), 3.69 (t, $J = 6.1$ Hz, 1H, H-5), 3.64 – 3.48 (m, 2H, H-2, $\text{CH}_{2\text{b}}$), 2.40 (s, 3H, PhCH_3), 1.07 – 0.77 (m, 2H, CH_2), -0.01 (s, 9H, $\text{Si}(\text{CH}_3)_3$); ^{13}C NMR (126 MHz, CDCl_3): δ 145.46, 145.17, 144.88, 132.76, 130.04, 128.02 (Ar-C), 102.46 (C-1), 73.24, 72.29, 70.95 (C-3, C-4, C-5), 68.81 (CH_2), 68.48 (C-2), 67.74 (CH_2), 21.73 (PhCH_3), 18.32 (CH_2Si), -1.36 ($\text{Si}(\text{CH}_3)_3$); HR-MS m/z calcd for $\text{C}_{18}\text{H}_{30}\text{O}_8\text{SSi} [\text{M}+\text{Na}]^+$: 457.1323, found: 457.1320.

2-(Trimethylsilyl)ethyl 6-deoxy- β -D-galactopyranoside (**26**)⁶¹

Compound **25** (148 mg, 0.34 mmol) was dissolved in anhydrous THF (1.5 ml) and LiAlH_4 (26 mg, 2 eq, 0.68 mmol) was added. The mixture was refluxed for 1h. After cooling, EtOAc (50 ml) was added to quench the excess of reagent and subsequently water was added. The organic layer was washed with water (50 ml), the aqueous phase was extracted with EtOAc (3x 50ml). The organic phase was dried over Na_2SO_4 , filtered, and concentrated. Flash column chromatography on silica gel ($\text{CH}_2\text{Cl}_2/\text{MeOH}$, 1:0 → 7:3) of the residue gave **26** (65 mg, 72%) as an amorphous mass.

Spectroscopic data are in accordance with literature.⁶¹

^1H NMR (500 MHz, CDCl_3): δ 4.21 (d, $J = 7.3$ Hz, 1H, H-1), 3.99 (ddd, $J = 11.8, 9.6, 5.6$ Hz, 1H, CH_{2a}), 3.72 (s, 1H, OH), 3.68 – 3.52 (m, 5H, H-2, H-3, H-4, H-5, CH_{2b}), 3.34 (s, 1H, OH), 2.97 (s, 1H, OH), 1.33 (d, $J = 6.5$ Hz, 3H, H-6), 1.12 – 0.93 (m, 2H, CH_2), 0.07 (s, 9H, $\text{Si}(\text{CH}_3)_3$); ^{13}C NMR (126 MHz, CDCl_3): δ 102.68 (C-1), 74.07, 71.79, 71.74, 70.68 (C-2, C-3, C-4, C-5), 67.49 (CH_2), 18.41 (CH_2), 16.45 (C-6), -1.29 ($(\text{CH}_3)_3$); ESI-MS m/z calcd for $\text{C}_{11}\text{H}_{24}\text{O}_5\text{Si}$ $[\text{M}+\text{Na}]^+$: 287.13, found: 286.97.

2-(Trimethylsilyl)ethyl 2,3,4-tri-*O*-benzoyl-6-deoxy- β -D-galactopyranoside (27)

Compound **26** (74 mg, 0.28 mmol) was dissolved in dry pyridine (1.5 ml). BzCl (113 μl , 3.5 eq, 0.98 mmol) was added at 0°C and the resulting mixture was stirred at r.t. until TLC showed complete conversion of the starting material (8 h). The solvent was removed by co-evaporation with toluene. The resulting residue was dissolved in CH_2Cl_2 (25 ml) and washed with satd. aq. NaHCO_3 solution (25 ml). The aq. phase was extracted with CH_2Cl_2 (3x 25 ml). The combined organic phases were dried over Na_2SO_4 , filtered and concentrated under reduced pressure. The crude product was purified by flash column chromatography (PE/EtOAc, 1:0 \rightarrow 2:1) to give **27** (155 mg, 96%) as a white solid.

$[\alpha]_{\text{D}}^{20} +179$ (c 0.28, CHCl_3); ^1H NMR (500 MHz, CDCl_3): δ 8.20 – 7.16 (m, 15H, Ar-H), 5.74 (m, 2H, H-2, H-4), 5.54 (d, $J = 10.4$ Hz, 1H, H-3), 4.77 (d, $J = 7.8$ Hz, 1H, H-1), 4.17 – 3.99 (m, 2H, H-5, O-CH_{2a}), 3.63 (dd, $J = 17.3, 9.1$ Hz, 1H, O-CH_{2b}), 1.36 (d, $J = 6.1$ Hz, 3H, H-6), 1.03 – 0.71 (m, 2H, $\text{CH}_2\text{-Si}$), -0.06 (s, 9H, $\text{Si}(\text{CH}_3)_3$); ^{13}C NMR (126 MHz, CDCl_3): δ 166.20, 165.88, 165.45, (3CO) 133.54, 133.31, 133.20, 130.16, 129.88, 129.81, 129.41, 129.09, 128.66, 128.42, 128.39 (18C, 18Ar-C) 100.99 (C-1), 72.45 (C-3), 71.26, 70.00, 69.81 (C-2, C-4, C-5), 67.77 (O-CH_2 -), 18.18 ($-\text{CH}_2\text{-Si}$), 16.51 (C-6), -1.35 ($\text{Si}(\text{CH}_3)_3$); ESI-MS: m/z calcd for $\text{C}_{32}\text{H}_{36}\text{O}_8\text{Si}$ $[\text{M}+\text{Na}]^+$: 599.21, found: 599.21; Combustion analysis: calcd: C 66.65, H 6.29, found: C 66.70, H 6.24.

Phenyl 2,3,4-tri-*O*-benzoyl-6-deoxy-1-thio- β -D-galactopyranoside (28)⁶²

Glycoside **27** (40 mg, 0.07 mmol) was dissolved in dry toluene (0.5 ml) and Ac_2O (100 μl , 15 eq, 1.1 mmol) was added followed by addition of $\text{BF}_3\cdot\text{Et}_2\text{O}$ (8 μl , 0.9 eq, 0.06 mmol) and the mixture was stirred at r.t. The reaction was monitored by TLC and diluted with CH_2Cl_2 (25 ml) after completion. The mixture was washed with satd. aq. NaHCO_3 solution (25 ml) and water (25 ml) and the aq. phases were extracted with CH_2Cl_2 (3x 25 ml). The combined organic phases were dried with Na_2SO_4 , filtered, and concentrated under reduced pressure.

The residue was purified by flash column chromatography on silica gel before usage for the next step. Yield: 36 mg, 99%.

The acetate (36 mg, 0.07 mmol) was dissolved in dry CH₂Cl₂ (0.5 ml) and PhSH (11 μ l, 1.5 eq, 0.1 mmol) was added followed by BF₃·Et₂O (14 μ l, 1.6 eq, 0.11 mmol). The mixture was stirred overnight at r.t. After complete transformation of the starting material the solution was diluted with CH₂Cl₂ and washed with satd. aq. NaHCO₃ solution and the aq. phase was extracted with CH₂Cl₂. The organic phase was dried over Na₂SO₄, filtered, and concentrated. The crude product was purified by flash column chromatography on silica gel (PE/EtOAc, 1:0→7:3). The β -anomer **20** (47%, 19 mg) was obtained as white solid.

$[\alpha]_{\text{D}}^{20} +136$ (*c* 0.1, CHCl₃); ¹H NMR (500 MHz, CD₃OD): δ 7.99 – 7.92 (m, 2H, Ar-H), 7.89 – 7.82 (m, 2H, Ar-H), 7.73 – 7.37 (m, 14H, Ar-H), 7.24 (t, *J* = 7.9 Hz, 2H, Ar-H), 5.73 – 5.58 (m, 3H, H-2, H-3, H-4), 5.17 (d, *J* = 9.4 Hz, 1H, H-1), 4.31 (q, *J* = 6.2 Hz, 1H, H-5), 1.31 (d, *J* = 6.4 Hz, 3H, H-6); ¹³C NMR (126 MHz, CD₃OD): δ 167.35, 167.30, 166.81, 166.67, (4 quart. Ar-C) 135.62, 134.75, 134.61, 134.47, 132.16, 130.82, 130.69, 130.57, 130.51, 130.33, 129.91, 129.81, 129.63, 129.40 (20C, 20Ar-C), 85.55 (C-1), 74.93, 74.50, 72.93, 69.47, (C-2, C-3, C-4, C-5), 16.90 (C-6); HR-MS: *m/z* calcd for C₃₃H₂₈O₇S [M+Na]⁺: 591.1448, found: 591.1449.

General procedure A (glycosylation):

Thioglycoside (0.13 mmol, 1.3 eq) and glycosyl acceptor **5**³³ (0.1 mmol, 1 eq) in dry CH₂Cl₂ (3 ml) were added via syringe to activated molecular sieves (4Å, 0.8 g). A suspension of DMTST (3 eq, 0.3 mmol) and activated molecular sieves (4Å, 0.4 g) in dry CH₂Cl₂ (1 ml) was prepared in a second flask. Both suspensions were stirred at r.t. for 4 h, then the DMTST suspension was added via syringe to the other suspension. The reaction was stopped after 16–24 h, filtered through celite and the celite was washed with CH₂Cl₂. The filtrate was successively washed with satd. aq. NaHCO₃ and water. The aqueous layers were extracted with CH₂Cl₂. The combined organic layers were dried with Na₂SO₄, filtered and concentrated under reduced pressure. The crude product was purified by column chromatography (PE/toluene/EtOAc, 10:10:1→5:5:1) to afford the trisaccharide mimic as a colorless foam.

General procedure B (deprotection):

A mixture of the according trisaccharide mimic (0.07 mmol) and Pd(OH)₂/C (10%) in dioxane/water (4:1, v/v, 2.5 ml) was shaken in a Parr shaker under a hydrogen atmosphere

(atm. pressure to 5 bar). After complete cleavage of the benzyl groups the reaction mixture was filtered through celite. The celite was washed with MeOH, the filtrate was evaporated to dryness and dried in *vacuo* for 4 h before usage for the next step. The intermediate was dissolved in MeOH (1 ml) and a catalytical amount of freshly prepared methanolic NaOMe solution (1 M) was added at r.t. After complete deprotection the mixture was neutralized with AcOH and evaporated. The residue was purified by column chromatography on silica gel (CH₂Cl₂/MeOH 10:4) to yield the trisaccharide mimics. For biological testing the compounds were further purified by preparative HPLC.

{(1R,2R,3S)-2-[(2,3,4-Tri-O-benzyl-6-deoxy- α -L-galactopyranosyl)oxy]-3-methyl-cyclohex-1-yl} 2,3,4-tri-O-benzoyl-6-O-benzyl- β -D-galactopyranoside (7)

Synthesized from **5** (55 mg, 0.1 mmol) and **6**³⁶ (81 mg, 0.13 mmol) according to general procedure A to give trisaccharide mimic **7** (55 mg, 0.049 mmol, 49%).

$[\alpha]_D^{20}$ -4.23 (c 0.25, CHCl₃); ¹H NMR (500 MHz, CDCl₃): δ 8.01 – 7.90 (m, 4H, Ar-H), 7.80 (d, J = 7.2 Hz, 2H, Ar-H), 7.56 – 7.47 (m, 2H, Ar-H), 7.45 – 7.07 (m, 29H, Ar-H), 5.96 (d, J = 3.3 Hz, 1H, Gal-H4), 5.70 (dd, J = 10.3, 8.2 Hz, 1H, Gal-H2), 5.51 (dd, J = 10.4, 3.5 Hz, 1H, Gal-H3), 5.11 (d, J = 3.3 Hz, 1H, Fuc-H1), 4.91 (m, 2H, PhCH_{2a}, Fuc-H5), 4.81 (m, 2H, PhCH_{2b}, Gal-H1), 4.71 (m, 2H, PhCH₂), 4.55 (m, 2H, PhCH₂), 4.47 – 4.35 (d, J = 11.9 Hz, 2H, PhCH₂), 4.11 – 4.02 (m, 3H, Fuc-H2, Fuc-H4, Gal-H5), 3.74 – 3.63 (m, 3H, Fuc-H3, MeCy-H1, Gal-H6a), 3.60 (m, 1H, Gal-H6b), 3.28 (t, J = 9.2 Hz, 1H, MeCy-H2), 2.00 (s, 1H, MeCy), 1.69 – 1.48 (m, 3H, MeCy), 1.42 (d, J = 6.5 Hz, 3H, Fuc-H6), 1.35 – 1.10 (m, 2H, MeCy), 1.06 (d, J = 6.6 Hz, 3H, Cy-CH₃), 0.9 (m, 1H, MeCy); ¹³C NMR (126 MHz, CDCl₃): δ 165.64, 165.55, 164.96 (3CO), 139.20, 138.91, 138.50, 137.41, 133.44, 133.17, 129.78, 129.71, 129.67, 129.58, 129.48, 128.96, 128.53, 128.42, 128.40, 128.37, 128.28, 128.26, 128.20, 127.80, 127.72, 127.68, 127.52, 127.37, 127.17 (42C, 42Ar-C), 99.91 (Gal-C1), 97.74 (Fuc-C1), 81.20 (MeCy-C2), 80.82 (MeCy-C1), 80.24 (Fuc-C2), 79.50 (Fuc-C3), 76.27 (Gal-C5), 75.01 (CH₂), 74.22 (CH₂), 73.69 (CH₂), 72.69 (CH₂), 72.64 (Fuc-C4), 72.29 (Gal-C3), 69.67 (Gal-C2), 68.68 (Gal-C4), 67.64 (Gal-C6), 66.47 (Fuc-C5), 38.91 (MeCy), 33.17 (MeCy), 30.74 (MeCy), 22.70 (Cy-CH₂), 18.81 (Cy-CH₃), 16.97 (Fuc-C6); ESI-MS m/z calcd for C₆₈H₇₀O₁₄ [M+Na]⁺: 1133.47 found: 1133.55.

{{(1*R*,2*R*,3*S*)-2-[(6-Deoxy- α -L-galactopyranosyl)oxy]-3-methyl-cyclohex-1-yl} β -D-galactopyranoside (8)

Compound **7** (54 mg, 0.049 mmol) was deprotected according to standard procedure B to yield title compound **8** (15 mg, 0.034 mmol, 70%).

$[\alpha]_D^{20}$ -89.1 (*c* 0.20, MeOH); ^1H NMR (500 MHz, D_2O): δ 4.99 (d, *J* = 4.1 Hz, 1H, Fuc-H1), 4.80 (1H, Fuc-H5), 4.35 (d, *J* = 7.8 Hz, 1H, Gal-H1), 3.79 – 3.73 (m, 2H, Gal-H4, Fuc-H3), 3.72 – 3.55 (m, 5H, Fuc-H2, Fuc-H3, Gal-H6, MeCy-H1), 3.50 (m, 2H, Gal-H3, Gal-H5), 3.40 (dd, *J* = 9.8, 7.9 Hz, 1H, Gal-H2), 3.10 (t, *J* = 9.6 Hz, 1H, MeCy-H2), 2.01 (s, 1H, MeCy), 1.52 – 1.58 (m, 3H, MeCy), 1.15 (d, *J* = 8.7 Hz, 2H, MeCy), 1.06 (d, *J* = 6.6 Hz, 3H, Fuc-H6), 0.97 (d, *J* = 6.4 Hz, 4H, Cy- CH_3 , MeCy); ^{13}C NMR (126 MHz, CD_3OD): δ 102.40 (Gal-C1), 100.31 (Fuc-C1), 84.60 (MeCy-C2), 79.89 (MeCy-C1), 74.94, 76.34 (Gal-C3, Gal-C5), 73.84 (Fuc-C4), 72.24 (Gal-C2), 70.31, 71.38 (Fuc-C2, Fuc-C3), 70.16 (Gal-C4), 67.54 (Fuc-C5), 62.93 (Gal-C6), 24.22, 31.90, 34.94, 40.35, (4C, MeCy), 19.59 (Fuc-C6), 16.74 (MeCy); HR-MS: *m/z* calcd for $\text{C}_{19}\text{H}_{34}\text{O}_{11}[\text{M}+\text{Na}]^+$: 461.1993, found: 461.2003; HPLC-purity > 99.5%, R_t = 5.335 min.

{{(1*R*,2*R*,3*S*)-2-[(2,3,4-Tri-*O*-benzyl-6-deoxy- α -L-galactopyranosyl)oxy]-3-methyl-cyclohex-1-yl} 2,3,4,6-tetra-*O*-acetyl- β -D-glucopyranoside (30)

Synthesized from **5** (55 mg, 0.1mmol) and **29**⁴² (51 mg, 0.13 mmol) according to general procedure A, to give trisaccharide mimic **30** (60 mg, 0.068 mmol, 68%).

^1H NMR (500 MHz, CDCl_3): δ 7.37 – 7.05 (m, 18H, Ar-H), 5.10 (m, 1H, Glc-H3), 5.00 (d, *J* = 3.8 Hz, 1H, Fuc-H1), 4.95 – 4.86 (m, 2H, Glc-H4, Ph CH_2), 4.84 – 4.56 (m, 7H, Glc-H2, Fuc-H5, Ph CH_2), 4.46 (d, *J* = 8.2 Hz, 1H, Glc-H1), 4.31 (dd, *J* = 12.3, 4.1 Hz, 1H, Glc-H6a), 4.04 (m, 1H, Fuc-H2), 3.93 – 3.88 (m, 2H, Fuc-H3, Glc-H6b), 3.65 (d, *J* = 1.6 Hz, 1H, Fuc-H4), 3.60 – 3.47 (m, 2H, Glc-H5, MeCy-H1), 3.18 (t, *J* = 9.1 Hz, 1H, MeCy-H2), 2.00 – 1.89 (m, 10H, 3 CH_3 , MeCy), 1.85 (s, 3H, CH_3), 1.76 – 1.46 (m, 3H, MeCy), 1.27 – 1.09 (m, 5H, Fuc-H6, MeCy), 1.08 – 0.91 (m, 4H, Cy- CH_3 , MeCy); ^{13}C NMR (126 MHz, CDCl_3): δ 170.54, 170.41, 169.65, 169.05 (4CO), 156.39, 139.05, 138.48, 129.15, 128.59, 128.41, 128.33, 128.31, 128.22, 127.69, 127.59, 127.44, 127.19 (Ar-C), 99.41 (Glc-C1), 98.20 (Fuc-C1), 81.98 (MeCy-C2), 81.11 (MeCy-C1), 80.31 (Fuc-C3), 78.25 (Fuc-C4), 76.47 (Fuc-C2), 74.69, 74.57, 73.10, 72.61, 72.00, 71.32, 68.15 (Glc-C2, Glc-C3, Glc-C4, Glc-C5, 3Ph CH_2), 66.35 (Fuc-C5), 62.04 (Glc-C6), 38.94, 33.28, 30.99, 22.76 (4MeCy), 20.79, 20.77, 20.74,

20.72 (4COCH₃), 18.85 (Cy-CH₃), 16.91 (Fuc-C6); ESI-MS: *m/z* calcd for C₄₈H₆₀O₁₅ [M+Na]⁺: 899.38, found: 899.41.

{{(1*R*,2*R*,3*S*)-2-[(6-Deoxy- α -L-galactopyranosyl)oxy]-3-methyl-cyclohex-1-yl} β -D-glucopyranoside (35)}

Compound **30** (50 mg, 0.057 mmol) was deprotected according to general procedure B and gave **35** (18mg, 0.041 mmol, 72%).

[α]_D²⁰ -78.4 (*c* 0.14, MeOH); ¹H NMR (500 MHz, D₂O): δ 4.96 (d, *J* = 4.0 Hz, 1H, Fuc-H1), 4.66 (m, 1H, Fuc-H5), 4.40 (d, *J* = 8.0 Hz, 1H, Glc-H1), 3.79 – 3.74 (m, 2H, Fuc-H3, Glc-H6_a), 3.72 – 3.62 (m, 2H, Fuc-H2, Fuc-H4), 3.56 (tt, *J* = 12.1, 6.0 Hz, 1H, MeCy-H1), 3.47 (m, 1H, Glc-H6_b), 3.34 (t, *J* = 9.2 Hz, 1H, Glc-H3), 3.27 (ddd, *J* = 9.4, 7.2, 2.0 Hz, 1H, Glc-H5), 3.16 – 3.04 (m, 3H, Glc-H2, D-Glc-H4, MeCy-H2), 1.98 (m, 1H, MeCy), 1.59 – 1.41 (m, 3H, MeCy), 1.20 – 1.08 (m, 2H, MeCy), 1.06 (m, 3H, Fuc-H6), 0.95 (m, 4H, MeCy, Cy-CH₃); ¹³C NMR (126 MHz, D₂O): δ 99.37 (Glc-C1), 99.02 (Fuc-C1), 84.48 (MeCy-C2), 78.98 (MeCy-C1), 75.72 (2C, Glc-C3, D-Glc-C5), 73.11, 71.94, 70.22 (Glc-C2, Glc-C4, Fuc-C4), 69.22 (Fuc-C3), 68.11 (Fuc-C2), 66.26 (Fuc-C5), 61.60 (Glc-C6), 38.65 (Cy-CH), 33.09, 30.34, 22.47 (3MeCy), 18.03 (Cy-CH₃), 15.56 (Fuc-C6); HR-MS *m/z* calcd for C₁₉H₃₄O₁₁ [M+Na]⁺: 461.1993, found: 461.1999; HPLC-purity > 99.5%, R_t = 5.496 min.

{{(1*R*,2*R*,3*S*)-2-[(6-Deoxy- α -L-galactopyranosyl)oxy]-3-methyl-cyclohex-1-yl} 2- deoxy- β -D-xyl α -hexopyranoside (36)}

A mixture of thioglycoside **11** (57 mg, 0.12 mmol, 1.2 eq), acceptor **5** (55 mg, 0.1 mmol), and flame-dried molecular sieves (3Å, 1g) was suspended in CH₂Cl₂/CH₃CN (10 ml, 1:3, v/v). The resulting mixture was stirred at room temperature for 10 min and at -65°C for an additional 20 min under argon, followed by the addition of *N*-iodosuccinimide (27 mg, 1.2 eq, 0.12 mmol) and trimethylsilyl trifluoro-methanesulfonate (4.4 μ l, 0.24 eq, 0.024 mmol). The reaction was monitored by TLC. After 2h the reaction mixture was quenched; a small volume of satd. aq. NaHCO₃ solution and lumps of Na₂S₂O₃ (s) were added and the mixture was warmed to r.t. The mixture was stirred and then filtered through a pad of celite. The filtrate was diluted with CH₂Cl₂ (30 ml) and washed with satd. aq. NaHCO₃ solution (30 ml) and water (30 ml). The aq. Phase was extracted with CH₂Cl₂ (3x 30 ml). The combined organic phases were dried over Na₂SO₄, filtered, and concentrated. The residue was purified by flash column chromatography on silica gel (Pe/toluene/EtOAc gradient). Unreacted

starting material **5** and β -glycosylated product **31** were not separable. Hence, the mixture (54 mg) was submitted to the deprotection step. Debenzylation was performed as described in general procedure B. Yield: 14% over 2 steps (6 mg, 0.014 mmol).

$[\alpha]_D^{20}$ -96.5 (*c* 0.18, MeOH); $^1\text{H NMR}$ (500 MHz, D_2O): δ 5.07 (d, $J = 3.9$ Hz, 1H, Fuc-H1), 4.75 (d, $J = 9.4$ Hz, 2H, Fuc-H5, Gal-H1), 3.92 – 3.83 (m, 2H, Fuc-H3, Gal-H3), 3.82 – 3.66 (m, 6H, Fuc-H2, Fuc-H4, MeCy-H2, Gal-H6a, Gal-H6b, Gal-H4), 3.46 (m, 1H, Gal-H5), 3.13 (s, 1H, MeCy-H1), 2.13 (s, 1H, MeCy), 1.88 (m, 1H, Gal-H2a), 1.74 – 1.51 (m, 4H, MeCy, Gal-H2b), 1.31 – 1.19 (m, 2H, MeCy), 1.16 (d, $J = 6.5$ Hz, 3H, Fuc-H6), 1.04 (m, 4H, Cy- CH_3 , MeCy); $^{13}\text{C NMR}$ (125 MHz, D_2O): δ 99.84 (Fuc-C1), 97.90 (Gal-C1), 85.13 (MeCy-C2), 79.37 (MeCy-C1), 76.10 (Gal-C5), 73.06 (Fuc-C4), 70.26, 69.24, 69.05 (Fuc-C3, Gal-C3, Gal-C4), 67.79 (Fuc-C2), 67.50 (Fuc-C5), 62.94 (Gal-C6), 39.80 (MeCy), 34.78 (Gal-C2), 34.17, 31.25, 23.64 (3MeCy), 19.21 (Cy- CH_3), 16.65 (Fuc-C6); HR-MS: m/z calcd for $\text{C}_{19}\text{H}_{34}\text{O}_{10}$ $[\text{M}+\text{Na}]^+$: 445.2044, found: 445.2051; HPLC-purity > 99.5%, $R_t = 7.696$ min.

{{(1*R*,2*R*,3*S*)-2-[(2,3,4-Tri-*O*-benzyl-6-deoxy- α -L-galactopyranosyl)oxy]-3-methyl-cyclohex-1-yl} 2,4,6-tri-*O*-benzoyl-3- deoxy- β -D-xylo-hexopyranoside (32**)**

Compound **32** was synthesized from **5** (27 mg, 0.05 mmol) and **24** (37 mg, 0.065 mmol) according to general procedure A. Yield: 27 mg, 0.027 mmol, 54 %.

$^1\text{H NMR}$ (500 MHz, CDCl_3): δ 8.10 – 7.95 (m, 6H, Ar-H), 7.63 – 7.27 (m, 20H, Ar-H), 7.24 – 7.16 (m, 4H, Ar-H), 5.47 (s, 1H, Gal-H4), 5.24 (s, 1H, Gal-H2), 5.09 (s, 1H, Fuc-H1), 4.98 (d, $J = 11.4$ Hz, 1H, PhCH_2), 4.90 (d, $J = 6.5$ Hz, 1H, Fuc-H5), 4.86-4.66 (m, 5H, Gal-H1, 2 PhCH_2), 4.56 (d, $J = 11.2$ Hz, 1H, PhCH_2), 4.45 – 4.31 (m, 2H, Gal-H6), 4.18 – 4.06 (m, 3H, Fuc-H2, Fuc-H3, Gal-H5), 3.75 (s, 1H, Fuc-H4), 3.67 (s, 1H, MeCy-H1), 3.26 (t, $J = 8.9$ Hz, 1H, MeCy-H2), 2.70 (d, $J = 13.0$ Hz, 1H, Gal-H3a), 2.08 (s, 1H, MeCy), 1.96 (t, $J = 12.9$ Hz, 1H, Gal-H3b), 1.58 (s, 3H, MeCy), 1.46 – 1.13 (m, 5H, Fuc-H6, MeCy), 1.08 (d, $J = 5.8$ Hz, 3H, Cy- CH_3), 1.02 – 0.76 (m, 4H, MeCy); $^{13}\text{C NMR}$ (DEPT-135, 126 MHz, CDCl_3): δ 133.48, 133.14, 133.07, 129.77, 129.53, 128.48, 128.44, 128.36, 128.14, 128.12, 127.75, 127.44, 127.29, 127.13, 127.03 (Ar-C), 100.63 (Gal-C1), 98.00 (Fuc-C1), 81.84 (MeCy-C2), 79.90, 79.81, 79.72, 76.37 (MeCy-C1, Fuc-C2, Fuc-C3, Fuc-C4), 75.06, 74.30, 74.18, 72.46 (3 PhCH_2 , Gal-C5), 67.93, 67.90 (Gal-C2, Gal-C4), 66.25 (Fuc-C5), 62.31 (Gal-C6), 38.87 (MeCy), 33.46 (Gal-C3), 33.15, 30.58, 22.72 (3MeCy), 18.69 (Cy- CH_3), 16.86 (Fuc-C6); ESI-MS: m/z calcd for $\text{C}_{61}\text{H}_{64}\text{O}_{13}$ $[\text{M}+\text{Na}]^+$: 1027.42, found: 1027.44.

{{(1R,2R,3S)-2-[(6-Deoxy- α -L-galactopyranosyl)oxy]-3-methyl-cyclohex-1-yl}-3-deoxy- β -D-xylo-hexopyranoside (37)}

Compound **32** was deprotected according to general procedure B to yield **37** (8 mg, 0.019 mmol, 70%).

$[\alpha]_D^{20}$ -65.1 (*c* 0.14, MeOH); $^1\text{H NMR}$ (500 MHz, D_2O): δ 5.06 (d, $J = 4.0$ Hz, 1H, Fuc-H1), 4.83 (m, 1H, Fuc-H5), 4.42 (d, $J = 7.9$ Hz, 1H, Gal-H1), 3.93 (s, 1H, Gal-H4), 3.85 (dd, $J = 10.5, 3.3$ Hz, 1H, Fuc-H3), 3.80 – 3.54 (m, 7H, Fuc-H2, Fuc-H4, MeCy-H1, Gal-H6a, Gal-H6b, Gal-H2, Gal-H5), 3.18 (t, $J = 9.6$ Hz, 1H, MeCy-H2), 2.20 – 2.03 (m, 2H, MeCy, Gal-H3a), 1.73 – 1.48 (m, 4H, MeCy, Gal-H3b), 1.23 (dd, $J = 18.9, 10.5$ Hz, 2H, MeCy), 1.13 (d, $J = 6.6$ Hz, 3H, Fuc-H6), 1.04 (d, $J = 6.4$ Hz, 4H, Cy- CH_3 , MeCy); $^{13}\text{C NMR}$ (125 MHz, D_2O): δ 102.68 (Gal-C1), 99.90 (Fuc-C1), 85.38 (MeCy-C2), 79.29 (MeCy-C1), 78.90 (Gal-C5), 73.08 (Fuc-C4), 70.28 (Fuc-C3), 69.22 (Fuc-C2), 67.51 (Fuc-C5), 66.72 (Gal-C4), 66.26 (Gal-C2), 62.83 (Gal-C6), 39.74 (MeCy), 37.90 (Gal-C3), 34.20 (MeCy), 31.41 (MeCy), 23.61 (MeCy), 19.15 (Cy- CH_3), 16.49 (Fuc-C-6); HR-MS: m/z calcd for $\text{C}_{19}\text{H}_{34}\text{O}_{10}$ $[\text{M}+\text{Na}]^+$: 445.2044, found: 445.2052; HPLC-purity > 99.5%, $R_t = 6.268$ min.

{{(1R,2R,3S)-2-[(2,3,4-Tri-*O*-benzyl-6-deoxy- α -L-galactopyranosyl)oxy]-3-methyl-cyclohex-1-yl} 2,3,6-tri-*O*-benzoyl-4-deoxy- β -D-xylo-hexopyranoside (33)}

Compound **33** was synthesized from **5** (43.7 mg, 0.08 mmol) and **17** (54mg, 0.1 mmol) according to general procedure A. Yield: 60 mg, 0.06 mmol, 75%.

$^1\text{H NMR}$ (500 MHz, CDCl_3): δ 8.09 – 8.03 (m, 2H, Ar-H), 8.01 – 7.93 (m, 4H, Ar-H), 7.51 (dt, $J = 7.2, 3.1$ Hz, 3H, Ar-H), 7.43 – 7.36 (m, 6H, Ar-H), 7.35 – 7.19 (m, 16H, Ar-H), 5.40 – 5.30 (m, 2H, Gal-H2, Gal-H3), 5.05 (d, $J = 3.1$ Hz, 1H, Fuc-H1), 4.85 (q, $J = 6.4$ Hz, 1H, Fuc-H5), 4.83 – 4.66 (m, 5H, PhCH_2 , Gal-H1), 4.60 (d, $J = 11.6$ Hz, 1H, PhCH_2), 4.46 (dd, $J = 11.5, 4.3$ Hz, 1H, Gal-H6a), 4.37 (dd, $J = 11.5, 3.0$ Hz, 2H, Gal-H6b, PhCH_2), 4.08 – 3.95 (m, 3H, Fuc-H2, Fuc-H3, Gal-H5), 3.69 – 3.60 (m, 2H, Fuc-H4, MeCy-H1), 3.22 (t, $J = 9.1$ Hz, 1H, MeCy-H2), 2.49 (dd, $J = 12.7, 2.2$ Hz, 1H, Gal-H4a), 2.00 (d, $J = 10.2$ Hz, 1H, MeCy), 1.88 (m, 1H, Gal-H4b), 1.81 – 1.56 (m, 2H, MeCy), 1.52 (d, $J = 10.4$ Hz, 2H, MeCy), 1.35 (d, $J = 6.5$ Hz, 3H, Fuc-H6), 1.07 (m, 5H, Cy- CH_3 , MeCy), 1.00 – 0.80 (m, 1H, MeCy); $^{13}\text{C NMR}$ (126 MHz, CDCl_3): δ 166.23, 166.13, 165.21 (3CO), 139.34, 139.21, 138.69, 133.52, 133.42, 133.20, 129.93, 129.91, 129.81, 129.78, 129.52, 128.76, 128.55, 128.48, 128.30, 128.27, 128.23, 128.05, 127.58, 127.41, 127.27 (Ar-C), 99.84 (Gal-H1), 98.33 (Fuc-H1), 82.19 (MeCy-C2), 80.88 (MeCy-C1), 80.24, 78.97, 76.45 (Fuc-C2, Fuc-C3, Fuc-C4), 74.95, 74.49 (2 PhCH_2), 72.58, 72.34, 72.16 (Gal-C2, Gal-C3, PhCH_2), 69.51 (Gal-

C5), 66.30 (Fuc-C5), 66.16 (Gal-C6), 38.94 (MeCy), 33.30, 33.17 (Gal-C4, MeCy), 30.99, 22.71 (MeCy), 18.79 (Cy-CH₃), 17.03 (Fuc-C6); ESI-MS: *m/z* calcd for C₆₁H₆₄O₁₃ [M+Na]⁺: 1027.42, found: 1027.51.

{{(1R,2R,3S)-2-[(6-Deoxy- α -L-galactopyranosyl)oxy]-3-methyl-cyclohex-1-yl} 4-deoxy- β -D-xyllo-hexopyranoside (38)}

Compound **33** (50mg, 0.05 mmol) was deprotected according to general procedure B to yield **38** (17 mg, 0.04 mmol, 81%).

$[\alpha]_D^{20}$ -99.4 (*c* 0.19, MeOH); ¹H NMR (500 MHz, D₂O): δ 5.04 (s, 1H, Fuc-H1), 4.79 (Fuc-H5 overlay with H₂O), 4.40 (d, *J* = 7.8 Hz, 1H, Gal-H1), 3.84 (d, *J* = 10.6 Hz, 1H, Fuc-H3), 3.79 – 3.71 (m, 2H, Fuc-H2, Fuc-H4), 3.71 – 3.46 (m, 5H, Gal-H3, Gal-H5, Gal-H6, MeCy-H1), 3.16 (t, *J* = 9.5 Hz, 1H, MeCy-H2), 3.08 (t, *J* = 8.4 Hz, 1H, Gal-H2), 2.07 (s, 1H, Cy-CH_{2a}'), 1.91 (d, *J* = 8.3 Hz, 1H, Gal-H4_b), 1.70 – 1.46 (m, 3H, MeCy), 1.24 (m, 3H, Gal-H4_a, MeCy), 1.13 (d, *J* = 6.3 Hz, 3H, Fuc-H6), 1.04 (d, *J* = 5.6 Hz, 4H, Cy-CH₃, MeCy); ¹³C NMR (125 MHz, D₂O, reference CD₃OD): δ 102.16 (Gal-C1), 101.45 (Fuc-C1), 87.00 (MeCy-C2), 81.22 (MeCy-C1), 77.31 (Gal-C2), 74.41, 74.40, 72.76 (Fuc-C4, Gal-C3, Gal-C5), 71.63 (Fuc-C3), 70.56 (Fuc-C2), 68.69 (Fuc-C5), 66.57 (Gal-C6), 41.07 (MeCy), 36.89 (Gal-C4), 35.53 (MeCy), 32.82 (MeCy), 24.90 (MeCy), 20.46 (Cy-CH₃), 18.02 (Fuc-C6); HR-MS: *m/z* calcd for C₁₉H₃₄O₁₀ [M+Na]⁺: 445.2044, found: 445.2053; HPLC-purity > 99.5%, R_t = 5.933 min.

{{(1R,2R,3S)-2-[(2,3,4-Tri-*O*-benzyl-6-deoxy- α -L-galactopyranosyl)oxy]-3-methyl-cyclohex-1-yl} 2,3,4-tri-*O*-benzoyl-6-deoxy- β -D-galactopyranoside (34)}

Compound **34** was synthesized from **5** (40 mg, 0.073 mmol) and **28** (48 mg, 1.15 eq, 0.84 mmol) according to general procedure. Yield: 35 mg, 0.035 mmol, 48%.

¹H NMR (500 MHz, CDCl₃): δ 8.06 (d, *J* = 7.5 Hz, 2H, Ar-H), 7.96 (d, *J* = 7.5 Hz, 2H, Ar-H), 7.81 (d, *J* = 7.6 Hz, 2H, Ar-H), 7.59 – 7.47 (m, 2H, Ar-H), 7.45 – 7.13 (m, 26H, Ar-H), 5.77 – 5.65 (m, 2H, Gal-H2, Gal-H4), 5.51 (dd, *J* = 10.4, 3.5 Hz, 1H, Gal-H3), 5.10 (d, *J* = 2.3 Hz, 1H, Fuc-H1), 5.01 (d, *J* = 6.5 Hz, 1H, Fuc-H5), 4.88 (d, *J* = 11.5 Hz, 1H, PhCH₂), 4.85 – 4.72 (m, 4H, PhCH₂, Gal-H1), 4.58 (d, *J* = 11.6 Hz, 1H, PhCH_{2a}), 4.48 (d, *J* = 11.5 Hz, 1H, PhCH₂), 4.13 – 4.05 (m, 2H, Fuc-H2, Fuc-H3), 4.02 (d, *J* = 6.5 Hz, 1H, Gal-H5), 3.73 – 3.64 (m, 2H, Fuc-H4, MeCy-H1), 3.29 (t, *J* = 9.3 Hz, 1H, MeCy-H2), 2.02 (d, *J* = 10.6 Hz, 1H, MeCy), 1.67 (s, 1H, MeCy), 1.54 (m, 1H, MeCy), 1.47 (d, *J* = 6.4 Hz, 3H, Fuc-H6),

1.28 (d, $J = 6.4$ Hz, 3H, Gal-H6), 1.16 (m, 1H, MeCy), 1.08 (d, $J = 6.6$ Hz, 3H, Cy-CH₃), 1.02 – 0.81 (m, 1H, MeCy); ¹³C NMR (125 MHz, CDCl₃): δ 166.29, 165.75, 165.19 (3CO), 139.38, 139.07, 138.60, 138.00, 133.65, 133.36, 133.24, 129.87, 129.78, 129.75, 129.67, 129.17, 129.03, 128.72, 128.67, 128.49, 128.42, 128.36, 128.33, 128.28, 127.86, 127.69, 127.43, 127.41, 127.27, 125.43 (Ar-C), 99.96 (Gal-C1), 97.92 (Fuc-C1), 81.21, 81.11, 80.19, 79.67, 76.28 (MeCy-C1, MeCy-C2, Fuc-C2, Fuc-C3, Fuc-C4), 75.11, 74.46, 72.61 (3PhCH₂), 72.53 (Gal-C3), 71.69, 69.83, 69.69 (Gal-C2, Gal-C4, Gal-C5), 66.51 (Fuc-C5), 39.22, 33.44, 31.14, 23.04 (4MeCy), 18.99 (Cy-CH₃), 17.08 (Fuc-C6), 16.71 (Gal-C6); ESI-MS: m/z calcd for C₆₁H₆₄O₁₃ [M+Na]⁺: 1027.42, found: 1027.44.

{{(1R,2R,3S)-2-[(6-Deoxy- α -L-galactopyranosyl)oxy]-3-methyl-cyclohex-1-yl} 6-deoxy- β -D-galactopyranoside (39)}

Compound **34** (35 mg, 0.035 mmol) was deprotected according to general procedure B to give **39** (11 mg, 0.26 mmol, 74%).

$[\alpha]_D^{20}$ -88.7 (c 0.2, MeOH); ¹H NMR (500 MHz, D₂O, CD₃OD as reference): δ 5.09 (d, $J = 3.8$ Hz, 1H, Fuc-H1), 4.84 (s, 1H, Fuc-H5), 4.47 (d, $J = 7.9$ Hz, 1H, Gal-H1), 3.90 (dd, $J = 10.5, 3.2$ Hz, 1H, Fuc-H3), 3.84 – 3.75 (m, 2H, Fuc-2, Fuc-H4), 3.75 – 3.60 (m, 4H, Gal-H3, Gal-H4, Gal-5H, MeCy-H1), 3.48 (t, $J = 8.9$ Hz, 1H, Gal-H2), 3.20 (t, $J = 9.5$ Hz, 1H, MeCy-H2), 2.14 (s, 1H, MeCy), 1.74 – 1.49 (m, 3H, MeCy), 1.27 – 1.20 (m, 5H, Gal-H6, MeCy), 1.18 (d, $J = 6.5$ Hz, 3H, Fuc-H6), 1.09 (d, $J = 6.2$ Hz, 4H, Cy-CH₃, MeCy); ¹³C NMR (125 MHz, D₂O, CD₃OD as reference): δ 100.51 (Gal-C1), 99.77 (Fuc-C1), 85.42 (MeCy-C2), 79.50 (MeCy-C1), 73.94 (Gal-H2), 72.99 (Fuc-C4), 72.30, 71.31, 71.3 (Gal-C3, Gal-C4, Gal-C5), 70.26 (Fuc-C3), 69.31 (Fuc-C2), 67.52 (Fuc-C5), 39.55 (MeCy), 34.15 (MeCy), 31.16 (MeCy), 23.51 (MeCy), 19.09 (Cy-CH₃), 16.63 (Gal-C6), 16.46 (Fuc-C6); HR-MS: m/z calcd for C₁₉H₃₄O₁₀ [M+Na]⁺: 445.2044, found: 445.2048; HPLC-purity > 99.5%, $R_t = 7.007$ min.

[(1R,2R,3S)-1-Hydroxy-3-methyl-cyclohex-2-yl] 6-deoxy- α -L-galactopyranoside (40)

Compound **5** (32.8 mg, 0.06 mmol) was deprotected with Pd(OH)₂/C (10%) in water/dioxane (1:4, 2.5 ml) under H₂ (5 psi) to yield compound **40** (15 mg, 0.054 mmol, 91%).

$[\alpha]_D^{20} = -119.3$ ($c = 0.60$, MeOH); ¹H NMR (500 MHz, D₂O): δ 5.00 (s, 1H, Fuc), 4.30 (m, 1H, Fuc-H5), 3.83 – 3.70 (m, 3H, Fuc-H2, Fuc-H3, Fuc-H4), 3.45 (s, 1H, MeCy-H1), 2.98 (t, $J = 8.9$ Hz, 1H, MeCy-H2), 1.91 (s, 1H, MeCy), 1.58 (m, 3H, MeCy), 1.23 (s, 2H, MeCy), 1.12 (t, $J = 5.8$ Hz, 3H, Fuc-H6), 1.00 (t, $J = 5.5$ Hz, 4H, Cy-CH₃, MeCy); ¹³C NMR (125

MHz, D₂O, CD₃OD as reference): δ 99.74 (Fuc-C1), 90.76 (MeCy-C2), 73.47 (MeCy-C1), 72.84, 70.42, 69.31 (Fuc-C2, Fuc-C3, Fuc-C4), 67.88 (Fuc-C5), 38.05 (MeCy), 34.17, 34.11, 23.75 (3MeCy), 18.88 (Cy-CH₃), 16.29 (Fuc-C6); HR-MS m/z calcd for C₁₃H₂₄O₆ [M+Na]⁺: 299.1465, found: 299.1471; HPLC-purity > 99.5%, R_t = 7.749 min.

Computational Methods

Structure Preparation and Docking. For ligand docking the 1.8 Å resolution crystal structure of the carbohydrate recognition domain of DC-SIGN (PDB code 1SL5) was used. The downloaded structure was pre-processed using Maestro's protein preparation wizard (Maestro, version 9.2, Schrödinger, LLC, New York, NY, 2011). Hydrogen atoms were added, bond orders were corrected, and protonation states were assigned to yield a fully atomistic model of the complex. Finally, this model was subjected to energy minimization using OPLS 2005 forcefield within heavy-atom RMSD of 0.3 Å to relieve strain and steric clashes. For docking experiments, the co-crystallized ligand LNFP III was used to define the binding site before it was deleted. Additionally, two water molecules were common to several available crystal structures of DC-SIGN (W437 and W439 according to 1SL5 numbering) and were, thus, used as part of the binding site. Ligand docking was then obtained through flexible docking using the default settings in Glide (Glide, version 5.5, Schrödinger, LLC, New York, NY, 2009). Resultant poses were visually inspected and the ones lacking key interactions with DC-SIGN (e.g. calcium coordination) were dismissed.

Free energy perturbation (FEP). FEP coupled to MD simulations with explicit solvent is considered one of the reference computational approaches for estimating free energies.⁶³ In FEP simulations, the system is gradually mutated from one state to another through multiple windows, and the effect of this perturbation onto the free energy is monitored.⁶⁴ Since the structural changes in the deoxy derivatives (**37**, **38**, **39**) are relatively small compared to **8** (replacing a hydroxyl group with a hydrogen), they are best suited for free energy predictions using FEP. For this purpose, the FEP implementation in Desmond was employed and the default settings were used. System setup similar to that used in our MD simulations was employed across 12 lambda-windows to simulate the transition from the un-perturbed (hydroxyl) to the fully perturbed (hydro) states. Due to the higher computational cost, the FEP simulations were 1.2 ns long.

Molecular Dynamics. Molecular dynamics (MD) simulations were carried out for docked ligands with Desmond⁶⁵ using the OPLS 2005 force field as implemented in the Schrödinger 2011 suite. Each system was solvated using an orthorhombic, TIP3P water⁶⁶ box with a minimum distance of 10 Å from the complex. Na⁺ and Cl⁻ ions were added to neutralize the charges and account for physiological salt concentration (0.15 M). All systems were equilibrated using the default relaxation protocol (Desmond 2.2; Schrödinger, Inc., New York, NY) and simulated over the span 30 ns with a time step of 2.0 fs. The SHAKE algorithm⁶⁷ was applied to all heavy-atom bound hydrogens. Production runs were carried out in the Martyna-Tobias-Klein isothermal-isobaric ensemble (NPT)⁶⁸ using the Nose-Hoover barostat to maintain a constant temperature of 300 K.⁶⁹ Energies and geometries were recorded in 1.2 ps intervals. Output trajectory were analyzed using component-interactions script in Maestro to compute interaction energies between the ligand and individual amino acids defining the binding site as well as the conserved calcium along the MD simulations. Non-bonded interactions were computed as the sum of OPLS 2005 Van der Waals and electrostatic terms. For Le^x (**1**) and **8** the solvent accessible surface areas (SASA) were calculated using a water probe simulated as a sphere of radius 1.4 Å to map the complex surface at a resolution of 0.2 Å.

Biological Evaluation

Protein expression, competitive polymer assay, and ITC experiments were performed as previously described (Chapter 2.2.1).

ACKNOWLEDGEMENTS

The authors gratefully acknowledge the financial support by the Swiss National Science Foundation (grant no. 200020_129935) and by GlycoMimetics Inc., Gaithersburg, MD, USA.

REFERENCES

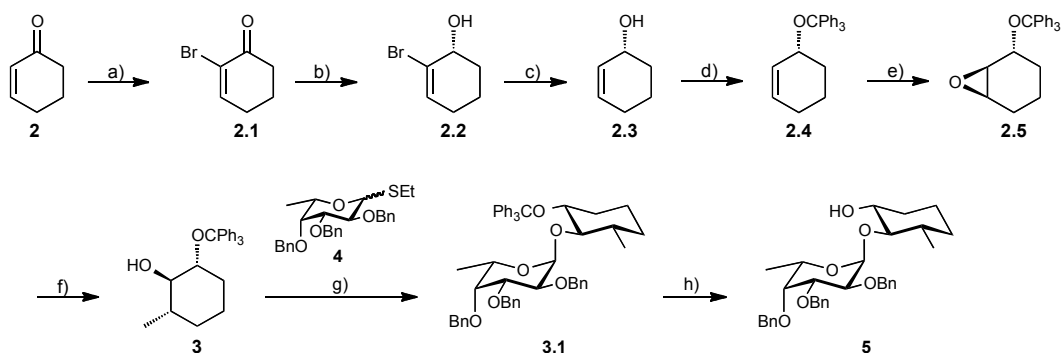
1. Banchereau, J.; Steinman, R. *Nature* **1998**, 245.
2. Geijtenbeek, T. B. H.; Torensma, R.; van Vliet, S. J.; van Duijnhoven, G. C. F.; Adema, G. J.; van Kooyk, Y.; Figdor, C. G. *Cell* **2000**, 100, 575.
3. Geijtenbeek, T. B. H.; Krooshoop, D.; Bleijs, D. A.; van Vliet, S. J.; van Duijnhoven, G. C. F.; Grabovsky, V.; Alon, R.; Figdor, C. G.; van Kooyk, Y. *Nat. Immunol.* **2000**, 1, 353.
4. Geijtenbeek, T. B. H.; Kwon, D. S.; Torensma, R.; van Vliet, S. J.; van Duijnhoven, G. C. F.; Middel, J.; Cornelissen, I. L. M. H. A.; Nottet, H. S. L. M.; KewalRamani, V. N.; Littman, D. R.; Figdor, C. G.; van Kooyk, Y. *Cell* **2000**, 100, 587.
5. Alvarez, C. P.; Lasala, F.; Carrillo, J.; Muniz, O.; Corbi, A. L.; Delgado, R. *J. Virol.* **2002**, 76, 6841.
6. Geijtenbeek, T.; van Vliet, S.; Koppel, E.; Sanchez-Hernandez, M.; Vandenbroucke-Grauls, C.; Appelmelk, B.; van Kooyk, Y. *J. Exp. Med.* **2003**, 7.
7. Appelmelk, B.; van Die, I.; van Vliet, S.; Vandenbroucke-Grauls, C.; Geijtenbeek, T.; van Kooyk, Y. *J. Immunol.* **2003**, 1635.
8. d'Ostiani, C. F. *J. Exp. Med.* **2000**, 191, 1661.
9. Geijtenbeek, T. B. H.; van Kooyk, Y. *APMIS* **2003**, 111, 698.
10. van Kooyk, Y.; Geijtenbeek, T. B. H. *Nat. Rev. Immunol.* **2003**, 3, 697.
11. Gringhuis, S. I.; den Dunnen, J.; Litjens, M.; Hof, B. V.; van Kooyk, Y.; Geijtenbeek, T. B. H. *Immunity* **2007**, 26, 605.
12. van Vliet, S. J.; den Dunnen, J.; Gringhuis, S. I.; Geijtenbeek, T. B. H.; van Kooyk, Y. *Curr. Opin. Immunol.* **2007**, 19, 435.
13. Gringhuis, S. I.; Geijtenbeek, T. B. H. *Methods in Enzymology, Vol 480: Glycobiology* **2010**, 480, 151.
14. Anderluh, M.; Jug, G.; Svajger, U.; Obermajer, N. *Curr. Med. Chem.* **2012**, 19, 992.
15. Bashirova, A. A.; Wu, L.; Cheng, J.; Martin, T. D.; Martin, M. P.; Benveniste, R. E.; Lifson, J. D.; KewalRamani, V. N.; Hughes, A.; Carrington, M. *J. Virol.* **2003**, 77, 217.
16. Hong, P. W. *J. Virol.* **2002**, 76, 12855.
17. Turville, S. G. *Blood* **2001**, 98, 2482.
18. Chung, N. P. Y.; Breun, S. K. J.; Bashirova, A.; Baumann, J. G.; Martin, T. D.; Karamchandani, J. M.; Rausch, J. W.; Le Grice, S. F. J.; Wu, L.; Carrington, M.; KewalRamani, V. N. *J. Biol. Chem.* **2010**, 285, 2100.
19. de Witte, L.; Nabatov, A.; Geijtenbeek, T. B. H. *Trends Mol. Med.* **2008**, 14, 12.
20. Engering, A.; Van Vliet, S. J.; Geijtenbeek, T. B.; van Kooyk, Y. *Blood* **2002**, 100, 1780.
21. Geijtenbeek, T.; Torensma, R.; van Vliet, S.; van Duijnhoven, G.; Middel, J.; Cornelissen, I.; Adema, G.; Nottet, H.; Figdor, C.; van Kooyk, Y. *Blood* **1999**, 94, 434A.
22. Geijtenbeek, T. B. H. *Cell* **2000**, 100, 587.
23. Geijtenbeek, T. B. H.; van Kooyk, Y. *Dendritic Cells and Virus Infection* **2003**, 276, 31.
24. Alvarez, C. P. *J. Virol.* **2002**, 76, 6841.
25. Baribaud, F.; Doms, R. W.; Pohlmann, S. *Expert Opin. Ther. Targets* **2002**, 6, 423.
26. Lasala, F.; Arce, E.; Otero, J. R.; Rojo, J.; Delgado, R. *Antimicrob. Agents Chemother.* **2003**, 47, 3970.
27. van Die, I.; van Vliet, S. J.; Nyame, A. K.; Cummings, R. D.; Bank, C. M. C.; Appelmelk, B.; Geijtenbeek, T. B. H.; van Kooyk, Y. *Glycobiology* **2003**, 13, 471.

28. Naarding, M. A.; Ludwig, I. S.; Groot, F.; Berkhout, B.; Geijtenbeek, T. B. H.; Pollakis, G.; Paxton, W. A. *J. Clin. Invest.* **2005**, *115*, 3256.
29. Guo, Y.; Feinberg, H.; Conroy, E.; Mitchell, D.; Alvarez, R.; Blixt, O.; Taylor, M.; Weis, W.; Drickamer, K. *Nat. Struct. Mol. Biol.* **2004**, *11*, 591.
30. Van Liempt, E.; Imberty, A.; Bank, C. M. C.; Van Vliet, S. J.; Van Kooyk, Y.; Geijtenbeek, T. B. H.; Van Die, I. *J. Biol. Chem.* **2004**, *279*, 33161.
31. van Liempt, E.; Bank, C. M. C.; Mehta, P.; GarcI'a-Vallejo, J. J.; Kawar, Z. S.; Geyer, R.; Alvarez, R. A.; Cummings, R. D.; Kooyk, Y. v.; van Die, I. *FEBS Lett.* **2006**, *580*, 6123.
32. Ernst, B.; Magnani, J. L. *Nat. Rev. Drug Discovery* **2009**, *8*, 661.
33. Schwizer, D.; Patton, J. T.; Cutting, B.; Smiesko, M.; Wagner, B.; Kato, A.; Weckerle, C.; Binder, F. P. C.; Rabbani, S.; Schwarzdt, O.; Magnani, J. L.; Ernst, B. *Chem. Eur. J.* **2012**, *18*, 1342.
34. Binder, F. P.; Lemme, K.; Preston, R. C.; Ernst, B. *Angew. Chem. Int. Ed. Engl.* **2012**, *51*, 7327.
35. Tyrrell, D.; James, P.; Rao, N.; Foxall, C.; Abbas, S.; Dasgupta, F.; Nashed, M.; Hasegawa, A.; Kiso, M.; Asa, D. *Proc. Natl. Acad. Sci. U. S. A.* **1991**, *88*, 10372.
36. Prodger, J. C.; Bamford, M. J.; Bird, M. I.; Gore, P. M.; Holmes, D. S.; Priest, R.; Saez, V. *Bioorg. Med. Chem.* **1996**, *4*, 793.
37. Thoma, G.; Magnani, J. L.; Patton, J. T.; Ernst, B.; Jahnke, W. *Angew. Chem., Int. Ed.* **2001**, *40*, 1941.
38. Ernst, B.; Wagner, B.; Baisch, G.; Katopodis, A.; Winkler, T.; Ohrlein, R. *Can. J. Chem.* **2000**, *78*, 892.
39. Paul, S.; Jayaraman, N. *Carbohydrate Research* **2004**, *339*, 2197.
40. Lindberg, J.; Svensson, S.; Pahlsson, P.; Konradsson, P. *Tetrahedron* **2002**, 5109.
41. Steinman, R. A.; Johnson, D. E. *Blood* **1999**, *94*, 160B.
42. Agnihotri, G.; Tiwari, P.; Misra, A. K. *Carbohydr. Res.* **2005**, *340*, 1393.
43. Chao, C. S.; Li, C. W.; Chen, M. C.; Chang, S. S.; Mong, K. K. T. *Chem. Eur. J.* **2009**, *15*, 10972.
44. Glide. Schrödinger LLC: New York, 2011.
45. Timpano, G.; Tabarani, G.; Anderluh, M.; Invernizzi, D.; Vasile, F.; Potenza, D.; Nieto, P. M.; Rojo, J.; Fieschi, F.; Bernardi, A. *ChemBioChem* **2008**, *9*, 1921.
46. Andreini, M.; Doknic, D.; Sutkeviciute, I.; Reina, J. J.; Duan, J.; Chabrol, E.; Thepaut, M.; Moroni, E.; Doro, F.; Belvisi, L.; Weiser, J.; Rojo, J.; Fieschi, F.; Bernardi, A. *Org. Biomol. Chem.* **2011**, *9*, 5778.
47. Ambrosi, M.; Cameron, N. R.; Davis, B. G. *Org. Biomol. Chem.* **2005**, *3*, 1593.
48. Dam, T. K.; Brewer, C. F. In *Chem. Rev.: United States*, 2002; Vol. 102, pp. 387.
49. Toone, E. J. *Curr. Opin. Struct. Biol.* **1994**, *4*, 719.
50. Klebe, G.; Bohm, H. J. *J. Recept. Signal Transduct. Res.* **1997**, *17*, 459.
51. Lemieux, R. U. *Acc. Chem. Res.* **1996**, *29*, 373.
52. Holla, A.; Skerra, A. *Protein Eng. Des. Sel.* **2011**, *24*, 659.
53. Thoma, G.; Magnani, J. L.; Patton, J. T. *Bioorg. Med. Chem. Lett.* **2001**, *11*, 923.
54. Paul, S.; Jayaraman, N. *Carbohydr. Res.* **2008**, *343*, 453.
55. Paul, S.; Jayaraman, N. *Carbohydr. Res.* **2007**, *342*, 1305.
56. Jiang, J. Q.; Biggins, J. B.; Thorson, J. S. *J. Am. Chem. Soc.* **2000**, *122*, 6803.
57. Murase, T.; Kameyama, A.; Kartha, K. P. R.; Ishida, H.; Kiso, M.; Hasegawa, A. *J. Carbohydr. Chem.* **1989**, *8*, 265.
58. Nikolaev, A.; Watt, G.; Ferguson, M.; Brimacombe, J. *J. Chem. Soc. [Perkin 1]* **1997**, 969.

59. Hasegawa, A.; Ishida, H.; Nagahama, T.; Kiso, M. *J. Carbohydr. Chem.* **1993**, *12*, 703.
60. Hansen, H. C.; Magnusson, G. *Carbohydr. Res.* **1998**, *307*, 233.
61. Komba, S.; Ishida, H.; Kiso, M.; Hasegawa, A. *Glycoconjugate J.* **1996**, *13*, 241.
62. Paulsen, H.; Rutz, V.; Brockhausen, I. *Liebigs Ann. Chem.* **1992**, 735.
63. Jorgensen, W. L. *In Encyclopedia of Computational Chemistry*; Schleyer, P. v. R., Ed.; Wiley: New York, 1998; Vol. 2, pp. 1061.
64. Kollman, P. *Chem. Rev.* **1993**, *93*, 2395.
65. Bowers, K. J.; Chow, E.; Xu, H.; Dror, R. O.; Eastwood, M. P.; Gregersen, B. A.; Klepeis, J. L.; Kolossvary, I.; Moraes, M. A.; Sacerdoti, F. D.; Salmon, J. K.; Shan, Y.; Shaw, D. E. *In Proceedings of the 2006 ACM/IEEE conference on Supercomputing*; ACM: Tampa, Florida, 2006, 84.
66. Jorgensen, W. L.; Chandrasekhar, J.; Madura, J. D.; Impey, R. W.; Klein, M. L. *J. Chem. Phys.* **1983**, *79*, 926.
67. Ryckaert, J. P.; Ciccotti, G.; Berendsen, H. J. C. *J. Comput. Phys.* **1977**, *23*, 327.
68. Martyna, G. J.; Tobias, D. J.; Klein, M. L. *J. Chem. Phys.* **1994**, *101*, 4177.
69. Nosé, S. *Mol. Phys.* **1984**, *52*, 255.

2.3.1.1 Synthesis of (1R,2R,3S)-3-methyl-cyclohexane-1,2-diol as D-GlcNAc mimic

The D-GlcNAc mimic **3**, used for the synthesis of Le^x trissacchride mimics (chapter 2.3.1), was synthesized according to a procedure developed by Daniel Schwizer, a former coworker, in the course of his PhD thesis.¹ Starting from cyclohex-2-en-one (**2**) the D-GlcNAc mimic **3** is accessible in a 6-step synthesis (Scheme 1). By bromination of the starting material **2** a sterically demanding group was introduced in α -position (\rightarrow **2.1**). Subsequent Corey-Bakshi-Shibata reduction led to alcohol **2.2** stereoselectively. After halogen-metal exchange with *tert*-BuLi and subsequent hydrolysis, the obtained secondary alcohol (*R*)-**2.3** was tritylated to give **2.4**. Epoxidation of compound **2.4** with *m*-chloroperoxybenzoic acid yielded epoxide **2.5** with an anti-preference (syn:anti \approx 7:3). The nucleophilic opening of epoxide **2.5** by higher-order cyanocuprate Me₂Cu(CN)Li₂ in presence of BF₃·Et₂O afforded **3** in high yields. Fucosylation of the D-GlcNAc mimic **3** with fucosyl donor **4**^{2,3} was performed under *in situ* anomerization conditions to yield predominantly the α -fucoside. Detritylation of the cyclohexane derivative **3.1** in presence of ZnBr₂ as mild Lewis acid and triethylsilane (TES) as trityl cation scavenger yielded the α -fucoside **5**.



Scheme 1. a) *i*) Br₂, CH₂Cl₂, 0°C, 2.5 h, *ii*) Et₃N, CH₂Cl₂, r.t., 2 h, 64%; b) (*S*)- α , α -diphenyl-prolinol, B(OMe)₃, BH₃·*N,N*-diethylaniline, THF, -10°C-0°C, 3.75 h, 93% (96% ee); c) *i*) *t*-BuLi, Et₂O, -78°C to -20°C, 4.75 h, *ii*) aq. NaHCO₃, -20°C-r.t., 1 h, 87%; d) Ph₃CCl, CH₂Cl₂, DBU, r.t., 12 h, 79%; e) *m*-CPBA, NaHCO₃, CH₂Cl₂; 0°C-r.t., 5 h, 70% f) MeLi, CuCN, BF₃·Et₂O, THF, -78°C to -30°C, 5-8 h, 96% g) TBAB, 2,6-di-*tert*-butyl-4-methylpyridine, MS 4Å, CuBr₂, DMF, CH₂Cl₂, r.t., 20 h, 43%; h) ZnBr₂, TES, CH₂Cl₂, r.t., 10 h, 63%.

References

1. Schwizer, D. et al. Pre-organization of the Core Structure of E-Selectin Antagonists. *Chem. Eur. J.* **18**, 1342-1351 (2012).
2. Ernst, B., Wagner, B., Baisch, G., Katopodis, A., Winkler, T. & Ohrlein, R. Substrate specificity of fucosyl transferase III: An efficient synthesis of sialyl Lewis(x)-, sialyl Lewis(a)-derivatives and mimetics thereof. *Can. J. Chem.* **78**, 892-904 (2000).
3. Prodger, J.C., Bamford, M.J., Bird, M.I., Gore, P.M., Holmes, D.S., Priest, R. & Saez, V. Mimics of the sialyl Lewis X tetrasaccharide. Replacement of the N-Acetylglucosamine sugar with simple C2-symmetric 1,2-diols. *Bioorg. Med. Chem.* **4**, 793-801 (1996).

2.3.2 (1*R*,2*R*)-cyclohexadiol as D-GlcNAc mimic

In a previous study (chapter 2.3.1) we identified (1*R*,2*R*,3*S*)-methylcyclohexadiol as a feasible replacement for D-GlcNAc in Le^x leading to a moderate improvement in affinity. However, the thermodynamic profile indicated non-optimal properties. Despite a gain in enthalpy ($\Delta\Delta H \approx -7.6$ kJ/mol), this replacement was accompanied by an unfavorable entropic term ($-T\Delta\Delta S \approx 6.3$ kJ/mol). For DC-SIGN, the concept of preorganization^{1,2} as realized for the Le^x mimic **2**^{*} was outranged by desolvation effects.

Since a cyclohexadiol-based mimic was shown to be more flexible, i.e. less preorganized compared to a methylcyclohexadiol-based,³ mimic **3** with (1*R*,2*R*)-cyclohexadiol replacing D-GlcNAc was synthesized (Figure 1).

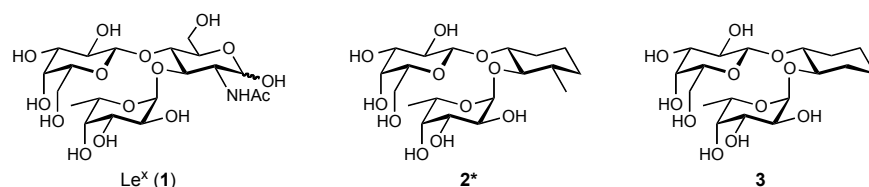
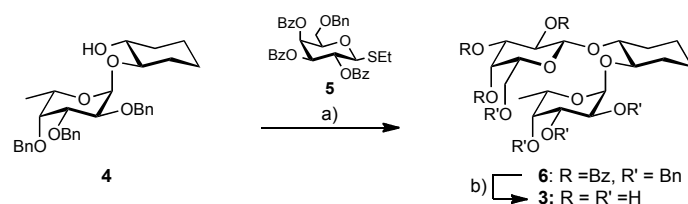


Figure 1. Le^x (**1**) and two Le^x mimics with (1*R*,2*R*,3*S*)-methylcyclohexadiol (\rightarrow **2**^{*}) and (1*R*,2*R*)-cyclohexadiol (\rightarrow **3**) as replacement for GlcNAc.

Trisaccharide mimic **3** was synthesized from pseudo-disaccharide **4**⁴ that was glycosylated β -selectively with galactosyl donor **5**⁵ using DMTST as promoter. Removal of benzoyl groups under *Zemplén* conditions and hydrogenolytic cleavage of benzyl groups yielded mimic **3** (Scheme 1).

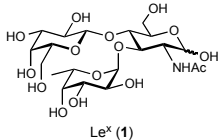
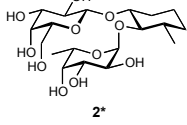
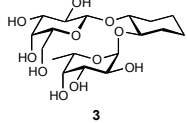


Scheme 1. a) Glycosyl acceptor **4**⁴ and donor **5**⁵, DMTST, MS4Å, CH₂Cl₂, r.t., 16 h; b) i) NaOMe, MeOH, 5 h; ii) Pd(OH)₂/C, dioxane/water, 6 h; 22% over three steps.

Mimic **3** was tested for affinity towards DC-SIGN in a target-based, competitive binding assay and by ITC experiments. The results are listed in Table 1 with data of Le^x (**1**) and the respective methylcyclohexadiol bearing mimic **2**^{*} for comparison.

* identical with **8** in chapter 2.3.1

Table 1. Results of the competitive polymer binding assay with DC-SIGN CRD and Le^a-PAA as competitor. ITC experiments were performed at 278 K with DC-SIGN CRD.

Entry	Structure	IC_{50} [mM]	K_D [μ M]	ΔG [kJ/mol]	ΔH [kJ/mol]	$-T\Delta S$ [kJ/mol]
1		3.8 (n=1)	1068 ± 13 (n=2)	-17.0 ± 0.0	-23.8 ± 0.3	6.9 ± 0.3
2		1.9 ± 0.4	645	-18.2 ± 0.5	-31.4	+13.2
3		0.7 ± 0.2	445	-19.1	-32.9	+13.8

As discussed in chapter 2.3.1, the exchange of D-GlcNAc in Le^x (**1**) by (1*R*,2*R*,3*S*)-methylcyclohexadiol (\rightarrow **2**^{*}) entailed an improvement in affinity by a factor of two. With mimic **3** a further improvement in affinity compared to **2**^{*} (0.7 mM vs. 1.9 mM, respectively) was observed (Table 1). ITC experiments reveal a less pronounced effect with a K_D of 445 μ M for **3** compared to 645 μ M for **2**^{*}.

The thermodynamic profile of **3** resembles the results found for **2**^{*}. Neither the enthalpic, nor the entropic contributions are significantly different. The cyclohexadiol derivative **3** is assumed to be more flexible.^{2,3,6} The degree of preorganization seems to be not relevant and with respect to **3** rather counterproductive for binding to DC-SIGN.

In summary, this example illustrates the complexity in designing the proper mimic for a solvent-exposed binding site, such as in DC-SIGN. The replacement of D-GlcNAc by a simple cyclohexyl moiety is obviously effective in terms of conformational freedom and gain in affinity. Further optimization of this moiety should be directed towards improvement of solvation properties.

* identical with **8** in chapter 2.3.1

EXPERIMENTAL SECTION

General Methods: see chapter 2.3.1

Synthesis of (1*R*,2*R*)-2-hydroxycyclohexyl-2,3,4-tris-*O*-benzyl-6-deoxy- α -L-galactopyranoside **4** was done by a co-worker (R.O. Duthaler) according to a published procedure.⁴

(1*R*,2*R*)-1-*O*-(2,3,4-Tri-*O*-benzoyl-6-*O*-benzyl- β -D-galactosyl)-2-*O*-(2,3,4-tri-*O*-benzyl-6-deoxy- α -L-galactosyl)-cyclohexane-1,2-diol (6**)**

Compound **4** (107 mg, 0.2 mmol) and **5** (163 mg, 1.3 eq. 0.26 mmol) were dissolved in anhydrous CH₂Cl₂ (4.0 ml). Powdered activated molecular sieves 4Å (0.4 g) were added and the mixture was stirred at r.t. under argon. After 3.5 h, a solution of DMTST (155 mg, 3 eq, 0.6 mmol) in anhydrous CH₂Cl₂ (1.5 mL) that had been stirred with molecular sieves 4Å (0.15 g) for 3.5 h, was added. After stirring for 30h, the solution was diluted with CH₂Cl₂ (30 ml), filtered, and successively washed with satd. aq. NaHCO₃ (50 ml) and brine (50 ml). The aqueous layers were extracted with CH₂Cl₂ (2x 50 ml) and the combined organic layers were dried over Na₂SO₄ and concentrated under reduced pressure. The crude product was purified by column chromatography (PE/MTBE, gradient) to afford an unseperable mixture of unreacted starting material and the trisaccharide mimic **6**. This mixture was directly used for the next step.

(1*R*,2*R*)-1-*O*-(β -D-galactosyl)-2-*O*-(α -L-fucosyl)-cyclohexane-1,2-diol (6**)**

Intermediate **6** (100 mg) was dissolved in MeOH (1 ml) and a catalytic amount of NaOMe (1M methanolic solution) was added at r.t. After stirring for 2h the mixture was neutralized with AcOH and evaporated. The residue was purified by column chromatography on silica gel (PE/EtOAc) and used for the next step.

A mixture of debenzoylated intermediate and Pd(OH)₂/C (10%) in dioxane/water (4:1, 1.5 ml) was treated with H₂ (atm. pressure) overnight. The reaction mixture was filtered over celite. The celite was washed with MeOH (15 ml). The filtrate was evaporated to dryness. The residue was purified by column chromatography on silica gel (DCM/MeOH, 1:0 →10:4) and to yield **3** (19 mg, 22% over 3 steps). For biological assays the product was further purified by preparative RP-HPLC.

[α]_D²⁰ -119.4 (*c* 0.14, MeOH); ¹H-NMR (500 MHz, MeOD): δ 4.89 (Fuc-H1), 4.61 (dd, *J* = 13.1, 6.5 Hz, 1H, Fuc-H5), 4.31 (m, 1H, Gal-H1), 3.89 (dd, *J* = 10.1, 3.3 Hz, 1H, Gal-H3),

3.84 (s, 1H, Gal-H4), 3.82 – 3.65 (m, 5H, Cy-H, Fuc-H2, Fuc-H4, Gal-H6), 3.58 (td, $J = 9.3$, 4.4 Hz, 1H, Cy-H), 3.53 – 3.43 (m, 3H, Fuc-H3, Gal-H2, Gal-H5), 2.07 (d, $J = 2.5$ Hz, 2H, Cy), 1.80 – 1.66 (m, 2H, Cy), 1.48 – 1.23 (m, 4H, Cy), 1.21 (d, $J = 6.6$ Hz, 3H, Fuc-H6); ^{13}C -NMR (126 MHz, MeOD) δ : 102.64 (Gal-C1), 97.26 (Fuc-C1), 79.23, 77.40 (Cy-C1, Cy-C2), 76.48, 74.97, 73.80, 72.67, 71.56, 70.22, 70.01 (Fuc-C2, Fuc-C3, Fuc-C4, Gal-C2, Gal-C3, Gal-C4, Gal-C5), 67.43 (Fuc-C5), 62.84 (Gal-C6), 30.84, 29.97, 24.38, 24.35 (Cy), 16.56 (Fuc-C6); HR-MS: m/z calcd for $\text{C}_{18}\text{H}_{32}\text{O}_{11}$ $[\text{M}+\text{Na}]^+$: 447.1837, found: 447.1843.

Biological evaluation

Polymer binding assays and ITC experiments with DC-SIGN CRD-Fc were performed as described in chapter 2.3.1 by Meike Scharenberg, and Roland Preston, respectively (at the Institute of Molecular Pharmacy, University of Basel).

References

1. Kolb, H.C. & Ernst, B. Development of tools for the design of selectin antagonists. *Chem.--Eur. J.* **3**, 1571-1578 (1997).
2. Thoma, G., Magnani, J.L., Patton, J.T., Ernst, B. & Jahnke, W. Preorganization of the bioactive conformation of sialyl Lewis(X) analogues correlates with their affinity to E-selectin. *Angew. Chem., Int. Ed.* **40**, 1941-1945 (2001).
3. Schwizer, D. et al. Pre-organization of the core structure of E-selectin antagonists. *Chemistry* **18**, 1342-51 (2012).
4. Bamford, M.J. et al. Synthesis and biological activity of conformationally constrained sialyl Lewis X analogues with reduced carbohydrate character. *Bioorg. Med. Chem. Lett.* **6**, 239-244 (1996).
5. Prodger, J.C. et al. Mimics of the sialyl Lewis X tetrasaccharide. Replacement of the N-Acetylglucosamine sugar with simple C2-symmetric 1,2-diols. *Bioorg. Med. Chem.* **4**, 793-801 (1996).
6. Binder, F.P.C., Lemme, K., Preston, R.C. & Ernst, B. Sialyl Lewisx: A "Pre-Organized Water Oligomer"? *Angew. Chem., Int. Ed.* **51**, 7327-7331 (2012).

2.3.3 Synthesis of tetrahydropyran-based DC-SIGN antagonists

BACKGROUND

Binding of monovalent oligosaccharides to DC-SIGN is of weak nature. DC-SIGN recognizes mannosidic as well as fucosidic ligands. As a consequence of the shallow, solvent-exposed binding pocket offered by DC-SIGN, ligands are bound in multiple binding poses.^{1,2} Therefore, the design of high-affinity ligands is still a challenging task.

Our analysis of binding modes of Lewis antigens with different aglycones (chapter 2.2.1) demonstrated that Le^a and Le^x bearing a phenyl moiety are able to establish an additional hydrophobic contact with Phe313 (Figure 1). During our studies, other research groups discovered as well the potential of this interaction to improve affinity of mannose- and fucose-based antagonists. Consequently, studies on introducing different residues allowing for an interaction with the hydrophobic cleft lined by Phe313 and Lys371 were initiated.³⁻⁵ Addressing this site is also related to selectivity of DC-SIGN antagonists and presents therewith an additional benefit.⁴

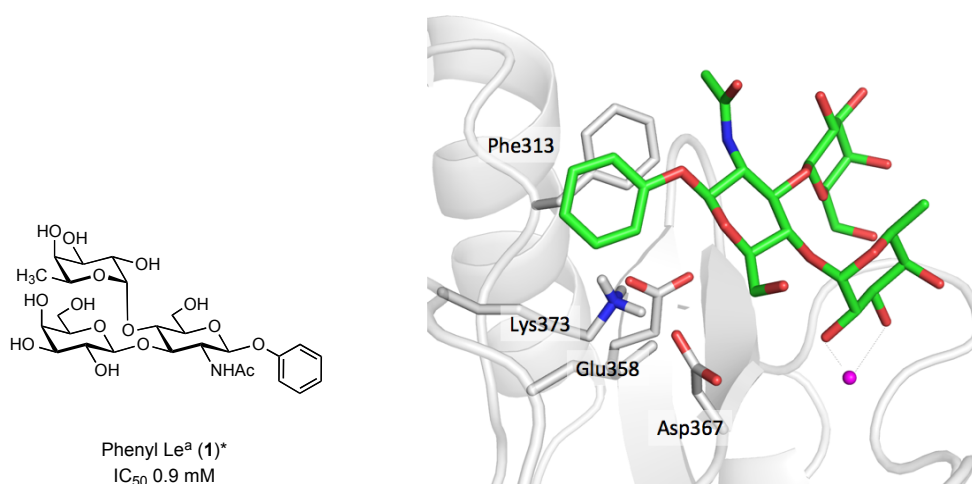
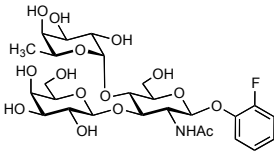
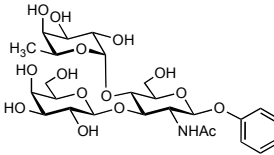
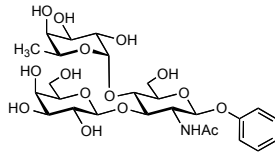


Figure 1. Structure of phenyl Le^a (**1**)* and binding mode derived from docking to the crystal structure of DC-SIGN (PDB 1SL5⁶, Sameh Eid, Institute of Molecular Pharmacy, University of Basel). The phenyl aglycone addresses the hydrophobic cleft formed by Phe313 and Leu371, the GlcNAc moiety is arranged in proximity to protein surface.

* identical with compound **4** in chapter 2.2.1

To investigate the nature of the π - π -interaction, we determined the binding affinity of a Le^a derivative bearing an electron-rich *p*-methoxyphenyl aglycone (Arjan Odedra, Institute of Molecular Pharmacy, University of Basel). This compound exhibited a twofold lower affinity to DC-SIGN CRD than phenyl Le^a (**1**) (competitive polymer assay performed by Meike Scharenberg, Institute of Molecular Pharmacy, University of Basel). This can be ascribed to weaker interaction of the aromatic moiety of the ligand with Phe313 and Lys373. Consequently, electron-withdrawing groups were considered favorable. Free energy perturbation (FEP) simulations were initiated to support this hypothesis (Table 1). These calculations indicate for derivatives of phenyl Le^a that both *o*- and *m*-fluoro-substitutions (**2** and **3**) at the phenyl aglycone are associated with improvement of interaction energy.

Table 1. FEP calculation of fluorophenyl Le^a derivatives. Changes in free energy of binding are given relative to phenyl Le^a (**1**). More negative values indicate a gain in affinity.

			
	<i>o</i> -Fluorophenyl Le ^a (2)	<i>m</i> -Fluorophenyl Le ^a (3)	<i>p</i> -Fluorophenyl Le ^a (4)
$\Delta\Delta G_{FEP}$ [kcal/mol]	-2.3 ± 0.3	-2.7 ± 0.3	$+1.6 \pm 0.3$

Based on these data, we designed a new series of DC-SIGN antagonists (Figure 2). As we previously exchanged the D-GlcNAc moiety with an improvement in affinity (chapter 3.2.1 and 3.2.2) we applied the same approach with this series. Consequently, an appropriate D-GlcNAc mimic as well as an aromatic moiety capable of addressing Phe313 were introduced.

We decided to start from a glucal-derived D-GlcNAc mimic which allows introduction of different aromatic moieties via amide coupling in a late step of the synthesis (Schemes 1 and 2). Our starting point for choosing an aromatic moiety were the FEP simulations of phenyl Le^a derivatives (Table 1), indicating *m*-fluoro-substituted phenyl residue to be most beneficial. Crystallographic data derived for various ligands binding to DC-SIGN imply Phe313 to be a rather flexible residue, able to adjust its orientation.⁷ Hence, the binding site is supposed to be flexible enough to orient the phenyl ring in fluoroanilides **5**, **6**, and **7** (Figure 2) close to Phe313.

In order to investigate effects of D-Gal in this series and the novel “lying” binding mode (described in chapter 2.2.1), D-Gal (**6**), hydroxyl (**5**) and hydrogen (**7**) at 3-position of the hexon amide based D-GlcNAc mimic were studied.

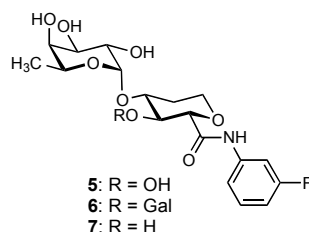
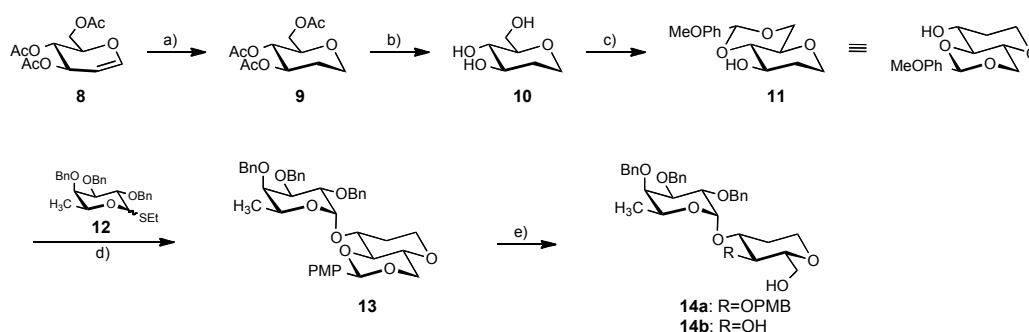


Figure 2. General structure of amides.

RESULTS AND DISCUSSION

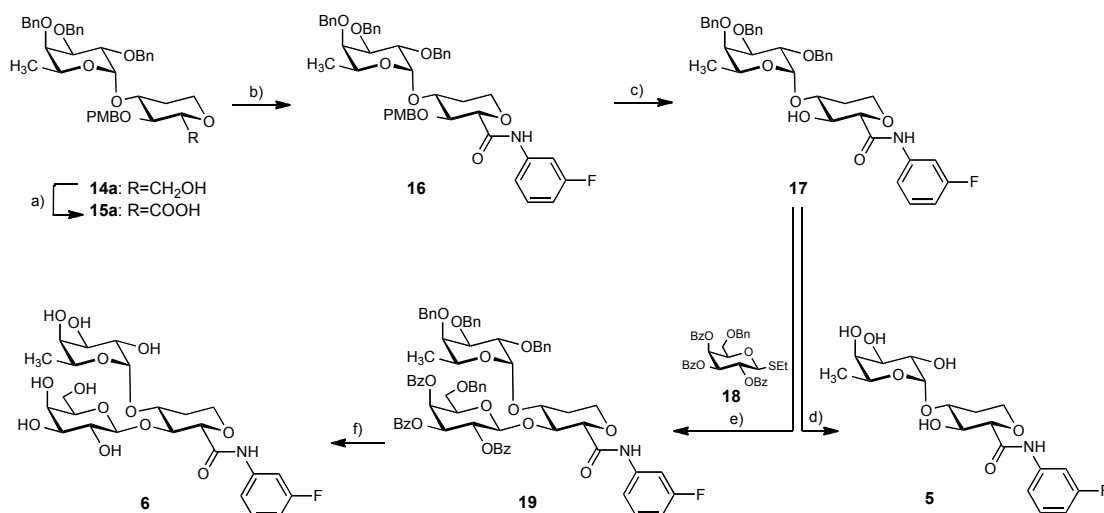
Synthesis of glucal building block⁸

Starting from the peracetylated glucal **8**, intermediate **11** was synthesized following a published procedure.⁸ Building block **11** was reacted with ethyl thiofucoside **12**⁹ under *Ogawa* conditions to yield **13** in up to 90% yield.¹⁰ Opening of the anisylidene acetal with $\text{NaCNBH}_3/\text{TMSCl}$ and $\text{BH}_3\cdot\text{THF}/\text{TMSOTf}$ as suggested by Spohr *et al.*⁸ yielded a mixture of 4-OH, 6-OH and 4,6-di-OH derivatives in an approximate 1:1:1 ratio. Regioselectivity could be improved with *n*- $\text{Bu}_2\text{BOTf}/\text{BH}_3\cdot\text{THF}$, leading predominantly to the formation of the 6-OH compound **14a**.¹¹ However, during work-up the dihydroxy derivative **14b** was formed in equal amount. Different work-up methods failed to improve this ratio.



Scheme 1. a) Pd/C, H_2 , EtOH/EtOAc 1:1, 4 h, quant.; b) NaOMe, MeOH, r.t. 12-24 h, 98%; c) 4-methoxybenzaldehyde dimethyl acetal, DMF, camphor sulfonic acid, 40°C, 12 h, 69%; d) TBAB, 2,6-di-*tert*-butyl-4-methylpyridine, MS 3Å, CuBr_2 , DMF, CH_2Cl_2 , r.t., 20 h, 76%; e) Bu_2BOTf , $\text{BH}_3\cdot\text{THF}$, 0°C, 1h, 72% of **14a**, 22% of **14b**.

Synthesis of anilides **5** and **6**



Scheme 2. a) TEMPO, NaOCl, NaBr, TBAB, NaHCO₃, r.t., 1h, 87%; b) DIC, HOBt, 73%; c) CAN, CH₃CN/H₂O (9:1), r.t., 44%; d) *i*) Pd(OH)₂/C, dioxane/H₂O, 52%; e) DMTST, MS 4Å, CH₂Cl₂, r.t., 12 h, 68%; f) *i*) Pd(OH)₂/C, dioxane/H₂O, *ii*) NaOMe, MeOH, 53%.

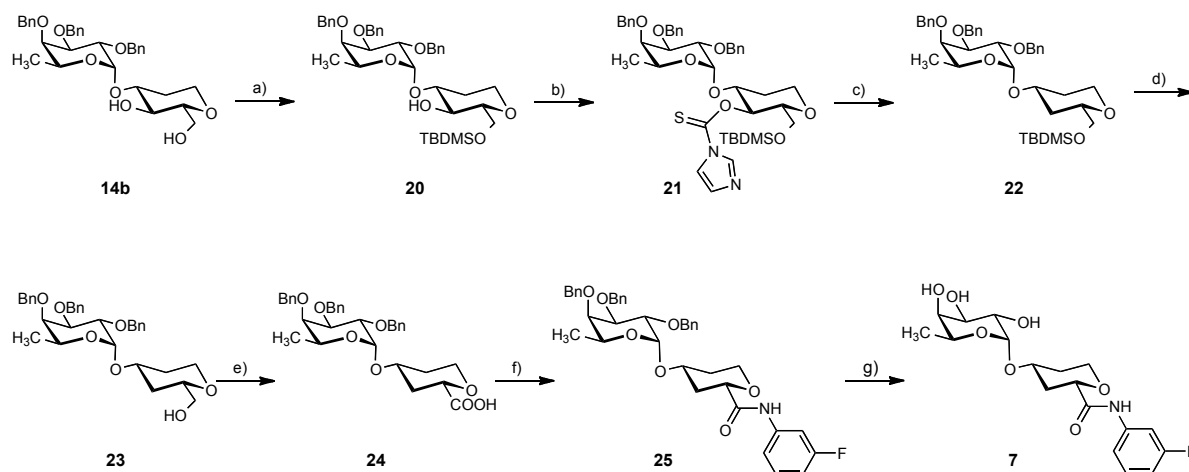
Following a procedure from Huang *et al.*¹⁷ the free 6-OH group was oxidized using 2,2,6,6-tetra-methylpiperidine-1-oxyl (TEMPO) and NaOCl. Spectroscopic characterization of the 4-*O*-PMB-6-COOH derivative **15a** was not possible most likely due to TEMPO remainders that could not be removed by excessive chromatographic purification. Direct transformation into the amide using standard coupling reagents yielded the 3-fluoro-anilide **16** in moderate yield. The PMB protection group was removed by treatment with ceric ammonium nitrate (CAN) to give **17**. Further hydrogenolytic cleavage of the benzyl groups afforded test compound **5**. Coupling of **17** with galactosyl donor **18**⁹ using dimethyl(methylthio)sulfonium triflate (DMTST) as promoter gave after deprotection test compound **6**.

Synthesis of deoxy derivative **7**

The attempt to access the deoxy derivative **7** via deoxygenation of compound **17** using Barton McCombie deoxygenation conditions failed, probably because transformation into the thiocarbonyl derivative is sterically and electronically disfavored. Therefore, the deoxygenated derivative was synthesized according to Scheme 3. The dihydroxy derivative **14b** was protected selectively in 6-*O*-position with TBDMS. **20** was transformed into the

imidazolylthiocarbonyl derivative (\rightarrow **21**) and deoxygenated with tributyltinhydride according to standard Barton McCombie deoxygenation conditions (\rightarrow **22**).

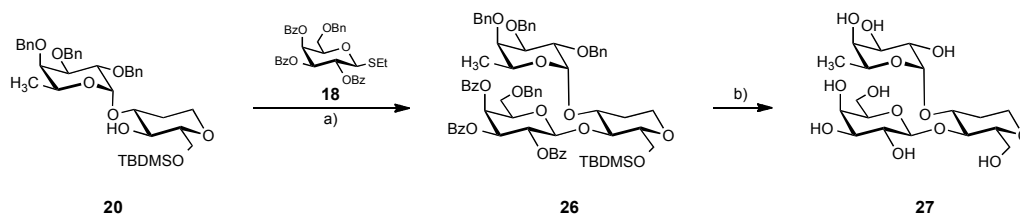
Deprotection of **22** yielded the 6-OH derivative (**23**) in 80% yield. Oxidation with TEMPO/NaOCl gave carboxylic acid **24** which was reacted with *m*-fluoroaniline to give amide **25**. Final deprotection led to the anilide **7**.



Scheme 3. a) TBDMSCl, Et₃N, pyridine, r.t., 1-3h, 73%; b) TCDI, DMAP, C₄H₄Cl₂, 6h, δ , 55%; c) Bu₃SnH, AIBN, PhCH₃, 4h, δ , 80%; d) TBAF, AcOH, THF, 10h, r.t., 40-80%; e) TEMPO, NaOCl, NaBr, TBAB, NaHCO₃, r.t., 1h, 75%; f) DIC, HOBT, DIPEA, CH₂Cl₂/DMF (1:1), 0°C, 12h, 65%; g) Pd(OH)₂/C, H₂ (atm.) dioxane/H₂O (4:1), 67%;

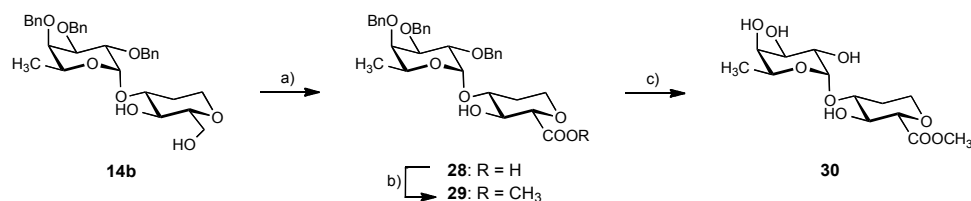
Synthesis of alcohol **27** and ester **30**

In addition to the three anilides, two compounds without aromatic moiety were synthesized. Compound **27** was obtained as outlined in Scheme 4. The silylether derivative **20** was glycosylated with **18**⁹ using DMTST to give primarily the β -galactoside **26**. Cleavage of the silyl ether with TBAF, hydrogenolytic cleavage of benzyl groups, and removal of benzoyl groups under *Zemplén* conditions yielded **27**.



Scheme 4. a) DMTST, 12h, r.t., 63%; b) i) TBAF; ii) NaOMe, methanol, r.t., 1h; iii) Pd(OH)₂/C, H₂ (atm. pressure), dioxane/water (4:1), 12h, 24%;

The methyl ester was obtained via esterification of the carboxylic acid of **14b** with *trimethylsilyldiazomethane* and subsequent deprotection of benzyl groups (Scheme 5).



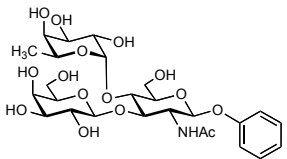
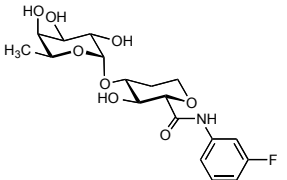
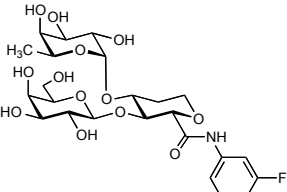
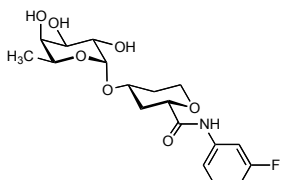
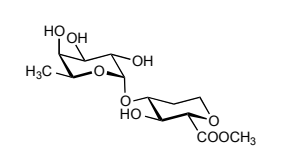
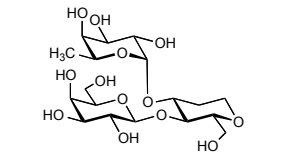
Scheme 5. a) TEMPO, NaOCl, NaBr, TBAB, NaHCO₃, r.t., 1h, 62 %; b) TMSCHN₂, toluene/methanol (3:2), r.t., 10h, 59%; b) Pd(OH)₂/C, H₂ (atm. pressure), dioxane/water (4:1), 12h, 53%;

Biological evaluation

Table 1 summarizes the results from a competitive polymer binding assay with DC-SIGN CRD-Fc vs. Le^a-polyacrylamide (performed by Meike Scharenberg, Institute of Molecular Pharmacy, University of Basel). These affinity data indicate no significant improvement of binding affinity originating from the fluorophenyl moiety. However, the results further support the assumption that the D-Gal moiety is indeed not crucial for binding.

Anilides **5**, **6**, and **7** have affinities around 1.1 mM, the respective methyl ester analogue **30** exhibits the same affinity. A slight improvement was detected for the trisaccharide mimic **27**. As a matter of fact, data for compound **27** are in accordance with the previous cyclohexadiol mimic (chapter 2.3.3). Most likely, this compound binds in the upright binding mode known from co-crystallization of LNFP III (Le^x) with DC-SIGN.⁶

Table 1. IC₅₀ values and relative IC₅₀ values with phenyl Le^a (**1**) as reference for binding to DC-SIGN CRD-Fc. (determined by Meike Scharenberg, University of Basel).

Compound No.	Structure	IC ₅₀ [mM]	rIC ₅₀
Phenyl Le ^a (1)		0.9	1
5		1.2 ± 0.8 (n=3)	1.3
6		1.1 ± 0.2 (n=2)	1.2
7		1 ± 0.5 (n=3)	1.1
30		1.1 ± 0.1 (n=2)	1.2
27		0.5 ± 0.2 (n=2)	0.7

Our initial assumption for synthesis of this series was a comparable binding mode of compounds **5**, **6**, **7**, and phenyl Le^a (**1**). However, docking studies revealed a complex picture with diverse binding modes for these structures (Sameh Eid, Institute of Molecular Pharmacy, University of Basel).

Figure 3 displays the top-ranked binding poses of **1** and **5**. Both adopt an overall similar orientation with coordination of Ca²⁺ via 2- and 3-OH of L-Fuc. However, the phenyl moiety of mimic **5** is suboptimally arranged resulting in poor interaction with Phe313. Consequently, the affinity towards DC-SIGN is not improved.

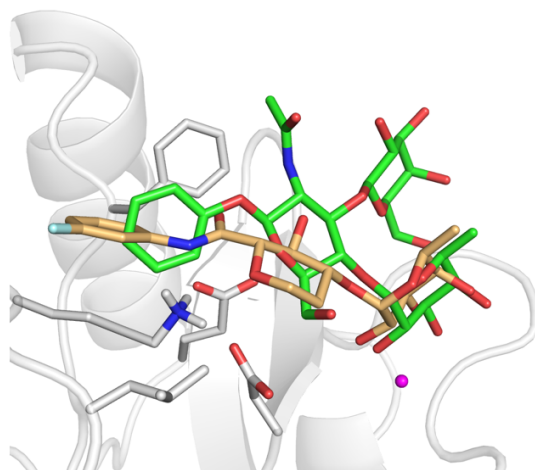


Figure 3. Overlay of top-ranked docking poses for phenyl Le^a (**1**, green carbons) and anilide **5** (orange carbons) derived by automated docking with DC-SIGN (PDB 1SL5⁶, Sameh Eid, University of Basel). The Ca²⁺ is illustrated as magenta sphere.

Compound **30** adopts an equal position as **5** (Figure 4). Despite no phenyl moiety being present in this mimic, the “lying” binding mode is favored. The D-GlcNAc mimic adopts an inverted orientation compared to **5**, which allows a van der Waals contact of its lipophilic part with Phe313. Additionally, H-bonds can be established via the hydroxyl and the ester group with the protein (not shown).

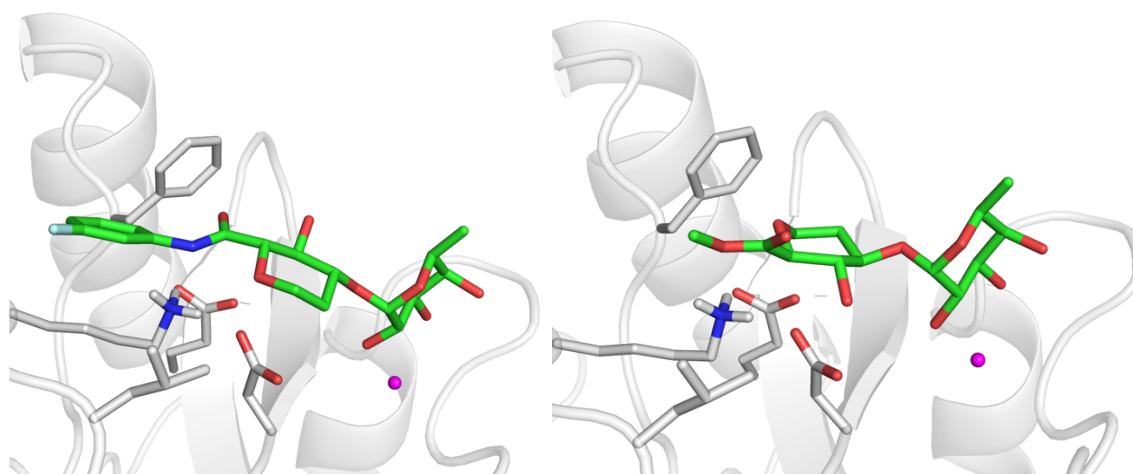


Figure 4. Comparison of top-ranked docking modes found for **5** (left) and **30** (right) obtained by automated docking with DC-SIGN CRD (PDB 1SL5⁶, Sameh Eid, University of Basel). Mimics are oriented similarly, i.e. L-Fuc coordinates the Ca²⁺ (magenta sphere) via 2- and 3-OH. In **30** van der Waals contacts with Phe313 are established via the D-GlcNAc mimic.

Mimic **6** that shows the closest resemblance to **1**, surprisingly, adopts favorably the upright binding position as seen for Le^x (Figure 5).⁶ In contrast to D-GlcNAc, the tetrahydropyran-

based mimic can not establish H-bond interactions with the protein, additionally the orientation of the phenyl moiety is non-optimal in the lying binding mode, resulting in the preference of an upright binding position. In this orientation compound **6** can form a H-bond network similar as seen for Le^x (Chapters 2.1 and 2.2.1), via its terminal D-Gal moiety. The deoxy mimic **7** revealed a top-ranked binding mode not related to any of the other binding modes (not shown).

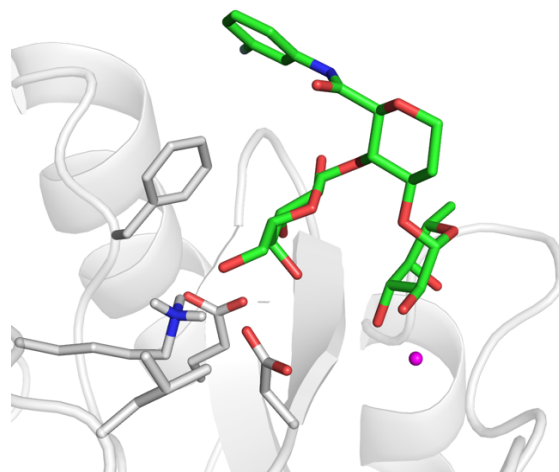


Figure 5. Mimic **6** docked into DC-SIGN CRD (PDB 1SL5⁶, Sameh Eid, University of Basel) preferably adopts an upright binding position allowing interaction with DC-SIGN via Fuc and Gal

Ultimately, coordination of calcium by L-Fuc is the only consistency in this series. Due to the poor interaction with Phe313 in the mimic series, the binding mode is adjusted individually by each ligand. The assumed advantageous contribution of a fluoro substituent, hence, could not be shown.

In summary, this series of anilides (**5**, **6**, **7**) presents no significant advantage over phenyl Le^a or other phenyl-lacking DC-SIGN antagonists (e.g. **27** and **30**). Yet, despite the non-optimal arrangement of these compounds affinities were comparable to **1**. The exchange of D-GlcNAc for a tetrahydropyran-based mimic is therewith feasible. Furthermore, affinity data for this series of compounds substantiates the insignificance of D-Gal for binding.

CONCLUSION

The shallow binding site of DC-SIGN accommodates different types of oligosaccharides in different binding modes.^{1,12} As found previously, the introduction of a phenyl aglycone leads to improved affinity for Le^a. When these findings were applied in this new series of DC-SIGN ligands, no further improvement of affinity was achieved. In spite of the flexibility of the DC-SIGN binding site and the ligands, the aromatic moiety present in this series could not be optimally positioned resulting in a poor interaction with Phe313. This led to different binding modes for each of the hexon amide derivatives.

Other researchers follow the same approach and address this hydrophobic cleft by according modifications of L-Fuc and D-Man-based monovalent ligands.^{4,5,13} Though, to the best of our knowledge, up to now no high-affine monovalent, carbohydrate-based ligands for DC-SIGN have been developed. Our series of compounds demonstrates the challenge of developing monovalent high-affinity antagonists for DC-SIGN. Crucial for the design of such ligands, is a comprehensive amount of experimental data, such as affinity data and crystallographic data.

EXPERIMENTAL SECTION

General Methods: Commercially available reagents were purchased from Fluka, Aldrich, Merck, and Abcr. Solvents were dried prior to use as indicated. Dichloromethane (CH₂Cl₂), 1,2-dichloroethane (DCE), and acetonitrile (MeCN) were dried by filtration over Al₂O₃ (Fluka, type 5016 A basic). DMF, pyridine, and toluene were dried by distillation from calcium hydride. Tetrahydrofuran (THF) was dried by distillation from sodium/benzophenone. Methanol (MeOH) was dried by refluxing with sodium methoxide and distilled immediately before use. Molecular sieves (3Å, 4Å) were activated under vacuum at 500°C for 1 h immediately before use. Reactions were monitored by TLC using glass plates coated with silica gel 60 F₂₅₄ (Merck) and visualized by using UV light and/or by charring with a molybdate solution (a 0.02 M solution of ammonium cerium sulfate dihydrate and ammonium molybdate tetrahydrate in aqueous 10% H₂SO₄). Column chromatography was performed on a CombiFlash Companion (Teledyne-ISCO, Inc.) using RediSep normal phase disposable flash columns (silica gel, 40-63 μm). Reversed phase chromatography was performed on LiChroprepRP-18 (Merck, 40-63 μm). LC-MS: separations were carried out using Sunfire C₁₈ columns (19 x 150 mm, 5.0 μm) on a Waters 2525 LC, equipped with Waters 2996 photodiode array and Waters micromass ZQ MS: for detection. Electron spray

ionization mass spectra (ESI-MS:) were obtained on a Waters micromass ZQ. HR-MS: analysis were carried out using a Agilent 1100 LC equipped with a photodiode array detector and a Micromass QTOF I equipped with a 4 GHz digital-time converter. Optical rotations were measured using Perkin-Elmer polarimeter 341. Microanalysis was performed at the Institute of Organic Chemistry at the University of Basel, Switzerland. Compound purity was determined on an Agilent 1200 HPLC; ELS detector, Waters 2420; column: Waters Atlantis dC18, 3 μ m, 4.6 x 75 mm; eluents: A: water + 0.1% TFA; B: 90% acetonitrile + 10% water + 0.1% TFA. Gradient A for compounds **5**, **6**, and **7**; linear gradient: 0 - 2 min 2% B; 2-15 min 2 to 50% B; 16 - 20 min 50 to 2% B flow: 0.5 mL/min. Gradient B for compound **30**; linear gradient: 0 - 1 min 5% B; 1 - 15 min 5 to 70% B; 16 - 20 min 70 to 5% B flow: 0.5 mL/min. NMR spectra were recorded on a Bruker Avance DMX-500 (500 MHz) spectrometer. Assignment of ^1H and ^{13}C NMR spectra was achieved using 2D methods (COSY, HSQC, HMBC, TOCSY). Chemical shifts are expressed in ppm in relation to the residual solvent signals (CHCl_3 , CHD_2OD , and HDO) on the: δ -scale. Coupling constants J are given in Hertz (Hz). Multiplicities were specified as follows: s (singlet), d (doublet), dd (doublet of a doublet), t (triplet), q (quartet), m (multiplet). For assignment of resonance signals to the appropriate nuclei the following abbreviations were used: Fuc (fucose), Gal (galactose), Hex (hexitol, hexonic acid, or hexon amide).

1,5-Anhydro-2-deoxy-D-arabino hexitol (10)

3,4,6-Tri-*O*-acetyl-1,5-anhydro-2-deoxy-D-*arabino*-hex-1-enitol (**8**) (4.50 g, 16.5 mmol) was dissolved in EtOAc/EtOH (1:1, v/v, 30 ml). Pd/C was added (0.4%, 20 mg) and the mixture was shaken overnight with a Parr shaker under H_2 atmosphere (5 bar). The catalyst was filtered off and the product was used without further purification for the next step. The 1,5-anhydro-2-deoxy-3,4,6-tri-*O*-acetyl-D-*arabino* hexitol (**9**) was dissolved in anhydrous MeOH (20 ml) and treated with a methanolic solution of NaOMe (1 M, 1 ml). Upon complete cleavage of the acetyl groups (12 h) the mixture was concentrated and purified by flash column chromatography ($\text{CH}_2\text{Cl}_2/\text{MeOH}$). Yield: 2.45 g, 96%.

Spectroscopic data were in accordance with literature.¹⁴⁻¹⁶

1,5-Anhydro-2-deoxy-4,6-*O*-(4-methoxybenzylidene)-D-*arabino* hexitol (11)

Compound **11** was synthesized according to a procedure from Spohr et al.⁸

A solution of **10** (2.40 g, 16.2 mmol), *p*-methoxybenzaldehyde dimethyl acetale (2.80 ml, 1 eq, 16.2 mmol) and camphorsulfonic acid (280 mg, 0.1 eq, 1.62 mmol) in DMF (20 ml) was stirred overnight at r.t. The solvent was co-evaporated with toluene, then EtOAc was added and the mixture was washed with water. The aqueous phase was extracted with EtOAc and the combined organic phases were dried over Na₂SO₄, filtered and concentrated. Successive crystallization of the product from EtOAc/*n*-hexane gave **11** (2.97 g, 69%).

General procedure A for oxidation (adapted from Huang *et al.*¹⁷):

Aqueous solutions of NaBr (1 M, 25 μL), tetrabutylammonium bromide (1 M, 50 μL), a satd. aq. solution of NaHCO₃ (125 μL) and 2,2,6,6-tetramethyl-1-piperidinyloxy (TEMPO) (2.2 mg, 0.014 mmol, 0.3 eq) were added to a solution of alcohol (0.045 mmol) in CH₂Cl₂ (1 mL) and H₂O (170 μL) in an ice-water bath. The resulted mixture was treated with an aqueous solution of NaOCl (150 μL, chlorine content not less than 4 %) and was stirred and warmed to r.t. After complete conversion (2 h) water and CH₂Cl₂ were added and the phases were separated. The aqueous phase was extracted with EtOAc. The organic phases were combined and dried over Na₂SO₄, filtered, and concentrated. Flash column chromatography (CH₂Cl₂/MeOH gradient +0.1% AcOH) yielded the product.

General procedure B for amide coupling:

Starting material (0.1 mmol) was dissolved in anhydrous CH₂Cl₂/DMF (1 ml, v/v, 1:1) or anhydrous CH₂Cl₂. Hydroxybenzotriazole (HOBt) (14.9 mg, 1.1 eq, 0.11 mmol) and amine (48 μl, 5 eq, 0.5 mmol) were added. The mixture was cooled to 0°C and *N,N'*-diisopropylcarbodiimide (DIC) (16.5 μl, 1.1 eq, 0.11 mmol) was added. The mixture was stirred overnight and warmed to r.t. The reaction mixture was diluted with CH₂Cl₂ and then washed with NaHCO₃ and brine. The aqueous phase was extracted with CH₂Cl₂ and the combined organic layers were dried with Na₂SO₄ and filtered. The solvent was evaporated under vacuum and the residue was purified by flash column chromatography.

General Procedure C for deprotection by hydrogenation:

A mixture of starting material (0.03 mmol) and Pd(OH)₂/C (10%) in dioxane/water (4:1, 1 ml) was treated with hydrogen at atmospheric pressure. The reaction was controlled by TLC. Upon completion the mixture was filtered, the solvent was removed under reduced pressure

and the resulting residue dried in *vacuo*. The crude product was either used for the next deprotection step or, in case of target compounds, purified by column chromatography on silica gel (CH₂Cl₂/MeOH).

General Procedure D for saponification with NaOMe:

To a solution of **12** (0.03 mmol) in dry MeOH (1 ml) was added a catalytical amount of freshly prepared NaOMe solution (1M) at r.t. Reaction was monitored by TLC. Upon completion the mixture was neutralized with 1N HCl and the solvent evaporated under reduced pressure. The residue was purified by column chromatography on silica gel (CH₂Cl₂/MeOH).

1,5-Anhydro-2-deoxy-4,6-*O*-(4-methoxybenzylidene)-3-*O*-(6-deoxy-2,3,4-tri-*O*-benzyl)- α -L-galactopyranosyl)-D-*arabino*-hexitol (**13**)

A mixture of **11** (506 mg, 1.90 mmol), ethyl 2,3,4-tri-*O*-benzyl-L-fucothiopyranoside (**12**)¹⁸ (1.82 g, 2 eq, 3.8 mmol), Bu₄NBr (1.84 g, 3 eq, 5.7 mmol), 2,6-di-*tert*-butyl-4-methylpyridine (1.17 g, 3 eq, 5.7 mmol), and powdered MS 4Å (3 g) in CH₂Cl₂ (12 mL) and DMF (3 mL) was stirred at r.t. under argon for 4 h. Then, CuBr₂ (1.27 g, 3 eq, 5.7 mmol) was added and the reaction mixture was stirred at r.t. for 15 h. The reaction mixture was filtered through celite, the filtrate was diluted with CH₂Cl₂ and successively washed with satd. aq. NaHCO₃ and brine. The aqueous layers were extracted successively with CH₂Cl₂. The combined organic layers were dried with Na₂SO₄, filtered and co-evaporated with toluene to dryness. The residue was purified by column chromatography (PE/Et₂O, 7:1 to 5:1) to yield compound **13** (631 mg, 76%) as yellowish oil.

[α]_D²⁰ -80.7 (*c* 0.47, CHCl₃); ¹H NMR (500 MHz, CDCl₃): δ 7.32 – 7.09 (m, 15H, Ar-H), 7.09 – 6.99 (m, 2H, Ar-H), 6.73 (d, *J* = 8.7 Hz, 2H, Ar-H), 5.39 (s, 1H, MeOPhCH), 4.89 – 4.79 (m, 2H, PhCH₂, Fuc-H1), 4.77 – 4.66 (m, 2H, PhCH₂), 4.63 – 4.46 (m, 3H, PhCH₂), 4.18 – 4.03 (m, 2H, Hex-H6b, Fuc-H5), 3.95 (dd, *J* = 10.1, 3.7 Hz, 1H, Fuc-H2), 3.90 – 3.77 (m, 3H, Hex-H1b, Hex-H3, Fuc-H3), 3.65 (s, 3H, O-CH₃), 3.62 – 3.52 (m, 2H, Hex-H4, Hex-H6a), 3.47 (d, *J* = 2.3 Hz, 1H, Fuc-H4), 3.38 (t, *J* = 11.3 Hz, 1H, Hex-H1a), 3.21 (td, *J* = 9.8, 4.9 Hz, 1H, Hex-H5), 1.89 (dd, *J* = 12.0, 3.8 Hz, 1H, Hex-H2b), 1.71 (qd, *J* = 12.9, 5.2 Hz, 1H, Hex-H2a), 0.89 (d, *J* = 6.5 Hz, 3H, Fuc-H6); ¹³C NMR (126 MHz, CDCl₃): δ 159.90, 138.97, 138.65, 138.57, 130.32 (5 quart. Ar-C), 129.01, 128.34, 128.33, 128.32, 128.20,

128.14, 128.02, 127.68, 127.52, 127.41, 127.37, 127.31, 125.28 (17C, 17 Ar-C), 113.40 (2C, Ar-C), 101.27 (PhCH), 94.13 (Fuc-C1), 80.92 (Hex-C4), 79.53 (Fuc-C3), 77.85 (Fuc-C4), 76.26 (Fuc-C2), 74.83, 73.39, 73.21, (3C, PhCH₂), 72.07, 72.00 (Hex-C3, Hex-C5), 68.87 Hex-C6), 66.27 (Hex-C1), 66.04 (Fuc-C5), 55.20 (O-CH₃), 30.79 (Hex-C2), 16.45 (Fuc-C6); ESI-MS: *m/z* calcd for C₄₁H₄₆O₉ [M+Na]⁺: 705.30, found: 705.37.

1,5-Anhydro-2-deoxy-3-*O*-(6-deoxy-2,3,4-tri-*O*-benzyl-4-*O*-(4-methoxy-benzylidene)- α -L-galactopyranosyl)-D-*arabino*-hexitol (14a) and 1,5-anhydro-2-deoxy-3-*O*-(6-deoxy-2,3,4-tri-*O*-benzyl- α -L-galactopyranosyl)-D-*arabino*-hexitol (14b)

The procedure for acetal opening was adapted from reference¹¹.

A solution of **13** (695 mg, 1.00 mmol) and BH₃·THF (1 M solution in THF, 8 ml, 8 eq, 8.00 mmol) was cooled to -20 °C and treated with Bu₂BOTf (1 M solution in CH₂Cl₂, 1 ml, 1 eq, 1 mmol). The reaction mixture was stirred and warmed from -20 to -5 °C over 1.5 h under argon, then quenched with Et₃N followed by the dropwise addition of MeOH. The reaction mixture was warmed to r.t. and evaporated to dryness. The residual syrup was coevaporated with toluene. Purification by flash chromatography on silica gel (PE/EtOAc gradient) afforded the C-6 alcohol **14a** (505 mg, 72%) and the dihydroxylated side product **14b** (125 mg, 22%).

Analytical data of **14a**:

[α]_D²⁰ -42.5 (*c* 0.22, CHCl₃); ¹H NMR (500 MHz, CDCl₃): δ 7.38 – 7.10 (m, 15H, Ar-H), 7.01 (d, *J* = 8.6 Hz, 2H, Ar-H), 6.71 (d, *J* = 8.6 Hz, 2H, Ar-H), 4.94 – 4.47 (m, 9H, 4 CH₂, Fuc-H1), 3.97 (dd, *J* = 10.1, 3.6 Hz, 1H, Fuc-H2), 3.92 – 3.80 (m, 3H, Hex-H1a, Fuc-H3, Fuc-H5), 3.77 – 3.66 (m, 5H, Hex-H3, Hex-H6a, OCH₃), 3.58 (d, *J* = 9.4 Hz, 1H, Hex-H6a), 3.45 – 3.35 (m, 2H, Hex-H4, Fuc-H4), 3.30 (t, *J* = 11.4 Hz, 1H, Hex-H1b), 3.13 (m, 1H, Hex-H5), 1.89 (m, 1H, Hex-H2a), 1.52 (m, 1H, Hex-H2b), 0.85 (t, *J* = 6.9 Hz, 3H, Fuc-H6); ¹³C NMR (126 MHz, CDCl₃): δ 159.08 (quart Ar-C, PMB), 138.77, 138.62, 138.54 (quart Ar-C), 130.31, 129.16, 128.41, 128.35, 128.30, 128.23, 128.12, 128.06, 128.01, 127.94, 127.63, 127.57, 127.52 (14C, 14 Ar-C), 113.66 (Ar-C), 92.92 (Fuc-C1), 79.82 (Hex-C5), 78.74 (Fuc-C3), 77.86 (Fuc-C4), 77.23 (Hex-C4), 76.17 (Fuc-C2), 75.20 (Hex-C3), 74.81, 74.61, 73.22, 73.10 (4C, CH₂), 66.26 (Fuc-C5), 65.34 (Hex-C1), 62.44 (Hex-C6), 55.21 (OCH₃), 29.72 (Hex-C2), 16.35 (Fuc-C6); ESI-MS: *m/z* calcd for C₄₁H₄₈O₉ [M+Na]⁺: 707.32, found: 707.30.

Analytical data of **14b**:

$[\alpha]_D^{20}$ -33.5 (*c* 0.44, CHCl₃); ¹H NMR (500 MHz, CDCl₃): δ 7.43 – 7.16 (m, 15H, Ar-H), 4.97 (t, *J* = 9.8 Hz, 1H, PhCH_{2a}), 4.92 (d, *J* = 3.9 Hz, 1H, Fuc-H1), 4.85 (2d, *J* = 11.8 Hz, 2H, PhCH₂), 4.74 (m, 1H, CH_{2b}), 4.64 (2d, *J* = 11.7 Hz, 2H, PhCH₂), 4.13 – 4.02 (m, 3H, Fuc-H2, H5), 4.02 – 3.83 (m, 3H, Hex-H1a, Hex-H6a, Fuc-H3), 3.76 (m, 1H, Hex-H6b), 3.68 (m, 1H, Fuc-H4), 3.48 – 3.31 (m, 4H, Hex-H1b, Hex-H3, Hex-H4), 3.17 (m, 1H, Hex-H5), 2.36 (s, 1H, OH), 2.13 (t, *J* = 6.3 Hz, 1H, OH), 1.97 (dd, *J* = 13.2, 4.7 Hz, 1H, Hex-H2a), 1.72 (m, 1H, Hex-H2b), 1.14 (d, *J* = 6.5 Hz, 3H, Fuc-H6); ¹³C NMR (126 MHz, CDCl₃): δ 138.65, 138.45 (3C, 3 quart. Ar-C), 129.18, 128.63, 128.57, 128.50, 128.43, 128.37, 128.06, 127.97, 127.90, 127.73, 127.59 (15C, 15 Ar-C), 97.59 (Fuc-C1), 82.74 (Hex-C3), 79.63 (Hex-C5), 79.13 (Fuc-C3), 77.48 (Fuc-C4), 76.31 (Fuc-C2), 75.12, 73.69, 73.32 (3C, CH₂), 71.77 (Hex-C4), 67.60 (Fuc-C5), 65.84 (Hex-C1), 63.47 (Hex-C6), 31.27 (Hex-C2), 16.81 (Fuc-C6); HR-MS: *m/z* calcd for C₃₃H₄₀O₈ [M+Na]⁺: 587.2615, found: 587.2625.

2,6-Anhydro-5-deoxy-3-O-(4-methoxybenzylidene)-4-O-(6-deoxy-2,3,4-tri-O-benzyl-α-L-galactopyranosyl)-D-lyxo-hexonic acid (15)

Compound **15** was synthesized according to general procedure A from **14a** (330 mg, 0.48 mmol). Yield: 87% (292 mg). Characterization by NMR failed presumably due to residual TEMPO. The product was therefore directly used for the amide coupling step.

HR-MS: *m/z* calcd for C₄₁H₄₆O₁₀ [M+Na]⁺: 721.2983, found: 721.2986.

2,6-Anhydro-5-deoxy-3-O-(4-methoxybenzylidene)-4-O-(6-deoxy-2,3,4-tri-O-benzyl-α-L-galactopyranosyl)-N-(3-fluorophenyl)-D-lyxo-hexonamide (16)

Carboxylic acid **15** (133 mg, 0.19 mmol), CH₂Cl₂ (1 ml), HOBT (28 mg, 1.1 eq, 0.21 mmol), 3-fluoro-aniline (91 μl, 5 eq, 0.95 mmol), and DIC (32 μl, 1.1 eq 0.21 mmol) were reacted according to general procedure B and yielded **16** (110 mg, 73%).

$[\alpha]_D^{20}$ -40.4 (*c* 0.34, CHCl₃); ¹H NMR (500 MHz, CD₃OD): δ 7.58 – 7.51 (m, 1H, Ar-H), 7.42 – 7.36 (m, 4H, Ar-H), 7.35 – 7.18 (m, 13H, Ar-H), 6.99 (d, *J* = 8.6 Hz, 2H, Ar-H), 6.82 (m, 1H, Ar-H), 6.66 (d, *J* = 8.6 Hz, 2H, Ar-H), 5.02 (d, *J* = 3.6 Hz, 1H, Fuc-H1), 4.88 (d, *J* = 11.3 Hz, 1H, PhCH_{2a}), 4.76 – 4.63 (m, 4H, PhCH₂), 4.57 (d, *J* = 11.3 Hz, 1H, PhCH_{2b}), 4.47 (d, *J* = 10.7 Hz, 2H, PhCH₂), 4.03 (dd, *J* = 7.4, 2.5 Hz, 1H, Hex-H6a), 4.00 – 3.92 (m, 2H, Fuc-H2, Fuc-H5), 3.86 (dd, *J* = 10.2, 2.8 Hz, 1H, Fuc-H3), 3.79 (m, 2H, Hex-H2, Hex-H4),

3.71 – 3.63 (m, 4H, Hex-H3, O-CH₃), 3.53 (d, $J = 1.8$ Hz, 1H, Fuc-H4), 3.45 (dd, $J = 11.8$, 9.9 Hz, 1H, Hex-H6b), 2.08 (d, $J = 9.0$ Hz, 1H, Hex-H5a), 1.62 (m, 1H, Hex-H5b), 0.95 – 0.84 (m, 3H, Fuc-H6); ¹³C NMR (126 MHz, CD₃OD): δ 170.15 (Hex-C1), 164.25 (d, $^1J_{CF} = 242.8$ Hz, Ar-CF), 160.72, 141.20 (d, $^3J_{CF} = 10.8$ Hz, C-NHCO), 140.15, 140.00, 139.94, 131.43 (5C, 5 quart. Ar-C), 131.29, 131.22, 130.83, 129.53, 129.50, 129.46, 129.29, 129.28, 129.04, 128.87, 128.77, 128.75, 116.77, 116.75, 114.61, 111.96, 111.79, 108.46, 108.25 (23C, 23 Ar-C), 94.37 (Fuc-C1), 81.55 (Hex-C2), 79.77, 79.55, 79.37 (Fuc-C3, Hex-C3, Fuc-C4), 77.41 (Fuc-C2), 76.28, 75.78 (2PhCH₂), 75.64 (Hex-C4), 74.11, 73.85 (2PhCH₂), 67.74 (Fuc-C5), 66.30 (Hex-C6), 55.70 (O-CH₃), 30.29 (Hex-C5), 16.79 (Fuc-C6); ESI-MS: m/z calcd for C₄₇H₅₀FN₉O₉ [M+Na]⁺: 814.29, found: 814.34.

2,6-Anhydro-5-deoxy-4-O-(6-deoxy-2,3,4-tri-O-benzyl- α -L-galactopyranosyl)-D-lyxo-hexonamide (17)

Compound **16** (32 mg, 0.04 mmol) was dissolved in CH₃CN/H₂O (9:1, 1 ml) and CAN (33 mg, 2 eq, 0.08 mmol) was added. The mixture was stirred at r.t. until TLC showed complete conversion (5-8 h), then diluted with CH₂Cl₂ and washed with satd. aq. NaHCO₃ solution. The aqueous phase was extracted with CH₂Cl₂, the combined organic phases were dried over Na₂SO₄, filtered and concentrated. The crude product was purified by flash column chromatography (PE/EtOAc gradient) to give **17** (27 mg, 44%).

¹H NMR (500 MHz, CD₃OD): δ 7.59 (dt, $J = 11.3$, 2.1 Hz, 1H, Ar-H), 7.42 – 7.22 (m, 17H, Ar-H), 6.86 – 6.79 (m, 1H, Ar-H), 5.03 (d, $J = 2.4$ Hz, 1H, Fuc-H1), 4.90 (d, $J = 11.2$ Hz, 1H, PhCH₂), 4.77 – 4.57 (m, 5H, CH₂), 4.28 (q, $J = 6.5$ Hz, 1H, Fuc-H5), 4.09 (m, 1H, Hex-H6a), 4.03 – 3.96 (m, 2H, Fuc-H2, -H3), 3.81 (s, 1H, Fuc-H4), 3.78 – 3.65 (m, 3H, Hex-H4, -H3, -H2), 3.53 (m, 1H, Hex-H6b), 2.14 – 2.04 (m, 1H, Hex-H5a), 1.72 – 1.58 (m, 1H, Hex-H5b), 1.15 (t, $J = 8.4$ Hz, 3H, Fuc-H6); ¹³C NMR (126 MHz, CD₃OD): δ 170.66 (Hex-C1), 164.25 (d, $^1J_{CF} = 242.6$ Hz), 141.08 (d, $^3J_{CF} = 10.9$ Hz), 140.30, 140.11, 139.87, 131.21, 131.14, 129.42, 129.38, 129.31, 129.24, 128.85, 128.74, 128.67, 128.58, 116.90 (d, $^4J_{CF} = 2.9$ Hz), 111.80 (d, $^2J_{CF} = 21.5$ Hz), 108.50 (d, $^2J_{CF} = 26.5$ Hz) (24C, Ar-C), 95.41 (Fuc-C1), 81.65 (Hex-C2), 80.31, 79.57, 77.58, 77.45 (Fuc-C2, Fuc-C3, Fuc-C4, Hex-C4), 76.37, 74.18, 73.88 (3PhCH₂), 72.09 (Hex-C3), 67.90 (Fuc-C5), 66.44 (Hex-C6), 30.59 (Hex-C5), 16.92 (Fuc-C6); HR-MS: m/z calcd for C₃₉H₄₂FNO₈ [M+Na]⁺: 694.2787, found: 694.2786.

2,6-Anhydro-5-deoxy-4-*O*-(6-deoxy- α -L-galactopyranosyl)-*N*-(3-fluorophenyl)-D-lyxo-hexonamide (5)

Compound **17** (19.5 mg, 0.029 mmol) was deprotected according to general procedure C. The product was further purified by preparative HPLC to give **5**. Yield: 6 mg, 52%.

$[\alpha]_D^{20}$ -31.3 (*c* 0.37, MeOH/CHCl₃, 2:1); ¹H NMR (500 MHz, CD₃OD): δ 7.60 (m, 1H, Ar-H), 7.38 – 7.26 (m, 2H, Ar-H), 6.86 (m, 1H, Ar-H), 4.95 (d, *J* = 3.8 Hz, 1H, Fuc-H1), 4.31 (q, *J* = 6.6 Hz, 1H, Fuc-H5), 4.08 (dd, *J* = 11.8, 3.4 Hz, 1H, Hex-H6a), 3.85 – 3.64 (m, 6H, Fuc-H2, Fuc-H3, Fuc-H4, Hex-H3, Hex-H4, Hex-H2), 3.55 (t, *J* = 11.2 Hz, 1H, Hex-H6b), 2.12 (dd, *J* = 13.3, 4.5 Hz, 1H, Hex-H5a), 1.69 (m, 1H, Glc-H5b), 1.20 (d, *J* = 6.6 Hz, 3H, Fuc-H6); ¹³C NMR (126 MHz, CD₃OD): δ 170.69 (CO), 164.26 (d, ¹*J*_{CF} = 242.5 Hz, Ar-CF), 131.17 (d, ³*J*_{CF} = 9.3 Hz, Ar-C), 116.86 (Ar-C), 111.82 (d, ²*J*_{CF} = 21.5 Hz, Ar-C), 108.48 (d, ²*J*_{CF} = 26.6 Hz, Ar-C), 101.42 (quart. Ar-C), 97.17 (Fuc-C1), 81.82 (Hex-C2), 78.15 (Hex-C4), 73.76, 72.45, 71.57, 69.83 (Hex-C3, Fuc-C2, Fuc-C3, Fuc-C4), 67.70 (Fuc-C5), 66.89 (Hex-C6), 30.83 (Hex-C5), 16.60 (Fuc-C6); HR-MS: *m/z* calcd for C₁₈H₂₄FNO₈ [M+Na]⁺: 424.1378, found: 424.1385; HPLC: Purity > 99.5 %, R_t 11.062 min.

2,6-Anhydro-5-deoxy-(6-deoxy-2,3,4-tri-*O*-benzyl- α -L-galactopyranosyl)-(1→4)-/2,3,4-tri-*O*-benzoyl-6-*O*-benzyl- β -D-galactopyranosyl-(1→3)]-*N*-(3-fluorophenyl)-D-lyxo-hexonamide (19)

A solution of thiogalactoside **18**¹⁹ (53 mg, 1.3 eq, 0.085 mmol) and glycosyl acceptor **17** (44 mg, 0.07 mmol, 1 eq) in dry CH₂Cl₂ (2.5 mL) was added to activated MS 4Å (0.6 g) under argon. A suspension of dimethyl(methylthio)sulfonium triflate (DMTST) (34 mg, 2 eq, 0.13 mmol) and activated MS 4Å (0.3 g) in CH₂Cl₂ (1.3 mL) was prepared in a second flask. Both suspensions were stirred at r.t. for 4 h, then the DMTST suspension was added via syringe to the first suspension. The reaction was stopped after 12 h, filtered through celite and the celite was washed with CH₂Cl₂. The filtrate was successively washed with satd. aq. NaHCO₃ and water. The aqueous layers were extracted with CH₂Cl₂. The combined organic layers were dried with Na₂SO₄, filtered and concentrated in *vacuo*. The crude product was purified by flash column chromatography (PE/toluene/EtOAc, 10:10:1 to 5:5:1) to afford **19** (55 mg, 68%) as colorless foam.

¹H NMR (500 MHz, CD₃OD): δ 8.04 (d, *J* = 7.2 Hz, 2H, Ar-H), 7.75 (d, *J* = 7.3 Hz, 2H, Ar-H), 7.71 – 7.63 (m, 3H, Ar-H), 7.57 – 7.47 (m, 3H, Ar-H), 7.46 – 7.37 (m, 2H, Ar-H), 7.34 –

7.05 (m, 26H, Ar-H), 6.85 (dd, $J = 11.0, 5.7$ Hz, 1H, Ar-H), 5.91 (d, $J = 2.8$ Hz, 1H, Gal-H4), 5.71 – 5.63 (m, 2H, Gal-H2, Gal-H3), 5.32 (d, $J = 7.6$ Hz, 1H, Gal-H1), 4.97 (d, $J = 3.4$ Hz, 1H, Fuc-H1), 4.74 – 4.45 (m, 6H, Fuc-H5, PhCH₂), 4.42 – 4.26 (m, 5H, PhCH₂, Gal-H5, Hex-H3), 4.07 – 3.87 (m, 4H, Hex-H6a, Fuc-H2, Fuc-H3, Hex-H4), 3.82 (d, $J = 7.4$ Hz, 1H, Hex-H2), 3.74 (dd, $J = 9.7, 6.0$ Hz, 1H, Gal-H6a), 3.70 – 3.62 (m, 2H, Fuc-H4, Gal-H6b), 3.47 (m, 1H, Hex-H6b), 2.09 (dd, $J = 13.5, 3.0$ Hz, 1H, Hex-H5a), 1.68 – 1.56 (m, 1H, Hex-H5b), 1.31 (t, $J = 7.1$ Hz, 3H, Fuc-H6); ¹³C NMR (126 MHz, CD₃OD): δ 169.19, 167.47, 167.03, 166.53 (3CO, Hex-C1), 164.28 (d, $^1J_{CF} = 242.9$ Hz, Ar-CF) 141.32, 140.19, 140.16, 139.99, 139.28, 134.97, 134.50, 134.31, 131.19, 130.80, 130.57, 130.46, 130.20, 130.03, 129.40, 129.37, 129.36, 129.31, 129.25, 129.20, 129.07, 128.75, 128.71, 128.62, 128.60, 128.47, 128.32, 116.83, 111.95, 108.46, 108.25, 101.54 (39C, 39Ar-C), 95.27 (Fuc-C1), 80.74, 80.69, 80.30, 77.48 (Fuc-C2, Fuc-C3, Fuc-C4, Hex-C2), 76.49, 76.44, 74.58, 73.98, 73.92, 73.87, 73.66, 73.56, 71.66 (4PhCH₂, Hex-C3, Hex-C4, Gal-C2, Gal-C3, Gal-C5), 70.68 (Gal-C4), 69.04 (Gal-C6), 67.83 (Fuc-C5), 65.62 (Hex-C6), 29.58 (Hex-C5), 17.29 (Fuc-C6); ESI-MS: m/z calcd for C₇₃H₇₀FNO₁₆ [M+Na]⁺: 1258.46, found: 1258.45.

2,6-Anhydro-5-deoxy-(6-deoxy- α -L-galactopyranosyl)-(1 \rightarrow 4)-/ β -D-galactopyranosyl-(1 \rightarrow 3)]-N-(3-fluorophenyl)-D-lyxo-hexonamide (6)

Compound **19** (24.7 mg, 0.02 mmol) was deprotected according to general procedures C and D. The product was further purified by preparative HPLC. Yield: 6 mg, 53%.

[α]_D²⁰ -85.7 (c 0.08, MeOH); ¹H NMR (500 MHz, CD₃OD): δ 7.96 (d, $J = 7.2$ Hz, NH), 7.57 (d, $J = 11.2$ Hz, 1H, Ar-H), 7.39 – 7.27 (m, 2H, Ar-H), 6.85 (t, $J = 8.2$ Hz, 1H, Ar-H), 4.91 (d, $J = 3.9$ Hz, 1H, Fuc-H1), 4.62 (q, $J = 6.5$ Hz, 1H, Fuc-H5), 4.32 (d, $J = 7.6$ Hz, 1H, Gal-H1), 4.12 – 4.06 (m, 1H, Hex-H6a), 4.03 (t, $J = 8.8$ Hz, 1H, Hex-H3), 3.96 – 3.82 (m, 3H, Hex-H2, Fuc-H3, Hex-H4), 3.81 – 3.63 (m, 5H, Gal-H4, Gal-H6, Fuc-H2, Fuc-H4), 3.57 (m, 1H, Hex-H6b), 3.48 (dd, $J = 9.6, 7.7$ Hz, 1H, Gal-H2), 3.39 (m, 1H, Gal-H5), 3.30 (m, 1H, Gal-H3), 2.17 (d, $J = 13.2$ Hz, 1H, Hex-H5a), 1.73 (m, 1H, Hex-H5b), 1.19 (d, $J = 6.6$ Hz, 3H, Fuc-H6); ¹³C NMR (126 MHz, CD₃OD): δ 170.08 (Hex-C1), 164.22 (d, $^1J_{C-F} = 242.7$ Hz, Ar-CF), 140.86 (quart. Ar-C), 131.12 (Ar-C), 128.58 (Ar-C), 117.32 (Ar-C), 112.04 (d, $^2J_{C-F} = 21.5$ Hz, Ar-C), 108.85 (d, $^2J_{C-F} = 26.2$ Hz, Ar-C), 103.63 (Gal-C1), 96.83 (Fuc-C1), 81.43 (Hex-C2), 76.96 (Hex-C3), 74.92, 74.70, 73.71, 73.04, 71.40, 70.00, 69.93 (Gal-C2, Gal-C3, Gal-C5, Fuc-C2, Fuc-C3, Fuc-C4, Hex-C4), 67.57 (Fuc-C5), 66.50 (Hex-C6), 62.79 (Gal-

C6), 30.68 (Hex-C5), 16.57 (Fuc-C6); HR-MS: m/z calcd for $C_{24}H_{34}FNO_{13}$ $[M+Na]^+$: 586.1906, found: 586.1914; HPLC: Purity > 99.5 %, R_t 9.336 min.

1,5-Anhydro-2-deoxy-6-*O*-[(1,1-dimethylethyl)dimethylsilyl]-3-*O*-(6-deoxy-2,3,4-tri-*O*-benzyl- α -L-galactopyranosyl)-D-*arabino*-hexitol (20)

The dihydroxyl compound **14b** (243 mg, 0.43 mmol) was dissolved in dry CH_2Cl_2 (5 ml). 1*H*-Imidazole (73 mg, 2.5 eq, 1.1 mmol), a catalytic amount of DAMP, and TBDMSCl (78 mg, 1.2 eq, 0.5 mmol) were added. The mixture was stirred at r.t. until TLC showed no further transformation (6 h). The reaction was quenched by addition of H_2O and the mixture was extracted with EtOAc. The organic phase was dried over Na_2SO_4 , filtered and the solvent removed under reduced pressure. The crude product was purified by flash column chromatography (PE/EtOAc gradient) to yield **20** (278 mg, 95%).

$[a]_D^{20}$ -41.2 (c 0.12, $CHCl_3$); 1H NMR (500 MHz, $CDCl_3$): δ 7.63 – 7.15 (m, 15H, Ar-H), 4.99 (d, J = 11.5 Hz, 1H, $PhCH_{2a}$), 4.94 (d, J = 3.8 Hz, 1H, Fuc-H1), 4.85-4.66 (m, 5H, $PhCH_2$), 4.14 (m, 1H, Fuc-H5), 4.07 (m, 1H, Fuc-H2), 4.03 – 3.92 (m, 2H, Fuc-H3, Hex-H1a), 3.86 (m, 2H, Hex-H6), 3.82 (s, 1H, OH), 3.71 (d, J = 1.8 Hz, 1H, Fuc-H4), 3.51 – 3.40 (m, 2H, Hex-H3, Hex-H4), 3.38 (m, 1H, Hex-H1b), 3.13 (m, 1H, Hex-H5), 1.94 (m, 1H, Hex-H2a), 1.71 (m, 1H, Hex-H2b), 1.13 (d, J = 6.5 Hz, 3H, Fuc-H6), 0.90 (s, 9H, $C(CH_3)_3$), 0.08 (s, 6H, $Si(CH_3)_2$); ^{13}C NMR (126 MHz, $CDCl_3$): δ 139.00, 138.74, 138.57 (3 quart. Ar-C), 128.64, 128.57, 128.52, 128.38, 128.05, 127.87, 127.82, 127.65, 127.55 (15C, 15 Ar-C), 96.74 (Fuc-C1), 81.51 (Hex-C3), 80.22 (Hex-C5), 79.31 (Fuc-C3), 77.61 (Fuc-C4), 76.42 (Fuc-C2), 75.05, 73.55, 73.37 (3 $PhCH_2$), 71.21 (Hex-C4), 67.20 (Fuc-C5), 65.73 (Hex-C1), 64.08 (Hex-C6), 30.94 (Hex-C2), 26.16 ($(CH_3)_3$), 18.66 ($SiC(CH_3)_3$), 16.75 (Fuc-C6), -5.14, -5.15 ($Si(CH_3)_2$); ESI-MS: m/z calcd for $C_{39}H_{54}O_8Si$ $[M+Na]^+$: 701.35, found: 701.30.

1,5-Anhydro-2-deoxy-6-*O*-[(1,1-dimethylethyl)dimethylsilyl]-4-(1*H*-imidazole-1-carbothioate)-3-*O*-(6-deoxy-2,3,4-tri-*O*-benzyl- α -L-galactopyranosyl)-D-*arabino*-hexitol (21)

Compound **20** (146 mg, 0.22 mmol) was dissolved in dry DCE (1 ml) under argon atmosphere. *N,N'*-Thiocarbonyldiimidazole (77 mg, 2 eq, 0.4 mmol) was added to the mixture. The flask was sealed and refluxed for 6 h. The solvent was evaporated and the

crude product was purified by flash column chromatography to yield the thioimidazolyl intermediate **21** (151 mg, 89%) which was directly used for the next step.

ESI-MS: m/z calcd for $C_{43}H_{56}N_2O_8SSi [M+H]^+$: 789.36, found: 789.38.

1,5-Anhydro-2,4-dideoxy-6-*O*-[(1,1-dimethylethyl)dimethylsilyl]-3-*O*-(6-deoxy-2,3,4-tri-*O*-benzyl- α -L-galactopyranosyl)- α -D-*threo*-hexitol (22**)**

The imidazolylthiocarbonyl intermediate **21** (139 mg, 0.17 mmol) was dissolved in anhydrous toluene (1.5 ml) under argon atmosphere. This solution was added dropwise to a refluxing solution of Bu_3SnH (67 μ l, 1.5 eq, 0.2 mmol) with a catalytic amount of AIBN in anhydrous toluene (4 ml). The resulting mixture was refluxed for 6 h. The solvent was evaporated under reduced pressure and the crude mixture purified by flash column chromatography (bigger batches were dissolved in acetonitrile and the tin organyl remainders removed by extraction with hexane prior to chromatography). Compound **22** was obtained as colorless foam (93 mg, 85%).

$[\alpha]_D^{20}$ -53.0 (c 0.23, $CHCl_3$); 1H NMR (500 MHz, CD_3OD): δ 7.44 – 7.22 (m, 15H, Ar-H), 5.02 (d, J = 3.1 Hz, 1H, Fuc-H1), 4.94 – 4.56 (m, 6H (overlaid by H_2O) $PhCH_2$), 4.03 – 3.90 (m, 4H, Fuc-H2, Fuc-H3, Fuc-H5, Hex-H1a), 3.82 (s, 1H, Fuc-H4), 3.73 (m, 1H, Fuc-H3), 3.66 (dd, J = 10.6, 5.4 Hz, 1H, Hex-H6a), 3.57 (dd, J = 10.6, 4.7 Hz, 1H, Hex-H6b), 3.45 – 3.34 (m, 2H, Hex-H1b, Hex-H5), 2.03 – 1.89 (m, 2H, Hex-H4a, Hex-H2a), 1.49 (m, 1H, Hex-H2b), 1.36 (dd, J = 19.2, 7.2 Hz, 1H, Hex-H4b), 1.13 (d, J = 6.5 Hz, 3H, Fuc-H6), 0.91 (s, 9H, $C(CH_3)_3$), 0.07 (d, J = 2.2 Hz, 2H, $Si(CH_3)_2$); ^{13}C NMR (126 MHz, CD_3OD): δ 140.27, 140.08, 139.92 (3 quart Ar-C), 129.39, 129.37, 129.28, 129.23, 128.81, 128.79, 128.66, 128.59 (15C, 15 Ar-C), 97.23 (Fuc-C1), 80.20 (Fuc-C3), 79.46 (Fuc-C4), 78.31 (Hex-C5), 77.44 (Fuc-C2), 76.35 ($PhCH_2$), 75.25 (Hex-C3), 74.02, 73.87 (2 $PhCH_2$), 67.92 (Fuc-C5), 67.52 (Hex-C1), 66.91 (Hex-C6), 37.11 (Hex-C2), 33.45 (Hex-C4), 26.42 ($C(CH_3)_3$), 19.24 ($C(CH_3)_3$), 16.96 (Fuc-C6), -5.18 ($Si(CH_3)_2$); ESI-MS: m/z calcd for $C_{39}H_{54}O_7Si [M+Na]^+$: 685.35, found: 685.41.

1,5-Anhydro-2,4-dideoxy-3-*O*-(6-deoxy-2,3,4-tri-*O*-benzyl- α -L-galactopyranosyl)- α -D-*threo*-hexitol (23**)**

Compound **22** (57 mg, 0.086 mmol) was dissolved in THF (abs., 1 ml) under an argon atmosphere. TBAF (86 μ l, 1 eq, 0.086 mmol) was added and the mixture stirred. AcOH

(100 μ l) was added. After 5 h another 0.5 eq of TBAF (43 μ l) was added and the mixture stirred for 10 h. The reaction mixture was diluted with H₂O and the aqueous phase extracted with EtOAc. The combined organic layers were dried over Na₂SO₄, filtered and concentrated. The crude product was purified by flash column chromatography (PE/EtOAc, 1:0 to 6:4) to yield **23** (38 mg, 81%).

¹H NMR (500 MHz, CDCl₃): δ 7.43 – 7.22 (m, 15H, Ar-H), 4.97 (m, 2H, PhCH_{2a}, Fuc-H1), 4.90 – 4.65 (m, 5H, PhCH₂), 4.10 – 3.99 (m, 2H, Hex-H1_a, Fuc-H2), 3.96 – 3.88 (m, 2H, Fuc-H3, Fuc-H5), 3.73 (m, 1H, Hex-H3), 3.66 (d, J = 2.0 Hz, 1H, Fuc-H4), 3.57 (m, 2H, Hex-H6), 3.47 – 3.37 (m, 2H, Hex-H1_b, Hex-H5), 1.90 (m, 1H, Hex-H2a), 1.78 (m, 1H, Hex-H4a), 1.58 (m, 1H, Hex-H2b), 1.47 (m, 1H, Hex-H4b), 1.10 (d, J = 6.5 Hz, 3H, Fuc-H6); ¹³C NMR (126 MHz, CDCl₃): δ 139.09, 138.82, 138.69 (3 quart. Ar-C), 128.59, 128.50, 128.47, 128.34, 128.10, 127.89, 127.75, 127.61, 127.57 (15C, 15 Ar-C), 95.76 (Fuc-C1), 79.49 (Fuc-C3), 77.82 (Fuc-C4), 76.85 (Hex-C5), 76.45 (Fuc-C2), 74.99, 73.42 (3C, 3 PhCH₂), 72.79 (Hex-C3), 66.57 (Fuc-C5), 66.20, 66.07 (Hex-C1, Hex-C6), 35.11 (Hex-C4), 32.05 (Hex-C2), 16.80 (Fuc-C6); HR-MS: m/z calcd for C₃₃H₄₀O₇ [M+Na]⁺: 571.2666, found: 571.2663.

2,6-Anhydro-3,5-dideoxy-4-O-(6-deoxy-2,3,4-tri-O-benzyl- α -L-galactopyranosyl)-D-threo-hexonic acid (24)

Alcohol **23** (45 mg, 0.082 mmol) was oxidized according to general procedure A. The crude product was purified on silica gel prior to usage in the next step. Yield: 34 mg (80% purity), 74%.

HR-MS: m/z calcd for C₃₃H₃₈O₈ [M+Na]⁺: 585.2459, found: 585.2457.

2,6-Anhydro-3,5-dideoxy-4-O-(6-deoxy-2,3,4-tri-O-benzyl- α -L-galactopyranosyl)-N-(3-fluorophenyl)-D-threo-hexonamide (25)

Carboxylic acid **24** (26 mg, 0.047 mmol) was coupled with 3-fluoroaniline (45 μ l, 10 eq, 0.47 mmol) using HOBt (7 mg, 1.1 eq, 0.052 mmol) and DIC (8 μ l, 1.1eq, 0.052 mmol) according to general procedure B with following modification: after 5 h DIPEA (4 μ l, 0.5 eq, 0.02 mmol) was added. Yield: 20 mg, 65%

¹H NMR (500 MHz, CD₃OD): δ 7.60 – 7.53 (m, 1H, Ar-H), 7.45 – 7.18 (m, 17H, Ar-H), 6.84 (dd, J = 10.9, 5.3 Hz, 1H, Ar-H), 5.05 (d, J = 3.6 Hz, 1H, Fuc-H1), 4.91 (m, 1H, CH_{2a}), 4.77 – 4.71 (m, 3H, CH₂), 4.70 – 4.59 (m, 2H, CH₂), 4.20 (dd, J = 11.6, 2.7 Hz, 1H, Hex-H6a),

4.04 – 3.79 (m, 6H, Fuc-H2, Fuc-H3, Fuc-H4, Fuc-H5, Hex-H2, Hex-H4), 3.56 (m, 1H, Hex-H6b), 2.38 (m, 1H, Hex-H3a), 1.99 (m, 1H, Hex-H5a), 1.66 – 1.51 (m, 2H, Hex-H5b, Hex-H3b), 1.18 – 1.14 (m, 3H, Fuc-H6); ^{13}C NMR (126 MHz, CDCl_3): δ 169.12 (Hex-C1), 163.13 (d, $^1J_{CF} = 244.9$ Hz, Ar-CF), 139.02, 138.91, 138.84, 138.69, 130.25, 130.17, 128.56, 128.49, 128.46, 128.34, 128.08, 127.79, 127.74, 127.61, 127.58, 115.16, 115.13 (20C, 20 Ar-C), 111.28 (d, $^2J_{CF} = 21.2$ Hz, Ar-C), 107.38 (d, $^2J_{CF} = 26.3$, Ar-C), 95.72 (C-1), 79.46 (Fuc-C2), 77.87 (Fuc-C4), 76.37, 76.13 (Fuc-C3, Hex-C2), 75.05, 73.51, 73.37 (3PhCH₂), 71.98 (Hex-C4), 66.80 (Fuc-C5), 66.15 (Hex-C6), 36.19 (Hex-C3), 31.55 (Hex-C5), 14.33 (Fuc-C6); ESI-MS: m/z calcd for $\text{C}_{39}\text{H}_{42}\text{FNO}_7$ $[\text{M}+\text{Na}]^+$: 678.28, found: 678.37.

2,6-Anhydro-3,5-dideoxy-4-*O*-(6-deoxy- α -L-galactopyranosyl)-*N*-(3-fluorophenyl)-*D*-threo-hexonamide (7)

Compound **25** (19 mg, 0.03 mmol) was deprotected according to standard procedure C to yield after HPLC purification title compound **7** (7 mg, 67%).

$[\alpha]_{\text{D}}^{20}$ -138.0 (c 0.06, MeOH); ^1H NMR (500 MHz, CD_3OD): δ 7.57 (m, 1H, Ar-H), 7.39 – 7.26 (m, 2H, Ar-H), 6.85 (m, 1H, Ar-H), 4.97 (d, $J = 11.0$ Hz, 1H, Fuc-H1), 4.20 (dd, $J = 11.8, 3.5$ Hz, 1H, Hex-H6a), 4.01 (m, 2H, Fuc-H5, Hex-H2), 3.89 (m, 1H, Hex-H4), 3.78 – 3.70 (m, 2H, Fuc-H2, Fuc-H3), 3.68 (m, 1H, Fuc-H4), 3.58 (dt, $J = 12.4, 2.1$ Hz, 1H, Hex-H6b), 2.45 (m, 1H, Hex-H3a), 2.04 (dd, $J = 12.9, 2.2$ Hz, 1H, Hex-H5a), 1.66 – 1.48 (m, 2H, Hex-H5b, Hex-H3b), 1.23 (t, $J = 9.3$ Hz, 3H, Fuc-H6); ^{13}C NMR (126 MHz, CD_3OD): δ 171.96 (Hex-C1), 165.23 ($^1J_{CF} = 242.9$ Hz, Ar-CF), 140.75 (d, $^3J_{CF} = 10.8$ Hz, Ar-C), 131.20 (d, $^2J_{CF} = 9.4$ Hz, Ar-C), 117.12 (Ar-C), 111.95 (d, $^2J_{CF} = 21.5$ Hz, Ar-C), 108.65 (d, $^2J_{CF} = 26.5$ Hz, Ar-C), 98.99 (Fuc-C1), 77.32 (Hex-C2), 74.59 (Hex-C4), 73.68 (Fuc-C4), 71.64, 69.83 (Fuc-C2, Fuc-C3), 67.91 (Fuc-C5), 67.11 (Hex-C6), 37.72 (Hex-C3), 32.76 (Hex-C5), 16.47 (Fuc-C6); HR-MS: m/z calcd for $\text{C}_{18}\text{H}_{24}\text{FNO}_7$ $[\text{M}+\text{Na}]^+$: 408.1429, found: 408.1437; HPLC: Purity > 99.5%, R_t 13.029 min.

1,5-Anhydro-2-deoxy-6-*O*-[(1,1-dimethylethyl)dimethylsilyl]-(6-deoxy-2,3,4-tri-*O*-benzyl- α -L-galactopyranosyl)-(1 \rightarrow 3)-/2,3,4-tri-*O*-benzoyl-6-*O*-benzyl- β -*D*-galactopyranosyl-(1 \rightarrow 4)]-*D*-arabino-hexitol (26)

A solution of thiogalactoside **12**¹⁹ (81 mg, 1.3 eq, 0.13 mmol) and glycosyl acceptor **20** (68 mg, 0.1 mmol) in dry CH_2Cl_2 (3 ml) was added to activated MS 3Å (0.8 g) under argon. A

suspension of DMTST (83 mg, 0.32 mmol, 3.2 eq) and activated MS 3Å (0.4 g) in CH₂Cl₂ (1.6 mL) was prepared in a second flask. Both suspensions were stirred at r.t. for 4 h, then the DMTST suspension was added via syringe to the other suspension. The reaction was stopped after 12 h, filtered through celite and the celite washed with CH₂Cl₂. The filtrate was successively washed with satd. aq. NaHCO₃ and water. The aqueous layers were extracted with CH₂Cl₂. The combined organic layers were dried with Na₂SO₄, filtered and concentrated under reduced pressure. The crude product was purified by flash column chromatography (petroleum ether/toluene/ethyl acetate, 10:10:1 to 5:5:1) to afford compound **26** as colourless foam. Yield: 78 mg, 63%.

¹H NMR (500 MHz, CD₃OD): δ 8.09 – 8.04 (m, 2H, Ar-H), 7.97 – 7.92 (m, 2H, Ar-H), 7.76 – 7.71 (m, 2H, Ar-H), 7.67 (t, *J* = 7.5 Hz, 1H, Ar-H), 7.60 – 7.51 (m, 3H, Ar-H), 7.47 – 7.40 (m, 3H, Ar-H), 7.34 – 7.21 (m, 15H, Ar-H), 7.20 – 7.14 (m, 4H, Ar-H), 7.13 – 7.05 (m, 3H, Ar-H), 5.90 (d, *J* = 3.2 Hz, 1H, Gal-H4), 5.76 (dd, *J* = 10.4, 8.2 Hz, 1H, Gal-H2), 5.59 (dd, *J* = 10.4, 3.6 Hz, 1H, Gal-H3), 5.26 (d, *J* = 8.2 Hz, 1H, Gal-H1), 4.94 (d, *J* = 3.7 Hz, 1H, Fuc-H1), 4.77 (q, *J* = 6.5 Hz, 1H, Fuc-H5), 4.73 – 4.50 (m, 5H, PhCH₂), 4.44 – 4.30 (m, 3H, PhCH₂), 4.16 (t, *J* = 6.5 Hz, 1H, Gal-H5), 4.06 (dd, *J* = 10.1, 2.8 Hz, 1H, Fuc-H3), 3.98 – 3.90 (m, 3H, Fuc-H2, Hex-H5, Hex-H6a), 3.85 (dd, *J* = 11.7, 3.9 Hz, 1H, Hex-H1a), 3.79 – 3.63 (m, 5H, Fuc-H4, Gal-H6, Hex-H6b, Hex-H3), 3.30 (m, 1H, Hex-H1b), 2.93 (d, *J* = 8.1 Hz, 1H, Hex-H4), 2.01 (d, *J* = 8.2 Hz, 1H, Hex-H2a), 1.55 (m, 1H, Hex-H2b), 1.41 (d, *J* = 6.5 Hz, 3H, Fuc-H6), 0.98 (s, 9H, C(CH₃)₃), 0.16 (s, 3H, SiCH₃), 0.10 (s, 3H, SiCH₃); ¹³C NMR (126 MHz, CD₃OD): δ 167.43, 166.57 (3C, 3 CO), 140.21, 140.15, 139.85, 139.28, 135.09, 134.77, 134.62, 131.20, 130.75, 130.55, 130.49, 130.09, 129.76, 129.47, 129.37, 129.35, 129.31, 129.26, 128.91, 128.76, 128.64, 128.59, 128.53, 128.50, 128.24 (42C, 42 Ar-C), 101.76 (Gal-C1), 94.72 (Fuc-C1), 81.91 (Hex-C4), 80.72, 80.63 (Fuc-C3, -C4), 77.45 (Fuc-C2), 76.61 (Hex-C5), 76.47 (PhCH₂), 75.01 (Hex-C3), 74.58 (PhCH₂), 74.51 (Gal-C5), 73.87, 73.80 (2PhCH₂), 73.55 (Gal-C3), 71.82 (Gal-C2), 70.73 (Gal-C4), 69.07 (Gal-C6), 67.55 (Fuc-C5), 66.34 (Hex-C1), 62.93 (Hex-C6), 31.67 (Hex-C2), 26.61 (C(CH₃)₃), 19.28 (C(CH₃)₃), 17.34 (Fuc-C6), -4.70, -5.01 (Si(CH₃)₂); ESI-MS: *m/z* calcd for C₇₃H₈₂O₁₆Si [M+Na]⁺: 1265.53, found: 1265.50.

1,5-anhydro-2-deoxy-6-*O*-[(1,1-dimethylethyl)dimethylsilyl]-(6-deoxy- α -L-galactopyranosyl)-(1 \rightarrow 3)-/ β -D-galactopyranosyl-(1 \rightarrow 4)]-D-arabino-hexitol (27)

Trisaccharide mimic **26** (78 mg, 0.063 mmol) was deprotected with TBAF (1 eq, 63 μ l) to yield the 6-OH compound. After aqueous work up and purification on silica gel the compound was deprotected according to general procedures C and D to yield **27** (7 mg, 24%).

^1H NMR (500 MHz, D_2O): δ 5.04 (d, $J = 3.8$ Hz, 1H, Fuc-H1), 4.72 (q, $J = 6.7$ Hz, 1H, Fuc-H5), 4.46 (d, $J = 7.7$ Hz, 1H, Gal-H1), 4.03 (dd, $J = 11.7, 4.4$ Hz, 1H, Hex-H6a), 3.94 (dd, $J = 17.7, 8.5$ Hz, 3H, Fuc-H3, Gal-H4, Hex-H6a), 3.88 – 3.70 (m, 7H, Fuc-H2, Fuc-H4, Gal-H6, Hex-H3, Hex-H5, Hex-H6b), 3.70 – 3.59 (m, 2H, Gal-H3, Gal-H5), 3.57 – 3.47 (m, 2H, Gal-H2, Hex-H1b), 3.44 (m, 1H, Hex-H4), 2.20 (d, $J = 11.6$ Hz, 1H, Hex-H2a), 1.63 (d, $J = 6.6$ Hz, 1H, Hex-H2b), 1.21 (d, $J = 6.6$ Hz, 3H, Fuc-H6); ^{13}C NMR (126 MHz, D_2O): δ 102.02 (Gal-C1), 94.78 (Fuc-C1), 80.09 (Hex-C4), 74.93 Gal-C5), 74.46, 74.13 (Hex-C3, Hex-C5) 72.49 (Fuc-C4), 71.98 (Gal-C3), 71.49 (Gal-C2), 69.53, 68.37, 67.76 (Fuc-C2, Fuc-C3, Gal-C4), 66.52 (Fuc-C5), 65.23 (Hex-C1), 61.42 (Gal-C6), 60.21 (Hex-C1), 29.72 (Hex-C2), 15.14 (Fuc-C6); HR-MS: m/z calcd for $\text{C}_{73}\text{H}_{82}\text{O}_{16}\text{Si}$ $[\text{M}+\text{Na}]^+$: 479.1735, found: 479.1744.

2,6-Anhydro-5-deoxy-4-*O*-(6-deoxy-2,3,4-tri-*O*-benzyl- α -L-galactopyranosyl)-D-lyxo-hexonic acid (28)

14b (230 mg, 0.41 mmol) was oxidized according to general procedure A. The crude product was purified on silica gel and used directly for the next step. Yield: 147 mg, 62%. HR-MS: m/z calcd for $\text{C}_{34}\text{H}_{40}\text{O}_9$ $[\text{M}+\text{Na}]^+$: 615.2565, found: 615.2572.

Methyl 2,6-anhydro-5-deoxy-4-*O*-(6-deoxy-2,3,4-tri-*O*-benzyl- α -L-galacto-pyranosyl)-D-lyxo-hexonate (29)

Carboxylic acid **28** (42 mg, 0.1 mmol) was dissolved in toluene/MeOH (3:2, v/v, 1 ml), and a solution of TMSCHN_2 (75 μ l, 2M in hexane, 1.1 eq, 0.11 mmol) was added. The mixture was stirred at r.t. until TLC showed no further transformation (5 h). The solvent was removed under reduced pressure and the crude product purified by flash column chromatography ($\text{CH}_2\text{Cl}_2/\text{EtOAc}$ 1:0 to 7:3) to give **29**. Yield: 24 mg, 58%.

^1H NMR (500 MHz, CD_3OD): δ 7.43 – 7.23 (m, 15H, Ar-H), 5.00 (d, $J = 8.9$ Hz, 1H, Fuc-H1), 4.91 (d, $J = 11.2$ Hz, 1H, CH_{2a}), 4.79 – 4.59 (m, 5H, CH_2), 4.19 (q, $J = 6.5$ Hz, 1H, Fuc-H5), 4.03 (m, 1H, Hex-H6a), 3.99 – 3.95 (m, Fuc-H2, Fuc-H3), 3.81 (s, 1H, Fuc-H4), 3.78 (dd, $J = 8.0, 4.0$ Hz, 1H, Hex-H3), 3.75 – 3.70 (m, 3H, CH_3), 3.69 – 3.60 (m, 2H, Hex-H2, Hex-H4), 3.46 (m, 1H, Hex-H6b), 2.06 (m, 1H, Hex-H5a), 1.58 (ddd, $J = 14.7, 12.4, 4.6$ Hz, 1H, Hex-H5b), 1.14 (d, $J = 6.5$ Hz, 3H, Fuc-H6); ^{13}C NMR (126 MHz, CD_3OD): δ 171.91 (Hex-C1), 140.29, 140.10, 139.86 (3 quart. Ar-C), 129.41, 129.39, 129.30, 129.23, 128.83, 128.74, 128.66, 128.59 (15C, 15Ar-C), 95.41 (Fuc-C1), 80.72, 80.22, 79.54, 77.38, 76.81 (5C, Hex-C3, Hex-C2, Fuc-C2, Fuc-C3, Fuc-C4), 76.35, 74.16, 73.85 (3Ph CH_2), 71.85 (Hex-C4), 67.94 (Fuc-C5), 66.01 (Hex-C6), 52.63 (COOCH_3), 30.11 (Hex-C5), 16.89 (Fuc-C6); HR-MS: m/z calcd for $\text{C}_{34}\text{H}_{40}\text{O}_9$ [$\text{M}+\text{Na}$] $^+$: 615.2565, found: 615.2572.

2,6-Anhydro-5-deoxy-4-*O*-(6-deoxy- α -L-galactopyranosyl)-D-lyxo-hexonic acid methyl ester (30)

Compound **29** (24 mg, 0.04 mmol) was deprotected according to general procedure C to yield title compound **30** after purification via flash column chromatography on silica gel and preparative HPLC. Yield: 7 mg, 53%.

$[\alpha]_{\text{D}}^{20}$ -117.9 (c 0.13, MeOH); ^1H NMR (500 MHz, CD_3OD): δ 4.92 (d, $J = 3.5$ Hz, 1H, Fuc-H1), 4.23 (q, $J = 6.4$ Hz, 1H, Fuc-H5), 4.03 (ddd, $J = 11.8, 4.6, 2.9$ Hz, 1H, Hex-H6a), 3.83 – 3.71 (m, 6H, CH_3 , Fuc-H2, Fuc-H3, Hex-H3), 3.71 – 3.58 (m, 3H, Fuc-4, Hex-2, Hex-4), 3.49 (m, 1H, Hex-H6b), 2.10 (m, 1H, Hex-H5a), 1.62 (m, 1H, Hex-H5b), 1.20 (d, $J = 6.6$ Hz, 3H, Fuc-H6); ^{13}C NMR (126 MHz, CD_3OD): δ 172.02 (Hex-C1), 97.27 (Fuc-C1), 80.95 (Hex-C2), 77.36, 73.74, 72.12, 71.56, 69.78, (5C, Fuc-C2, Fuc-C3, Fuc-C4, Hex-C3, Hex-C4), 67.77 (Fuc-C5), 66.40 (Hex-C6), 52.66 (CH_3), 30.33 (Hex-C5), 16.58 (Fuc-C6); HR-MS: m/z calcd for $\text{C}_{13}\text{H}_{22}\text{O}_9$ [$\text{M}+\text{Na}$] $^+$: 345.1156, found: 345.1165; HPLC: Purity > 99%, $R_t = 4.877$ min.

Abbreviations: AIBN, Azobisisobutyronitrile; CAN, ceric ammonium nitrate; CRD, carbohydrate recognition domain; DCs, Dendritic cells; DC-SIGN, Dendritic cell-specific intercellular adhesion molecule-3 grabbing nonintegrin; DIC, *N,N'*-Diisopropylcarbodiimide; DIPEA, *N,N*-Diisopropylethylamine; DMAP, 4-Dimethylaminopyridine; DMF, *N,N*-Dimethyl-formamide; DMTST, Dimethyl(methylthio)-sulfonium triflates; Fuc, fucose; Gal, galactose; HOBt, *N*-Hydroxybenzotriazol; HPLC, High performance/pressure

liquid chromatography; IC₅₀, Inhibitory concentration 50%; Le^a, Lewis^a; Le^x, Lewis^x; LNFP III, lacto-*N*-fucopentaose III; Man, mannose; MHC, major histocompatibility complex; MD, molecular dynamics; NMR, nuclear magnetic resonance; PAA, polyacrylamide; PDB, protein data bank; rIC₅₀, Relative IC₅₀; TBAB, Tetrabutyl-ammonium bromide; TBAF, Tetrabutylammonium fluoride; TBDMSCl, tert-Butyldimethylsilyl chloride; TEMPO, 2,2,6,6-Tetramethylpiperidine-1-oxyl; TMSE, Trimethylsilylethyl.

REFERENCES

1. Feinberg, H., Castelli, R., Drickamer, K., Seeberger, P.H. & Weis, W.I. Multiple modes of binding enhance the affinity of DC-SIGN for high mannose N-linked glycans found on viral glycoproteins. *J. Biol. Chem.* **282**, 4202-4209 (2007).
2. Angulo, J., Diaz, I., Reina, J.J., Tabarani, G., Fieschi, F., Rojo, J. & Nieto, P.M. Saturation Transfer Difference (STD) NMR Spectroscopy Characterization of Dual Binding Mode of a Mannose Disaccharide to DC-SIGN. *Chembiochem* **9**, 2225-2227 (2008).
3. Anderluh, M., Obermajer, N., Svajger, U. & Bernardi, A. DC-SIGN antagonists with mannose anchor. *Eur. J. Pharm. Sci.* **44**, 179-180 (2011).
4. Andreini, M. et al. Second generation of fucose-based DC-SIGN ligands: affinity improvement and specificity versus Langerin. *Org. Biomol. Chem.* **9**, 5778-5786 (2011).
5. Obermajer, N., Sattin, S., Colombo, C., Bruno, M., Švajger, U., Anderluh, M. & Bernardi, A. Design, synthesis and activity evaluation of mannose-based DC-SIGN antagonists. *Mol. Diversity*, 1-14 (2010).
6. Guo, Y., Feinberg, H., Conroy, E., Mitchell, D., Alvarez, R., Blixt, O., Taylor, M., Weis, W. & Drickamer, K. Structural basis for distinct ligand-binding and targeting properties of the receptors DC-SIGN and DC-SIGNR. *Nat. Struct. Mol. Biol.* **11**, 591-598 (2004).
7. Meyer, S., van Liempt, E., Imberty, A., van Kooyk, Y., Geyer, H., Geyer, R. & van Die, I. DC-SIGN Mediates Binding of Dendritic Cells to Authentic Pseudo-LewisY Glycolipids of *Schistosoma mansoni* Cercariae, the First Parasite-specific Ligand of DC-SIGN. *J. Biol. Chem.* **280**, 37349-37359 (2005).
8. Spohr, U. Inhibitors of endo- α -mannosidase. Part I. Derivatives of 3-O-(α -D-glucopyranosyl)-D-mannopyranose. Vol. 71 (ed. Bach, M.) 1919-1927 (Can. J. Chem., 1993).
9. Prodger, J.C., Bamford, M.J., Bird, M.I., Gore, P.M., Holmes, D.S., Priest, R. & Saez, V. Mimics of the sialyl Lewis X tetrasaccharide. Replacement of the N-Acetylglucosamine sugar with simple C2-symmetric 1,2-diols. *Bioorg. Med. Chem.* **4**, 793-801 (1996).
10. Sato, S., Mori, M., Ito, Y. & Ogawa, T. An Efficient Approach to O-Glycosides through CuBr₂·Bu₄Nr Mediated Activation of Glycosides. *Carbohydr. Res.* **155**, C6-C10 (1986).
11. Fan, R.-H., Achkar, J., Hernández-Torres, J.M. & Wei, A. Orthogonal Sulfation Strategy for Synthetic Heparan Sulfate Ligands. *Org. Lett.* **7**, 5095-5098 (2005).
12. Feinberg, H., Mitchell, D.A., Drickamer, K. & Weis, W.I. Structural basis for selective recognition of oligosaccharides by DC-SIGN and DC-SIGNR. *Science* **294**, 2163-2166 (2001).

13. Obermajer, N., Sattin, S., Colombo, C., Bruno, M., Svajger, U., Anderluh, M. & Bernardi, A. Design, synthesis and activity evaluation of mannose-based DC-SIGN antagonists. *Mol. Diversity* **15**, 347-360 (2011).
14. Foster, A.B., Stacey, M. & Vardheim, S. Action of alkali on methyl 2,3-anhydro- α -D-allopyranoside and 1,5-anhydro-2-deoxy-3-O-p-tolylsulfonyl-D-arabinohexitol. *Acta Chem. Scand.* **12**, 1819-24 (1958).
15. Van Rijsbergen, R., Anteunis, M.J.O. & De Bruyn, A. On the nature of the side-products formed during the hydrogenolysis of 1,6:2,3-dianhydro-4-O-benzyl- β -D-mannopyranose. *Carbohydr. Res.* **105**, 269-270 (1982).
16. v, R.E. & Tulloch, A.P. Hydrogenolysis of carbohydrates. III. Further observations on the reduction of methyl α -D-glucopyranoside. *Can. J. Chem.* **35**, 1504-10 (1957).
17. Huang, L., Teumelsan, N. & Huang, X. A Facile Method for Oxidation of Primary Alcohols to Carboxylic Acids and Its Application in Glycosaminoglycan Syntheses. *Chem.--Eur. J.* **12**, 5246-5252 (2006).
18. Thoma, G., Magnani, J.L., Patton, J.T., Ernst, B. & Jahnke, W. Preorganization of the bioactive conformation of sialyl Lewis(X) analogues correlates with their affinity to E-selectin. *Angew. Chem., Int. Ed.* **40**, 1941-1945 (2001).
19. Ernst, B., Wagner, B., Baisch, G., Katopodis, A., Winkler, T. & Ohrlein, R. Substrate specificity of fucosyl transferase III: An efficient synthesis of sialyl Lewis(x)-, sialyl Lewis(a)-derivatives and mimetics thereof. *Can. J. Chem.* **78**, 892-904 (2000).

3. FimH

3.1 Introduction

Microbial Lectins

Plant-derived hemagglutinins were the first lectins to be discovered in the late 19th century.¹ In the following century, the agglutinating effect on erythrocytes was also noted for bacteria demonstrating the existence of microbial lectins. Until today, the family of *Enterobacteriaceae* lectins is the best investigated one. These lectins are involved in various biological functions such as recognition, signaling, and as especially important for bacterial pathogens in adhesion. Recognition of glycoconjugates on mammalian cell surfaces for adherence and invasion of bacteria is the first and crucial step in infections.² By firm adhesion, the natural cleansing process is circumvented. Moreover, adhesion facilitates nutrition, release of toxins and entry of the bacteria into the cell.

Commonly, bacterial lectins assemble in a multimeric manner and form filamentous organelles, termed fimbriae or pili. These oligomers elevate from the bacterial surface and represent an important virulence factor.³⁻⁵

Fimbriae of the *enterobacterial* family include mannose-specific type 1 fimbriae,⁶ galabiose-specific P-fimbriae,⁷ N-acetylglucosamine-specific F17 fimbriae.⁸ Type 1 fimbriae are present on e.g. *Escherichia coli* (*E. coli*), *Salmonella typhimurium*, and *Nisseria gonorrhoea*. The carbohydrate recognition domain (CRD) is located at the tip of the fimbrium as part of the terminal subunit, designated FimH in type 1 fimbriae,⁹ PapG for P fimbriae,¹⁰ and F17G for F17 fimbriae.¹¹ The carbohydrate-specificity of these lectins determines ultimately the tissue tropism. As aforementioned, P fimbriae favor galabiose (Gal α 1-4Gal β) structures which are expressed in the upper part of the kidneys,¹² whereas type 1 fimbriae recognize mannose-containing glycoproteins such as uroplakin Ia (UPIa) that is highly abundant on urothelial bladder cells.^{13,14} This explains the involvement of these lectins in urinary tract infections (UTIs) and kidney infections caused by *E. coli*.¹⁵

Urinary Tract Infection

Uropathogenic *E. coli* (UPEC) is the major causative agent in UTIs, one of the most prevalent and cost-intensive infectious disease.¹⁵⁻¹⁷ Women are particularly affected,^{16,18} however, also patients suffering from diabetes, spinal cord injuries, or suppressed immune system have a high risk of experiencing an UTI.¹⁹⁻²¹ The host defense mechanisms includes cleansing by flow of urine, myriad antimicrobial molecules, and effector immune cells. Expression of fimbriae allowing for adherence of bacteria is an important virulence factor to circumvent these defense mechanisms. Type 1 pili with the lectin FimH at their very tip are

responsible for initial colonization of the bladder cells with UPEC by recognition of the mannose-bearing UPIa.^{4,14} An untreated UTI can ascend and lead to infection of the bladder (cystitis) and in a late stage to infection of the kidneys (pyelonephritis).¹⁵

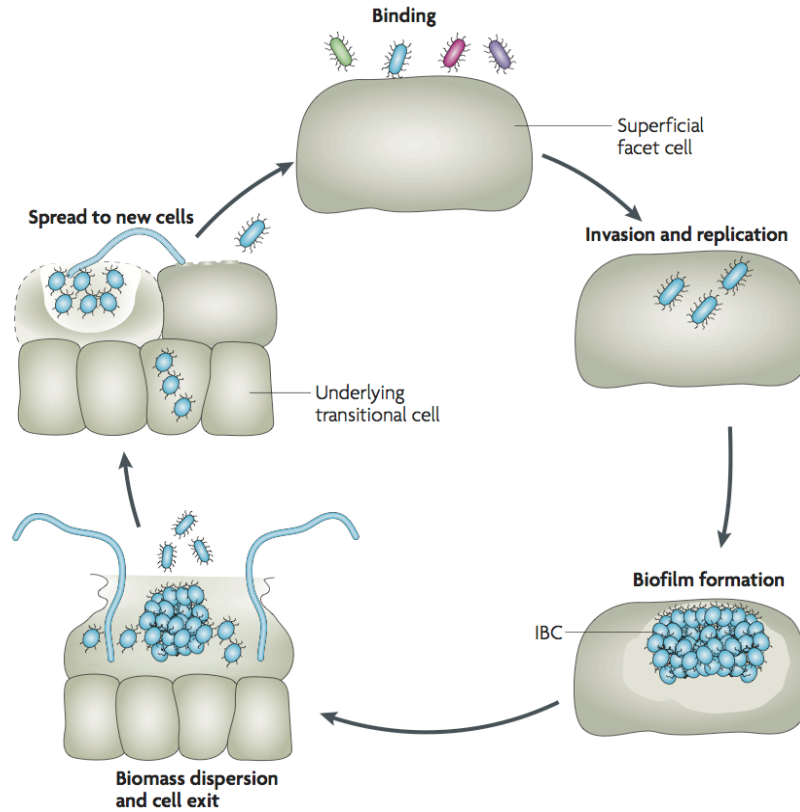


Figure 1. Infection cycle of uropathogenic *Escherichia coli* (UPEC), taken from Cegelski *et al.*²². Binding of UPEC to the urothelial bladder cells is mediated by type 1 pili, in particular FimH – uroplakin Ia interaction. This results in invasion into the host cells, replication, and formation of biofilm-like intracellular bacterial communities (IBCs). Within the IBCs bacteria are protected from host immune response and antibiotic treatment and can persist for months in a quiescent state. UPECs can re-emerge from IBCs and infect neighboring cells, which is associated with recurrence of infection. Furthermore, UPECs can penetrate deeper into the bladder tissue.

The adherence of bacteria is the initial and crucial step of an infection cycle (Figure 1); it protects the bacteria from being washed out by the flow of urine and allows for entry into the tissue resulting in an UTI.^{23,24} However, this also activates the innate immune defense, such as the influx of neutrophils to the site of infection, exfoliation of infected bladder cells, and further inflammatory responses.²⁵ Nonetheless, UPEC developed means to evade these responses and instead invade deeper into the tissue. The bacteria form biofilm-like structures, termed intracellular bacterial communities (IBCs), which allows them to stay in a quiescent

state and survive for an extended period of time.^{26,27} Protected from external influences, such as host immune response or antibiotics, bacteria can re-emerge from IBCs and infect neighboring cells (Figure 1). Formation of IBCs is considered to be the reason for recurrence of infection as well as resistance to treatment with antibiotics. As a matter of fact, up to 50% of the infected patients will experience a relapse of the infection within the first six month.^{17,28}

Type 1 Fimbriae

Type 1 fimbriae are filamentous organelles.^{6,29} A single type 1 fimbriae is a 7 nm wide and 1-3 μm long surface polymer and built up of thousands of copies of the major subunit protein FimA. These subunits are organized as a rigid, helical rod followed by a short linear and flexible tip composed of the subunits FimF, FimG, and FimH. The lectin FimH is located at the distal end of this linear fimbriar tip and comprises the mannose-specific CRD.^{9,30-32}

The assembly of type 1 pili takes place in the periplasm via the chaperone/usher pathway (Figure 2).³³ This pathway is a conserved bacterial secretion system and is also used for the assembling of other fimbriae, such as P fimbriae.³⁴ The periplasmic scaffolding protein FimC, the chaperone, and outer membrane assembly platform FimD, the usher, are needed for the biogenesis of the pilus. The FimC forms binary complexes with the monomeric pili subunits in the periplasmic space and guarantees their proper folding and delivery to FimD. The latter catalyzes the assembly of the subunits and enables the translocation of the growing fiber across the outer membrane to the cell surface.³⁴⁻³⁷

Each subunit presents an incomplete immunoglobulin (Ig)-like fold, missing a C-terminal β -strand. The chaperone FimC provides the missing β -strand until the diffusion to FimD and the integration of the subunit in the growing pili. Then, FimC is replaced and the Ig-like fold is completed by an N-terminal extension from the following subunit. This donor strand complementation process accounts for strong intermolecular interactions between the subunits and a considerable stability of the type 1 pili.³⁸⁻⁴⁰

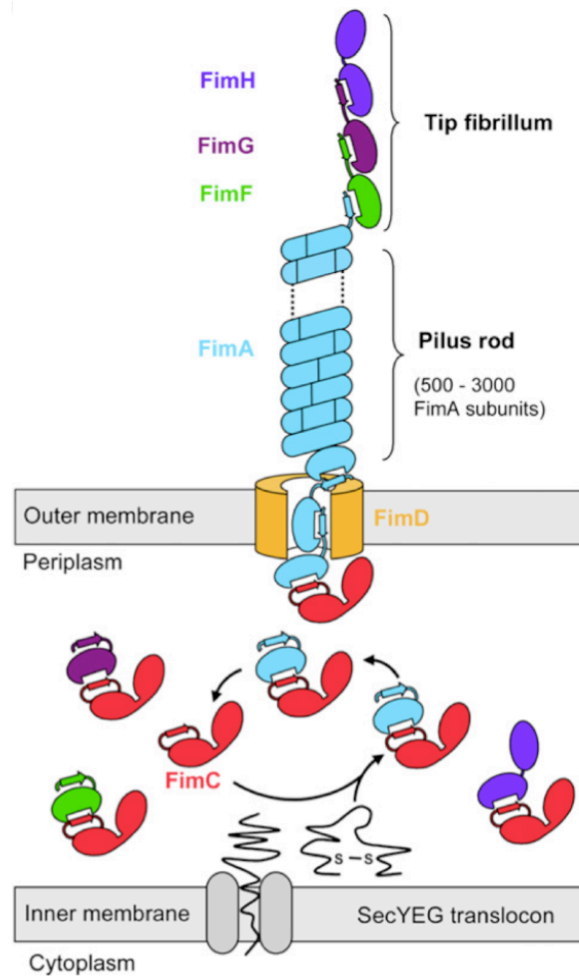


Figure 2. Schematic representation of pilus assembly taken from Puorger *et al.*³⁹ The chaperone FimC forms complexes with the newly translocated subunits (FimA, FimG, FimF and FimH) in the periplasm thereby mediating correct folding and delivery to the assembly platform FimD (usher). The usher catalyzes pilus subunit assembly and enables translocation of folded subunits across the outer membrane.

The expression of type 1 pili is a phase variable process alternating between fimbriated and non-fimbriated states of the bacterium. Nine *fim* genes contain the genetic information for the assembly of fimbriae. The mentioned phase variation is controlled by an invertible promoter region which is located upstream of *fimA* gene and controls the transcription of downstream *fim* genes (FimA, FimC, FimD, FimF, FimG, and FimH).⁴¹ The orientation of this promoter determines the fate of pili and can either be ‘on-phase’ resulting in pili expression or ‘off-phase’ resulting in silencing of the *fim* gene cluster.^{42,43} FimB and FimE can both regulate the inversion of the promoter, FimE from on-to-off and FimB in both directions.⁴⁴

Several factors influence the phase switch including activity of these recombinases dependent on growth conditions.^{43,45} Moreover, cross-talk between different gene clusters, e.g. the activated P fimbriae gene switches the *fim* gene to off-phase results in no simultaneous expression of type 1 and P pili. This allows for ascending of bacteria into the kidneys. Hence,

the fimbriae expression is adjusted to the infection status and environmental conditions and seems to be crucial for the survival and pathogenicity of the bacteria.⁴⁶

FimH

FimH is a 29 kDa protein composed of 279 amino acid residues. In contrast to the other Fim subunits, FimH consists of two Ig-like domains, the N-terminal pilin domain and the C-terminal lectin domain. The pilin domain connects FimH with the following FimG protein (compare Figure 2) and is characterized by the structural relation to the other pilus subunits, i.e. the incomplete Ig-like fold. The lectin domain comprises two β -sheets, one large and continuous, the other one smaller and split. At the distal end of the β -sandwich, opposite to the region where the lectin domain is connected with the pilin domain, a single CRD is located that is capable of accommodating α -D-mannosides.

Due to the missing donor strand for a complete fold, the monomeric FimH unit is not stable and proteolytically degraded, hence, crystallization was not achieved so far.⁴⁷ The first crystal structure of FimH in complex with the chaperone FimC (and cyclohexylbutanoyl-*N*-hydroxyethyl-D-glucamide that was added for crystallization) was solved in 1999.³¹ To date, five more crystal structures of FimH(–FimC) have been solved.^{30,48-51} Based on these data, it was found that FimH adopts two conformations, the low- and the high-affinity conformation; a comparison is depicted in Figure 3.^{31,51} In the low-affinity state the pilin and the lectin domain of FimH interact with each other via the interdomain region. This interaction induces a twist in the β -sandwich fold of the lectin domain and results in a compressed overall structure accompanied by an opening of the mannose-binding site.⁵¹ The high-affinity state is characterized by a separation of the the lectin and pilin domain due to a disrupted interdomain region. This leads to an untwist of the pilin domain and an elongated overall structure, though, the mannose binding pocket is tightened and referred to as active.⁵¹

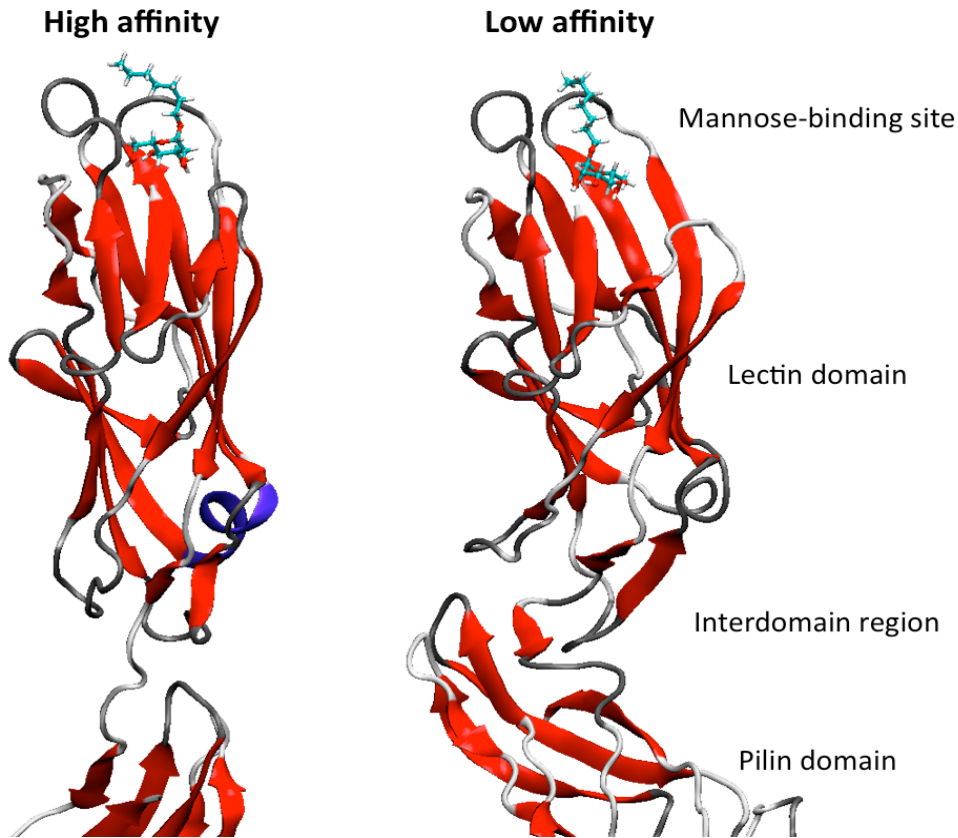


Figure 3. Comparison of low-affinity (left side, PDB 3JWN) and high-affinity (right side, PDB 1KLF) conformation of FimH (Modeled by Adam Zalewski, University of Basel).⁵¹ In the high-affinity state the lectin domain is elongated with a tight mannose-binding site. In the low-affinity state the lectin domain interacts with the pilin domain at the interdomain region. These interdomain interactions lead to a twist in the β -sandwich fold of the lectin domain, which results in a compressed overall structure and an open mannose-binding site.

A switch from the low- to the high-affinity state can be achieved upon tensile force. The mechanical force is capable of disrupting the interdomain region resulting in the allosteric switch.^{52,53} Since the low-affinity conformation is stabilized by intra-molecular interactions, this mechanism is also called allosteric autoinhibition.⁵¹ Such a force-induced switch along with enhanced affinity to a ligand are characteristic for catch bonds.⁵⁴ The physiological function of catch bonds is considered to facilitate adhesion under flow conditions. A critical step in UTIs is the adherence of bacteria to the urothelium, which is challenged by the flow of urine that is nothing else than application of force. It was found that, according to the catch bond behavior, the FimH–UPIa interaction becomes stronger under sheer stress, which results in stabilized attachment and bacterial accumulation.⁵⁵⁻⁵⁷

The Carbohydrate Recognition Domain

The CRD of FimH represents a deep negatively charged pocket with hydrophobic amino acid residues lining the rim. (Figure 4).

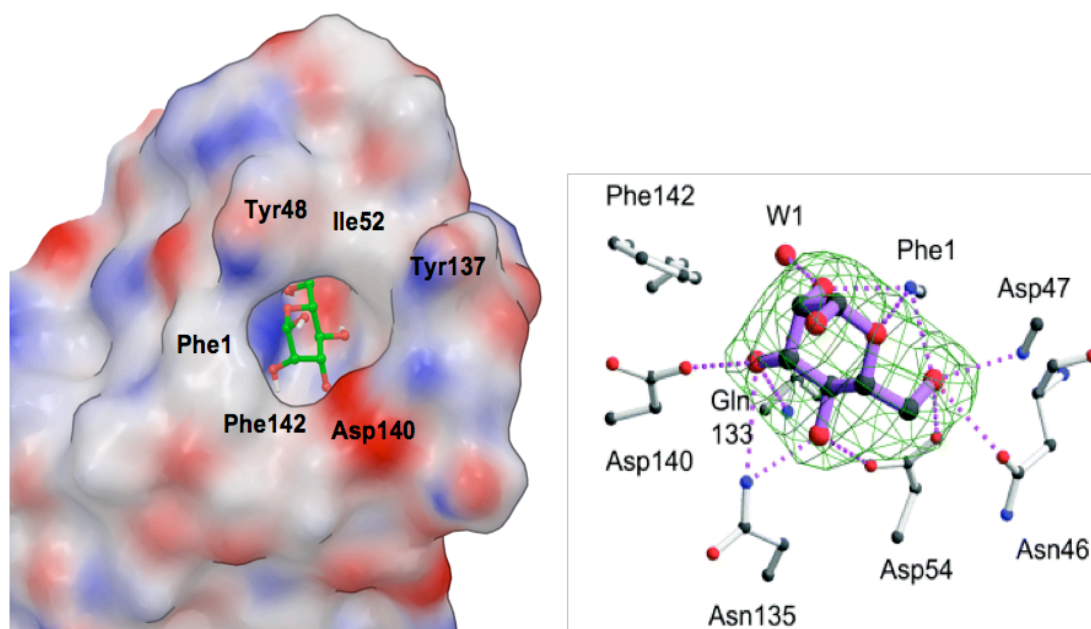


Figure 4. Crystal structure of FimC–FimH complex bound to α -D-methyl-mannoside (left, PDB 1KLF³⁰, modeled by Adam Zalewski, Institute of Molecular Pharmacy, University of Basel) and the interacting protein residues with the same ligand (right), adapted from Hung *et al.*³⁰. Coloring of the receptor resembles the electrostatic potential surface with positively charged residues shown in blue, negatively charged residues in red, and neutral and hydrophobic residues in white. Residues of the hydrophobic ridge are labeled; Tyr48, Ile52 and Tyr137 form the ‘tyrosine gate’ at the entrance of the binding site. D-mannose establishes an extensive H-bond network with the residues Phe1, Asn46, Asp47, Asp54, Gln133, Asn135, Asp140, and Phe142 (shown in ball-and-stick, H-bonds are highlighted in purple, W1: water molecule in the binding site).³⁰

FimH selectively binds α -configured D-mannose ligands. Hydrophilic side chains of the amino acids in the binding pocket establish a vast network of hydrogen bonds with each of the hydroxyl groups (except for the anomeric oxygen) of an α -D-mannopyranoside. Additionally, hydrophobic interactions are formed. The interacting residues are Phe1, Asn46, Asp47, Asp54, Gln133, Asn135, Asp140, and Phe142. Three hydrophobic amino acids at the entrance of the binding pocket (Tyr48, Ile52 and Tyr137) form the so called “tyrosine gate”.³⁰

FimH Antagonists

UTIs are generally treated with antibiotics. However, the excessive use of the latter encounters resistance development of bacteria, which entails recurrence of infections and high medical costs.⁵⁸ This explains the urgent need for alternative treatment and prevention strategies. An anti-adhesion therapy provides a promising approach.⁵⁹⁻⁶² FimH antagonists that are capable of blocking the lectin FimH would avoid adhesion of the bacterium to the urothelium and hence ultimately lead to clearance of the microbes by the bulk flow of urine. This different mode of action is advantageous to antibiotics in terms of susceptibility to resistance development.

α -D-mannosides can prevent the type 1 pili-mediated agglutination of yeast cells.⁶³⁻⁶⁵ Mannose, methyl α -D-mannoside (**1**), and mannan were among the first ligands to be identified to inhibit yeast aggregation in the presence of UPEC. Thereupon, many natural oligomannosides and multimeric mannose dendrimers have been studied followed by mannosides bearing aromatic aglycones (**3**, **4**, Figure 5). The latter have been proven significantly more potent than their methyl analogue **1**.⁶⁶ Without any information on the CDR, Sharon and Ofek proposed a model on the increments the binding site should present. Thus, a hydrophobic region was assumed to be in proximity to the carbohydrate binding site that overall has strong specificity for α -configuration.⁶⁶ By now, crystallographic data elucidated the 3D structure of the FimH CRD and various bound ligands and furnish evidence for the initial model.^{48,67} Based on these data aromatic aglycones were supposed to insert between both sides of the hydrophobic rim, in that manner a π - π stacking with Tyr48 and Tyr137 is established. Hence, this binding mode is termed ‘in-binding mode’. A similar binding mode is assumed for alkyl aglycones.⁴⁸ Affinity of these alkyl mannosides towards FimH was found to be increasing with growing chain length. The best inhibitory potency was achieved with a seven-membered alkyl chain (**2**).⁴⁸

Antagonists developed since then can be categorized accordingly as, long-chain alkyl mannosides and mannosides with variously substituted aromatic aglycones.⁶⁸ The most recent group of antagonists includes mannosides with extended aglycones.⁶⁸ An overview of antagonists is given in Figure 5.

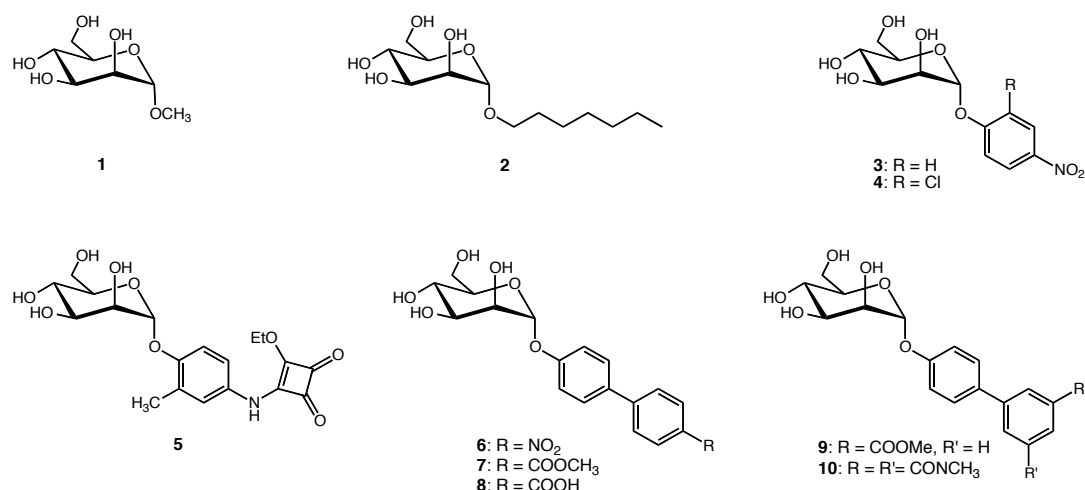


Figure 5. FimH antagonists. Alkyl α -D-mannopyranoside: Methyl α -D-mannopyranoside (**1**)⁶⁹, *n*-heptyl α -D-mannopyranoside (**2**);⁴⁸ *p*-nitrophenyl α -D-mannopyranosides, *p*-NPMan (**3**) and *p*-NoCIPMan (**4**);⁶⁶ squaric acid derivative **5**;⁷⁰ *p*-substituted biphenyl α -D-mannopyranosides **6**, **7**, **8**;^{50,71} drug and ester prodrug: 3,5, disubstituted biphenyl α -D-mannopyranosides **9**, **10**^{50,72}.

To date, the squaric acid derivatives (e.g. **5**, Figure 5) and biphenyl mannosides (e.g. **6-10**, Figure 5) are amongst the most promising antagonists for FimH with affinity in the low nanomolar range.^{50,70,72}

Crystallography studies of compound **9** with FimH revealed a novel binding mode for biphenyl mannosides.⁵⁰ Instead of the aglycone located within the tyrosine gate this ligand binds in the so called ‘out binding mode’ addressing only Tyr48 by π - π interaction (Figure 6). Additionally, an electrostatic interaction with Arg98 is discussed.⁵⁰

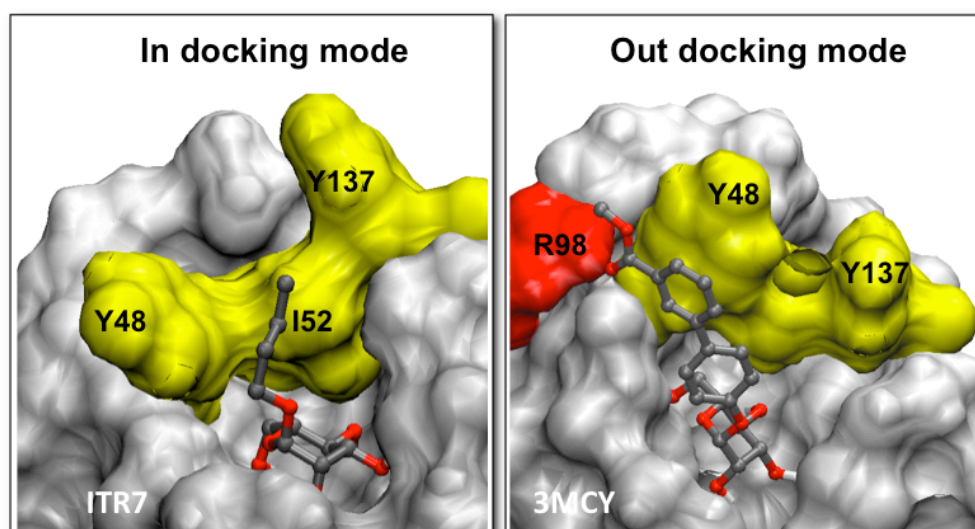


Figure 6. ‘In’ and ‘out’ binding mode of FimH-ligand complexes. FimH CRD in complex with *n*-butyl α -D-mannopyranoside (left, PDB entry 1TR7⁴⁸) reveals in-binding, and with the biphenyl derivative **9** (right, PDB entry 3MCY⁵⁰) out-binding.

The first assays for biological evaluation of these mannosidic compounds were based on measuring the effect, i.e. the inhibitory potency, on agglutination of yeast cells in presence of UPEC.^{66,73} Equivalent approaches involve hemagglutination of erythrocytes.⁶⁹ Up to now, many more assay formats have been developed, including ELISA-based^{74,75}, surface plasmon resonance^{48,76}, and cell-based adhesion assays (e.g. fluorescence-activated cell sorting)⁷⁷.

Depending on the assay format the inhibitory potencies reported as IC₅₀ values differ. Amongst others, the reason for that are differences in the UPEC strains used, such as FimH mutations, or on the conformational state of the FimH subunit depending e.g. on shear stress and resulting in distinct affinities for ligands. For comparability, generally relative IC₅₀ values are presented with either methyl α -D-mannoside (**1**) or *n*-heptyl α -D-mannoside (**2**) as reference compounds that exhibit low micromolar and nanomolar affinity, respectively.

The potential of α -D-mannosides as alternative treatment strategy was demonstrated with *in vivo* mouse infections studies where the bacterial infections could be reduced considerably by application of α -D-mannoside (**1**) or *n*-heptyl α -D-mannoside (**2**).^{49,78,79} Concerning the development of an orally available drug good pharmacokinetics and -dynamics are a prerequisite. Intestinal absorption and renal clearance are key issues for orally dosed FimH antagonists to reach the therapeutic target in the bladder and the optimization of these properties is still a challenging task. One approach to address that matter was the design of ester-prodrugs.⁷¹ The ester form of a biphenylcarboxylate (**7**) is expected to facilitate intestinal absorption due to higher lipophilicity and the subsequent hydrolysis by carboxyl esterases in the small intestine and liver releases the active principle (**8**) that is prone to renal elimination. This study revealed a small molecule FimH antagonist with a proven reducing effect on colony forming units in the bladder. Ultimately, this substantiates the potential of orally available FimH antagonists as anti-adhesives for the treatment of UTIs.

References

1. Kilpatrick, D.C. Animal lectins: a historical introduction and overview. *Bba-Gen Subjects* **1572**, 187-197 (2002).
2. Patti, J.M. & Hook, M. Microbial Adhesins Recognizing Extracellular-Matrix Macromolecules. *Curr. Opin. Cell Biol.* **6**, 752-758 (1994).
3. Connell, H., Agace, W., Hedlund, M., Klemm, P., Shembri, M. & Svanborg, C. Fimbriae-mediated adherence induces mucosal inflammation and bacterial clearance - Consequences for anti-adhesion therapy. *Toward Anti-Adhesion Therapy for Microbial Diseases* **408**, 73-80 (1996).
4. Connell, H., Agace, W., Klemm, P., Schembri, M., Marild, S. & Svanborg, C. Type 1 fimbrial expression enhances Escherichia coli virulence for the urinary tract. *Proc. Natl. Acad. Sci. U. S. A.* **93**, 9827-9832 (1996).
5. Oelschlaeger, T.A., Dobrindt, U. & Hacker, J. Pathogenicity islands of uropathogenic E-coli and the evolution of virulence. *Int. J. Antimicrob. Agents* **19**, 517-521 (2002).
6. Jones, C.H., Pinkner, J.S., Roth, R., Heuser, J., Nicholes, A.V., Abraham, S.N. & Hultgren, S.J. Fimh Adhesin of Type-1 Pili Is Assembled into a Fibrillar Tip Structure in the Enterobacteriaceae. *Proc. Natl. Acad. Sci. U. S. A.* **92**, 2081-2085 (1995).
7. Kuehn, M.J., Heuser, J., Normark, S. & Hultgren, S.J. P Pili in Uropathogenic Escherichia-Coli Are Composite Fibers with Distinct Fibrillar Adhesive Tips. *Nature* **356**, 252-255 (1992).
8. Bertin, Y., Girardeau, J.P., Darfeuille-Michaud, A. & Contrepolis, M. Characterization of 20K fimbria, a new adhesin of septicemic and diarrhea-associated Escherichia coli strains, that belongs to a family of adhesins with N-acetyl-D-glucosamine recognition. *Infect. Immun.* **64**, 332-342 (1996).
9. Hanson, M.S. & Brinton, C.C. Identification and Characterization of Escherichia-Coli Type-1 Pilus Tip Adhesion Protein. *Nature* **332**, 265-268 (1988).
10. Lindberg, F., Lund, B., Johansson, L. & Normark, S. Localization of the Receptor-Binding Protein Adhesin at the Tip of the Bacterial Pilus. *Nature* **328**, 84-87 (1987).
11. Buts, L., Wellens, A., Van Molle, I., Wyns, L., Loris, R., Lahmann, M., Oscarson, S., De Greve, H. & Bouckaert, J. Impact of natural variation in bacterial F17G adhesins on crystallization behaviour. *Acta Crystallogr D* **61**, 1149-1159 (2005).
12. Leffler, H. & Svanborgeden, C. Glycolipid Receptors for Uropathogenic Escherichia-Coli on Human-Erythrocytes and Uroepithelial Cells. *Infect. Immun.* **34**, 920-929 (1981).
13. Xie, B., Zhou, G., Chan, S.Y., Shapiro, E., Kong, X.P., Wu, X.R., Sun, T.T. & Costello, C.E. Distinct glycan structures of uroplakins Ia and Ib - Structural basis for the selective binding of FimH adhesin to uroplakin Ia. *J. Biol. Chem.* **281**, 14644-14653 (2006).
14. Zhou, G., Mo, W.J., Sebbel, P., Min, G.W., Neubert, T.A., Glockshuber, R., Wu, X.R., Sun, T.T. & Kong, X.P. Uroplakin Ia is the urothelial receptor for uropathogenic Escherichia coli: evidence from in vitro FimH binding. *J. Cell Sci.* **114**, 4095-4103 (2001).
15. Ronald, A. The etiology of urinary tract infection: Traditional and emerging pathogens. *Am. J. Med.* **113**, 14S-19S (2002).
16. Foxman, B., Barlow, R., D'Arcy, H., Gillespie, B. & Sobel, J.D. Urinary tract infection: Self reported incidence and associated costs. *Ann. Epidemiol.* **10**, 509-515 (2000).
17. Foxman, B. Recurring urinary tract infection: incidence and risk factors. *Am. J. Public Health* **80**, 331-333 (1990).

18. Foxman, B., Somsel, P., Tallman, P., Gillespie, B., Raz, R., Colodner, R., Kandula, D. & Sobel, J.D. Urinary tract infection among women aged 40 to 65: Behavioral and sexual risk factors. *J. Clin. Epidemiol.* **54**, 710-718 (2001).
19. Patterson, J.E. & Andriole, V.T. Bacterial Urinary-Tract Infections in Diabetes. *Infect. Dis. Clin. North Am.* **9**, 25-51 (1995).
20. Patterson, J.E. & Andriole, V.T. Bacterial urinary tract infections in diabetes. *Infect. Dis. Clin. North Am.* **11**, 735-750 (1997).
21. Mahan, K.T. & Wang, J. Spinal Morphine Anesthesia and Urinary Retention. *J. Am. Podiatr. Med. Assoc.* **83**, 607-614 (1993).
22. Cegelski, L., Marshall, G.R., Eldridge, G.R. & Hultgren, S.J. The biology and future prospects of antivirulence therapies. *Nat. Rev. Microbiol.* **6**, 17-27 (2008).
23. Wiles, T.J., Kulesus, R.R. & Mulvey, M.A. Origins and virulence mechanisms of uropathogenic Escherichia coli. *Exp. Mol. Pathol.* **85**, 11-19 (2008).
24. Mulvey, M.A. Adhesion and entry of uropathogenic Escherichia coli. *Cell. Microbiol.* **4**, 257-271 (2002).
25. Mulvey, M.A., Lopez-Boado, Y.S., Wilson, C.L., Roth, R., Parks, W.C., Heuser, J. & Hultgren, S.J. Induction and evasion of host defenses by type 1-piliated uropathogenic Escherichia coli. *Science* **282**, 1494-1497 (1998).
26. Justice, S.S., Hung, C., Theriot, J.A., Fletcher, D.A., Anderson, G.G., Footer, M.J. & Hultgren, S.J. Differentiation and developmental pathways of uropathogenic Escherichia coli in urinary tract pathogenesis. *Proc. Natl. Acad. Sci. U. S. A.* **101**, 1333-1338 (2004).
27. Anderson, G.G., Goller, C.C., Justice, S., Hultgren, S.J. & Seed, P.C. Polysaccharide Capsule and Sialic Acid-Mediated Regulation Promote Biofilm-Like Intracellular Bacterial Communities during Cystitis. *Infect. Immun.* **78**, 963-975 (2010).
28. Ikaheimo, R., Siitonen, A., Heiskanen, T., Karkkainen, U., Kuosmanen, P., Lipponen, P. & Makela, P.H. Recurrence of urinary tract infection in a primary care setting: Analysis of a 1-year follow-up of 179 women. *Clin. Infect. Dis.* **22**, 91-99 (1996).
29. Russell, P.W. & Orndorff, P.E. Lesions in 2 Escherichia-Coli Type-1 Pilus Genes Alter Pilus Number and Length without Affecting Receptor-Binding. *J. Bacteriol.* **174**, 5923-5935 (1992).
30. Hung, C.S. et al. Structural basis of tropism of Escherichia coli to the bladder during urinary tract infection. *Mol. Microbiol.* **44**, 903-915 (2002).
31. Choudhury, D., Thompson, A., Stojanoff, V., Langermann, S., Pinkner, J., Hultgren, S.J. & Knight, S.D. X-ray structure of the FimC-FimH chaperone-adhesin complex from uropathogenic Escherichia coli. *Science* **285**, 1061-1066 (1999).
32. Hahn, E. et al. Exploring the 3D molecular architecture of Escherichia coli type 1 pili. *J. Mol. Biol.* **323**, 845-857 (2002).
33. Hung, D.L. & Hultgren, S.J. Pilus biogenesis via the chaperone/usher pathway: An integration of structure and function. *J. Struct. Biol.* **124**, 201-220 (1998).
34. Dodson, K.W., Jacobdubuisson, F., Striker, R.T. & Hultgren, S.J. Outer-Membrane Papc Molecular Usher Discriminately Recognizes Periplasmic Chaperone Pilus Subunit Complexes. *Proc. Natl. Acad. Sci. U. S. A.* **90**, 3670-3674 (1993).
35. Sauer, F.G., Barnhart, M., Choudhury, D., Knights, S.D., Waksman, G. & Hultgren, S.J. Chaperone-assisted pilus assembly and bacterial attachment. *Curr. Opin. Struct. Biol.* **10**, 548-556 (2000).
36. Sauer, F.G., Remaut, H., Hultgren, S.J. & Waksman, G. Fiber assembly by the chaperone-usher pathway. *Biochim. Biophys. Acta, Mol. Cell Res.* **1694**, 259-267 (2004).
37. Klemm, P. & Christiansen, G. The Fimd Gene Required for Cell-Surface Localization of Escherichia-Coli Type-1 Fimbriae. *Mol. Gen. Genet.* **220**, 334-338 (1990).

38. Nishiyama, M. & Glockshuber, R. The Outer Membrane Usher Guarantees the Formation of Functional Pili by Selectively Catalyzing Donor-Strand Exchange between Subunits That Are Adjacent in the Mature Pilus. *J. Mol. Biol.* **396**, 1-8 (2010).
39. Puorger, C., Eidam, O., Capitani, G., Erilov, D., Grutter, M.G. & Glockshuber, R. Infinite kinetic stability against dissociation of supramolecular protein complexes through donor strand complementation. *Structure* **16**, 631-642 (2008).
40. Sauer, F.G., Futterer, K., Pinkner, J.S., Dodson, K.W., Hultgren, S.J. & Waksman, G. Structural basis of chaperone function and pilus biogenesis. *Science* **285**, 1058-1061 (1999).
41. Adiciptaningrum, A.M., Blomfield, I.C. & Tans, S.J. Direct observation of type 1 fimbrial switching. *EMBO Rep.* **10**, 527-532 (2009).
42. Sohanpal, B.K., Kulasekara, H.D., Bonnen, A. & Blomfield, I.C. Orientational control of fimE expression in Escherichia coli. *Mol. Microbiol.* **42**, 483-494 (2001).
43. Gally, D.L., Rucker, T.J. & Blomfield, I.C. The Leucine-Responsive Regulatory Protein Binds to the Fim Switch to Control Phase Variation of Type-1 Fimbrial Expression in Escherichia-Coli K-12. *J. Bacteriol.* **176**, 5665-5672 (1994).
44. Klemm, P. 2 Regulatory Fim Genes, Fimb and Fime, Control the Phase Variation of Type-1 Fimbriae in Escherichia-Coli. *Embo Journal* **5**, 1389-1393 (1986).
45. Tsai, K.W., Lai, H.T., Tsai, T.C., Wu, Y.C., Yang, Y.T., Chen, K.Y., Chen, C.M., Li, Y.S.J. & Chen, C.N. Difference in the regulation of IL-8 expression induced by uropathogenic E. coli between two kinds of urinary tract epithelial cells. *J. Biomed. Sci.* **16**(2009).
46. Xia, Y., Gally, D., Forsman-Semb, K. & Uhlin, B.E. Regulatory cross-talk between adhesin operons in Escherichia coli: inhibition of type 1 fimbriae expression by the PapB protein. *EMBO J.* **19**, 1450-1457 (2000).
47. Tewari, R., Macgregor, J.I., Ikeda, T., Little, J.R., Hultgren, S.J. & Abraham, S.N. Neutrophil Activation by Nascent Fimh Subunits of Type-1 Fimbriae Purified from the Periplasm of Escherichia-Coli. *J. Biol. Chem.* **268**, 3009-3015 (1993).
48. Bouckaert, J. et al. Receptor binding studies disclose a novel class of high-affinity inhibitors of the Escherichia coli FimH adhesin. *Mol. Microbiol.* **55**, 441-455 (2005).
49. Wellens, A. et al. Intervening with Urinary Tract Infections Using Anti-Adhesives Based on the Crystal Structure of the FimH-Oligomannose-3 Complex. *PLoS ONE* **3**(2008).
50. Han, Z.F. et al. Structure-Based Drug Design and Optimization of Mannoside Bacterial FimH Antagonists. *J. Med. Chem.* **53**, 4779-4792 (2010).
51. Le Trong, I. et al. Structural Basis for Mechanical Force Regulation of the Adhesin FimH via Finger Trap-like beta Sheet Twisting. *Cell* **141**, 645-655 (2010).
52. Yakovenko, O., Tchesnokova, V., Aprikian, P., Forero, M., Vogel, V., Sokurenko, E. & Thomas, W. Mechanical force activates an adhesion protein through allosteric regulation. *Biophys. J.*, 348A-349A (2007).
53. Yakovenko, O. et al. FimH forms catch bonds that are enhanced by mechanical force due to allosteric regulation. *J. Biol. Chem.* **283**, 11596-11605 (2008).
54. Dembo, M., Torney, D.C., Saxman, K. & Hammer, D. The Reaction-Limited Kinetics of Membrane-to-Surface Adhesion and Detachment. *Proc. R. Soc. B* **234**, 55-83 (1988).
55. Konstantopoulos, K., Hanley, W.D. & Wirtz, D. Receptor-ligand binding: 'Catch' bonds finally caught. *Curr. Biol.* **13**, R611-R613 (2003).
56. Isberg, R.R. & Barnes, P. Dancing with the host: Flow-dependent bacterial adhesion. *Cell* **110**, 1-4 (2002).

57. Thomas, W.E., Trintchina, E., Forero, M., Vogel, V. & Sokurenko, E.V. Shear prevents detachment of target cells bound to E-coli via the bacterial adhesin, FimH. *Second Joint Embs-Bmes Conference 2002, Vols 1-3, Conference Proceedings*, 707-708 (2002).
58. Levy, S.B. Antibiotic resistance - the problem intensifies. *Adv. Drug Delivery. Rev.* **57**, 1446-1450 (2005).
59. Ofek, I., Kahane, I. & Sharon, N. Toward anti-adhesion therapy for microbial diseases. *Trends Microbiol.* **4**, 297-299 (1996).
60. Ofek, I. & Sharon, N. Visions & reflections - A bright future for anti-adhesion therapy of infectious diseases. *Cell. Mol. Life Sci.* **59**, 1666-1667 (2002).
61. Ofek, I., Hasy, D.L. & Sharon, N. Anti-adhesion therapy of bacterial diseases: prospects and problems. *FEMS Immunol. Med. Microbiol.* **38**, 181-191 (2003).
62. Sharon, N. Carbohydrates as future anti-adhesion drugs for infectious diseases. *Bba-Gen Subjects* **1760**, 527-537 (2006).
63. Sharon, N. & Lis, H. Lectins - Cell-Agglutinating and Sugar-Specific Proteins. *Science* **177**, 949-959 (1972).
64. Ofek, I., Mirelman, D. & Sharon, N. Adherence of Escherichia-Coli to Human Mucosal Cells Mediated by Mannose Receptors. *Nature* **265**, 623-625 (1977).
65. Sharon, N. Bacterial lectins, cell-cell recognition and infectious disease. *FEBS Lett.* **217**, 145-157 (1987).
66. Firon, N., Ashkenazi, S., Mirelman, D., Ofek, I. & Sharon, N. Aromatic Alpha-Glycosides of Mannose Are Powerful Inhibitors of the Adherence of Type-1 Fimbriated Escherichia-Coli to Yeast and Intestinal Epithelial-Cells. *Infect. Immun.* **55**, 472-476 (1987).
67. Hung, C.-S. et al. Structural basis of tropism of Escherichia coli to the bladder during urinary tract infection. *Mol. Microbiol.* **44**, 903-915 (2002).
68. Hartmann, M. & Lindhorst, T.K. The Bacterial Lectin FimH, a Target for Drug Discovery - Carbohydrate Inhibitors of Type 1 Fimbriae-Mediated Bacterial Adhesion. *Eur. J. Org. Chem.*, 3583-3609 (2011).
69. Lindhorst, T.K., Kieburg, C. & Krallmann-Wenzel, U. Inhibition of the type 1 fimbriae-mediated adhesion of Escherichia coli to erythrocytes by multiantennary alpha-mannosyl clusters: The effect of multivalency. *Glycoconjugate J.* **15**, 605-613 (1998).
70. Grabosch, C., Hartmann, M., Schmidt-Lassen, J. & Lindhorst, T.K. Squaric Acid Monoamide Mannosides as Ligands for the Bacterial Lectin FimH: Covalent Inhibition or Not? *Chembiochem* **12**, 1066-1074 (2011).
71. Klein, T. et al. FimH Antagonists for the Oral Treatment of Urinary Tract Infections: From Design and Synthesis to in Vitro and in Vivo Evaluation. *J. Med. Chem.* **53**, 8627-8641 (2010).
72. Han, Z.F. et al. Lead Optimization Studies on FimH Antagonists: Discovery of Potent and Orally Bioavailable Ortho-Substituted Biphenyl Mannosides. *J. Med. Chem.* **55**, 3945-3959 (2012).
73. Firon, N., Ofek, I. & Sharon, N. Carbohydrate Specificity of the Surface Lectins of Escherichia-Coli, Klebsiella-Pneumoniae, and Salmonella-Typhimurium. *Carbohydr. Res.* **120**, 235-249 (1983).
74. Sokurenko, E.V., Courtney, H.S., Ohman, D.E., Klemm, P. & Hasty, D.L. Fimh Family of Type-1 Fimbrial Adhesins - Functional-Heterogeneity Due to Minor Sequence Variations among Fimh Genes. *J. Bacteriol.* **176**, 748-755 (1994).
75. Sperling, O., Fuchs, A. & Lindhorst, T.K. Evaluation of the carbohydrate recognition domain of the bacterial adhesin FimH: design, synthesis and binding properties of mannoside ligands. *Org. Biomol. Chem.* **4**, 3913-3922 (2006).

76. Durka, M., Buffet, K., Iehl, J., Holler, M., Nierengarten, J.F., Taganna, J., Bouckaert, J. & Vincent, S.P. The functional valency of dodecamannosylated fullerenes with *Escherichia coli* FimH-towards novel bacterial antiadhesives. *Chem. Commun. (Camb.)* **47**, 1321-1323 (2011).
77. Horst, A.K., Kotter, S., Lindhorst, T.K., Ludwig, A., Brandt, E. & Wagener, C. Binding inhibition of type 1 fimbriae to human granulocytes: a flow cytometric inhibition assay using trivalent cluster mannosides. *Med. Microbiol. Immunol.* **190**, 145-149 (2001).
78. Eden, C.S., Freter, R., Hagberg, L., Hull, R., Hull, S., Leffler, H. & Schoolnik, G. Inhibition of Experimental Ascending Urinary-Tract Infection by an Epithelial Cell-Surface Receptor Analog. *Nature* **298**, 560-562 (1982).
79. Aronson, M., Medalia, O., Schori, L., Mirelman, D., Sharon, N. & Ofek, I. Prevention of Colonization of the Urinary-Tract of Mice with *Escherichia-Coli* by Blocking of Bacterial Adherence with Methyl Alpha-D-Mannopyranoside. *J. Infect. Dis.* **139**, 329-332 (1979).

3.2 Synthesis of Antagonists for FimH

3.2.1 *Manuscript 3: Water: to be or not to be displaced?*

Author contributions:

Katharina Mayer: synthesis of 2-*O*-modified mannoside, collection of data, preparation of manuscript.

Adam Zalewski: molecular modeling studies, preparation of manuscript.

Roland Preston: ITC experiments.

Dr. Said Rabbani: protein expression.

Manuscript for **Bioorganic & Medicinal Chemistry Letters**

Water: to be or not to be displaced?

Katharina Mayer,^{‡^a} Adam Zalewski,^{‡^a} Roland Preston,^a Said Rabbani,^a and Beat Ernst^{*^a}

^a *Institute of Molecular Pharmacy, Pharmacenter, University of Basel, Klingelbergstr.50, 4056 Basel, Switzerland*

* Corresponding author: Prof. Dr. Beat Ernst, Institute of Molecular Pharmacy, Pharmacenter, University of Basel, Klingelbergstrasse 50, CH-4056 Basel, Switzerland, Tel: +41 61 2671551, Fax: +41 61 2671552; e-mail: beat.ernst@unibas.ch

‡ These authors contributed equally to this work

Keywords: FimH · 2-*O*-modification of mannose · water displacement · ITC · molecular dynamics.

Abbreviations: CRD, carbohydrate recognition domain; CSA, camphor sulfonic acid; DMF, dimethylformamide; *E. coli*, *Escherichia coli*; HPLC, high-performance liquid chromatography; ITC, isothermal titration calorimetry; MD, molecular dynamics; MS, molecular sieves; TBAB, tetrabutyl ammonium bromide; TLC, thin layer chromatography; UPEC, uropathogenic *E. coli*; UTI, urinary tract infection.

ABSTRACT

FimH is a bacterial lectin enabling the adhesion of *E. coli* to urothelial cells, the initial interaction leading to urinary tract infections. X-ray data of mannose derivatives co-crystallized with FimH reveal a conserved water molecule deep within the binding pocket. This study is focused on the displaceability of this water by a *n*-heptyl α -D-mannoside modified in the 2-position. In case the water molecule is no structural water its replacement can lead to a substantially improved binding affinity. Since binding studies with the modified mannoside **2** revealed a complete loss of affinity, a detailed molecular modeling investigation was performed. The results indicated a distortion of the ligand binding pose with a nonoptimal interaction profile explaining the loss in affinity.

INTRODUCTION

Adhesion to host cells is the initial step, when bacteria establish infections. In urinary tract infections (UTIs), uropathogenic *Escherichia coli* (UPEC) are the causative pathogens.¹⁻⁴ With the lectin FimH located at the tip of filamentous organelles, attachment of bacteria to the urothelial cells is provided.⁵⁻⁷ This first step of recognition and therewith adherence is crucial for the establishment of an infection. Adherence prevents bacteria from being washed out by the bulk flow of urine. FimH is a mannose-specific lectin recognizing glycoconjugates such as uroplakin Ia prevalent on the urothelial cells. Treatment of UTIs with antibiotics is causing increasingly resistance problems. Therefore, alternative therapeutics are urgently required. The development of anti-adhesive agents that are able to prevent the crucial interaction with the urothelial cells presents a promising approach.^{8,9}

In the course of developing small-molecule FimH antagonists, various alkyl and aryl α -D-mannosides have been reported with low nanomolar affinities for FimH.^{10,11-14} All of these FimH antagonists bear an unmodified mannose moiety. Approaches towards the replacement of this entity by other carbohydrates or deoxy mannosides lead to a substantial loss in affinity indicating the high specificity of FimH for α -D-mannosides. The latter was rationalized by crystallographic data revealing that each of the hydroxyl groups in mannose establishes one or more H-bonds (Figure 1).¹⁵

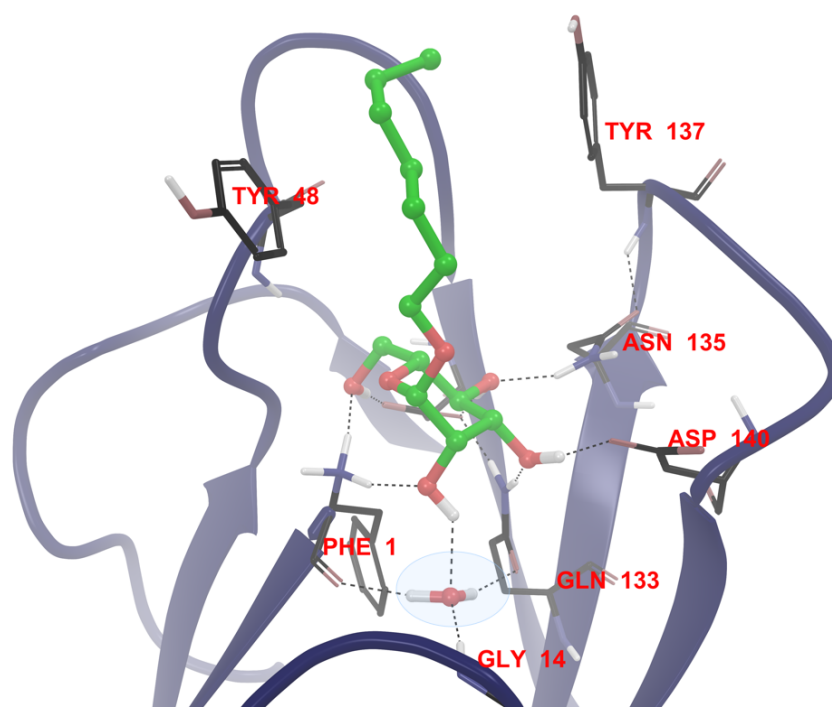


Figure 1. Binding mode of *n*-heptyl mannoside **1** as ribbon representation with highlighted H-bonding network derived from docking to the CRD of FimH (PDB 1UWF¹⁶). The water molecule maintains on average a maximum of two hydrogen bonds at a time.

The analysis of X-ray data on apo and holo FimH crystal structures revealed a conserved water molecule within the mannoside binding pocket (Figure 1).^{12, 16-20} The successful displacement of such a water molecule by a proper modification of the ligand is associated with an affinity improvement driven by the entropic gain upon release of the water molecule.²¹ This concept has successfully been applied in drug-discovery before.²²

The goal of this study was to investigate the displacement of the conserved water molecule in the CRD of FimH. Therefore, a modified ligand was designed and synthesized expected to result in a gain in binding energy, while also offering a structurally new antagonist species which can be beneficial regarding selectivity.²³

RESULTS AND DISCUSSION

Design and synthesis of the new ligand

In several crystal structures^{12, 16-20} a water molecule mediated the interaction of 2-OH of mannose with FimH (Figure 1). Since molecular dynamics (MD) simulations indicated that this water molecule does not form stable interactions with the protein, its displacement through an antagonist modified in the 2-position offers the opportunity to increase affinity, predominantly by an improved entropy term.²⁴

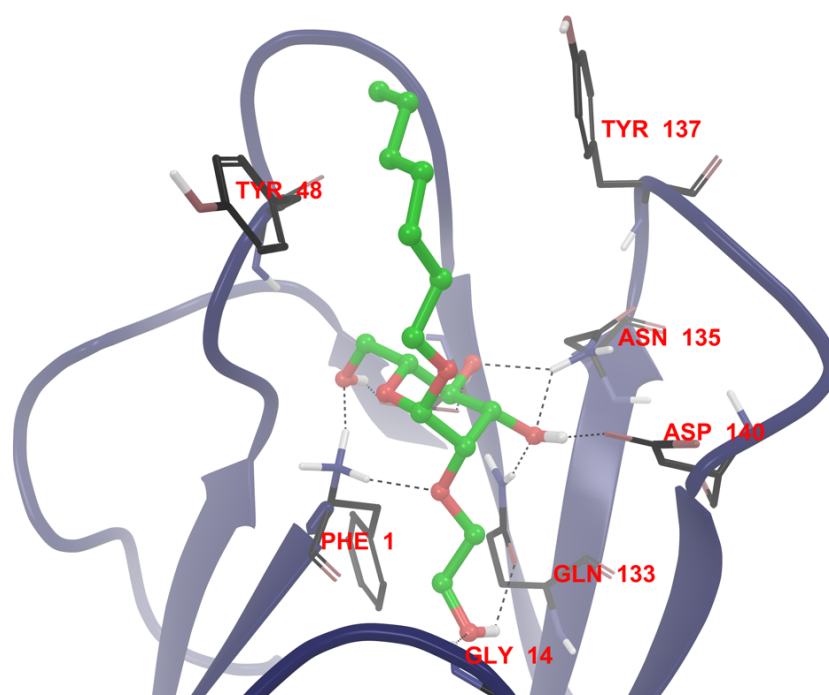


Figure 2. Modified 2-*O*-extended analogue **2** docked in FimH (PDB 1UWF¹⁶) representing the optimal scenario with displacement of water.

Molecular modeling studies suggested that an extension at the C2 position of mannose could offer the mentioned benefits. Accordingly, a *n*-heptyl α -D-mannoside (**1**) with the 2-OH group replaced by an 2-hydroxyethoxy moiety (\rightarrow **2**) was selected for chemical synthesis and subsequent biological evaluation (Figure 2).

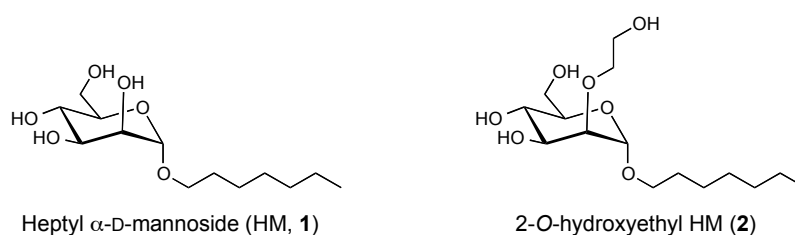
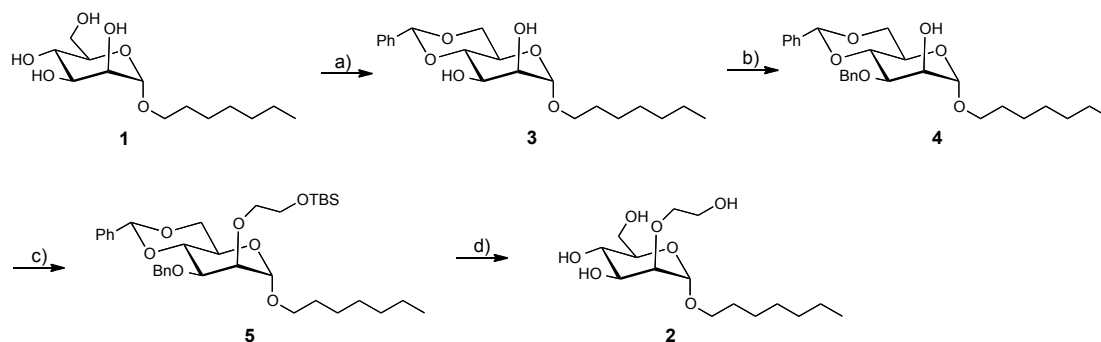


Figure 3. Heptyl mannoside (**1**)¹⁶ and modified ligand with extension at position C2 of mannose (**2**).

The 2-*O*-modified mannoside **2** was synthesized from *n*-heptyl α -D-mannoside (**1**)¹⁶ in four steps (Scheme 2). Firstly, the 4,6-*O*-benzylidene acetal (\rightarrow **3**) was formed, followed by 3-selective benzylation (\rightarrow **4**). The ethoxy moiety was introduced as TBS protected 2-bromoethanol (\rightarrow **5**) an final deprotection under *Zemplén* conditions yielded the target compound **2**.



Scheme 2. a) benzaldehyde dimethyl acetal, DMF, CSA, 12h, r.t., 63%; b) i) Bu_2SnO , toluene, Δ , 5h, ii), BnBr , TBAB, toluene, Δ , 8h, 80%; c) (2-bromoethoxy)-*tert*-butyldimethylsilane, NaH , DMF, 12h, r.t., 36%; d) $\text{Pd}(\text{OH})_2/\text{C}$, H_2 (atm. pressure), toluene/ H_2O (4:1), 12h, 91%.

We performed isothermal titration calorimetry (ITC) to determine the dissociation constant and the thermodynamic fingerprint of **2**. However, these experiments showed no binding of the mannoside **2** to FimH. To elucidate this unexpected loss in affinity, with respect to **1** ($K_D = 7.3 \pm 1.8 \text{ nM}$)²⁵, more in-depth computational methods were initiated.

Molecular dynamics

A suitable ligand structure does not guarantee improved binding energetics. Among other reasons, this is due to the fact that for obtaining a desired binding mode, enthalpic costs for partly desolvation of protein and ligand have to be paid. The additional rotatable bonds introduced in **2** that are restrained upon binding might have led to increased ligand internal strain and entropic costs. These penalties needed to be overcompensated by a gain in solvent entropy upon release of the water molecule (up to 2 kcal/mol for displacing a single water molecule²¹) and improved protein-ligand interactions. To inspect the interplay of these energy contributions, ensembles of frames obtained from MD simulations for both **2** and **1** were post-processed with the Molecular Mechanics *Generalized* Born Surface Area (MM-GBSA) method. The calculations were further augmented with Rigid Rotor-Harmonic Oscillator (RRHO) entropy approximations. Though the current field of molecular modeling

provides potentially more advanced methods²⁶, the chosen setup allowed for uniquely detailed insight into the contributions of specific binding energy components (Table 1).

Table 1. Results of MM-GBSA/RRHO calculations, including selected energy components. All values [kcal/mol] obtained as averages over 250 frames extracted from 30 ns simulations for the parent (**1**) and child (**2**) compound. Due to the method specifics and lack of some entropy components, these values are expected to be overestimated.

	1	2
MM-GBSA $\Delta G_{\text{Coulomb}}$	-31.9	-37.5
MM-GBSA $\Delta G_{\text{Lipophilic}}$	-30.6	-37.8
MM-GBSA $\Delta G_{\text{Solvation}}$	18.8	19.0
MM-GBSA ΔG_{vdW}	-23.7	-28.9
MM-GBSA ΔG_{Total}	-67.1	-81.8
Ligand strain	4.5	6.5
Protein strain	11.1	12.4
RRHO entropy	17.8	19.7
MM-GBSA + RRHO	-49.3	-62.1

The obtained data strongly indicated that if the modified ligand were to displace the conserved water molecule and assume the favorable docking conformation (Figure 2) while maintaining the same interactions as **1**, it would benefit from a substantial increase in binding energy. This increase would be in fact large enough (relative calculated $\Delta\Delta G$ of 12.8 kcal/mol) to insure correct compound ranking in spite of potential inaccuracies of the implemented methods²⁷. Based on these findings we conclude that the modified compound failed to assume the favorable docking pose.

In order to obtain the most favorable pose (Figure 2B), the employed docking software required removal of the conserved water molecule from the FimH binding site. Although this approach was justified by the exchange of the molecule with the bulk solvent (observed in a corresponding simulation of the apo FimH structure), an attempt to dock the modified compound in presence of the molecule was also made. As a result, a pose with an inferior score compared to **1** and a noticeable distortion of the hydrogen-bond network was obtained (Figure 3). A subsequent MD simulation did not yield an improvement of this pose. Interactive inspection of the simulation revealed that the buried water molecule was immobilized by a steric clash with the ligand impairing the exchange with the bulk solvent and hampering an optimal binding. Further simulations revealed progression of the distortion to a point where several crucial interactions with the protein were lost.

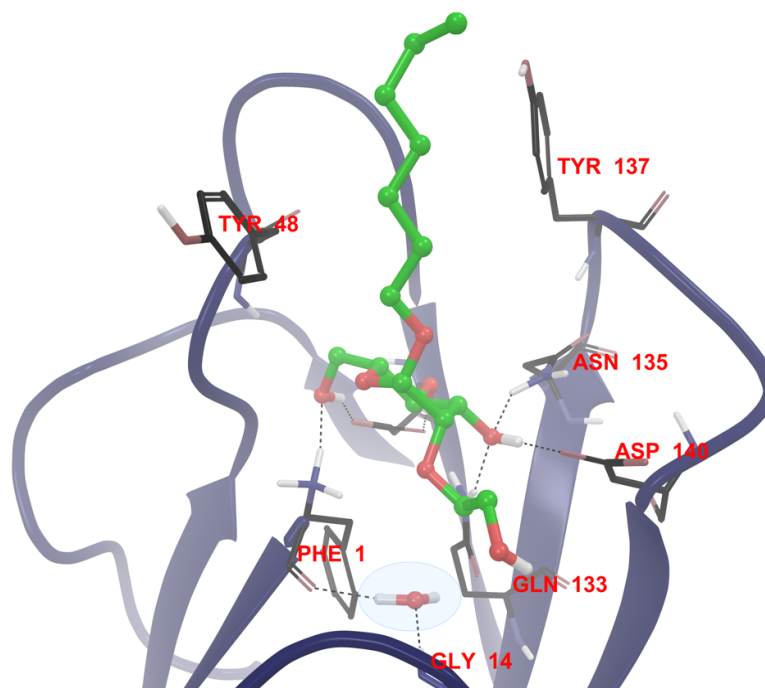


Figure 3. Binding mode (probable scenario) of ligand **2** to the crystal structure of FimH (PDB 1UWF¹⁶). Ligand accommodates a distorted binding mode, impairing optimal interaction. The water molecule is not displaced. (left: ribbon representation, right: shell presentation).

Finally, we compared the bound and solution conformations of the extended ligand **2**. An analysis of the free ligand MD simulations implied that conformations close to the one required for favorable binding were scarcely populated (Figure 4). Taken together, this implied that the modified ligand could neither approach the receptor in a favorable conformation nor adapt its shape within the binding site. This scenario likely reflects the obtained ITC data.

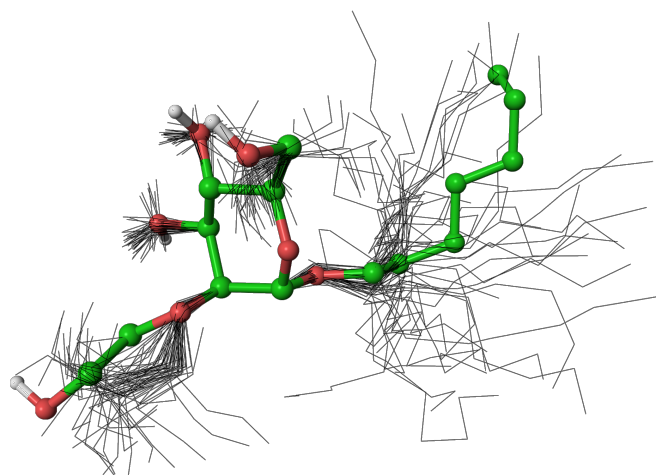


Figure 4. Superposition (mannose heavy atoms) of docked (ball and stick) and MD poses (black wires; 50 representative frames) for the modified mannosidic compound **2**.

CONCLUSION

This study was focused on the displacement of a water molecule within the mannose binding pocket of FimH. Although, we had no indication for a structural role of this water molecule, an antagonist designed to replace it, showed no affinity for FimH in the ITC experiment. MD studies revealed that the proper spatial arrangement of the hydroxyethoxy chain, i.e. the bioactive conformation, was not populated in solution. Ligand rearrangement inside the binding site is not possible due to steric clashes with the protein and the trapped water molecule. This forces a distorted binding mode of **2** impairing optimal binding interaction as reflected by the experimental data. Furthermore, molecular modeling allowed for some additional insights. Specifically, desolvation energy, strain and entropy penalties prevent the ligand from assuming the pose necessary for binding. Given the previously unsuccessful attempts of replacing the mannose with other carbohydrate moieties¹⁶, our results further indicate that the CRD of FimH does not tolerate modifications on the physiological ligand D-mannose. In addition, this is an example that the displacement of a water molecule is not a unambiguous concept to improve affinity. Even if the water molecule in question is not of structural type, failing to displace a single solvent molecule with a ligand modification may have devastating effects on the potency of the latter.

EXPERIMENTAL SECTION

Synthesis

General Methods: NMR spectra were recorded on a Bruker Avance DMX-500 (500 MHz) spectrometer. Assignment of ¹H and ¹³C NMR spectra was achieved using 2D methods (COSY, HSQC, HMBC, TOCSY). Chemical shifts are expressed in ppm in relation to the residual solvent signals (CHCl₃, CHD₂OD, and HDO) on the δ-scale. Coupling constants J are given in Hertz (Hz). Multiplicities were specified as follows: s (singlet), d (doublet), dd (doublet of a doublet), t (triplet), q (quartet), m (multiplet). For assignment of resonance signals to the appropriate nuclei the following abbreviation was used: hep (heptyl). Commercially available reagents were purchased from Fluka, Aldrich, Merck, Abcr. Solvents were dried prior to use as indicated. Dichloromethane (CH₂Cl₂) was dried by filtration over Al₂O₃ (Fluka, type 5016 A basic). *N,N*-dimethylformamide (DMF), pyridine, and toluene were dried by distillation from calcium hydride. Methanol (MeOH) was dried by refluxing with sodium methoxide and distilled immediately before use. Molecular sieves were activated under vacuum at 500°C for 1 h immediately before use. Reactions were monitored

by TLC using glass plates coated with silica gel 60 F₂₅₄ (Merck) and visualized by using UV light and/or by charring with a molybdate solution (a 0.02 M solution of ammonium cerium sulfate dihydrate and ammonium molybdate tetrahydrate in aqueous 10% H₂SO₄). Column chromatography was performed on a CombiFlash Companion (Teledyne-ISCO, Inc.) using RediSep normal phase disposable flash columns (silica gel, 40-63 μm). Reversed phase chromatography was performed on LiChroprepRP-18 (Merck, 40-63 μm). LC-MS separations were carried out using Sunfire C₁₈ columns (19 x 150 mm, 5.0 μm) on a Waters 2525 LC, equipped with Waters 2996 photodiode array and Waters micromass ZQ MS for detection. Electron spray ionization mass spectra (ESI-MS) were obtained on a Waters micromass ZQ. HR-MS analysis were carried out using a Agilent 1100 LC equipped with a photodiode array detector and a Micromass QTOF I equipped with a 4 GHz digital-time converter. Optical rotations were measured using Perkin-Elmer polarimeter 341. Microanalysis was performed at the Institute of Organic Chemistry at the University of Basel, Switzerland. Compound purity was determined on an Agilent 1100 HPLC; detector ELS, Waters 2420; column: Waters Atlantis dC18, 3 μm, 4.6 x 75 mm; eluents: A: water + 0.1% TFA; B: 90% acetonitrile + 10% water + 0.1% TFA.

***n*-Heptyl 4,6-*O*-benzylidene- α -D-mannopyranoside (3)**

To a solution of *n*-heptyl α -D-mannopyranoside **1**¹⁶ (120 mg, 0.43 mmol) in dry DMF (6.0 ml) benzaldehyde dimethylacetate (98 μl, 1.5 eq) and camphor sulfonic acid (catalytic amount) were added at r.t. The reaction mixture was stirred at 50°C for 5 h, then diluted with DCM (50 ml), washed with 5% aq. NaHCO₃ solution (50 ml), brine (50 ml), and dried over Na₂SO₄. The solvent was removed under reduced pressure and the residue was purified by flash chromatography on silica gel (PE/EtOAc 3:1 to 3:2) to give **3** (100 mg, 63%) as a glassy solid.

¹H NMR (500 MHz, CD₃OD): δ 7.51-7.49 (m, 2H, Ar-H), 7.37-7.33 (m, 3H, Ar-H), 5.60 (s, 1H, PhCH), 4.77 (d, *J* = 1.0 Hz, 1H, H-1), 4.18 (dd, *J* = 10.0, 4.5 Hz, 1H, H-6a), 3.95-3.90 (m, 2H, H-3, H-4), 3.88 (m, 1H, H-2), 3.81 (t, *J* = 10.0 Hz, 1H, H-6b), 3.76-3.41 (m, 2H, H-5, OCH₂C₆H₁₃), 3.46 (dt, *J* = 9.5, 6.5 Hz, 1H, OCH₂C₆H₁₃), 1.62 (m, 2H, OCH₂CH₂C₅H₁₁), 1.36 (m, 8H, OC₂H₄C₄H₈CH₃), 0.91 (t, *J* = 7.0 Hz, 3H, OC₂H₄C₄H₈CH₃); ¹³C NMR (126 MHz, CD₃OD): δ 139.31, 129.87, 129.02, 127.52 (Ar-C), 103.36 (PhCH), 102.59 (C-1), 80.20 (C-3), 72.74 (C-2), 69.87 (C-6), 69.61 (C-4), 68.77 (OCH₂C₆H₁₃), 65.25 (C-5), 33.01,

30.57, 30.17, 27.29, 23.70, 14.46 (OCH₂C₆H₁₃); ESI-MS: calcd for C₂₀H₃₀O₆ [M+Na]⁺, 389.19, found 389.06.

***n*-Heptyl 3-*O*-benzyl-4,6-*O*-benzylidene- α -D-mannopyranoside (4)**

To a solution of **3** (80 mg, 0.218 mmol) in dry toluene (4 ml) was added dibutyltin oxide (112 mg, 0.456 mmol) at rt. The reaction suspension was refluxed for 6 h, concentrated to dryness under reduced pressure. To a solution of the product generated above in dry toluene (8 ml) was added tetrabutylammonium bromide (TBAB) (147 mg, 0.456 mmol) and benzyl bromide (59 μ L, 0.5 mmol). The mixture was stirred at 95°C overnight, concentrated to dryness, and purified by flash chromatography on silica gel (PE/EtOAc 9:1 to 4:1) to give **4** (172 mg, 91%) as colorless oil.

$[\alpha]_D^{20}$ +34.2 (*c* 1.43, MeOH); ¹H NMR (500 MHz, CDCl₃): δ 7.51-7.49 (m, 2H, Ar-H), 7.40-7.33 (m, 8H, Ar-H), 5.62 (s, 1H, PhCH), 4.86 (m, 1H, H-1), 4.87 (d, *J* = 11.5 Hz, 1H, PhCH₂), 4.73 (d, *J* = 11.5 Hz, 1H, PhCH₂), 4.27 (m, 1H, H-6a), 4.14-4.06 (m, 2H, H-4, H-2), 3.94 (dd, *J* = 9.5, 3.0 Hz, 1H, H-3), 3.88-3.82 (m, 2H, H-5, H-6b), 3.67 (m, 1H, OCH₂C₆H₁₃), 3.41 (m, 1H, OCH₂C₆H₁₃), 2.64 (s, 1H, OH), 1.57 (m, 2H, OCH₂CH₂C₅H₁₁), 1.29 (m, 8H, OC₂H₄C₄H₈CH₃), 0.89 (t, *J* = 7.0 Hz, 3H, OC₂H₄C₄H₈CH₃); ¹³C NMR (126 MHz, CDCl₃): δ 138.05, 137.53, 128.90, 128.45, 128.22, 127.88, 127.77, 126.01 (Ar-C), 101.52 (PhCH), 99.87 (C-1), 78.93 (C-4), 75.79 (C-3), 73.04 (PhCH₂), 70.10 (C-2), 68.92 (C-6), 67.97 (OCH₂C₆H₁₃), 63.19 (C-5), 32.75, 29.37, 29.05, 26.04, 22.61, 14.09 (OCH₂C₆H₁₃); HR-MS: calcd for C₂₇H₃₆O₆ [M+Na]⁺, 479.2410, found 479.2414.

***n*-Heptyl 3-*O*-benzyl-4,6-*O*-benzylidene-2-*O*-(2-((*tert*-butyldimethylsilyl)oxy)-ethoxy))- α -D-mannopyranoside (5)**

A solution of **4** (60 mg, 0.131 mmol) in anhydrous DMF (1 ml) was cooled to 0°C. NaH (60% dispersion in oil, 15.7 mg, 3 eq, 0.39 mmol) was added and the resulting suspension was stirred for 10 min. (2-Bromoethoxy)-*tert*-butyldimethylsilane (110 μ l, 3 eq, 0.39 mmol) was added and the mixture was stirred for 8 h and warmed to r.t. The mixture was poured on ice and the resulting emulsion was extracted repeatedly with EtOAc. The combined organic phases were dried with Na₂SO₄, filtered, concentrated and the solvent removed under reduced pressure. The crude product was purified by flash column chromatography on silica gel

(Petroleum ether/EtOAc gradient with 0.1% NEt₃). The product **5** was isolated (29 mg, 39%) along with unreacted starting material (17 mg, 28%) and TBS-protected product.

[α]_D²⁰ +27.4 (*c* 0.78, CHCl₃); ¹H NMR (500 MHz, CDCl₃): δ 7.51 (dd, *J* = 8.1, 6.4 Hz, 2H, Ar-H), 7.43 – 7.21 (m, 8H, Ar-H), 5.62 (s, 1H, PhHC), 4.90 – 4.82 (m, 2H, H-1, PhCH_{2a}), 4.73 (d, *J* = 12.2 Hz, 1H, PhCH_{2b}), 4.25 (dd, *J* = 10.0, 4.5 Hz, 1H, H-6a), 4.15 (m, 1H, H-4), 3.97 – 3.62 (m, 9H, H-2, H-3, H-5, H-6b, OCH_{2a}C₆H₁₃, 2PhCH₂), 3.37 (dt, *J* = 9.5, 6.6 Hz, 1H, OCH_{2b}C₆H₁₃), 1.56 (p, *J* = 6.7 Hz, 2H, OCH₂CH₂C₅H₁₁), 1.38 – 1.22 (m, 8H, OC₂H₄C₄H₈CH₃), 0.97 – 0.83 (m, 12H, OC₂H₄C₄H₈CH₃, SiC(CH₃)₃), 0.08 (d, *J* = 1.5 Hz, 6H, Si(CH₃)₂); ¹³C NMR (126 MHz, CDCl₃): δ 138.97, 137.90, 128.89, 128.39, 128.29, 127.57, 127.54, 126.17 (12, Ar-C), 101.53 (CH-Ph), 100.01 (C-1), 79.39 (C-4), 78.86 (C-2), 76.72 (H-3), 73.85 (CH₂), 73.23 (CH₂Ph), 69.09 (C-6), 67.96 (CH₂C₆H₁₃), 64.21 (C-5), 63.43 (CH₂OTBS), 31.89, 29.61, 29.22, 26.24 (4C, CH₂C₆H₁₃, SiC(CH₃)₃), 26.06 (SiC(CH₃)₃), 22.76 (C₅H₁₀CH₂CH₃), 14.23 (C₆H₁₂CH₃), -5.14, -5.20 (2C, Si(CH₃)₂); ESI-MS: calcd for C₃₅H₅₄O₇Si [M+Na]⁺: 637.35, found 637.36.

***n*-Heptyl 2-*O*-(2-hydroxyethyl)- α -D-mannopyranoside (**2**)**

Compound **5** (23 mg, 0.073 mmol) was dissolved in dioxane/water (4:1, v/v, 1.2 ml). Pd(OH)₂/C (10%) was added and the benzyl groups were hydrogenolytically cleaved by treatment with H₂ under atmospheric pressure. The dispersion was stirred overnight and upon completion of the reaction the catalyst was filtered off. ESI-MS indicated complete cleavage of TBS group. The crude product was purified by column chromatography, preparative HPLC, and P2 size exclusion chromatography. The product was obtained as colorless resin (11 mg, 91%).

[α]_D²⁰ +44.4 (*c* 0.97, MeOH); ¹H NMR (500 MHz, CD₃OD): δ 4.87 (d, *J* = 1.4 Hz, 1H, H-1), 3.81 (dd, *J* = 11.7, 2.3 Hz, 1H, H-6a), 3.76 – 3.58 (m, 8H, H-3, hep-C(1)H_{2a}, 2 PhCH₂, H-6b, H-4), 3.56 (dd, *J* = 3.5, 1.6 Hz, 1H, H-2), 3.49 (ddd, *J* = 9.6, 5.8, 2.3 Hz, 1H, H-5), 3.42 (dt, *J* = 9.6, 6.4 Hz, 1H, hep-C(1)H_{2b}), 1.67 – 1.52 (m, 2H, hep-CH₂), 1.45 – 1.24 (m, 8H, hep-CH₂), 0.91 (t, *J* = 7.0 Hz, 3H, hep-CH₃); ¹³C NMR (126 MHz, CD₃OD): δ 98.74 (C-1, ¹*J*_{CH} = 168 Hz), 81.08 (C-2), 74.63 (C-5), 73.88 (CH₂), 72.72 (C-3), 69.04 (C-4), 68.66 (hep-C-1), 62.86 (C-6), 62.47 (CH₂), 32.99, 30.66, 30.25, 27.34, 23.68 (5C, CH₂), 14.41 (CH₃); HR-MS: calcd for C₁₅H₃₀O₇ [M+Na]⁺: 345.1884, found 345.1883; HPLC: purity > 99.5 %, R_t 9.740 min; gradient: 5% → 70% MeCN over 20 min, 1.0 ml/min.

Molecular Modeling

For all experiments a 1.69 Å resolution crystal structure (PDB code 1UWF) of the FimH-CRD was used. Initial protein-ligand complexes were obtained through flexible docking using Glide (Glide, version 5.5, Schrödinger, LLC, New York, NY, 2009). Molecular dynamics (MD) simulations were carried out with Desmond²⁸ using the OPLS 2005 force field as implemented in the Schrödinger 2011 suite (Maestro, version 9.2, Schrödinger, LLC, New York, NY, 2011). Each system was solvated using an orthorhombic, TIP3P water²⁹ box with a minimum distance of 10 Å from the complex. Na⁺ and Cl⁻ ions were added to neutralize the charges and account for physiological salt concentration (0.15 M). Long-range electrostatic interactions were handled using the particle mesh Ewald summation.³⁰ All systems were equilibrated using the default relaxation protocol (Desmond 2.2; Schrodinger, Inc., New York, NY) and simulated over the span 30 ns (2 ns for the initial compound screening) with a time step of 2.0 fs. The SHAKE algorithm³¹ was applied to all heavy-atom bound hydrogens. Production runs were carried out in the Martyna-Tobias-Klein isothermal-isobaric ensemble (NPT)³² using the Nose-Hoover barostat to maintain a constant temperature of 300 K.³³ Energetic and structural data were recorded in 3.0 ps intervals. To obtain representative poses, trajectory clustering was performed based on ligand heavy atom RMSDs (1000 snapshots per simulation with 0.5 Å cutoff between clusters) using a hierarchical average-linkage algorithm. Molecular mechanics-generalized Born surface area (MM-GBSA) and Rigid Rotor-Harmonic Oscillator (RRHO) calculations were performed on ensembles of 250 MD snapshots using the default settings implemented in Prime (Prime, version 3.0, Schrödinger, LLC, New York, NY, 2011.) and MacroModel (MacroModel, version 9.9, Schrodinger, LLC, New York, NY, 2011.). All images were generated using Maestro.

Isothermal Titration Calorimetry

ITC experiments were performed according to a previously reported procedure.³⁴ FimH-CRD was dialyzed over night at 4 °C against assay buffer using Slide-A-Lyzer dialysis cassettes with 10 kDa cut-off (Thermo Fisher Scientific, Waltham, MA, USA). A final protein concentration of 18 µM was used. The ligand was diluted to 300 µM in assay buffer (20 mM HEPES, 150 mM NaCl, and 1 mM CaCl₂, pH 7.4). The measurements were performed with a MicroCalTM VP-ITC instrument (GE Healthcare, Northampton, MA, USA; sample cell

volume of 1.4523 mL) at 25 °C or 37 °C, 307 rpm stirring speed, and 10 µcal/s reference power. The samples were preheated to 3°C below the measurement temperature and degassed for 5 minutes prior to the measurements. Titration was started after steady baseline equilibration was reached with an initial 2 µL injection. Ligand was injected in 15 µL steps with a spacing of 10 minutes to ensure non-overlapping peaks. Baseline adjustments and peak integration were performed using the Origin 7 software (OriginLab, Northampton, MA, USA). No heat of interaction was observed at 25 °C. Since this may be a consequence of an silent reaction in terms of enthalpy, the measurement was repeated at 37 °C with the same outcome.

ACKNOWLEDGEMENTS

The authors gratefully acknowledge the financial support by the Swiss National Science Foundation (grant no. 200020_129935).

REFERENCES

1. Mahan, K. T.; Wang, J. *J. Am. Podiatr. Med. Assoc.* **1993**, *83*, 607.
2. Ronald, A. *Am. J. Med.* **2002**, *113*, 14S.
3. Foxman, B. *American Journal of Public Health* **1990**, *80*, 331.
4. Foxman, B.; Barlow, R.; D'Arcy, H.; Gillespie, B.; Sobel, J. D. *Ann. Epidemiol.* **2000**, *10*, 509.
5. Wiles, T. J.; Kulesus, R. R.; Mulvey, M. A. *Exp. Mol. Pathol.* **2008**, *85*, 11.
6. Mulvey, M. A. *Cell. Microbiol.* **2002**, *4*, 257.
7. Knight, S. D.; Berglund, J.; Choudhury, D. *Curr. Opin. Chem. Biol.* **2000**, *4*, 653.
8. Ofek, I.; Hasy, D. L.; Sharon, N. *FEMS Immunol. Med. Microbiol.* **2003**, *38*, 181.
9. Sharon, N. *Bba-Gen Subjects* **2006**, *1760*, 527.
10. Firon, N.; Ashkenazi, S.; Mirelman, D.; Ofek, I.; Sharon, N. *Infect. Immun.* **1987**, *55*, 472.
11. Grabosch, C.; Hartmann, M.; Schmidt-Lassen, J.; Lindhorst, T. K. *Chembiochem* **2011**, *12*, 1066.
12. Han, Z. F.; Pinkner, J. S.; Ford, B.; Obermann, R.; Nolan, W.; Wildman, S. A.; Hobbs, D.; Ellenberger, T.; Cusumano, C. K.; Hultgren, S. J.; Janetka, J. W. *J. Med. Chem.* **2010**, *53*, 4779.
13. Klein, T.; Abgottspon, D.; Wittwer, M.; Rabbani, S.; Herold, J.; Jiang, X. H.; Kleeb, S.; Luthi, C.; Scharenberg, M.; Bezencon, J.; Gubler, E.; Pang, L. J.; Smiesko, M.; Cutting, B.; Schwardt, O.; Ernst, B. *J. Med. Chem.* **2010**, *53*, 8627.
14. Schwardt, O.; Rabbani, S.; Hartmann, M.; Abgottspon, D.; Wittwer, M.; Kleeb, S.; Zalewski, A.; Smiesko, M.; Cutting, B.; Ernst, B. *Bioorg. Med. Chem.* **2011**, *19*, 6454.

15. Hung, C.-S.; Bouckaert, J.; Hung, D.; Pinkner, J.; Widberg, C.; DeFusco, A.; Auguste, C. G.; Strouse, R.; Langermann, S.; Waksman, G.; Hultgren, S. J. *Mol. Microbiol.* **2002**, *44*, 903.
16. Bouckaert, J.; Berglund, J.; Schembri, M.; De Genst, E.; Cools, L.; Wuhrer, M.; Hung, C. S.; Pinkner, J.; Slattegard, R.; Zavialov, A.; Choudhury, D.; Langermann, S.; Hultgren, S. J.; Wyns, L.; Klemm, P.; Oscarson, S.; Knight, S. D.; De Greve, H. *Mol. Microbiol.* **2005**, *55*, 441.
17. Choudhury, D.; Thompson, A.; Stojanoff, V.; Langermann, S.; Pinkner, J.; Hultgren, S. J.; Knight, S. D. *Science* **1999**, *285*, 1061.
18. Hung, C. S.; Bouckaert, J.; Hung, D.; Pinkner, J.; Widberg, C.; DeFusco, A.; Auguste, C. G.; Strouse, R.; Langermann, S.; Waksman, G.; Hultgren, S. J. *Mol. Microbiol.* **2002**, *44*, 903.
19. Wellens, A.; Garofalo, C.; Nguyen, H.; Van Gerven, N.; Slattegard, R.; Hernalsteens, J. P.; Wyns, L.; Oscarson, S.; De Greve, H.; Hultgren, S.; Bouckaert, J. *PLoS ONE* **2008**, *3*.
20. Le Trong, I.; Aprikian, P.; Kidd, B. A.; Forero-Shelton, M.; Tchesnokova, V.; Rajagopal, P.; Rodriguez, V.; Interlandi, G.; Klevit, R.; Vogel, V.; Stenkamp, R. E.; Sokurenko, E. V.; Thomas, W. E. *Cell* **2010**, *141*, 645.
21. Dunitz, J. D. *Science* **1994**, *264*, 670.
22. Chen, J. M.; Xu, S. L.; Wawrzak, Z.; Basarab, G.S.; Jordan, D. B. *Biochemistry* **1998**, *37*, 17735.
23. Scharenberg, M.; Schwardt, O.; Rabbani, S.; Ernst, B. *J. Med. Chem.* **2012**.
24. Kadirvelraj, R.; Foley, B. L.; Dyekjær, J. D.; Woods, R. J. *J. Am. Chem. Soc.* **2008**, *130*, 16933.
25. Wellens, A.; Lahmann, M.; Touaibia, M.; Vaucher, J.; Oscarson, S.; Roy, R.; Remaut, H.; Bouckaert, J. *Biochemistry* **2012**, *51*, 4790.
26. Gohlke, H.; Klebe, G. *Angew. Chem., Int. Ed.* **2002**, *41*, 2644.
27. Guimarães, C. R. W.; Cardozo, M. *J. Chem. Inf. Model.* **2008**, *48*, 958.
28. Bowers, K. J.; Chow, E.; Xu, H.; Dror, R. O.; Eastwood, M. P.; Gregersen, B. A.; Klepeis, J. L.; Kolossvary, I.; Moraes, M. A.; Sacerdoti, F. D.; Salmon, J. K.; Shan, Y.; Shaw, D. E. In *Proceedings of the 2006 ACM/IEEE conference on Supercomputing*; ACM: Tampa, Florida, 2006, 84.
29. Jorgensen, W. L.; Chandrasekhar, J.; Madura, J. D.; Impey, R. W.; Klein, M. L. *J. Chem. Phys.* **1983**, *79*, 926.
30. Darden, T.; York, D.; Pedersen, L. *J. Chem. Phys.* **1993**, *98*, 10089.
31. Ryckaert, J. P.; Ciccotti, G.; Berendsen, H. J. C. *J. Comput. Phys.* **1977**, *23*, 327.
32. Martyna, G. J.; Tobias, D. J.; Klein, M. L. *J. Chem. Phys.* **1994**, *101*, 4177.
33. Nosé, S. *Mol. Phys.* **1984**, *52*, 255.
34. Pang, L.; Kleeb, S.; Lemme, K.; Rabbani, S.; Scharenberg, M.; Zalewski, A.; Schadler, F.; Schwardt, O.; Ernst, B. *Chemmedchem* **2012**, *7*, 1404.

3.2.2 *Manuscript 4: Topliss Approach Applied to FimH Antagonists*

Author contributions:

Katharina Mayer: synthesis of biphenyl mannosides, data collection and coordination, preparation of manuscript.

Simon Kleeb: physicochemical evaluation of antagonists, contribution to manuscript.

Dr. Said Rabbani: protein expression, competitive polymer binding assay.

Pascal Zihlmann and Roland Preston: ITC experiments.

Manuscript in preparation for **ChemMedChem**

Topliss Approach Applied to FimH Antagonists

Katharina Mayer,^{‡a} Simon Kleeb,^{‡a} Said Rabbani,^a Pascal Zihlmann,^a Roland Preston,^a and Beat Ernst^{*a}

^a *Institute of Molecular Pharmacy, Pharmacenter, University of Basel, Klingelbergstr.50, 4056 Basel, Switzerland*

* Corresponding author: Prof. Dr. Beat Ernst, Institute of Molecular Pharmacy, Pharmacenter, University of Basel, Klingelbergstrasse 50, CH-4056 Basel, Switzerland, Tel: +41 61 2671551, Fax: +41 61 2671552; e-mail: beat.ernst@unibas.ch

‡ These authors contributed equally to this work

Keywords: bacterial adhesion · *E. coli* · FimH antagonists · biphenyl mannosides · *Topliss* · SAR · urinary tract infections

Abbreviations: Caco-2 cells, colorectal adenocarcinoma cells; CRD, carbohydrate recognition domain; D, octanol/water distribution coefficient; DMSO, dimethyl sulfoxide; *E. coli*, *Escherichia coli*; HPLC, high-performance liquid chromatography; IC₅₀, halfmaximal inhibitory concentration; ITC, isothermal titration calorimetry; PAMPA, parallel artificial membrane permeability assay; P_{app}, apparent permeability coefficient; SAR, structure–activity relationship; UPEC, uropathogenic *E. coli*; UTI, urinary tract infection.

ABSTRACT

Urinary tract infections (UTIs) are a serious health issue affecting millions of people and accounting for intensive medical costs. Increasing resistance to antibiotics demands a new strategy to deal with this infectious disease. FimH is a bacterial lectin on the tip of filamentous organelles expressed on *E. coli*, the causative agent of UTIs. This lectin establishes the attachment on bladder epithelial cells by recognizing mannosidic glycoproteins. Blocking this bacterial interaction with host cells would lead to clearance of the bacterium by the bulk flow of urine, which rationalizes the extensive search for potent FimH antagonists.

In this study, we synthesized a series of *o*-chloro-biphenyl α -D-mannosides with different substituents at the outer aromatic moiety applying the *Topliss* approach. We evaluated their potency as FimH antagonists in a target-based assay and determined solubility, lipophilicity, and for the most promising candidates, permeability properties. Our comprehensive study of these compounds revealed tolerated properties and hinted to a promising cyano substituted FimH antagonist.

INTRODUCTION

Adhesion to host cells is a prerequisite for microbes to efficiently establish infections. This initial contact is mediated by lectins located at the tip of bacterial fimbriae recognizing carbohydrate structures on the cell surface.

Escherichia coli (*E. coli*) is the causative pathogen in urinary tract infections (UTIs).^[1] UTIs are among the most prevalent and widespread infectious diseases.^[1b,1c] Therewith, UTIs account for significant morbidity as well as high medical costs.^[1b,2] A treatment with antibiotics frequently encounters resistance.^[3] New therapeutic strategies for the treatment and prevention of UTIs are therefore urgently required.

FimH is a bacterial lectin located at the tip of type 1 fimbriae that are expressed on *E. coli*. It recognizes glycoproteins located on urothelial cells such as uroplakin Ia and mediates the attachment of the bacterium to the host cell. This is a crucial step for bacterial survival. It prevents clearance of *E. coli* by the bulk flow of urine and furthermore facilitates the invasion into host cells.^[2b,4] Hence, inhibiting this first interaction is a promising therapeutic approach to prevent and treat UTIs.^[5]

FimH is a mannose-specific lectin, which contains a monomeric carbohydrate recognition domain (CRD) that is responsible for binding to the carbohydrate epitope of the host tissue.

Sharon and coworkers explored various mannosides and oligomannosides with micromolar to millimolar affinities as potential antagonists for FimH.^[6] The first crystal structure of FimH was solved in 1999^[7], and since then various crystallographic studies of FimH ligands have followed.^[8] Based on these studies the reported affinities can be rationalized. The CRD of FimH accommodates the mannose in a deep cavity with the hydroxyl groups forming an extensive hydrogen bond network. At the entrance to this cavity a hydrophobic rim is formed by the amino acids Tyr48, Tyr137, and Ile52, referred to as “tyrosine gate”.^[8a] The latter enables the accommodation of aliphatic and aromatic aglycones. Already the introduction of a simple alkyl aglycone, such as in *n*-heptyl α -D-mannopyranoside (**1**), led to nanomolar affinity.^[8b] With aromatic aglycones a further improvement of the inhibitory potency was achieved.^[9] To date, biphenyl mannosides, such as **2-4** (Figure 1), are among the most promising inhibitors with excellent pharmacodynamic and pharmacokinetic properties.^[10]

In a recently published study, we reported a beneficial effect on binding affinity by introducing substituents at the biphenyl moiety vicinal to the mannose moiety.^[10c] A chloro (\rightarrow **4**) or trifluoromethyl substituent in this position allows for a van der Waals contact leading to an improvement in affinity by a factor of two to three.

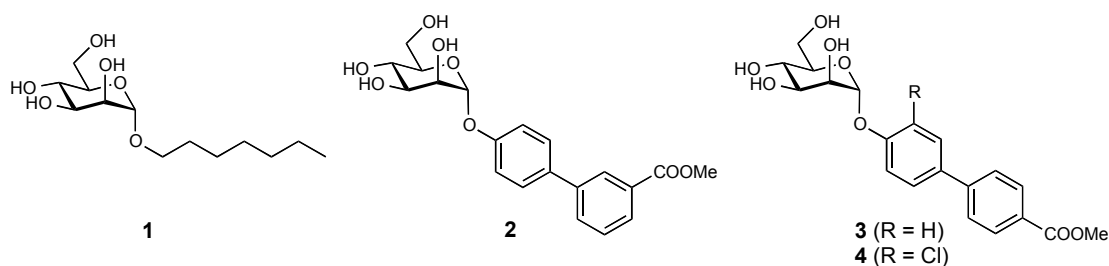


Figure 1. FimH antagonists; *n*-heptyl α -D-mannopyranoside (**1**) used as reference compound, the *meta*-substituted biphenyl derivative **2**^[11] and the *para*-substituted analogues **3**^[10b] and **4**^[10b] exhibit nanomolar affinities.

The crystal structure of FimH co-crystallized with biphenyl mannoside **2** (Figure 2) demonstrated the mannose moiety being involved in a vast H-bond network similar to heptyl mannoside **1**. The biphenyl aglycone binds in the out-docking mode establishing a π - π stacking interaction of the second phenyl moiety with Tyr48 of the tyrosine gate.^[11] For the biphenyl derivative **4** a similar out-docking mode was suggested.^[10b]

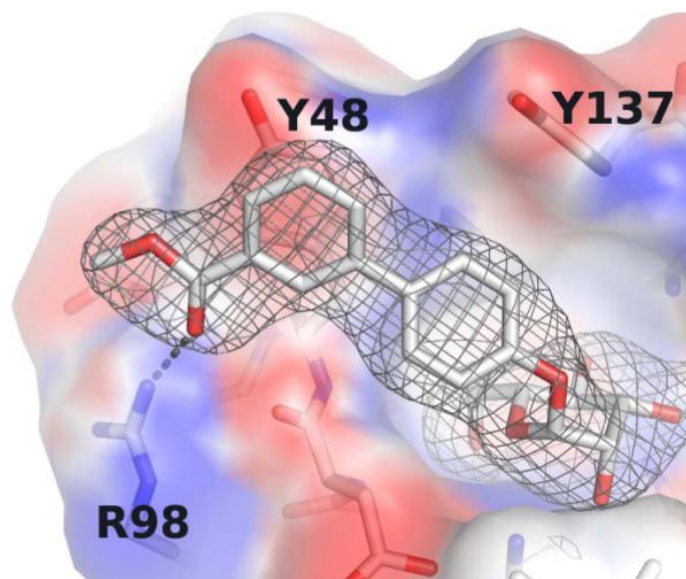


Figure 2. X-ray structure of biphenyl mannoside **2** taken from Han *et al.*^[11] (PDB 3MCY). Electron density (mesh) and surface electrostatic potential of FimH with positive and negative potential displayed in blue and red, respectively. Amino acids Tyr48, Tyr137, and Arg98 are involved in interactions with the biphenyl aglycones.

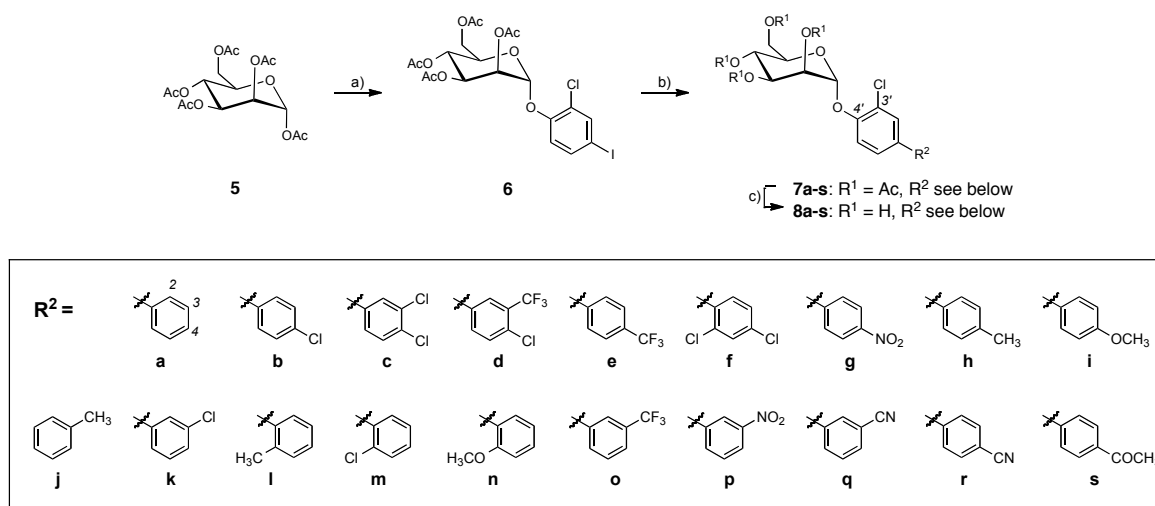
In this study, we focused on modifications of the outer phenyl ring of the biphenyl aglycone. In order to investigate the nature of the π - π stacking with Tyr48 the *Topliss* approach was applied.^[12] Based on the Hansch analysis^[13], this approach is a step-by-step SAR study of substituents on aromatic moieties. Each substituent has specific properties regarding hydrophobic, electronic, and steric effects. The *Topliss* operational scheme (*vide infra*) is used as a guideline to efficiently optimize the substitution pattern on aromatic rings.^[12]

Starting from the optimized 3'-chloro-biphenyl aglycone, substituents were introduced on the outer phenyl ring according to the *Topliss* protocol^[12] and binding affinities were tested in a target-based competitive polymer assay. We furthermore determined basic pharmacokinetic properties, i.e. solubility and lipophilicity of the compounds. Finally, for the most promising candidates, permeability was tested.

RESULTS AND DISCUSSION

Synthesis

We synthesized a series of biphenyl mannosides in analogy to previously described routes.^[10b,10c] Peracetylated α -D-mannose (**5**) was coupled with 2-chloro-4-iodophenole using $\text{BF}_3 \cdot \text{Et}_2\text{O}$. Introduction of substituted phenyl moieties via Suzuki coupling with aryl boronic acids or pinacol ester (in case of 3-CN) gave after deprotection under *Zemplén* conditions compound **8a-s** (Scheme 1).



Scheme 1. a) 2-chloro-4-iodophenole, $\text{BF}_3 \cdot \text{Et}_2\text{O}$, 40°C, 20h, 76%; b) Aryl boronic acid derivative, $\text{Pd}(\text{dppf})_2 \cdot \text{CH}_2\text{Cl}_2$, K_3PO_4 , DMF, 80°C, 5-12h; 45-90%; c) NaOMe, MeOH, 5-12h, 34-95%.

For choosing substituents on this second phenyl moiety, we applied the *Topliss* approach. This approach categorizes substituents according to their hydrophobicity π and their electronic effects σ ; steric effects are only partially considered. Depending on the affinity towards FimH (IC_{50} values) the substituents were successively chosen according to the *Topliss* scheme (Figure 3).

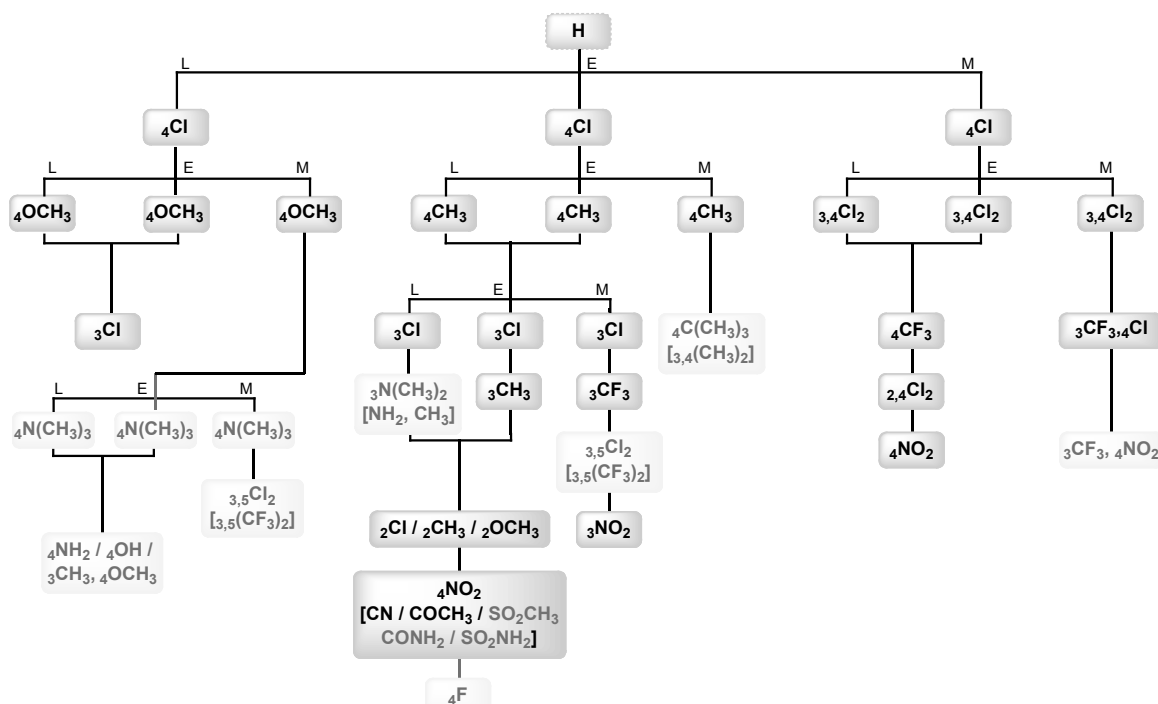


Figure 3. Operational scheme adapted from *Topliss*^[12]. Flow diagram allows the identification of most promising substituents with respect to binding affinity (M = more active, E = equally active, L = less active, compare to previous compound). Faded substituents were not investigated.

Biological Evaluation

In this study, we envisaged investigating the effects of various substituents on binding affinity and physicochemical properties. The affinity to the FimH CRD was determined in a cell-free competitive binding assay.^[14] Furthermore, solubility, lipophilicity, and permeability data predictive for intestinal absorption into circulation and subsequent excretion into the urine were determined. Aqueous solubility limits the maximal concentration of antagonist dissolved in the intestinal fluids and hence availability for absorption. Therefore, a minimal solubility of at least 50 µg/ml was envisaged.^[15] Lipophilicity quantified by the octanol water distribution coefficient (logD)^[16] is a key determinant for both, membrane permeability and renal excretion.^[17] The former improves with increase in lipophilicity unless transporter mediated processes are involved. The latter is favored by hydrophilicity, limiting antagonist reabsorption from the glomerular filtrate and non-renal elimination pathways.^[18]

Table 1. The cell-free competitive binding assay^[14] is based on the interaction of biotinylated polymer-bound trimannoside as competitor with the CRD of FimH. The affinities are reported as IC₅₀ and relative to parent compound **8a** as rIC₅₀. Heptyl α -D-mannoside (**1**) was tested on each plate as reference compound. Aqueous solubility and lipophilicity ($\log D_{7.4}$) were determined according to standard protocols. Promising compounds were further tested in a PAMPA assay for information on permeability.

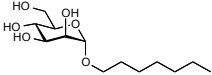
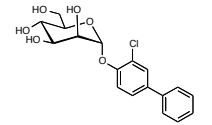
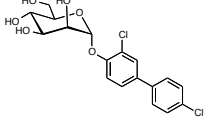
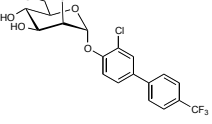
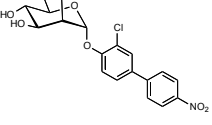
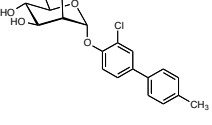
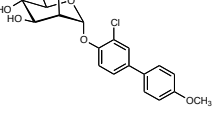
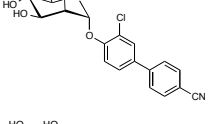
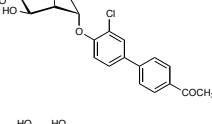
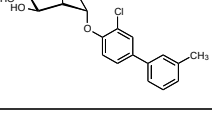
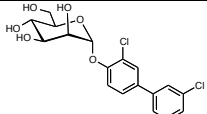
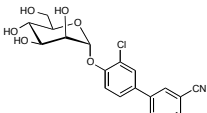
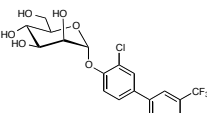
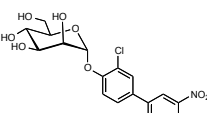
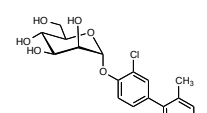
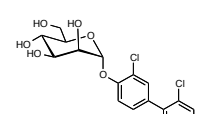
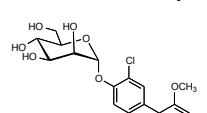
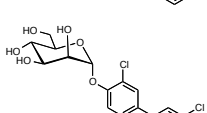
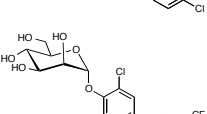
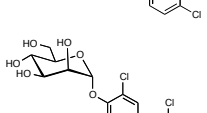
Compound	IC ₅₀ [nM]	rIC ₅₀	$\log D_{7.4}$ (mean \pm SD)	Solubility [μ g/ml] (mean \pm SD) / pH	PAMPA $\log P_e$ [log cm/s] (mean \pm SD) / pH
1 	73 \pm 7.9	2.4	1.7 \pm 0.0	>3000	n.d.
8a 	30.2	1	2.6 \pm 0.1	5.5 \pm 0.2 / 7.4	n.d.
8b 	22.0	0.73	3.3 \pm 0.1	3.5 \pm 0.3 / 7.4	n.d.
8c 	39.5	1.31	3.4 \pm 0.1	22 \pm 0 / 7.4	n.d.
8g 	37.6	1.24	2.3 \pm 0.0	117 \pm 7 / 7.4	-5.0 \pm 0.1 / 7.4
8h 	18.5	0.61	3.3 \pm 0.0	7.4 \pm 0.2 / 7.4	n.d.
8i 	23.2	0.77	2.7 \pm 0.1	3.8 \pm 0.4 / 7.4	n.d.
8r 	10.1	0.33	2.1 \pm 0.0	192 \pm 5 / 7.4	-5.2 \pm 0.0 / 7.4
8s 	21.3	0.71	2.1 \pm 0.1	16 \pm 0 / 7.4	n.d.
8j 	15.6	0.52	3.0 \pm 0.0	7.1 \pm 0.6 / 7.4	n.d.

Table 1. (Continued)

Compound	IC ₅₀ [nM]	rIC ₅₀	logD _{7.4} (mean ± SD)	Solubility [μg/ml] (mean ± SD) / pH	PAMPA log P _e [log cm/s] (mean ± SD) / pH
8k 	17.3	0.57	3.2 ± 0.0	5.7 ± 0.7 / 7.4	n.d.
8q 	17.9	0.59	2.1 ± 0.0	227 ± 5 / 7.4	-5.1 ± 0.0 / 7.4
8o 	25.4	0.84	3.3 ± 0.1	36 ± 1 / 7.4	n.d.
8p 	13.1	0.43	2.4 ± 0.1	23 ± 2 / 7.4	-4.9 ± 0.1 / 7.4
8l 	18.3	0.61	2.9 ± 0.0	135 ± 24 / 7.4	-4.6 ± 0.2 / 7.4
8m 	20.9	0.69	3.1 ± 0.1	28 ± 1 / 7.4	-4.4 ± 0.1 / 7.4
8n 	48.5	1.61	2.4 ± 0.0	> 280 / 7.4	-4.6 ± 0.1 / 7.4
8c 	17.2	0.57	n.d.	2.3 ± 0.2 / 7.4	n.d.
8d 	34.2	1.13	n.d.	1.0 ± 0.2 / 7.4	n.d.
8f 	21.9	0.73	n.d.	8.0 ± 0.8 / 7.4	n.d.

Binding Affinity

Affinity of the unsubstituted parent compound **8a** was in the low nanomolar range and exhibited a twofold higher binding affinity compared to *n*-heptyl mannoside (**1**). Introduction of hydrophobic residues is often accompanied by affinity improvement.^[12] Accordingly, the first substitution proposed is the introduction of a 4-chloro substituent. In the present case, the 4-chlorophenyl **8b** showed a slight improvement in affinity compared to the unsubstituted parent compound **8a**. Following the outer right branch of the *Topliss* tree (Figure 3), hydrophobicity was further increased by the introduction of a 3,4-dichloro substituted phenyl (\rightarrow **8c**), leading to only marginally improved affinity. With a 3-trifluoromethyl-4-chlorophenyl (\rightarrow **8d**) the affinity was slightly reduced to the level of the unsubstituted biphenyl **8a**. These observations indicate a too pronounced electron withdrawing and hydrophobic character of the latter substituents. Therefore, also the neighboring branches of the *Topliss* scheme were investigated. To elucidate whether the biological activity depends mainly on the electron withdrawing effect, the 4-trifluoromethyl (\rightarrow **8e**), the 2,4-dichloro (\rightarrow **8f**), and the 4-nitro (\rightarrow **8g**) bearing compounds were tested. These strong electron-withdrawing groups did not improve binding affinity compared to the chloro-substituted compounds **8b** and **8c**.

These results clearly indicate a non-optimal π/σ -balance. Since the effect of the 4-chloro substituent (\rightarrow **8b**) on affinity was not significantly different compared to the parent compound **8a**, a less electron withdrawing or a less hydrophobic group might be favorable. We therefore introduced substituents according to the middle branch of the *Topliss* scheme. Starting with a substituent with $-\sigma$, i.e. electron-donating, and $+\pi$ properties, a methyl group was introduced in 4-position (\rightarrow **8h**). This compound showed a retained binding affinity. Both substituents, chloro and methyl, have similar properties concerning hydrophobicity, however, the methyl group has a weak electron-donating effect. In order to investigate whether electron donating groups are acceptable, we synthesized the 4-methoxy compound (\rightarrow **8i**). In fact, binding affinity was in the same range as for the 4-chloro derivative **8b**. Proceeding according to the *Topliss* scheme, we introduced methyl and chloro in the 3-position (\rightarrow **8j**, \rightarrow **8k**). However, the affinity was unchanged. Introduction of these substituents in the 2-position (2-CH₃ \rightarrow **8l**, 2-Cl \rightarrow **8m**) resulted in a marginally reduced binding affinity compared to the respective 3- or 4-substituted compounds. Introducing a 2-methoxy group (\rightarrow **8n**), which has strong electron-releasing properties and a low hydrophobicity parameter, gave the lowest binding affinity in this series. Considering the volume of this group, the loss in affinity

could also result from steric hindrance and hence a non-optimal binding geometry. A trifluoromethyl group in the 3-position (\rightarrow **8o**), being less electron withdrawing than in the 4-position led to a slightly better affinity than in the 4-position, however, no improvement compared to chloro or methyl substituents.

Up to that point, none of the substituents introduced improved the affinity notably comparing to 4-chloro substitution. Therefore, a less hydrophobic but still electron withdrawing group might yield better results. When introduced in the 3-position (\rightarrow **8p**), a nitro group has lower hydrophobic and electron withdrawing effects compared to the 4-nitro and, indeed, binding affinity of **8p** was increased almost threefold with respect to **8g**. A cyano group was shown to be advantageous in many aspects and a suitable replacement for a chloro substituent.^[19] Introducing cyano in the 3-position (\rightarrow **8q**) could not improve affinity, however, when introduced in the 4-position (\rightarrow **8r**), the highest binding affinity in this series was obtained. An acetyl group in 4-position (\rightarrow **8s**) was expected to have similar properties. However, the binding affinity was in same range as for the 4-chloro derivative **8b**. Obviously, a range of different substituents can support this π - π interaction. However, our results indicate that strongly electron withdrawing groups (4-nitro) or sterically demanding groups (2-methoxy) are less favoured.

With the *Topliss* approach, a cyano-group in the 4-position was identified as suitable substituent for improved affinity. Looking at the π and σ values of a cyano group (4-CN: $\pi = -0.57$, $\sigma = 0.66$)^[13b] the similarity to a carboxylic acid group that is present in previous, highly affine biphenyl mannosides^[10b] (4-COOH: $\pi = -0.32$, $\sigma = 0.45$)^[13b] becomes apparent. Both groups show rather low hydrophobicity and considerable electron withdrawing effects. The nitro group shows the same tendency. However the electron withdrawing character in the *para*-position is relatively strong (NO_2 : $\pi = -0.28$, $\sigma_p = 0.78$, $\sigma_m = 0.71$). The less electron withdrawing *meta*- NO_2 shows a threefold improved affinity over its *para*-analogue (**8p** vs. **8g**), which can be seen as an indication for the importance of the optimal π/σ -balance.

Undertaking a similar approach, Han *et al.* found that the introduction of electron-withdrawing substituents in 3- and 5-position is advantageous in case of an unsubstituted first phenyl ring.^[11] The best inhibitor in their study was an 3,5-di-amide-bearing biphenyl mannoside. An additional contact of the introduced substituents with Arg89 was discussed in this context. However, based on our findings of a rather small range in affinity, this seems rather unlikely. Interestingly, in their series with an unsubstituted inner phenyl ring, the

cyano substituted compounds showed a vice-versa effect compared to our results, i.e. in a hemagglutination assay the 3-cyano showed better inhibitory potency than a 4-cyano. The chloro-substituent on the inner ring surely influences the electronic properties of the second outer ring and therewith the affinity towards FimH. In our case, the electron poor inner phenyl can account for the preference of the cyano in 4-position, with a more electron-withdrawing effect, over 3-position.

In summary, compared to the unsubstituted biphenyl compound **8a** an electron-withdrawing or even a slightly electron-donating substituent are both advantageous leading to a two- to threefold improvement in binding affinity. Introduction of strongly electron-withdrawing substituents at the 4-position seems disadvantageous regarding the nitro (**8g**) and the trifluoromethyl (**8e**) substituted derivatives. Likewise, the introduction of a bulky electron-donating group at the 2-position (methoxy, **8n**) is unfavourable in terms of affinity. A significant improvement in affinity was obtained with the 4-cyano substituted compound **8r**. We further evaluated the affinity of this compound by isothermal titration calorimetry (ITC). The experiment revealed enthalpically driven binding of **8r** to FimH CRD with a K_D of 0.75 nM (ΔG° : -52.1 kJ/mol, ΔH° : -61.5 kJ/mol, $T\Delta S^\circ$: +9.4 kJ/mol at 25°C).

Physicochemical Properties

Obviously, small substituents in position 2, 3, or 4 of the biphenyl aglycone affect aqueous solubility and lipophilicity of the FimH antagonist. As the hydrophobicity parameter $\pi^{[20]}$ is defined by its $\log P_{(\text{octanol/water})}$ value the same general trend is reflected by our data, e.g.

$$\pi_{\text{Cl}} = \log P_{\text{chlorobenzene}} - \log P_{\text{benzene}} = 0.7^{[12,20]}$$

$$\pi_{\text{Cl}}(\text{experimental}) = \log D_{7.4}(\mathbf{8b}) - \log D_{7.4}(\mathbf{8a}) = 3.3 - 2.6 = 0.7$$

$$\pi_{\text{CN}} = \log P_{\text{chlorobenzene}} - \log P_{\text{benzene}} = -0.57^{[12]}$$

$$\pi_{\text{CN}}(\text{experimental}) = \log D_{7.4}(\mathbf{8r}) - \log D_{7.4}(\mathbf{8a}) = 2.1 - 2.6 = -0.5$$

Low solubility and moderate lipophilicity were determined for the unsubstituted parent compound (**8a**). Adding apolar substituents in position 3 or 4, such as methyl (\rightarrow **8h**, **8j**), chloro (\rightarrow **8b**, **8k**), or trifluoro methyl (\rightarrow **8c**, **8o**) markedly increased $\log D_{7.4}$, whereas 4-methoxy (\rightarrow **8i**) and 4-acetyl (\rightarrow **8s**) lead to lower lipophilicity. However, none of these substituents enhanced solubility beyond 50 $\mu\text{g/ml}$. By contrast, the 4-nitro substituted derivative **8g** showed markedly higher solubility, however, the same substituent in position 3

(→**8p**) was much less effective. The cyano substituent (→**8q**, **8r**) enhanced solubility above the critical limit as well, regardless of its position. Both, nitro and cyano reduced lipophilicity of the antagonist and, as a result, permeability. However, the permeation through an artificial membrane (PAMPA) still predicted high *in vivo* absorption.^[21]

In contrast to the 3- or 4-substituents, which did either not improve solubility at all or only on the expense of lipophilicity, 2-methyl (→**8l**) and 2-methoxy (→**8n**) increased both, lipophilicity and the maximum amount of dissolved antagonist. This is in agreement with the v. d. Waals volumes of these groups which result in a bigger distortion angle of the two phenyl moieties compared to a H-substituent at this position (data not shown). Nonetheless, we observed that moving methyl, methoxy, or chloro from the 4- or 3- position to the 2-position lowered logD_{7.4}, as a general trend. As for 3,4-disubstituted and 2,4-disubstituted biphenyl derivatives, the antagonists **8c**, **8d**, and **8f** were scarcely soluble in aqueous medium.

In summary, only few substituents (2-methyl, 2-methoxy, 3- and 4-cyano, and 4-nitro) rose aqueous solubility beyond 50 µg/ml leading to sufficient antagonist concentrations in the intestinal fluids. Nevertheless, all biphenyl derivatives bearing these substituents achieved substantial permeability, which, in combination with high aqueous solubility, suggested high systemic availability after oral dosing. Finally, we consider the nitro and cyano substituents most favorable for renal excretion. Adding nitro or cyano to the outer aromatic ring moderately reduced lipophilicity and therefore susceptibility to tubular reabsorption or hepatic metabolism, which results in high availability of the biphenyl mannoside in the urinary bladder.

CONCLUSION

The crystal structure for biphenyl mannosides binding to FimH has been solved^[11], yet, the electronic property of Tyr48 is not entirely understood. To address this matter, we synthesized a series of substituted biphenyl mannosides following the *Topliss* decision tree. The biological evaluation of these compounds indicated that a broad range of substituents is accepted and mostly improves affinity. Both, electron-withdrawing as well as weakly electron-releasing groups, lead to an improvement in affinity compared to the parent compound **8a**, though, the former effect appears more relevant. The sensitive balance of hydrophobic and electronic properties in addition to steric effects has been proven fundamental. The *Topliss*-based approach gave an insight into hydrophobic and electronic

properties and their influence on affinity. Physicochemical data complete this SAR study by elucidating the correlation of substitution pattern with solubility and permeability properties. As a result, the 2'-chloro-4-cyano substituted biphenyl mannoside **8r** was identified as FimH antagonist with improved affinity accompanied by appropriate physicochemical properties.

EXPERIMENTAL SECTION

Synthesis

General Methods

NMR spectra were recorded on a Bruker Avance DMX-500 (500 MHz) spectrometer. Assignment of ^1H and ^{13}C NMR spectra was achieved using 2D methods (COSY, HSQC, HMBC, TOCSY). Chemical shifts are expressed in ppm in relation to the residual solvent signals (CHCl_3 , CHD_2OD , and HDO) on the δ -scale. Coupling constants J are given in Hertz (Hz). Multiplicities were specified as follows: s (singlet), d (doublet), dd (doublet of a doublet), t (triplet), q (quartet), m (multiplet). For assignment of resonance signals to the appropriate nuclei the following abbreviations were used: Ar, aryl. Commercially available reagents were purchased from Fluka, Aldrich, Acros, and Abcr. Solvents were dried prior to use as indicated. Dichloromethane (CH_2Cl_2) was dried by filtration over Al_2O_3 (Fluka, type 5016 A basic). *N,N*-dimethylformamide (DMF) was dried by distillation from calcium hydride. Methanol (MeOH) was dried by refluxing with sodium methoxide and distilled immediately before use. Molecular sieves were activated under vacuum at 500°C for 1 h immediately before use. Reactions were monitored by TLC using glass plates coated with silica gel 60 F₂₅₄ (Merck) and visualized by using UV light and/or by charring with a molybdate solution (a 0.02 M solution of ammonium cerium sulfate dihydrate and ammonium molybdate tetrahydrate in aqueous 10% H_2SO_4). Column chromatography was performed on a CombiFlash Companion (Teledyne-ISCO, Inc.) using RediSep normal phase disposable flash columns (silica gel, 40-63 μm). Reversed phase chromatography was performed on LiChroprepRP-18 (Merck, 40-63 μm). LC-MS separations were carried out using Sunfire C₁₈ columns (19 x 150 mm, 5.0 μm) on a Waters 2525 LC, equipped with Waters 2996 photodiode array and Waters micromass ZQ MS for detection. Electron spray ionization mass spectra (ESI-MS) were obtained on a Waters micromass ZQ. HR-MS analysis were carried out using a Agilent 1100 LC equipped with a photodiode array detector and a Micromass QTOF I equipped with a 4 GHz digital-time converter. Optical rotations were measured using Perkin-Elmer polarimeter 341. Microanalysis was performed at the

Institute of Organic Chemistry at the University of Basel, Switzerland. Compound purity was determined on an Agilent 1200 HPLC; ELS detector, Waters 2420; column: Waters Atlantis dC18, 3 μ m, 4.6 x 75 mm; eluents: A: water + 0.1% TFA; B: 90% acetonitrile + 10% water + 0.1% TFA. Linear gradient: 0 - 1 min 5% B; 1 - 15 min 5 to 70% B; 16 - 20 min 70 to 5% B flow rate: 0.5 ml/min. All compounds used for biological assays are at least of 95% purity based on HPLC analytical results.

Compound **2** was prepared according to a published procedure.^[22]

2-Chloro-4-iodo-phenyl 2,3,4,6-tetra-O-acetyl- α -D-mannopyranoside (2)

In a dry flask activated MS4Å (300 mg), α -D-mannose pentaacetate (390 mg, 0.77 mmol), 2-chloro-4-iodophenol (235 mg, 1.2 eq, 0.9 mmol) were dissolved in dry CH₂Cl₂ (3 ml) under argon atmosphere. BF₃·Et₂O (freshly distilled, 290 μ l, 3eq, 2.3 mmol) was added dropwise and the mixture and stirred for 20h at 40°C. After cooling to room temperature the mixture was diluted with CH₂Cl₂ (75 ml), filtered through celite, washed with satd. aq. NaHCO₃ (75 ml) solution, water (75 ml), and brine (75 ml). The organic phase was dried over Na₂SO₄ and concentrated under reduced pressure. The crude product was purified via flash column chromatography (PE->PE/EE 1:1) to yield the product in 76% (345 mg).

Spectroscopic data were in accordance with literature.^[22]

General procedure A for the synthesis of biphenyl compounds

A two-neck flask was charged with **2** (100 mg, 1.0 eq), phenylboronic acid or boronate (1.1 eq), Pd(Cl₂)dppf·CH₂Cl₂ (0.03 eq), K₃PO₄ (2 eq), and a stirring bar under argon atmosphere. Then anhydrous DMF (2 ml) was added. The mixture was flushed with argon and degassed for 5min, then heated to 80°C and stirred 5-12h. The reaction mixture was cooled to r.t., diluted with EtOAc (50 ml), washed with H₂O (50 ml), brine (50 ml), and then dried over Na₂SO₄, concentrated and purified by normal phase flash chromatography (PE/EtOAc, gradient) to afford biphenyl compounds **7a-s**.

General procedure B for deacetylation. To a solution of **7** (1.0 eq) in dry MeOH (2 mL) was added freshly prepared methanolic NaOMe solution (1 M, 0.1 eq) under argon. The mixture was stirred at r.t. until the reaction was complete (monitored by TLC, 2-8h), then neutralized with acetic acid, filtered and concentrated in vacuo. The residue was purified by normal phase flash chromatography (CH₂Cl₂/MeOH, 10:1->8:1) to afford **8a-s** as white

solids. Further purification for biological testing was performed via reversed phase preparative HPLC.

3'-Chloro-4'-(2,3,4,6-tetra-*O*-acetyl- α -D-mannopyranosyloxy)-biphenyl (7a)

In a dry flask activated MS4Å (150 mg), α -D-mannose pentaacetate (156 mg, 1 eq, 0.4 mmol), 2-chloro-4-phenylphenol (98 mg, 1.2 eq, 0.48 mmol) were dissolved in dry CH₂Cl₂ (1.5 ml) under argon atmosphere. BF₃·Et₂O (freshly distilled, 148 μ l, 3 eq, 1.2 mmol) was added and the mixture stirred for 24 h at 40°C. After cooling down to room temperature the mixture was diluted with CH₂Cl₂ (50 ml), filtered through celite, washed with satd. aq. NaHCO₃ solution (50 ml), H₂O (50 ml), and brine (50 ml). The organic phase was dried over Na₂SO₄ and concentrated under reduced pressure. The crude product was purified via flash column chromatography (PE/EE, 1:0 to 1:1) to yield compound **7a** (166 mg, 77%).

[α]_D²⁰ +72.0 (*c* 0.47, CHCl₃); ¹H NMR (500 MHz, CDCl₃): δ 7.56 (d, *J* = 1.6 Hz, 1H, Ar-H), 7.45 (d, *J* = 7.4 Hz, 2H, Ar-H), 7.32 (dt, *J* = 39.4, 7.4 Hz, 4H, Ar-H), 7.17 (m, 1H, Ar-H), 5.63 – 5.42 (m, 3H, H-1, H-2, H-3), 5.33 (t, *J* = 10.1 Hz, 1H, H-4), 4.22 (dd, *J* = 12.2, 5.3 Hz, 1H, H-6a), 4.14 (m, 1H, H-5), 4.04 (d, *J* = 12.2 Hz, 1H, H-6b), 2.14 (s, 3H, CH₃), 2.06 – 1.88 (m, 9H, 3CH₃); ¹³C NMR (126 MHz, CDCl₃): δ 170.61, 170.08, 169.91, 169.90 (4CO), 150.64, 139.28, 137.64, 129.25, 129.06, 127.78, 126.97, 126.40, 124.82, 117.43 (12C, Ar-C), 96.86 (C-1), 69.90 (C-5), 69.50 (C-2), 68.93 (C-3), 66.01 (C-4), 62.26 (C-6), 21.01, 20.85, 20.82, 20.80 (4CH₃); ESI-MS: *m/z* calcd for C₂₆H₂₇ClO₁₀ [M+Na]⁺: 557.12, found: 557.17.

3'-Chloro-4'-(2,3,4,6-tetra-*O*-acetyl- α -D-mannopyranosyloxy)-4-chloro-biphenyl (7b)

Prepared according to general procedure A from **2** (30 mg, 0.052 mmol), 4-chloro-phenylboronic acid (9 mg, 0.57 mmol), Pd(dppf)Cl₂·CH₂Cl₂ (1.3 mg, 1.6 μ mol) and K₃PO₄ (22 mg, 0.1 mmol). Yield: 16 mg (54%) as a white solid.

[α]_D²⁰ +97.8 (*c* 0.54, CHCl₃); ¹H NMR (500 MHz, CD₃OD): δ 7.66 – 7.23 (m, 7H, Ar-H), 5.67 (s, 1H, H-1), 5.49 – 5.43 (m, 2H, H-2, H-3), 5.25 (t, *J* = 10.0 Hz, 1H, H-4), 4.13 (dd, *J* = 12.1, 5.4 Hz, 1H, H-6a), 4.05 (ddd, *J* = 10.1, 5.4, 2.1 Hz, 1H, H-5), 3.98 (dd, *J* = 12.2, 2.2 Hz, 1H, H-6b), 2.14 – 1.80 (m, 12H, 4CH₃); ¹³C NMR (126 MHz, CD₃OD): δ 172.17, 171.51, 171.48 (4C, CO), 151.81, 139.07, 137.34, 134.80, 130.12, 129.73, 129.31, 127.49, 125.65, 118.86 (12C, Ar-C), 97.67 (C-1), 71.23 (C-5), 70.50, 70.24 (C-2, C-3), 66.97 (C-4), 63.29 (C-6), 20.58, 20.55 (4C, CH₃); ESI-MS: *m/z* calcd for C₂₆H₂₆Cl₂O₁₀ [M+Na]⁺: 591.08, found: 591.11.

3'-Chloro-4'-(2,3,4,6-tetra-*O*-acetyl- α -D-mannopyranosyloxy)-3,4-dichloro-biphenyl (7c)

Prepared according to general procedure A from **2** (79 mg, 0.135 mmol), 3,4-dichlorophenylboronic acid (228mg, 0.15 mmol), Pd(dppf)Cl₂·CH₂Cl₂ (3.3 mg, 4 μ mol) and K₃PO₄ (57 mg, 0.27 mmol). Yield: 52 mg (64%) as a white solid.

$[\alpha]_D^{20}$ +66.5 (*c* 0.23, CHCl₃); ¹H NMR (500 MHz, CDCl₃): δ 7.59 (dt, *J* = 8.9, 4.4 Hz, 2H, Ar-H), 7.50 (d, *J* = 8.3 Hz, 1H, Ar-H), 7.41 – 7.31 (m, 2H, Ar-H), 7.24 (d, *J* = 8.6 Hz, 1H, Ar-H), (5.66 – 5.58 (m, 2H, H-1, H-2), 5.55 (d, *J* = 1.9 Hz, 1H, H-3), 5.41 (t, *J* = 10.1 Hz, 1H, H-4), 4.29 (dd, *J* = 12.3, 5.2 Hz, 1H, H-6a), 4.18 (ddd, *J* = 10.1, 5.1, 2.1 Hz, 1H, H-5), 4.10 (m, 1H, H-6b), 2.21 (d, *J* = 6.2 Hz, 3H, CH₃), 2.15 – 1.97 (m, 9H, 3CH₃); ¹³C NMR (126 MHz, CDCl₃): δ 170.60, 170.11, 169.92, 169.89 (4CO), 151.29, 139.26, 135.03, 133.24, 132.06, 131.01, 129.15, 128.81, 126.32, 126.18, 125.12, 117.41 (12Ar-C), 96.80 (C-1), 69.99 (C-5), 69.45 (C-3), 68.88 (C-2), 65.93 (C-4), 62.22 (C-6), 21.01, 20.85, 20.83 (4C, CH₃); ESI-MS: *m/z* calcd for C₂₆H₂₆Cl₃O₁₀ [M+Na]⁺: 625.04, found: 625.02.

3'-Chloro-4'-(2,3,4,6-tetra-*O*-acetyl- α -D-mannopyranosyloxy)-3-trifluoromethyl-4-chloro-biphenyl (7d)

Prepared according to general procedure A from **2** (80 mg, 0.137 mmol), 3-trifluoro-4-chlorophenylboronic acid (34 mg, 0.151 mmol), Pd(dppf)Cl₂·CH₂Cl₂ (3.4 mg, 4 μ mol) and K₃PO₄ (58 mg, 0.27 mmol). Yield: 70 mg (80%) as a white solid.

$[\alpha]_D^{20}$ +60.7 (*c* 0.27, CHCl₃); ¹H NMR (500 MHz, CD₃OD): δ 7.95 (d, *J* = 1.9 Hz, 1H, Ar-H), 7.84 (dd, *J* = 8.3, 2.0 Hz, 1H, Ar-H), 7.79 (d, *J* = 2.3 Hz, 1H, Ar-H), 7.72 – 7.58 (m, 2H, Ar-H), 7.44 (m, 1H, Ar-H), 5.80 (s, 1H, H-1), 5.60 – 5.51 (m, 2H, H-2, H-3), 5.36 (t, *J* = 10.0 Hz, 1H, H-4), 4.24 (dd, *J* = 12.2, 5.3 Hz, 1H, H-6a), 4.18 – 4.05 (m, 2H, H-5, H-6b), 2.20 (d, *J* = 3.4 Hz, 3H, CH₃), 2.08 (d, *J* = 3.0 Hz, 3H, CH₃), 2.02 (d, *J* = 2.8 Hz, 3H, CH₃), 1.96 (d, *J* = 3.9 Hz, 3H, CH₃); ¹³C NMR (126 MHz, CD₃OD): δ 172.17, 171.49, 171.47 (4C, CO), 152.43, 139.86, 135.79, 133.40, 132.76, 130.00, 127.78, 126.84, 125.87, 118.88 (12C, Ar-C), 97.65 (C-1), 71.28 (C-5), 70.49, 70.21 (C-2, C-3), 66.94 (C-4), 63.28 (C-5), 20.59, 20.56, (4C, CH₃); ESI-MS: *m/z* calcd for C₂₇H₂₅Cl₂F₃O₁₀ [M+Na]⁺: 659.07, found: 659.03.

3'-Chloro-4'-(2,3,4,6-tetra-*O*-acetyl- α -D-mannopyranosyloxy)-4-trifluoromethylbiphenyl (7e)

Prepared according to general procedure A from **2** (79 mg, 0.135 mmol), 4-trifluoromethylphenylboronic acid (28 mg, 0.15 mmol), Pd(dppf)Cl₂·CH₂Cl₂ (3.3 mg, 4 μ mol) and K₃PO₄ (57 mg, 0.27 mmol). Yield: 46 mg (57%) as a white solid.

$[\alpha]_{\text{D}}^{20}$ +63.8 (*c* 0.31, CHCl₃); ¹H NMR (500 MHz, CD₃OD): δ 7.84 – 7.77 (m, 3H, Ar-H), 7.74 (d, *J* = 8.3 Hz, 2H, Ar-H), 7.64 (dd, *J* = 8.6, 2.3 Hz, 1H, Ar-H), 7.43 (d, *J* = 8.6 Hz, 1H, Ar-H), 5.81 (s, 1H, H-1), 5.60 – 5.54 (m, 2H, H-2, H-3), 5.36 (t, *J* = 10.0 Hz, 1H, H-4), 4.24 (dd, *J* = 12.2, 5.4 Hz, 1H, H-6a), 4.14 (ddd, *J* = 10.0, 5.4, 2.2 Hz, 1H, H-5), 4.09 (dd, *J* = 12.2, 2.2 Hz, 1H, H-6b), 2.20 (s, 3H, CH₃), 2.07 (s, 3H, CH₃), 2.01 (d, *J* = 5.3 Hz, 3H, CH₃), 1.95 (s, 3H, CH₃); ¹³C NMR (126 MHz, CD₃OD): δ 172.18, 171.52, 171.50, 171.48 (4CO), 152.30, 144.19, 136.90, 130.12, 128.39, 127.89, 126.94, 126.91, 125.75, 118.82 (12C, Ar-C), 97.62 (C-1), 71.26 (C-5), 70.49, 70.21 (C-2, C-3), 66.95 (C-4), 63.28 (C-6), 20.59, 20.58, 20.55 (4C, CH₃); ESI-MS: *m/z* calcd for C₂₇H₂₆ClF₃O₁₀ [M+Na]⁺: 625.11, found: 625.02.

3'-Chloro-4'-(2,3,4,6-tetra-*O*-acetyl- α -D-mannopyranosyloxy)-2,4-dichlorobiphenyl (7f)

Prepared according to general procedure A from **2** (79 mg, 0.14 mmol), 2,4-dichlorophenylboronic acid (28 mg, 0.15 mmol), Pd(dppf)Cl₂·CH₂Cl₂ (3.3 mg, 4 μ mol) and K₃PO₄ (57 mg, 0.27 mmol). Yield: 48 mg (59%) as a white solid.

$[\alpha]_{\text{D}}^{20}$ +58.8 (*c* 0.56, CHCl₃); ¹H NMR (500 MHz, CD₃OD): δ 7.60 – 7.30 (m, 6H, Ar-H), 5.79 (s, 1H, H-1), 5.61 – 5.53 (m, 2H, H-2, H-3), 5.35 (m, 1H, H-4), 4.24 (dt, *J* = 11.9, 5.9 Hz, 1H, H-6a), 4.18 – 4.06 (m, 2H, H-5, H-6b), 2.19 (d, *J* = 7.8 Hz, 3H, CH₃), 2.10 – 2.05 (m, 3H, CH₃), 2.01 (d, *J* = 5.9 Hz, 3H, CH₃), 1.98 – 1.94 (m, 3H, CH₃); ¹³C NMR (126 MHz, CD₃OD): δ 172.18, 171.51, 171.48 (4C, CO), 152.01, 138.68, 135.51, 135.36, 134.29, 133.49, 132.33, 130.72, 130.24, 128.66, 124.79, 118.03 (12Ar-C), 97.63 (C-1), 71.27 (C-5), 70.49 (C-3), 70.23 (C-2), 66.96 (C-4), 63.30 (C-6), 20.60, 20.56, (4C, CH₃); ESI-MS: *m/z* calcd for C₂₆H₂₅Cl₃O₁₀ [M+Na]⁺: 652.04, found: 653.04.

3'-Chloro-4'-(2,3,4,6-tetra-*O*-acetyl- α -D-mannopyranosyloxy)-4-nitro-biphenyl (7g)

Prepared according to general procedure A from **2** (41 mg, 0.07 mmol), 4-nitrophenylboronic acid (13 mg, 0.08 mmol), Pd(dppf)Cl₂·CH₂Cl₂ (1.7 mg, 2 μ mol) and K₃PO₄ (30 mg, 0.14 mmol). Yield: 31 mg (76%) as a light-yellow solid.

[α]_D²⁰ +77.1 (*c* 0.58, CHCl₃); ¹H NMR (500 MHz, CD₃OD): δ 8.34 – 8.26 (m, 2H, Ar-H), 7.89 – 7.77 (m, 3H, Ar-H), 7.67 (dd, *J* = 8.6, 2.3 Hz, 1H, Ar-H), 7.43 (d, *J* = 8.7 Hz, 1H, Ar-H), 5.81 (s, 1H, H-1), 5.60 – 5.52 (m, 2H, H-2, H-3), 5.36 (m, 1H, H-4), 4.23 (dd, *J* = 12.1, 5.3 Hz, 1H, H-6a), 4.18 – 4.04 (m, 2H, H-5, H-6b), 2.20 (s, 3H, CH₃), 2.07 (s, 3H, CH₃), 2.02 (s, 3H, CH₃), 1.95 (s, 3H, CH₃); ¹³C NMR (126 MHz, CD₃OD): δ 172.14, 171.49, 171.48, 171.45 (4CO), 152.73, 148.64, 146.63, 135.95, 130.32, 128.73, 128.11, 125.84, 125.18, 118.76 (12C, Ar-C), 97.59 (C-1), 71.28 (C-5), 70.45, 70.17 (C-2, C-3), 66.91 (C-4), 63.26 (C-6), 20.59, 20.58, 20.56 (4C, CH₃); ESI-MS: *m/z* calcd for C₂₆H₂₆ClNO₁₂ [M+Na]⁺: 602.10, found: 602.06.

3'-Chloro-4'-(2,3,4,6-tetra-*O*-acetyl- α -D-mannopyranosyloxy)-4-methyl-biphenyl (7h)

Prepared according to general procedure A from **2** (79 mg, 0.135 mmol), 4-methylphenylboronic acid (20 mg, 0.15 mmol), Pd(dppf)Cl₂·CH₂Cl₂ (3.3 mg, 4 μ mol) and K₃PO₄ (57 mg, 0.27 mmol). Yield: 50 mg (67%) as a white solid.

[α]_D²⁰ +71.9 (*c* 0.43, CHCl₃); ¹H NMR (500 MHz, CD₃OD): δ 7.67 (d, *J* = 2.2 Hz, 1H, Ar-H), 7.52 (dd, *J* = 8.6, 2.2 Hz, 1H, Ar-H), 7.47 (t, *J* = 7.3 Hz, 2H, Ar-H), 7.35 (d, *J* = 8.6 Hz, 1H, Ar-H), 7.25 (d, *J* = 7.9 Hz, 2H, Ar-H), 5.75 (s, 1H, H-1), 5.59 – 5.52 (m, 2H, H-2, H-3), 5.34 (t, *J* = 10.0 Hz, 1H, H-4), 4.23 (dd, *J* = 12.1, 5.5 Hz, 1H, H-6a), 4.17 (m, 1H, H-5), 4.09 (dd, *J* = 12.1, 2.1 Hz, 1H, H-6b), 2.37 (s, 3H, PhCH₃), 2.20 (s, 3H, CH₃), 2.12 – 1.92 (m, 9H, 3CH₃); ¹³C NMR (126 MHz, CDCl₃): δ 170.64, 170.10, 169.94, 169.91 (4CO), 150.42, 137.66, 137.63, 136.41, 129.78, 129.03, 126.81, 126.18, 124.80, 117.47 (12C, Ar-C), 96.90 (C-1), 69.89, 69.53, 68.95 (C-5, C-3, C-2), 66.04 (C-4), 62.29 (C-6), 21.23, 21.02, 20.86, 20.83, 20.82 (5CH₃); ESI-MS: *m/z* calcd for C₂₇H₂₉ClO₁₀ [M+Na]⁺: 571.13, found: 571.08.

3'-Chloro-4'-(2,3,4,6-tetra-*O*-acetyl- α -D-mannopyranosyloxy)-4-methoxy-biphenyl (7i)

Prepared according to general procedure A from **2** (59.6 mg, 0.1 mmol), 4-methoxyphenylboronic acid (17 mg, 0.112 mmol), Pd(dppf)Cl₂·CH₂Cl₂ (2.5 mg, 3 μ mol) and K₃PO₄ (43 mg, 0.2 mmol). Yield: 52 mg (90 %) as a white solid.

$[\alpha]_{\text{D}}^{20} +73.7$ (*c* 0.53, CHCl₃); ¹H NMR (500 MHz, CD₃OD): δ 7.64 (d, *J* = 2.2 Hz, 1H, Ar-H), 7.56 – 7.46 (m, 3H, Ar-H), 7.33 (d, *J* = 8.6 Hz, 1H, Ar-H), 7.05 – 6.95 (m, 2H, Ar-H), 5.73 (s, 1H, H-1), 5.56 (dd, *J* = 8.1, 3.4 Hz, 2H, H-2, H-3), 5.35 (dd, *J* = 15.7, 5.7 Hz, 1H, H-4), 4.23 (dd, *J* = 12.1, 5.5 Hz, 1H, H-6a), 4.17 (ddd, *J* = 10.0, 5.6, 2.1 Hz, 1H, H-5), 4.09 (dd, *J* = 12.1, 2.1 Hz, 1H, H-6b), 3.83 (s, 3H, OCH₃), 2.19 (s, 3H, CH₃), 2.09 – 1.92 (m, 9H, 3CH₃); ¹³C NMR (126 MHz, CD₃OD): δ 172.19, 171.52, 171.48 (4C, CO), 161.04, 151.01, 138.58, 132.80, 129.26, 128.85, 127.01, 125.50, 118.93, 115.43 (12C, Ar-C), 97.76 (C-1), 71.18 (C-5), 70.52, 70.30 (C-2, C-3), 67.01 (C-4), 63.32 (C-6), 55.77 (OCH₃), 20.59, 20.58, 20.56 (4C, CH₃); ESI-MS: *m/z* calcd for C₂₇H₂₉ClO₁₁ [M+K]⁺: 603.12, found: 602.99.

3'-Chloro-4'-(2,3,4,6-tetra-*O*-acetyl- α -D-mannopyranosyloxy)-3-methyl-biphenyl (7j)

Prepared according to general procedure A from **2** (79 mg, 0.135 mmol), 3-methylphenylboronic acid (20 mg, 0.15 mmol), Pd(dppf)Cl₂·CH₂Cl₂ (3.3 mg, 4 μ mol) and K₃PO₄ (57 mg, 0.27 mmol). Yield: 51 mg (69%) as a white solid.

$[\alpha]_{\text{D}}^{20} +78.2$ (*c* 0.36, CHCl₃); ¹H NMR (500 MHz, CD₃OD): δ 7.68 (d, *J* = 2.1 Hz, 1H, Ar-H), 7.53 (dd, *J* = 8.6, 2.1 Hz, 1H, Ar-H), 7.34 (dt, *J* = 15.1, 10.4 Hz, 4H, Ar-H), 7.17 (d, *J* = 7.4 Hz, 1H, Ar-H), 5.76 (s, 1H, H-1), 5.59 – 5.52 (m, 2H, H-2, H-3), 5.35 (t, *J* = 9.9 Hz, 1H, H-4), 4.24 (dd, *J* = 12.1, 5.5 Hz, 1H, H-6a), 4.17 (m, 1H, H-5), 4.09 (dd, *J* = 12.1, 2.1 Hz, 1H, H-6b), 2.40 (s, 3H, PhCH₃), 2.19 (d, *J* = 6.1 Hz, 3H, CH₃), 2.09 – 1.94 (m, 9H, 3CH₃); ¹³C NMR (126 MHz, CD₃OD): δ 172.20, 171.53, 171.49 (4C, CO), 151.44, 140.37, 139.83, 138.93, 129.93, 129.75, 129.40, 128.41, 127.52, 125.47, 124.90, 118.82 (12Ar-C), 97.71 (C-1), 71.19 (C-5), 70.51, 70.28 (C-2, C-3), 66.99 (C-4), 63.31 (C-6), 21.52 (PhCH₃), 20.60, 20.59, 20.56 (4C, CH₃); ESI-MS: *m/z* calcd for C₂₇H₂₉ClO₁₀ [M+Na]⁺: 571.13, found: 571.13.

3'-Chloro-4'-(2,3,4,6-tetra-*O*-acetyl- α -D-mannopyranosyloxy)-3-chloro-biphenyl (7k)

Prepared according to general procedure A from **2** (81 mg, 0.138 mmol), 3-chlorophenylboronic acid (24 mg, 0.15 mmol), Pd(dppf)Cl₂·CH₂Cl₂ (3.4 mg, 4 μ mol) and K₃PO₄ (59 mg, 0.28 mmol). Yield: 57 mg (75%) as a white solid.

$[\alpha]_{\text{D}}^{20} +67.3$ (*c* 0.27, CHCl₃); ¹H NMR (500 MHz, CD₃OD): δ 7.71 (t, *J* = 7.8 Hz, 1H, Ar-H), 7.66 – 7.31 (m, 6H, Ar-H), 5.78 (s, 1H, H-1), 5.61 – 5.51 (m, 2H, H-2, H-3), 5.35 (t, *J* = 10.1 Hz, 1H, H-4), 4.23 (dd, *J* = 12.2, 5.4 Hz, 1H, H-6a), 4.19 – 4.02 (m, 2H, H-5, H-6b), 2.19 (s, 3H, CH₃), 2.11 – 1.92 (m, 9H, 3CH₃); ¹³C NMR (126 MHz, CD₃OD): δ 172.18, 171.50, 171.48 (4C, CO), 152.04, 142.44, 137.09, 135.96, 131.56, 129.89, 128.65, 127.75,

127.67, 126.23, 125.67, 118.82 (12C, Ar-C) 97.66 (C-1), 71.23, 70.49, 70.23 (C-2, C-3, C-5), 66.95 (C-4), 63.28 (C-6), 20.59, 20.58, 20.55 (4C, CH₃); ESI-MS: *m/z* calcd for C₂₆H₂₆Cl₂O₁₀ [M+Na]⁺: 591.08, found: 590.99.

3'-Chloro-4'-(2,3,4,6-tetra-*O*-acetyl- α -D-mannopyranosyloxy)-2-methyl-biphenyl (7l)

Prepared according to general procedure A from **2** (79 mg, 0.14 mmol), 2-methylphenylboronic acid (20 mg, 0.15 mmol), Pd(dppf)Cl₂·CH₂Cl₂ (3.3 mg, 4 μ mol) and K₃PO₄ (57 mg, 0.27 mmol). Yield: 39 mg (53%) as a white solid.

[α]_D²⁰ +62.9 (*c* 0.42, CHCl₃); ¹H NMR (500 MHz, CD₃OD): δ 7.37 (dd, *J* = 12.9, 5.2 Hz, 2H, Ar-H), 7.29 – 7.19 (m, 4H, Ar-H), 7.16 (d, *J* = 6.9 Hz, 1H, Ar-H), 5.76 (s, 1H, H-1), 5.59 – 5.54 (m, 2H, H-2, H-3), 5.35 (m, 1H, H-4), 4.28 – 4.03 (m, 3H, H-5, H-6), 2.25 (s, 3H, CH₃), 2.19 (d, *J* = 6.8 Hz, 3H, CH₃), 2.08 (s, 3H, CH₃), 2.02 (s, 3H, CH₃), 1.98 (s, 3H, CH₃); ¹³C NMR (126 MHz, CD₃OD): δ 172.19, 171.54, 171.50 (4C, CO), 151.24, 141.25, 139.60, 136.36, 132.01, 131.48, 130.60, 129.93, 128.82, 127.04, 124.80, 118.24 (12Ar-C), 97.81 (C-1), 71.21 (C-5), 70.52, 70.31 (2C, C-2, C-3), 67.02 (C-4), 63.35 (C-6), 20.60, 20.56, 20.52 (5C, CH₃); ESI-MS: *m/z* calcd for C₂₇H₂₉ClO₁₀ [M+Na]⁺: 571.13, found: 571.08.

3'-Chloro-4'-(2,3,4,6-tetra-*O*-acetyl- α -D-mannopyranosyloxy)-2-chloro-biphenyl (7m)

Prepared according to general procedure A from **2** (81 mg, 0.138 mmol), 2-chlorophenylboronic acid (24 mg, 0.15 mmol), Pd(dppf)Cl₂·CH₂Cl₂ (3.4 mg, 4 μ mol) and K₃PO₄ (59 mg, 0.28 mmol). Yield: 52 mg (66%) as a white solid.

[α]_D²⁰ +64.7 (*c* 0.42, CHCl₃); ¹H NMR (500 MHz, CD₃OD): δ 7.48 (dd, *J* = 8.9, 1.7 Hz, 2H, Ar-H), 7.39 – 7.30 (m, 5H, Ar-H), 5.77 (s, 1H, H-1), 5.64 – 5.52 (m, 2H, H-2, H-3), 5.35 (m, 1H, H-4), 4.24 (dd, *J* = 12.1, 5.6 Hz, 1H, H-6a), 4.17 (ddd, *J* = 10.0, 5.6, 2.0 Hz, 1H, H-5), 4.08 (m, 1H, H-6b), 2.19 (s, 3H, CH₃), 2.07 (s, 3H, CH₃), 2.01 (s, 3H, CH₃), 1.96 (s, 3H, CH₃); ¹³C NMR (126 MHz, CD₃OD): δ 172.16, 171.50, 171.45 (4C, CO), 151.72, 139.84, 136.70, 133.35, 132.42, 132.34, 131.10, 130.31, 130.24, 128.37, 124.63, 117.98 (12Ar-C), 97.64 (C-1), 71.22 (C-5), 70.47, 70.24 (C-2, C-3), 66.96 (C-4), 63.29 (C-6), 20.62, 20.61, 20.60, 20.57 (4CH₃); ESI-MS: *m/z* calcd for C₂₆H₂₆Cl₂O₁₀ [M+Na]⁺: 591.08, found: 591.00.

3'-Chloro-4'-(2,3,4,6-tetra-*O*-acetyl- α -D-mannopyranosyloxy)-2-methoxy-biphenyl (7n)

Prepared according to general procedure A from **2** (79 mg, 0.135 mmol), 2-methoxyphenylboronic acid (23 mg, 0.15 mmol), Pd(dppf)Cl₂·CH₂Cl₂ (3.3 mg, 4 μ mol) and K₃PO₄ (57 mg, 0.27 mmol). Yield: 34 mg (45%) as a white solid.

$[\alpha]_{\text{D}}^{20} +75.0$ (*c* 0.52, CHCl₃); ¹H NMR (500 MHz, CD₃OD): δ 7.58 (d, *J* = 2.1 Hz, 1H, Ar-H), 7.42 (dd, *J* = 8.6, 2.1 Hz, 1H, Ar-H), 7.38 – 7.25 (m, 3H, Ar-H), 7.08 (d, *J* = 8.2 Hz, 1H, Ar-H), 7.02 (m, 1H, Ar-H), 5.76 (s, 1H, H-1), 5.58 (dd, *J* = 8.5, 3.2 Hz, 2H, H-2, H-3), 5.37 (dd, *J* = 15.7, 5.8 Hz, 1H, H-4), 4.26 (dd, *J* = 12.1, 5.6 Hz, 1H, H-6a), 4.19 (ddd, *J* = 10.0, 5.7, 2.0 Hz, 1H, H-5), 4.12 (dt, *J* = 8.5, 5.3 Hz, 1H, H-6b), 3.82 (s, 3H, OCH₃), 2.21 (s, 3H, CH₃), 2.10 (s, 3H, CH₃), 2.04 (s, 3H, CH₃), 1.98 (s, 3H, CH₃); ¹³C NMR (126 MHz, CD₃OD): δ 172.23, 171.54, 171.49 (4C, CO), 157.81, 150.91, 136.27, 132.31, 131.42, 130.27, 130.11, 129.80, 124.42, 122.00, 118.00, 112.60 (12Ar-C), 97.63 (C-1), 71.16, 70.53, 70.30 (C-2, C-3, C-5), 67.02 (C-4), 63.31 (C-6), 55.99 (OCH₃), 20.60, 20.59, 20.57 (4C, CH₃); ESI-MS: *m/z* calcd for C₂₇H₂₉ClO₁₁ [M+Na]⁺: 587.13, found: 587.17.

3'-Chloro-4'-(2,3,4,6-tetra-*O*-acetyl- α -D-mannopyranosyloxy)-3-trifluoromethyl-biphenyl (7o)

Prepared according to general procedure A from **2** (80 mg, 0.137 mmol), 3-trifluoromethylphenylboronic acid (29 mg, 0.15 mmol), Pd(dppf)Cl₂·CH₂Cl₂ (3.4 mg, 4 μ mol) and K₃PO₄ (58 mg, 0.27 mmol). Yield: 69 mg (83%) as a white solid.

$[\alpha]_{\text{D}}^{20} +62$ (*c* 0.49, CHCl₃); ¹H NMR (500 MHz, CD₃OD): δ 7.86 (d, *J* = 11.7 Hz, 2H, Ar-H), 7.77 (d, *J* = 2.2 Hz, 1H, Ar-H), 7.71 – 7.59 (m, 3H, Ar-H), 7.43 (d, *J* = 8.6 Hz, 1H, Ar-H), 5.80 (s, 1H, H-1), 5.66 – 5.53 (m, 2H, H-2, H-3), 5.38 (dd, *J* = 13.1, 6.9 Hz, 1H, H-4), 4.31 – 4.06 (m, 3H, H-5, H-6), 2.28 – 1.93 (m, 12H, 4CH₃); ¹³C NMR (126 MHz, CD₃OD): δ 172.15, 171.49, 171.47, 171.46 (4C, CO), 152.19, 141.43, 136.92, 132.36 (q, ²*J*_{CF} = 32 Hz), 131.56, 130.93, 128.9 (q, ¹*J*_{CF} = 279 Hz), 126.69, 125.77, 125.29 (q, ³*J*_{CF} = 3.76 Hz), 124.53, 124.35 (q, ³*J*_{CF} = 3.89 Hz), 118.88 (12C, Ar-C), 97.66 (C-1), 71.24 (C-5), 70.47 (C-3), 70.22 (C-2), 66.94 (C-4), 63.27 (C-6), 20.59, 20.58, 20.56, 20.55 (4CH₃). ESI-MS: *m/z* calcd for C₂₇H₂₆ClF₃O₁₀ [M+Na]⁺: 641.08, found: 641.07.

3'-Chloro-4'-(2,3,4,6-tetra-*O*-acetyl- α -D-mannopyranosyloxy)-3-nitro-biphenyl (7p)

Prepared according to general procedure A from **2** (80 mg, 0.137 mmol), 3-nitrophenylboronic acid (25 mg, 0.151 mmol), Pd(dppf)Cl₂·CH₂Cl₂ (3.4 mg, 4 μ mol) and K₃PO₄ (58 mg, 0.27 mmol). Yield: 55 mg (69%) as a white solid.

$[\alpha]_{\text{D}}^{20} +70.6$ (*c* 0.23, CHCl₃); ¹H NMR (500 MHz, CD₃OD): δ 8.44 (t, *J* = 1.9 Hz, 1H, Ar-H), 8.23 (m, 1H, Ar-H), 8.02 (dd, *J* = 7.8, 0.6 Hz, 1H, Ar-H), 7.82 (d, *J* = 2.3 Hz, 1H, Ar-H), 7.77 – 7.61 (m, 2H, Ar-H), 7.44 (d, *J* = 8.7 Hz, 1H, Ar-H), 5.81 (s, 1H, H-1), 5.63 – 5.54 (m, 2H, H-2, H-3), 5.38 (dd, *J* = 12.4, 7.6 Hz, 1H, H-4), 4.26 (dd, *J* = 12.2, 5.3 Hz, 1H, H-6a),

4.16 (ddd, $J = 10.1, 5.3, 2.2$ Hz, 1H, H-5), 4.10 (m, 1H, H-6a), 2.22 (s, 3H, CH₃), 2.10 – 1.92 (m, 9H, 3CH₃); ¹³C NMR (126 MHz, CD₃OD): δ 172.16, 171.49, 171.47, 171.46 (4CO), 152.47, 150.23, 142.04, 136.00, 133.90, 131.33, 130.07, 127.85, 125.86, 123.29, 122.34, 118.88 (12Ar-C), 97.66 (C-1), 71.26 (C-5), 70.45, 70.21 (2C, C-2, C-3), 66.92 (C-4), 63.26 (C-6), 20.60, 20.59, 20.56 (4C, CH₃); ESI-MS: m/z calcd for C₂₆H₂₆ClNO₁₂ [M+Na]⁺: 602.10, found: 602.11.

3'-Chloro-4'-(2,3,4,6-tetra-*O*-acetyl- α -D-mannopyranosyloxy)-3-cyano-biphenyl (7q)

Prepared according to general procedure A from **2** (80 mg, 0.137 mmol), 3-cyanophenylboronic acid pinacol ester; (35 mg, 0.151 mmol), Pd(dppf)Cl₂·CH₂Cl₂ (3.4 mg, 4 μ mol) and K₃PO₄ (58 mg, 0.27 mmol). Yield: 57 mg (74%) as a white solid.

$[\alpha]_D^{20} +66.2$ (c 0.6, CHCl₃); ¹H NMR (500 MHz, CDCl₃): δ 7.83 – 7.73 (m, 2H, Ar-H), 7.62 (dd, $J = 10.4, 5.0$ Hz, 2H, Ar-H), 7.55 (t, $J = 7.8$ Hz, 1H, Ar-H), 7.41 (dd, $J = 8.6, 2.2$ Hz, 1H, Ar-H), 7.33 – 7.23 (m, 2H, Ar-H), 5.61 (dt, $J = 7.8, 3.7$ Hz, 2H, H-1, H-3), 5.54 (dd, $J = 3.3, 1.9$ Hz, 1H, H-2), 5.39 (t, $J = 10.1$ Hz, 1H, H-4), 4.27 (dd, $J = 12.3, 5.2$ Hz, 1H, H-6a), 4.22 – 4.05 (m, 2H, H-5, H-6b), 2.21 (s, 3H, CH₃), 2.14 – 1.99 (m, 9H, 3CH₃); ¹³C NMR (126 MHz, CDCl₃): δ 170.83, 170.23, 170.12, 170.04 (4CO), 151.35, 140.43, 134.98, 131.29, 131.11, 130.39, 129.89, 129.18, 126.39, 125.07 (10Ar-C), 118.60 (CN), 117.37, 113.04 (Ar-C), 96.60 (C-1), 69.83 (C-5), 69.29 (C-3), 68.85 (C-2), 65.80 (C-4), 62.14 (C-6), 24.54, 20.78, 20.64, 20.62 (4C, CH₃); ESI-MS: m/z calcd for C₂₇H₂₆ClNO₁₀ [M+Na]⁺: 582.11, found: 582.11.

3'-Chloro-4'-(2,3,4,6-tetra-*O*-acetyl- α -D-mannopyranosyloxy)-biphenyl-4-carbonitril (7r)

Prepared according to general procedure A from **2** (79 mg, 0.135 mmol), 4-cyanophenylboronic acid (22 mg, 0.15 mmol), Pd(dppf)Cl₂·CH₂Cl₂ (3.3 mg, 4 μ mol) and K₃PO₄ (57 mg, 0.27 mmol). Yield: 57 mg (75%) as a white solid.

$[\alpha]_D^{20} +77.7$ (c 0.5, CHCl₃); ¹H NMR (500 MHz, CDCl₃): δ 7.72 (d, $J = 8.3$ Hz, 2H, Ar-H), 7.63 (dd, $J = 10.4, 5.2$ Hz, 3H, Ar-H), 7.43 (dd, $J = 8.6, 2.2$ Hz, 1H, Ar-H), 7.27 (d, $J = 8.6$ Hz, 1H, Ar-H), 5.64 – 5.59 (m, 2H, H-1, H-2), 5.54 (dd, $J = 3.2, 1.9$ Hz, 1H, H-3), 5.41 (t, $J = 10.1$ Hz, 1H, H-4), 4.28 (dd, $J = 12.3, 5.2$ Hz, 1H, H-6a), 4.17 (ddd, $J = 10.0, 5.1, 2.1$ Hz, 1H, H-5), 4.10 (dd, $J = 12.3, 2.2$ Hz, 1H, H-6b), 2.21 (s, 3H, CH₃), 2.12 – 2.00 (m, 9H, 3CH₃); ¹³C NMR (126 MHz, CDCl₃): δ 170.54, 170.08, 169.90, 169.84, (4C, CO) 151.67, 143.61, 135.29, 132.87, 129.41, 127.53, 126.60, 125.20, 118.79, 117.36, 111.47 (13C, Ar-C,

CN), 96.72 (C-1), 70.00 (C-5), 69.39 (C-3), 68.82 (C-2), 65.86 (C-4), 62.16 (C-6), 20.98, 20.81, 20.79, 20.78 (4C, CH₃); ESI-MS: m/z calcd for C₂₇H₂₆ClNO₁₀ [M+Na]⁺: 582.11, found: 582.05.

3'-Chloro-4'-(2,3,4,6-tetra-*O*-acetyl- α -D-mannopyranosyloxy)-4-acetyl-biphenyl (7s)

Prepared according to general procedure A from **2** (64.3 mg, 0.11 mmol), 4-acetylphenylboronic acid (27 mg, 0.12 mmol), Pd(dppf)Cl₂·CH₂Cl₂ (2.7 mg, 3 μ mol) and K₃PO₄ (47 mg, 0.22 mmol). Yield: 52 mg (82%) as a white solid.

[α]_D²⁰ +76.9 (*c* 0.62, CHCl₃); ¹H NMR (500 MHz, CD₃OD): δ 8.04 (d, J = 8.4 Hz, 2H, Ar-H), 7.77 (d, J = 2.2 Hz, 1H, Ar-H), 7.71 (d, J = 8.4 Hz, 2H, Ar-H), 7.61 (dd, J = 8.6, 2.2 Hz, 1H, Ar-H), 7.38 (d, J = 8.7 Hz, 1H, Ar-H), 5.78 (s, 1H, H-1), 5.60 – 5.51 (m, 2H, H-2, H-3), 5.35 (dd, J = 13.0, 7.0 Hz, 1H, H-4), 4.23 (dd, J = 12.2, 5.4 Hz, 1H, H-6a), 4.17 – 4.01 (m, 2H, H-5, H-6b), 2.62 (s, 3H, PhCOCH₃), 2.20 (s, 3H, CH₃), 2.01 (dd, J = 33.9, 30.1 Hz, 9H, 3CH₃); ¹³C NMR (126 MHz, CD₃OD): δ 199.93 (PhCOCH₃), 172.14, 171.49, 171.46, 171.45 (4CO), 152.26, 144.91, 137.30, 137.07, 130.24, 130.03, 127.92, 127.82, 125.70, 118.78 (12C, Ar-C), 97.62 (C-1), 71.23 (C-5), 70.46, 70.21 (C-2, C-3), 66.93 (C-4), 63.27 (C-6), 26.73 (PhCOCH₃), 20.61, 20.59, 20.57 (4C, CH₃); ESI-MS: m/z calcd for C₂₈H₂₉ClO₁₁ [M+Na]⁺: 599.13, found 599.05.

3'-Chloro-4'-(α -D-mannopyranosyloxy)-biphenyl (8a)

Prepared according to general procedure B from **7a** (101 mg, 0.19 mmol). Yield: 65 mg (93%) as a white solid.

[α]_D²⁰ +87.5 (*c* 0.067, MeOH/CHCl₃ 1:1); ¹H NMR (500 MHz, CD₃OD): δ 7.63 (d, J = 2.2 Hz, 1H, Ar-H), 7.59 – 7.48 (m, 3H, Ar-H), 7.42 (dd, J = 12.3, 5.0 Hz, 3H, Ar-H), 7.32 (t, J = 7.4 Hz, 1H, Ar-H), 5.58 (d, J = 1.5 Hz, 1H, H-1), 4.12 (dd, J = 3.3, 1.8 Hz, 1H, H-2), 4.01 (dd, J = 9.5, 3.4 Hz, 1H, H-3), 3.83 – 3.64 (m, 4H, H-4, H-5, H-6); ¹³C NMR (126 MHz, CD₃OD): δ 152.67, 140.68, 137.91, 129.99, 129.49, 128.52, 127.72, 127.50, 125.24, 118.73 (12C, Ar-C), 100.86 (C-1), 75.97 (C-5), 72.43 (C-3), 71.90 (C-2), 68.26 (C-4), 62.69 (C-6); HR-MS: m/z calcd for C₁₈H₁₉ClO₆ [M+Na]⁺: 389.0762, found 389.0764; HPLC-purity: 98.9%, R_t = 10.371 min.

3'-Chloro-4'-(α -D-mannopyranosyloxy)-4-chloro-biphenyl (8b)

Prepared according to general procedure B from **7b** (45.6 mg, 0.08 mmol). Yield: 20 mg (62%) as a white solid.

$[\alpha]_{\text{D}}^{20} +69.9$ (*c* 0.42, MeOH); ^1H NMR (500 MHz, CD_3OD): δ 7.66 (d, $J = 2.2$ Hz, 1H), 7.59 – 7.54 (m, 2H), 7.51 (dd, $J = 8.6, 2.3$ Hz, 1H), 7.46 – 7.40 (m, 3H) 7xaryl CH, 5.58 (d, $J = 1.6$ Hz, 1H, H-1), 4.11 (dd, $J = 3.3, 1.8$ Hz, 1H, H-2), 3.99 (dd, $J = 9.5, 3.4$ Hz, 1H, H-3), 3.81 – 3.69 (m, 3H, H-4, H-6), 3.65 (ddd, $J = 9.8, 5.5, 2.4$ Hz, 1H, H-5); ^{13}C NMR (126 MHz, CD_3OD): δ 152.92, 139.33, 136.43, 134.57, 130.05, 129.44, 129.23, 127.44, 125.32, 118.70 (12 C, Ar-C), 100.79 (C-1), 75.99 (C-5), 72.40 (C-3), 71.86 (C-2), 68.23 (C-4), 62.66 (C-6); HR-MS: m/z calcd for $\text{C}_{18}\text{H}_{18}\text{Cl}_2\text{O}_6$ $[\text{M}+\text{Na}]^+$: 423.0373, found 423.0378; HPLC-purity > 99.5%, $R_t = 11.334$ min.

3'-Chloro-4'-(α -D-mannopyranosyloxy)-3,4-dichloro-biphenyl (8c)

Prepared according to general procedure B from **7c** (45.3 mg, 0.08 mmol). Yield: 26 mg, (80%) as a white solid.

$[\alpha]_{\text{D}}^{20} +92.8$ (*c* 0.24, MeOH); ^1H NMR (500 MHz, CD_3OD): δ 7.70 (d, $J = 2.1$ Hz, 1H, Ar-H), 7.63 (d, $J = 2.2$ Hz, 1H, Ar-H), 7.56 – 7.41 (m, 4H, Ar-H), 5.60 (d, $J = 1.6$ Hz, 1H, H-1), 4.12 (dd, $J = 3.3, 1.8$ Hz, 1H, H-2), 4.00 (dd, $J = 9.5, 3.4$ Hz, 1H, H-3), 3.81 – 3.69 (m, 3H, H-4, H-6), 3.64 (ddd, $J = 9.7, 5.4, 2.4$ Hz, 1H, H-5); ^{13}C NMR (126 MHz, CD_3OD): δ 153.28, 140.97, 134.91, 133.84, 132.38, 131.98, 129.50, 129.49, 127.51, 127.42, 125.38, 118.60 (12Ar-C), 100.68 (C-1), 75.99 (C-5), 72.38 (C-3), 71.81 (C-2), 68.19 (C-4), 62.63 (C-6); IR (KBr), $\nu = 3370$ (O-H stretch), 1468cm^{-1} ; HR-MS: m/z calcd for $\text{C}_{18}\text{H}_{17}\text{Cl}_3\text{O}_6$ $[\text{M}+\text{Na}]^+$: 456.9983, found 456.9984; HPLC-purity > 99.5%, $R_t = 12.021$ min.

3'-Chloro-4'-(α -D-mannopyranosyloxy)-3-trifluoromethyl-4-chloro-biphenyl (8d)

Prepared according to general procedure B from **7d** (76 mg, 0.12 mmol). Yield: 18 mg, (36%) as a white solid.

$[\alpha]_{\text{D}}^{20} +83$ (*c* 0.34, MeOH); ^1H NMR (500 MHz, CD_3OD): δ 7.95 – 7.44 (m, 6H, Ar-H), 5.61 (d, $J = 1.4$ Hz, 1H, H-1), 4.11 (dd, $J = 3.3, 1.8$ Hz, 1H, H-2), 4.00 (dd, $J = 9.5, 3.4$ Hz, 1H, H-3), 3.83 – 3.68 (m, 3H, H-4, H-6), 3.63 (ddd, $J = 9.6, 5.4, 2.3$ Hz, 1H, H-5); ^{13}C NMR (126 MHz, CD_3OD): δ 153.48, 140.08, 134.83, 133.32, 132.64, 132.04, 129.79 (7Ar-C), 128.7 (PhCF_3 , q, $^1J_{\text{CF}} = 246$ Hz), 126.71, 126.67, 125.51, 123.27, 118.69 (5Ar-C), 100.70 (C-1), 76.05 (C-5), 72.39 (C-3), 71.82 (C-2), 68.21 (C-4), 62.66 (C-6); HR-MS: m/z calcd for $\text{C}_{19}\text{H}_{17}\text{Cl}_2\text{F}_3\text{O}_6$ $[\text{M}+\text{Na}]^+$: 491.0246, found 491.0250; HPLC-purity > 99.5%, $R_t = 12.207$ min.

3'-Chloro-4'-(α -D-mannopyranosyloxy)-4-trifluoromethyl-biphenyl (8e)

Prepared according to general procedure B from **7e** (36.2 mg, 0.06 mmol). Yield: 25 mg, (95%) as a white solid.

$[\alpha]_D^{20} +83$ (*c* 0.24, MeOH); $^1\text{H NMR}$ (500 MHz, CD_3OD): δ 7.84 – 7.40 (m, 7H, Ar-H), 5.62 (d, $J = 1.2$ Hz, 1H, H-1), 4.13 (dt, $J = 12.0, 6.0$ Hz, 1H, H-2), 4.01 (dd, $J = 9.5, 3.4$ Hz, 1H, H-3), 3.84 – 3.71 (m, 3H, H-4, H-6), 3.65 (m, 1H, H-5); $^{13}\text{C NMR}$ (126 MHz, CD_3OD): δ 153.33, 144.34, 135.92, 130.42 (q, $^2J_{CF} = 32$ Hz), 128.3 (q, $^1J_{CF} = 246$ Hz), 128.28, 126.90 (q, $^3J_{CF} = 3.7$ Hz), 125.38, 124.69, 118.62, (12C, Ar-C), 100.65 (C-1), 75.96 (C-5), 72.38 (C-3), 71.80 (C-2), 68.16 (C-4), 62.57 (C-6); HR-MS: *m/z* calcd for $\text{C}_{19}\text{H}_{18}\text{ClF}_3\text{O}_6$ $[\text{M}+\text{Na}]^+$: 457.0636, found 457.0641; HPLC-purity > 99.5%, $R_t = 12.068$ min.

3'-Chloro-4'-(α -D-mannopyranosyloxy)-2,4-dichloro-biphenyl (8f)

Prepared according to general procedure B from **7f** (28.4 mg, 0.05 mmol). Yield: 15 mg, (73%) as a white solid.

$[\alpha]_D^{20} +82.2$ (*c* 0.22, MeOH); $^1\text{H NMR}$ (500 MHz, CD_3OD): δ 7.59 – 7.28 (m, 6H, Ar-H), 5.60 (d, $J = 1.4$ Hz, 1H, H-1), 4.12 (dd, $J = 3.3, 1.8$ Hz, 1H, H-2), 4.00 (dd, $J = 9.4, 3.4$ Hz, 1H, H-3), 3.83 – 3.61 (m, 4H, H-4, H-5, H-6); $^{13}\text{C NMR}$ (126 MHz, CD_3OD): δ 153.12, 138.93, 135.19, 134.62, 134.33, 133.51, 132.03, 130.68, 130.18, 128.60, 124.47, 117.95, (12Ar-C), 100.82 (C-1), 76.05 (C-5), 72.41 (C-3), 71.86 (C-2), 68.25 (C-4), 62.69 (C-6); HR-MS: *m/z* calcd for $\text{C}_{18}\text{H}_{17}\text{Cl}_3\text{O}_6$ $[\text{M}+\text{Na}]^+$: 456.9983, found 456.9989; HPLC-purity > 99.5%, $R_t = 11.922$ min.

3'-Chloro-4'-(α -D-mannopyranosyloxy)-4-nitro-biphenyl (8g)

Prepared according to general procedure B from **7g** (27.3 mg, 0.05 mmol). Yield: 16 mg, (83%) as a white solid.

$[\alpha]_D^{20} +100.2$ (*c* 0.20, MeOH); $^1\text{H NMR}$ (500 MHz, CD_3OD): δ 8.32 (d, $J = 8.8$ Hz, 2H, Ar-H), 8.00 (s, 1H, Ar-H), 7.86 (d, $J = 8.8$ Hz, 2H, Ar-H), 7.82 (d, $J = 2.2$ Hz, 1H, Ar-H), 7.67 (dd, $J = 8.6, 2.2$ Hz, 1H, Ar-H), 7.52 (d, $J = 8.7$ Hz, 1H, Ar-H), 5.66 (d, $J = 1.3$ Hz, 1H, H-1), 4.14 (dd, $J = 3.2, 1.8$ Hz, 1H, H-2), 4.02 (dd, $J = 9.5, 3.4$ Hz, 1H, H-3), 3.85 – 3.71 (m, 3H, H-4, H-6), 3.65 (ddd, $J = 9.6, 5.4, 2.3$ Hz, 1H, H-5); $^{13}\text{C NMR}$ (126 MHz, CD_3OD): δ 153.86, 148.53, 146.97, 135.06, 130.04, 128.64, 128.10, 125.53, 125.16, 118.60 (12C, Ar-C), 100.68 (C-1), 76.09 (C-5), 72.41 (C-3), 71.82 (C-2), 68.22 (C-4), 62.67 (C-6); HR-MS: *m/z* calcd for $\text{C}_{18}\text{H}_{18}\text{ClNO}_8$ $[\text{M}+\text{Na}]^+$: 434.0613, found 434.0614; HPLC-purity > 99.5%, $R_t = 10.199$ min.

3'-Chloro-4'-(α -D-mannopyranosyloxy)-4-methyl-biphenyl (8h)

Prepared according to general procedure B from **7h** (38 mg, 0.07 mmol). Yield: 14 mg, (53%) as a white solid.

$[\alpha]_D^{20} +95.1$ (*c* 0.22, MeOH); $^1\text{H NMR}$ (500 MHz, CD_3OD): δ 7.60 (d, $J = 2.2$ Hz, 1H, Ar-H), 7.51 – 7.37 (m, 4H, Ar-H), 7.23 (d, $J = 8.0$ Hz, 2H, Ar-H), 5.56 (d, $J = 1.4$ Hz, 1H, H-1), 4.11 (dd, $J = 3.2, 1.8$ Hz, 1H, H-2), 4.00 (dd, $J = 9.5, 3.4$ Hz, 1H, H-3), 3.82 – 3.64 (m, 4H, H-4, H-5, H-6), 2.36 (s, 3H, CH_3); $^{13}\text{C NMR}$ (126 MHz, CD_3OD): δ 152.40, 138.43, 137.87, 137.74, 130.59, 129.23, 127.53, 127.21, 125.18, 118.73, (12C, Ar-C), 100.86 (C-1), 75.91 (C-5), 72.41 (C-3), 71.89 (C-2), 68.24 (C-4), 62.66 (C-6), 21.08 (CH_3); HR-MS: m/z calcd for $\text{C}_{19}\text{H}_{21}\text{ClO}_6$ $[\text{M}+\text{Na}]^+$: 403.0919, found 403.0924; HPLC-purity: 97.3%, $R_t = 11.078$ min.

3'-Chloro-4'-(α -D-mannopyranosyloxy)-4-methoxy-biphenyl (8i)

Prepared according to general procedure B from **7i** (25 mg, 0.05 mmol). Yield: 13 mg, (72.8%) as a white solid.

$[\alpha]_D^{20} +84.5$ (*c* 0.16, $\text{CHCl}_3/\text{MeOH}$ 1:1); $^1\text{H NMR}$ (500 MHz, CD_3OD): δ 7.58 (d, $J = 2.2$ Hz, 1H, Ar-H), 7.53 – 7.43 (m, 3H, Ar-H), 7.39 (d, $J = 8.6$ Hz, 1H, Ar-H), 6.98 (d, $J = 8.8$ Hz, 2H, Ar-H), 5.55 (d, $J = 1.4$ Hz, 1H, H-1), 4.11 (dd, $J = 3.3, 1.8$ Hz, 1H, H-2), 3.99 (dt, $J = 11.8, 5.9$ Hz, 1H, H-3), 3.82 (s, 3H, CH_3), 3.82 – 3.62 (m, 4H, H-4, H-5, H-6); $^{13}\text{C NMR}$ (126 MHz, CD_3OD): δ 160.88, 152.14, 137.70, 133.08, 129.00, 128.77, 126.97, 125.20, 118.81, 115.38 (12C, Ar-C), 100.92 (C-1), 75.91 (C-5), 72.41 (C-3), 71.90 (C-2), 68.26 (C-4), 62.68 (C-6), 55.76 (CH_3); HR-MS: m/z calcd for $\text{C}_{19}\text{H}_{21}\text{ClO}_6$ $[\text{M}+\text{Na}]^+$: 419.0868, found 419.0865; HPLC-purity > 99.5%, $R_t = 10.135$ min.

3'-Chloro-4'-(α -D-mannopyranosyloxy)-3-methyl-biphenyl (8j)

Prepared according to general procedure B from **7j** (40.6 mg, 0.07 mmol). Yield: 26 mg, (92%) as a white solid.

$[\alpha]_D^{20} +98.5$ (*c* 0.304, MeOH); $^1\text{H NMR}$ (500 MHz, CD_3OD): δ 7.61 (d, $J = 2.2$ Hz, 1H, Ar-H), 7.39 (ddt, $J = 26.7, 15.1, 4.9$ Hz, 5H, Ar-H), 7.15 (d, $J = 7.3$ Hz, 1H, Ar-H), 5.56 (d, $J = 1.5$ Hz, 1H, H-1), 4.11 (dd, $J = 3.3, 1.8$ Hz, 1H, H-2), 3.99 (dd, $J = 9.5, 3.4$ Hz, 1H, H-3), 3.84 – 3.62 (m, 4H, H-4, H-5, H-6), 2.39 (s, 3H, CH_3); $^{13}\text{C NMR}$ (126 MHz, CD_3OD): δ 152.59, 140.64, 139.76, 138.07, 129.88, 129.48, 129.21, 128.37, 127.48, 125.18, 124.85, 118.71, (12Ar-C) 100.87 (C-1), 75.95 (C-5), 72.43 (C-3), 71.91 (C-2), 68.27 (C-4), 62.68 (C-6), 21.53 (CH_3); HR-MS: m/z calcd for $\text{C}_{19}\text{H}_{21}\text{ClO}_6$ $[\text{M}+\text{Na}]^+$: 403.0919, found 403.0925; HPLC-purity > 99.5%, $R_t = 11.092$ min.

3'-Chloro-4'-(α -D-mannopyranosyloxy)-3-chloro-biphenyl (8k)

Prepared according to general procedure B from **7k** (34 mg, 0.06 mmol). Yield: 15 mg, (62%) as a white solid.

$[\alpha]_D^{20} +96.1$ (*c* 0.21, MeOH); $^1\text{H NMR}$ (500 MHz, CD_3OD): δ 7.64 (d, $J = 1.9$ Hz, 1H, Ar-H), 7.57 (s, 1H, Ar-H), 7.55 – 7.29 (m, 5H, Ar-H), 5.59 (s, 1H, H-1), 4.12 (s, 1H, H-2), 4.00 (dd, $J = 9.5, 3.3$ Hz, 1H, H-3), 3.83 – 3.69 (m, 3H, H-4, H-6), 3.64 (m, 1H, H-5); $^{13}\text{C NMR}$ (126 MHz, CD_3OD): δ 153.12, 142.67, 136.15, 135.88, 131.47, 129.57, 128.42, 127.66, 127.59, 126.13, 125.32, 118.64 (12Ar-C), 100.74 (C-1), 75.98 (C-5), 72.39 (C-3), 71.84 (C-2), 68.21 (C-4), 62.65 (C-6); HR-MS: m/z calcd for $\text{C}_{18}\text{H}_{18}\text{Cl}_2\text{O}_6$ $[\text{M}+\text{Na}]^+$: 423.0373, found 423.0378; HPLC-purity > 99.5%, $R_t = 11.211$ min.

3'-Chloro-4'-(α -D-mannopyranosyloxy)-2-methyl-biphenyl (8l)

Prepared according to general procedure B from **7l** (26 mg, 0.05 mmol). Yield: 17 mg, (95%) as a white solid.

$[\alpha]_D^{20} +88$ (*c* 0.22, MeOH); $^1\text{H NMR}$ (500 MHz, CD_3OD): δ 7.40 – 6.93 (m, 7H, Ar-H), 5.47 (d, $J = 1.5$ Hz, 1H, H-1), 4.02 (dd, $J = 3.3, 1.8$ Hz, 1H, H-2), 3.90 (dd, $J = 9.4, 3.4$ Hz, 1H, H-3), 3.74 – 3.55 (m, 4H, H-4, H-5, H-6), 2.14 (s, 3H, CH_3); $^{13}\text{C NMR}$ (126 MHz, CD_3OD): δ 152.30, 141.49, 138.70, 136.37, 131.70, 131.42, 130.62, 129.84, 128.67, 126.97, 124.50, 118.20, (12Ar-C), 100.97 (C-1), 75.97 (C-5), 72.42 (C-3), 71.91 (C-2), 68.28 (C-4), 62.70 (C-6), 20.52 (CH_3); HR-MS: m/z calcd for $\text{C}_{19}\text{H}_{21}\text{ClO}_6$ $[\text{M}+\text{Na}]^+$: 403.0919, found 403.0922; HPLC-purity > 99.5%, $R_t = 10.895$ min.

3'-Chloro-4'-(α -D-mannopyranosyloxy)-2-chloro-biphenyl (8m)

Prepared according to general procedure B from **7m** (38.7 mg, 0.07 mmol). Yield: 20 mg, (73%) as a white solid.

$[\alpha]_D^{20} +85.6$ (*c* 0.3, MeOH); $^1\text{H NMR}$ (500 MHz, CD_3OD): δ 7.53 – 7.24 (m, 7H, Ar-H), 5.60 (d, $J = 1.3$ Hz, 1H, H-1), 4.13 (dd, $J = 3.2, 1.8$ Hz, 1H, H-2), 4.01 (dd, $J = 9.5, 3.4$ Hz, 1H, H-3), 3.86 – 3.64 (m, 4H, H-4, H-5, H-6); $^{13}\text{C NMR}$ (126 MHz, CD_3OD): δ 152.84, 140.11, 135.85, 133.40, 132.43, 132.05, 131.05, 130.18, 130.15, 128.30, 124.32, 117.89, (12Ar-C), 100.83 (C-1), 75.98 (C-5), 72.39, 71.86, (C-3, C-2), 68.23 (C-4), 62.66 (C-6); HR-MS: m/z calcd for $\text{C}_{18}\text{H}_{18}\text{Cl}_2\text{O}_6$ $[\text{M}+\text{Na}]^+$: 423.0373, found 423.0378; HPLC-purity > 99.5%, $R_t = 9.782$ min.

3'-Chloro-4'-(α -D-mannopyranosyloxy)-2-methoxy-biphenyl (8n)

Prepared according to general procedure B from **7n** (26.6 mg, 0.05 mmol). Yield: 15 mg, (80%) as a white solid.

$[\alpha]_D^{20} +81.2$ (*c* 0.12, MeOH); $^1\text{H NMR}$ (500 MHz, CD_3OD): δ 7.51 (s, 1H, Ar-H), 7.41 – 6.93 (m, 6H, Ar-H), 5.56 (d, *J* = 1.4 Hz, 1H, H-1), 4.11 (dd, *J* = 3.3, 1.8 Hz, 1H, H2), 4.00 (dd, *J* = 9.4, 3.4 Hz, 1H, H-3), 3.82 – 3.79 (m, 3H, CH_3), 3.79 – 3.66 (m, 4H, H-4, H-5, H-6); $^{13}\text{C NMR}$ (126 MHz, CD_3OD): δ 157.83, 152.11, 135.39, 132.06, 131.40, 130.08, 130.05, 124.14, 121.98, 117.93, 112.62, (12C, Ar-C) 100.87 (C-1), 75.89 (C-5), 72.41 (C-3), 71.91 (C-2), 68.26 (C-4), 62.67 (C-6), 56.01 (CH_3); HR-MS: *m/z* calcd for $\text{C}_{19}\text{H}_{21}\text{ClO}_7$ $[\text{M}+\text{Na}]^+$: 419.0868, found 419.0871; HPLC-purity > 99.5%, R_t = 10.475 min.

3'-Chloro-4'-(α -D-mannopyranosyloxy)-3-trifluoromethyl-biphenyl (8o)

Prepared according to general procedure B from **7o** (60 mg, 0.1 mmol). Yield: 39 mg, (91%) as a white solid.

$[\alpha]_D^{20} +84.3$ (*c* 0.42, MeOH); $^1\text{H NMR}$ (500 MHz, CD_3OD): δ 7.87 – 7.78 (m, 2H, Ar-H), 7.70 – 7.44 (m, 5H, Ar-H), 5.61 (d, *J* = 1.1 Hz, 1H, H-1), 4.13 (dd, *J* = 3.0, 1.7 Hz, 1H, H-2), 4.01 (dd, *J* = 9.5, 3.4 Hz, 1H, H-3), 3.84 – 3.60 (m, 4H, H-4, H-5, H-6); $^{13}\text{C NMR}$ (126 MHz, CD_3OD): δ 153.25, 141.66, 135.98, 132.30 (PhCF_3 , q, $^1J_{\text{CF}}$ = 246 Hz), 131.45, 130.85, 128.68 (q, $^2J_{\text{CF}}$ = 32 Hz), 126.71, 125.42, 125.05 (q, $^3J_{\text{CF}}$ = 3.8 Hz) 124.55, 124.23 (q, $^3J_{\text{CF}}$ = 3.8 Hz), 118.68 (12Ar-C), 100.71 (C-1), 75.99 (C-5), 72.39 (C-3), 71.82 (C-2), 68.20 (C-4), 62.64 (C-6); HR-MS: *m/z* calcd for $\text{C}_{19}\text{H}_{18}\text{ClF}_3\text{O}_6$ $[\text{M}+\text{Na}]^+$: 457.0636, found 457.0640; HPLC-purity: 97%, R_t = 11.743 min.

3'-Chloro-4'-(α -D-mannopyranosyloxy)-3-nitro-biphenyl (8p)

Prepared according to general procedure B from **7p** (48 mg, 0.08 mmol). Yield: 32 mg, (94%) as a white solid.

$[\alpha]_D^{20} +93.2$ (*c* 0.52, MeOH); $^1\text{H NMR}$ (500 MHz, CD_3OD): δ 8.47 – 7.97 (m, 3H, Ar-H), 7.80 – 7.48 (m, 4H, Ar-H), 5.63 (s, 1H, H-1), 4.11 (m, 1H, H-2), 4.00 (dd, *J* = 9.5, 3.4 Hz, 1H, H-3), 3.82 – 3.58 (m, 4H, H-4, H-5, H-6); $^{13}\text{C NMR}$ (126 MHz, CD_3OD): δ 153.56, 150.26, 142.38, 135.13, 133.86, 131.29, 129.78, 127.82, 125.53, 123.09, 122.28, 118.70 (12Ar-C), 100.71 (C-1), 76.06 (C-5), 72.40 (C-3), 71.82 (C-2), 68.21 (C-4), 62.66 (C-6); HR-MS: *m/z* calcd for $\text{C}_{18}\text{H}_{18}\text{ClNO}_8$ $[\text{M}+\text{Na}]^+$: 434.0613, found 434.0612; HPLC-purity > 99.5%, R_t = 10.172 min.

3'-Chloro-4'-(α -D-mannopyranosyloxy)-biphenyl-3-carbonitril (8q)

Prepared according to general procedure B from **7q** (84 mg, 0.15 mmol). Yield: 14 mg, (34%) as a white solid.

$[\alpha]_{\text{D}}^{20} +96.3$ (*c* 0.23, MeOH); $^1\text{H NMR}$ (500 MHz, CD_3OD): δ 8.03 – 7.88 (m, 2H, Ar-H), 7.71 (dd, *J* = 16.5, 5.0 Hz, 2H, Ar-H), 7.65 – 7.54 (m, 2H, Ar-H), 7.48 (d, *J* = 8.6 Hz, 1H, Ar-H), 5.61 (d, *J* = 1.4 Hz, 1H, H-1), 4.12 (dd, *J* = 3.3, 1.8 Hz, 1H, H-2), 4.00 (dd, *J* = 9.5, 3.4 Hz, 1H, H-3), 3.85 – 3.56 (m, 4H, H-4, H-5, H-6); $^{13}\text{C NMR}$ (126 MHz, CD_3OD): δ 153.45, 142.02, 135.30, 132.39, 132.00, 131.28, 131.15, 129.71, 127.74, 125.49 (10Ar-C), 119.62 (CN), 118.68, 114.15 (2Ar-C), 100.72 (C-1), 76.04 (C-5), 72.40 (C-3), 71.83 (C-2), 68.21 (C-4), 62.66 (C-6); HR-MS: *m/z* calcd for $\text{C}_{19}\text{H}_{18}\text{ClNO}_6$ $[\text{M}+\text{Na}]^+$: 414.0715, found 414.0715; HPLC-purity > 99.5%, R_t = 9.759 min.

3'-Chloro-4'-(α -D-mannopyranosyloxy)-biphenyl-4-carbonitril (8r)

Prepared according to general procedure B from **7r** (36 mg, 0.06 mmol). Yield: 12 mg (48%) as a white solid.

$[\alpha]_{\text{D}}^{20} +109.4$ (*c* 0.23, MeOH); $^1\text{H NMR}$ (500 MHz, CD_3OD): δ 7.80 – 7.72 (m, 5H, Ar-H), 7.59 (dd, *J* = 8.6, 2.2 Hz, 1H, Ar-H), 7.48 (d, *J* = 8.7 Hz, 1H, Ar-H), 5.62 (d, *J* = 1.4 Hz, 1H, H-1), 4.12 (dd, *J* = 3.3, 1.8 Hz, 1H, H-2), 4.00 (dd, *J* = 9.5, 3.4 Hz, 1H, H-3), 3.83 – 3.68 (m, 3H, H-4, H-6), 3.63 (ddd, *J* = 9.6, 5.4, 2.3 Hz, 1H, H-5); $^{13}\text{C NMR}$ (126 MHz, CD_3OD): δ 153.65, 145.15, 135.42, 133.86, 129.82, 128.53, 127.87, 125.47, 119.70, 118.59 (12C, Ar-C), 111.97 (CN), 100.66 (C-1), 76.05 (C-5), 72.39 (C-3), 71.80 (C-2), 68.20 (C-4), 62.65 (C-6); IR (KBr), ν = 3400 (O-H stretch), 2227 ($\text{C}\equiv\text{N}$ stretch), 1606, 1487 (Ar C=C bending) cm^{-1} ; HR-MS: *m/z* calcd for $\text{C}_{19}\text{H}_{18}\text{ClNO}_6$ $[\text{M}+\text{Na}]^+$: 414.0715, found 414.0721; HPLC-purity > 99.5%, R_t = 9.785 min.

3'-Chloro-4'-(α -D-mannopyranosyloxy)-4-acetyl-biphenyl (8s)

Prepared according to general procedure B **7s** (32 mg, 0.06 mmol). Yield: 21 mg, (93%) as a white solid.

$[\alpha]_{\text{D}}^{20} +103.2$ (*c* 0.27, MeOH); $^1\text{H NMR}$ (500 MHz, CD_3OD): δ 8.06 (d, *J* = 8.4 Hz, 2H, Ar-H), 7.74 (dd, *J* = 8.6, 5.3 Hz, 3H, Ar-H), 7.61 (dd, *J* = 8.6, 2.2 Hz, 1H, Ar-H), 7.48 (d, *J* = 8.7 Hz, 1H, Ar-H), 5.61 (d, *J* = 1.3 Hz, 1H, H-1), 4.12 (dd, *J* = 3.3, 1.8 Hz, 1H, H-2), 4.00 (dd, *J* = 9.5, 3.4 Hz, 1H, H-3), 3.83 – 3.59 (m, 4H, H-4, H-5, H-6), 2.63 (s, 3H, CH_3); $^{13}\text{C NMR}$ (126 MHz, CD_3OD): δ 200.02 (CO), 153.40, 145.29, 137.16, 136.20, 130.22, 129.76, 127.86, 127.80, 125.39, 118.61 (12C, Ar-C), 100.72 (C-1), 76.03 (C-5), 72.40 (C-3), 71.83 (C-2),

68.22 (C-4), 62.66 (C-6), 26.71 (CH₃); HR-MS: m/z calcd for C₂₀H₂₁ClO₇ [M+Na]⁺: 431.0868, found 431.0869; HPLC-purity: 98.8%, R_t = 9.375 min.

Biological Evaluation

Competitive binding assay. A recombinant protein consisting of the CRD of FimH linked with a thrombin cleavage site (Th) to a His₆-tag (FimH-CRD-Th-His₆) was expressed in *E. coli* strain HM125 and purified by affinity chromatography.^[14] To determine the affinity of the various FimH antagonists, a competitive binding assay described previously^[14] was applied. Microtiter plates (F96 MaxiSorp, Nunc) were coated with 10 µg/ml solution of FimH-CRD-Th-His₆ in 20 mM HEPES, 50 mM NaCl, and 1 mM CaCl₂, pH 7.4 (assay buffer), 100 µl per well, overnight at 4°C. The coating solution was discarded, and the wells were blocked with 3 % BSA in assay buffer (150 µl per well) for 2 h at 4°C. After three washing steps with assay buffer (150 µl per well), a fourfold serial dilution of the test compound (50 µl per well) in assay buffer containing 5% DMSO and streptavidinperoxidase coupled Man-α(1–3)[Man-α(1–6)]-Man-β(1–4)-GlcNAc-β(1–4)-GlcNAcβ polyacrylamide (TM-PAA) polymer (50 µl per well of a 0.5 µg/ml solution) were added. On each individual microtiter plate, *n*-heptyl α-D-mannopyranoside (**1**) was tested in parallel. The plates were incubated for 3 h at 25°C and 350 rpm and then carefully washed four times with 150 µl per well assay buffer. After the addition of 100 µl per well of 2,2'-azino-di-(3-ethylbenzthiazoline-6-sulfonic acid) (ABTS) substrate, the colorimetric reaction was allowed to develop for 4 min and then was stopped by the addition of 2% aqueous oxalic acid before the optical density (OD) was measured at 415 nm on a microplate reader (Spectramax 190, Molecular Devices, CA, USA). The IC₅₀ values of the compounds tested in duplicate were calculated with Prism software (GraphPad Software Inc., La Jolla, CA, USA). The IC₅₀ defines the molar concentration of the test compound that decreases the maximal specific binding of TM-PAA polymer to FimH-CRD by 50%. The relative IC₅₀ (rIC₅₀) is the ratio of the IC₅₀ of the test compound to the IC₅₀ of *n*-heptyl α-D-mannopyranoside (**1**).

Isothermal Titration Calorimetry. The thermodynamic characterization of the interactions between FimH CRD and the ligand was measured by ITC as previously described.^[10c] The protein was dialyzed over night at 4 °C against assay buffer using Slide-A-Lyzer dialysis cassettes with 10 kDa cut-off (Thermo Fisher Scientific, Waltham, MA, USA). The final protein concentration was 4.8 µM. The ligand was diluted to 60 µM in assay buffer (20 mM

HEPES, 150 mM NaCl, and 1 mM CaCl₂, pH 7.4). Dilution enthalpy was determined by ligand in assay buffer titration. A final concentration of 0.5 % DMSO was present in the ligand and protein solution. The measurements were performed with a MicroCalTM VP-ITC instrument (GE Healthcare, Northampton, MA, USA; sample cell volume of 1.4523 mL) at 25 °C, 307 rpm stirring speed, and 10 μcal/s reference power. The samples were preheated to 22 °C and degassed for 5 minutes prior to the measurements. Titration was started after steady baseline equilibration was reached with an initial 2 μL injection, which was excluded from subsequent data analysis. Ligand was injected in 5 μL steps with a spacing of 10 minutes to ensure non-overlapping peaks. Sigmoidal binding curves with complete saturation at the end of each experiment were obtained. Baseline adjustments and peak integration were performed using the Origin 7 software (OriginLab, Northampton, MA, USA). The parameters K_D (dissociation constant), N (stoichiometry), and ΔH° (change in enthalpy) were determined using non-linear least-square fitting in Microsoft Excel and the Solver add-in (Frontline Systems Inc., Incline Village, NV) according to Ziegler *et al.*^[23] The thermodynamic parameters ΔG° (change in free energy) and $T\Delta S^\circ$ (change in enthalpy) were calculated using equation 1,

$$\Delta G^\circ = \Delta H^\circ - T\Delta S^\circ = RT\ln K_A = -RT\ln K_D \quad (\text{Eq. 1})$$

where T is the absolute temperature and R is the universal gas constant (8.314 J mol⁻¹ K⁻¹). The quantity $c = Mt(0) K_D^{-1}$, where $Mt(0)$ is the initial macromolecule concentration, was above 1000. The determination of K_D and $T\Delta S^\circ$ is therefore not reliable, ΔH is nonetheless accurate.^[24]

Physicochemical and *in vitro* Pharmacokinetic Studies

Materials. DMSO, 1-Propanol, and 1-Octanol were purchased from Sigma-Aldrich. PAMPA System Solution, GIT-0 Lipid Solution, and Acceptor Sink Buffer were ordered from pIon (Woburn, MA, USA). Acetonitrile (MeCN) was bought from Acros Organics (Geel, Belgium).

logD_{7.4} determination. The *in silico* prediction tool ALOGPS^[25] was used to estimate the logP values of the compounds. Depending on these values, the compounds were classified into three categories: hydrophilic compounds (logP below zero), moderately lipophilic compounds (logP between zero and one) and lipophilic compounds (logP above one). For

each category, two different ratios (volume of 1-Octanol to volume of buffer) were defined as experimental parameters (Table 2).

Table 2. Compound classification based on estimated logP values.

Compound type	logP	ratio (1-Octanol / buffer)
hydrophilic	< 0	30:140, 40:130
moderately lipophilic	0 - 1	70:110, 110:70
lipophilic	> 1	3:180, 4:180

Equal amounts of phosphate buffer (0.1 M, pH 7.4) and 1-Octanol were mixed and shaken vigorously for 5 min to saturate the phases. The mixture was left until separation of the two phases occurred, and the buffer was retrieved. Stock solutions of the test compounds were diluted with buffer to a concentration of 1 μ M. For each compound, six determinations, i.e. three determinations per 1-Octanol:buffer ratio, were performed in different wells of a 96-well plate. The respective volumes of buffer containing analyte (1 μ M) were pipetted to the wells and covered by saturated 1-Octanol according to the chosen volume ratio. The plate was sealed with aluminum foil, shaken (1350 rpm, 25 °C, 2 h) on a Heidolph Titramax 1000 plate-shaker (Heidolph Instruments GmbH & Co. KG, Schwabach, Germany) and centrifuged (2000 rpm, 25 °C, 5 min, 5804 R Eppendorf centrifuge, Hamburg, Germany). The aqueous phase was transferred to a 96-well plate for analysis by LC-MS.

$\log D_{7.4}$ was calculated from the 1-Octanol:buffer ratio (o/b), the initial concentration of the analyte in buffer (1 μ M), and the concentration of the analyte in buffer (c_B) with equation (1):

$$\log D_{7.4} = \log \left(\frac{1\mu M - c_B}{c_B} \times \frac{1}{o:b} \right) \quad (1)$$

LC-MS measurements. Analyses were performed using an 1100/1200 Series HPLC System coupled to a 6410 Triple Quadrupole mass detector (Agilent Technologies, Inc., Santa Clara, CA, USA) equipped with electrospray ionization. The system was controlled with the Agilent MassHunter Workstation Data Acquisition software (version B.01.04). The column used was an Atlantis® T3 C18 column (2.1 x 50 mm) with a 3- μ m particle size (Waters Corp., Milford, MA, USA). The mobile phase consisted of two eluents: eluent A (H₂O, containing 0.1% formic acid, v/v) and eluent B (acetonitrile, containing 0.1% formic acid, v/v), both delivered at 0.6 mL/min. The gradient was ramped from 95% A/5% B to 5% A/95% B over 1 min, and then hold at 5% A/95% B for 0.1 min. The system was then brought back to 95%

A/5% B, resulting in a total duration of 4 min. MS parameters such as fragmentor voltage, collision energy, polarity were optimized individually for each analyte, and the molecular ion was followed for each compound in the multiple reaction monitoring mode. The concentrations of the analytes were quantified by the Agilent Mass Hunter Quantitative Analysis software (version B.01.04).

Solubility. Solubility was determined in a 96-well format using the μ SOL Explorer solubility analyzer (pIon, version 3.4.0.5). Measurements were performed at pH 7.4 in triplicates. Three wells of a deep well plate were filled with 300 μ L of aqueous universal buffer solution. Aliquots (3 μ L) of compound stock solution (100 mM in DMSO) were added and thoroughly mixed. The final sample concentration was 1 mM, the residual DMSO concentration was 1.0% (v/v) in the buffer solutions. After 15 h, the solutions were filtrated (0.2 μ m 96-well filter plates) using a vacuum to collect manifold (Whatman Ltd., Maidstone, UK) to remove any precipitates. Equal amounts of filtrate and 1-Propanol were mixed and transferred to a 96-well plate for UV detection (190 to 500 nm, SpectraMax 190, Molecular Devices, Sunnyvale, CA, USA). The amount of material dissolved was calculated by comparison with UV spectra obtained from reference samples, which were prepared by dissolving compound stock solution in a 1:1 mixture of buffer and 1-Propanol (final concentrations 0.167 mM).

Parallel Artificial Membrane Permeation Assay (PAMPA). Values of $\log P_e$ were determined in a 96-well format with the PAMPA^[21b] permeation assay. Measurements were performed at pH 7.4 in quadruplicates. Four wells of a deep well plate were filled with 650 μ L System Solution. Samples (150 μ L) were withdrawn from each well to determine the blank spectra by UV-spectroscopy (SpectraMax 190). Then, analyte dissolved in DMSO was added to the remaining System Solution to yield 50 μ M solutions. To exclude precipitation, the optical density was measured at 650 nm, with 0.01 being the threshold value. Solutions exceeding this threshold were filtrated. Afterwards, samples (150 μ L) were withdrawn to determine the reference spectra. Further 200 μ L were transferred to each well of the donor plate of the PAMPA sandwich (pIon, P/N 110 163). The filter membranes at the bottom of the acceptor plate were infused with 5 μ L of GIT-0 Lipid Solution, and 200 μ L of Acceptor Sink Buffer were filled into each acceptor well. The sandwich was assembled, placed in the GutBoxTM, and left undisturbed for 16 h. Then, it was disassembled and samples (150 μ L) were transferred from each donor and acceptor well to UV-plates. Quantification was

performed by UV spectroscopy. The logP_e-values were calculated with the aid of the PAMPA Explorer Software (pIon, version 3.5).

ACKNOWLEDGEMENTS

The authors gratefully acknowledge the financial support by the Swiss National Science Foundation (grant no. 200020_129935).

REFERENCES

- [1] a) H. Connell, W. Agace, P. Klemm, M. Schembri, S. Marild, C. Svanborg, *Proc. Natl. Acad. Sci. U. S. A.* **1996**, 93(18), 9827-9832; b) T. M. Hooton, W. E. Stamm, *Infect. Dis. Clin. North Am.* **1997**, 11(3), 551-581; c) C. Svanborg, G. Godaly, *Infect. Dis. Clin. North Am.* **1997**, 11(3), 513-529.
- [2] a) S. D. Fihn, *N. Engl. J. Med.* **2003**, 349(3), 259-266; b) T. J. Wiles, R. R. Kulesus, M. A. Mulvey, *Exp. Mol. Pathol.* **2008**, 85(1), 11-19.
- [3] a) J. D. Schilling, S. J. Hultgren, *Int. J. Antimicrob. Agents* **2002**, 19(6), 457-460; b) M. G. Blango, M. A. Mulvey, *Antimicrob. Agents Chemother.* **2010**, 54(5), 1855-1863.
- [4] M. A. Mulvey, *Cell. Microbiol.* **2002**, 4(5), 257-271.
- [5] N. Sharon, *Bba-Gen Subjects* **2006**, 1760(4), 527-537.
- [6] a) N. Firon, I. Ofek, N. Sharon, *Carbohydr. Res.* **1983**, 120(Aug), 235-249; b) N. Firon, S. Ashkenazi, D. Mirelman, I. Ofek, N. Sharon, *Infect. Immun.* **1987**, 55(2), 472-476.
- [7] D. Choudhury, A. Thompson, V. Stojanoff, S. Langermann, J. Pinkner, S. J. Hultgren, S. D. Knight, *Science* **1999**, 285(5430), 1061-1066.
- [8] a) C. S. Hung, J. Bouckaert, D. Hung, J. Pinkner, C. Widberg, A. DeFusco, C. G. Auguste, R. Strouse, S. Langermann, G. Waksman, S. J. Hultgren, *Mol. Microbiol.* **2002**, 44(4), 903-915; b) J. Bouckaert, J. Berglund, M. Schembri, E. De Genst, L. Cools, M. Wuhler, C. S. Hung, J. Pinkner, R. Slattegard, A. Zavialov, D. Choudhury, S. Langermann, S. J. Hultgren, L. Wyns, P. Klemm, S. Oscarson, S. D. Knight, H. De Greve, *Mol. Microbiol.* **2005**, 55(2), 441-455; c) A. Wellens, C. Garofalo, H. Nguyen, N. Van Gerven, R. Slattegard, J. P. Hernalsteens, L. Wyns, S. Oscarson, H. De Greve, S. Hultgren, J. Bouckaert, *PLoS ONE* **2008**, 3(4).
- [9] N. Sharon, *FEBS Lett.* **1987**, 217(2), 145-157.
- [10] a) Z. Han, J. S. Pinkner, B. Ford, E. Chorell, J. M. Crowley, C. K. Cusumano, S. Campbell, J. P. Henderson, S. J. Hultgren, J. W. Janetka, *J. Med. Chem.* **2012**, 55(8), 3945-3959; b) T. Klein, D. Abgottspon, M. Wittwer, S. Rabbani, J. Herold, X. H. Jiang, S. Kleeb, C. Luthi, M. Scharenberg, J. Bezencon, E. Gubler, L. J. Pang, M. Smiesko, B. Cutting, O. Schwaradt, B. Ernst, *J. Med. Chem.* **2010**, 53(24), 8627-8641; c) L. Pang, S. Kleeb, K. Lemme, S. Rabbani, M. Scharenberg, A. Zalewski, F. Schädler, O. Schwaradt, B. Ernst, *Chemmedchem* **2012**, 7(8), 1404-1422.
- [11] Z. F. Han, J. S. Pinkner, B. Ford, R. Obermann, W. Nolan, S. A. Wildman, D. Hobbs, T. Ellenberger, C. K. Cusumano, S. J. Hultgren, J. W. Janetka, *J. Med. Chem.* **2010**, 53(12), 4779-4792.

- [12] J. G. Topliss, *J. Med. Chem.* **1972**, *15*(10), 1006-1011.
- [13] a) C. Hansch, T. Fujita, *J. Am. Chem. Soc.* **1964**, *86*(8), 1616-1626; b) C. Hansch, A. Leo, S. H. Unger, K. H. Kim, Nikaitan.D, E. J. Lien, *J. Med. Chem.* **1973**, *16*(11), 1207-1216.
- [14] S. Rabbani, X. H. Jiang, O. Schwardt, B. Ernst, *Anal. Biochem.* **2010**, *407*(2), 188-195.
- [15] C. A. Lipinski, *J. Pharmacol. Toxicol. Methods* **2000**, *44*(1), 235-249.
- [16] J. C. Dearden, G. M. Bresnen, *Quant. Struct-Act. Relat.* **1988**, *7*(3), 133-144.
- [17] M. J. Waring, *Expert. Opin. Drug Dis.* **2010**, *5*(3), 235-248.
- [18] a) H. van de Waterbeemd, D. A. Smith, K. Beaumont, D. K. Walker, *J. Med. Chem.* **2001**, *44*(9), 1313-1333; b) M. V. S. Varma, B. Feng, R. S. Obach, M. D. Troutman, J. Chupka, H. R. Miller, A. El-Kattan, *J. Med. Chem.* **2009**, *52*(15), 4844-4852.
- [19] L. H. Jones, N. W. Summerhill, N. A. Swain, J. E. Mills, *Medchemcomm* **2010**, *1*(5), 309-318.
- [20] T. Fujita, C. Hansch, J. Iwasa, *J. Am. Chem. Soc.* **1964**, *86*(23), 5175-5180.
- [21] a) A. Avdeef, S. Bendels, L. Di, B. Faller, M. Kansy, K. Sugano, Y. Yamauchi, *J. Pharm. Sci.* **2007**, *96*(11), 2893-2909; b) M. Kansy, F. Senner, K. Gubernator, *J. Med. Chem.* **1998**, *41*(7), 1007-1010.
- [22] B. H. C. H. M. Ernst, J. H. C. H. B. Herold, Mannose Derivatives as Antagonists of Bacterial Adhesion, Vol. EP2010/069436 (Ed.: P. C. H. B. University Of Basel), WO, **2011**.
- [23] A. Ziegler, J. Seelig, *Biophys. J.* **2004**, *86*(1), 254-263.
- [24] T. Wiseman, S. Williston, J. F. Brandts, L. N. Lin, in *Anal. Biochem.*, Vol. 179, United States, **1989**, pp. 131-137.
- [25] a) VCCLAB, Virtual Computational Chemistry Laboratory, Vol. (accessed September 13, 2012), <http://www.vcclab.org>, **2005**; b) I. V. Tetko, J. Gasteiger, R. Todeschini, A. Mauri, D. Livingstone, P. Ertl, V. Palyulin, E. Radchenko, N. S. Zefirov, A. S. Makarenko, V. Y. Tanchuk, V. V. Prokopenko, *J. Comput.-Aided Mol. Des.* **2005**, *19*(6), 453-463.

3.2.3 *Manuscript 5: FimH Antagonists - Bioisosteres to improve the *in vitro* and *in vivo* PK/PD Profile*

Author contributions:

Katharina Mayer: synthesis of antagonist 11j (high-affinity biphenyl mannoside with improved PK/PD profile), contribution to manuscript.

Simon Kleeb: physicochemical evaluation of antagonists, preparation of manuscript.

Lijuan Pang: synthesis of antagonists, preparation of manuscript.

Deniz Eris: competitive fluorescence polarization assay, contribution to manuscript.

Manuscript submitted to **Journal of Medicinal Chemistry**

FimH Antagonists - Bioisosteres to Improve the *in vitro* and *in vivo* PK/PD Profile

Simon Kleeb,^{a)}# Lijuan Pang,^{a)}# Katharina Mayer,^{a)}# Deniz Eris,^{a)}# Anja Sigl,^{a)} Roland C. Preston,^{a)} Pascal Zihlmann,^{a)} Timothy Sharpe,^{c)} Roman P. Jakob,^{b)} Daniela Abgottspon,^{a)} Aline S. Hutter,^{a)} Meike Scharenberg,^{a)} Xiaohua Jiang,^{a)} Giulio Navarra,^{a)} Said Rabbani,^{a)} Martin Smiesko,^{a)} Nathalie Lüdin,^{a)} Jacqueline Bezencon,^{a)} Oliver Schwardt,^{a)} Timm Maier,^{b)} Beat Ernst^{a)*}

Equally contributed

^{a)} Institute of Molecular Pharmacy, Pharmacenter, University of Basel, Klingelbergstrasse 50, CH-4056 Basel, Switzerland

^{b)} Structural Biology, Biocenter, University of Basel, Klingelbergstrasse 70, CH-4056 Basel

^{c)} Biophysical Facility, Biocenter, University of Basel, Klingelbergstrasse 70, CH-4056 Basel

* To whom correspondence should be addressed: Prof. Dr. Beat Ernst, Institute of Molecular Pharmacy, Pharmacenter, University of Basel, Klingelbergstrasse 50, CH-4056 Basel, Switzerland; Tel: +41 61 267 15 51, Fax: +41 61 267 15 52; E-mail: beat.ernst@unibas.ch

Keywords: bacterial adhesion · urinary tract infections · *E. coli* · FimH antagonists · biphenyl mannosides · PK/PD profile · bioisosteres · fluorescence polarization assay ·

ABBREVIATIONS:

ΔH , change in enthalpy; ΔS , change in entropy; AUC, Area under the curve; BSA, bovine serum albumin; C_{\max} , maximal concentration; Caco-2 cells, colorectal adenocarcinoma cells; CFU, colony forming units; CL_{tot} , total clearance; CRD, carbohydrate recognition domain; C_0 , initial concentration; FITC, fluorescein isothiocyanate; FP, fluorescence polarization; ITC, isothermal titration calorimetry; K_D , dissociation constant; MAC_{90} , minimal anti-adhesion concentration to inhibit 90% adhesion; PAMPA, parallel artificial membrane permeation assay; P_{app} , apparent permeability; PD, pharmacodynamics; P_e , effective permeability; PK, pharmacokinetics; po, per os; UPEC, uropathogenic *Escherichia coli*; UTI, urinary tract infection; V_z , volume of distribution in terminal phase.

ABSTRACT

Urinary tract infections (UTIs), predominantly caused by uropathogenic *Escherichia coli* (UPEC) belong to the most prevalent infectious diseases worldwide. For the successful establishment of an UTI, the adhesion of bacteria to urothelial cells is a crucial first step, protecting the bacteria from the natural defense mechanisms as urine flow or the host immune system. The attachment of UPEC to host cells is mediated by FimH, a mannose-binding adhesin at the tip of type 1 pili, which are expressed on the bacterial surface. To date, UTIs are mainly treated with antibiotics, leading to the ubiquitous problem of increasing resistance against most of the currently available antimicrobials. Therefore, new treatment strategies are urgently needed, avoiding selection pressure and thereby affording a reduced risk of resistance. Here, we describe the development of an orally available FimH antagonist. Starting from the carboxylate substituted biphenyl α -D-mannoside **6** affinity as well as the relevant pharmacokinetic parameters (solubility, permeability, renal excretion) could be substantially improved by a bioisosteric approach. With 3'-chloro-4'-(α -D-mannopyranosyloxy)-biphenyl-4-carbonitrile (**11j**) a FimH antagonist with an optimal *in vitro* PK/PD profile was identified. The *para*-cyano substituent conferred lipophilicity and high binding to plasma proteins, which slowed down the rate of renal excretion. Despite higher lipophilicity, antagonist **11j** was unsusceptible to CYP450 mediated metabolism, and as a consequence predominantly eliminated via the renal pathway. Finally, *in vivo* experiments confirmed the excellent PK-profile of **11j** with steady renal excretion for more than eight hours after oral application, suggesting a long-lasting anti-adhesive effect. Finally, orally applied **11j** was effective in a mouse model of UTI by reducing the bacterial load in the bladder by over 1000-fold.

INTRODUCTION

Urinary tract infection (UTI) is one of the most frequent infectious diseases worldwide and affects millions of people every year.¹ In more than 70% of the reported cases, uropathogenic *Escherichia coli* (UPEC) is the causal pathogen.² Acute, uncomplicated lower urinary tract infection, commonly referred to as cystitis, requires an antibiotic treatment for symptom relief (i.e. reduction of dysuria, frequent and urgent urination, bacteriuria, pyuria) and for prevention of more devastating or even life threatening complications like pyelonephritis and urosepsis.^{3,4} However, the repeated use of antibacterial chemotherapeutics provokes antimicrobial resistance leading to treatment failure.⁵ Hence, a new approach for the prevention and treatment of UTI with orally applicable therapeutics is urgently needed.⁶

UPEC undergo a well-defined infection cycle within the host.⁷ The key step in pathogenesis is bacterial adhesion to the epithelial cells in the lower urinary tract.⁸ This interaction prevents UPEC from clearance by the bulk flow of urine and enables the bacteria to colonize the epithelial cells. The adhesion is mediated by the virulence factor FimH located at the tip of bacterial type 1 pili.^{9,10} FimH consists of two immunoglobulin-like domains: the N-terminal lectin domain and – connected by a short linker – the C-terminal pilin domain.¹¹ The lectin domain encloses the carbohydrate recognition domain (CRD) that binds to the oligomannosides of the glycoprotein uroplakin Ia on the epithelial cell surface.¹² The pilin domain anchors the adhesin to the pilus and regulates the switch between the two conformational states of the CRD with high and low affinity for mannosides, respectively.

More than three decades ago, Sharon and co-workers described various oligomannosides and aryl α -D-mannosides as potential antagonists of the FimH-mediated bacterial adhesion.^{13,14} However, only weak interactions in the milli- to micromolar range were observed. In recent years, several high-affinity monovalent α -D-mannopyranosides have been reported.¹⁵⁻²⁴ Their improved affinities are based on optimal interactions with the main structural features of the CRD.²⁵⁻²⁸ First, the mannose binding pocket accommodating the mannose moiety by means of an extended hydrogen bond network and, second, the entrance to the binding site composed of three hydrophobic amino acids (Tyr48, Tyr137, and Ile52) and therefore referred to as ‘tyrosine gate’ hosting aliphatic and aromatic aglycones. As an example, *n*-heptyl α -D-mannopyranoside (**1**) exhibits nanomolar affinity due to hydrophobic contacts of the alkyl aglycone with the hydrophobic residues of the tyrosine gate.¹⁵ Furthermore,

aromatic aglycones, such as present in the mannosides **2-10** (Figure 1), provide strong π - π stacking interactions with the tyrosine gate. These interactions are further favored by the addition of an electron withdrawing substituent on the terminal ring of the biaryl portion.^{18,19}

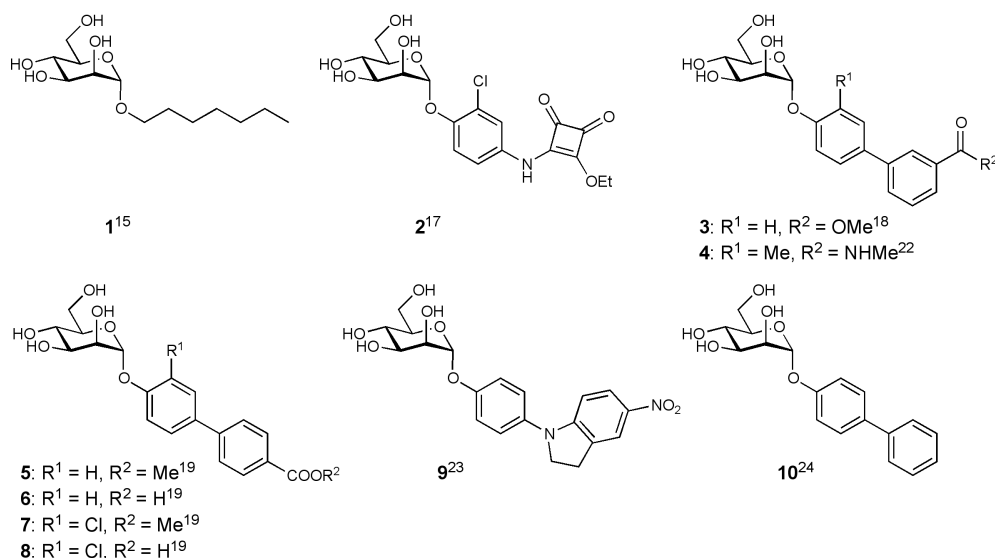


Figure 1. Monovalent FimH antagonists exhibiting nanomolar affinities.

Recent *in vivo* PK studies in mice proved the high potential of the biphenyl α -D-mannosides **4** and **7** for an oral treatment, although high doses (≥ 50 mg/kg) were necessary to achieve the minimal concentrations required for the anti-adhesive effect in the urinary bladder.^{19,21,22} Moreover, the therapeutic effect could only be maintained for a few hours, i.e. four hours for a po (per os) single-dose application of **7** (50 mg/kg), because of rapid elimination by glomerular filtration and low reabsorption from the primary urine in the renal tubules.¹⁹

To date, the physicochemical properties affecting the rate of renal excretion, i.e. lipophilicity and plasma protein binding (PPB), or metabolic liabilities promoting non-renal elimination pathways have been barely investigated for FimH antagonists. The goal of the present study was to optimize the biphenyl α -D-mannoside with respect to oral bioavailability and renal excretion. Starting from antagonist **6**, we synthesized new biphenyl derivatives, characterized their affinity to the CRD, structurally investigated their binding mode, and determined physicochemical and pharmacokinetic parameters predictive for intestinal absorption and renal elimination. Furthermore, we determined *in vivo* PK (pharmacokinetic) of the most promising new antagonists in a mouse model. The compound with the best PK profile

proved effective in reducing the bacterial loads upon bladder infection in a mouse model of UTI.

RESULTS AND DISCUSSION

As previously reported, the carboxylate substituent present in the biphenyl mannoside **6** – its electron withdrawing potential being essential for an enhanced drug target interaction – strongly decreases the lipophilicity of the antagonist ($\log D_{7.4} < -1.5^{19}$) in comparison to the *n*-heptyl (\rightarrow **1**, $\log P = 1.7^{19}$) or the unsubstituted biphenyl aglycone (\rightarrow **10**, $\log P = 2.1^{24}$). Since low lipophilicity is a major reason for low intestinal absorption and rapid renal excretion of the systemically available antagonist,^{19,23} we aspired to improve oral bioavailability as well as renal excretion by replacing the carboxylate in **6** with various bioisosteric groups²⁹ (Figure 2).

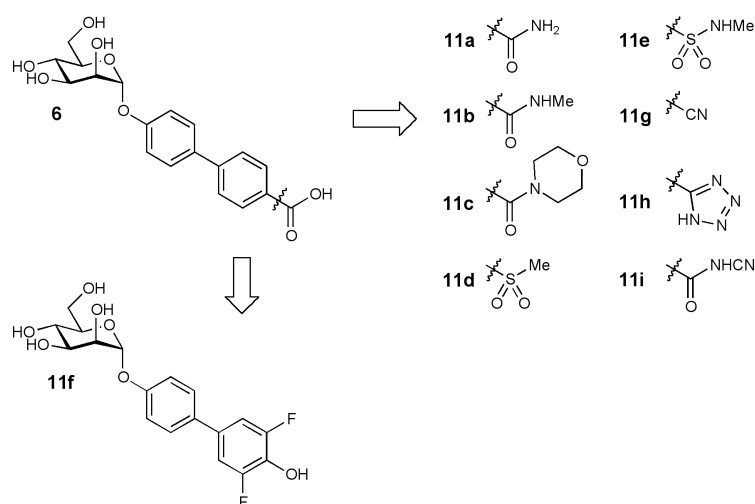
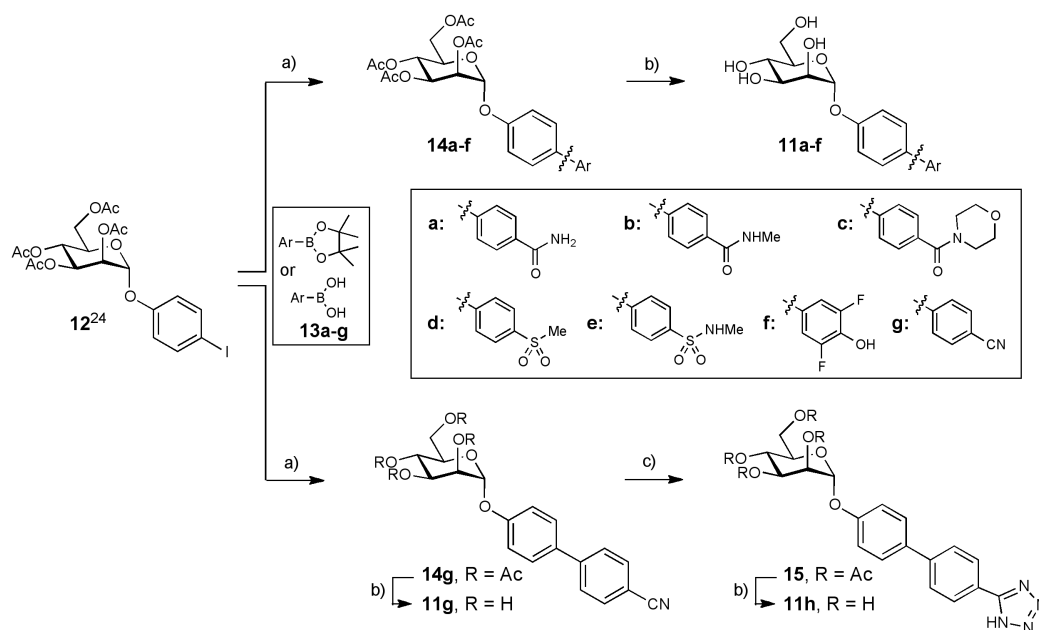


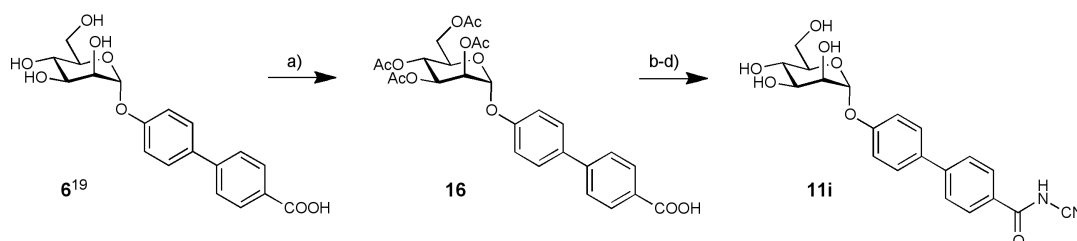
Figure 2. Bioisosteric replacement of the carboxylic acid substituent of biphenyl α -D-mannopyranoside **6**.

Synthesis. Iodide **12** was prepared from peracetylated mannose and 4-iodophenol in the presence of $\text{BF}_3 \cdot \text{Et}_2\text{O}$.²⁴ In a palladium-catalyzed Miyaura-Suzuki coupling³⁰ with the boronic acid or boronate derivatives **13a-g**, the biphenyl derivatives **14a-g** were obtained in good to excellent yields. Final deprotection yielded the test compounds **11a-g**. Utilizing microwave-assisted reaction condition,³¹ the conversion of aryl nitrile **14g** to tetrazole **15** proceeded rapidly and with good yield. After deprotection of **15** using Zemplén conditions, the test compound **11h** was obtained (Scheme 1).



Scheme 1. a) Pd(Cl₂)dppf·CH₂Cl₂, K₃PO₄, DMF, 80 °C, 4 h (**14a-g**, 44-99%); b) NaOMe, MeOH, rt, 4 h (**11a-h**, 29-86%); c) TMSN₃, Bu₂Sn(O), DME, 150 °C, μ W, 10 min, 81%.

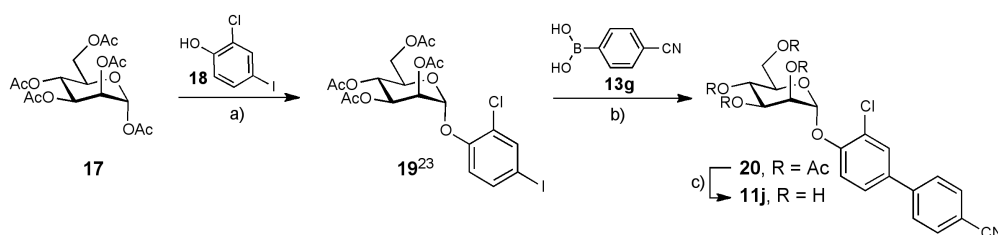
The cyanobenzamide derivative **11i** (Scheme 2) was obtained from **6** by peracetylation (\rightarrow **16**) followed by conversion of the carboxylic acid into its acid chloride with 1-chloro-*N,N*,2-trimethyl-1-propenylamine.³² Without isolation, the acid chloride was reacted with sodium hydrogen cyanide in DMF followed by deacetylation under Zemplén conditions to yield the test compound **11i**.



Scheme 2. a) i) Ac₂O, DMAP, pyridine, 0 °C to rt, overnight; ii) satd. NaHCO₃ aq., DCM, rt, 2 h (**16**, 53%); b) 1-chloro-*N,N*,2-trimethyl-1-propenylamine, toluene, 0 °C to rt, 2 h; c) NaH, NH₂CN, DMF, 0 °C to rt, overnight; d) NaOMe, MeOH, rt, 4 h (**11i**, 21% for three steps).

Finally, to further improve the pharmacokinetic properties of mannoside **11g** (see Table 3), a chloride substituent was introduced to the *ortho*-position of the aromatic ring adjacent to the anomeric oxygen. For its synthesis, peracetylated α -D-mannose (**17**) was coupled with 2-chloro-4-iodophenol (**18**) using BF₃·Et₂O as promotor (\rightarrow **19**, 76%). After the introduction of

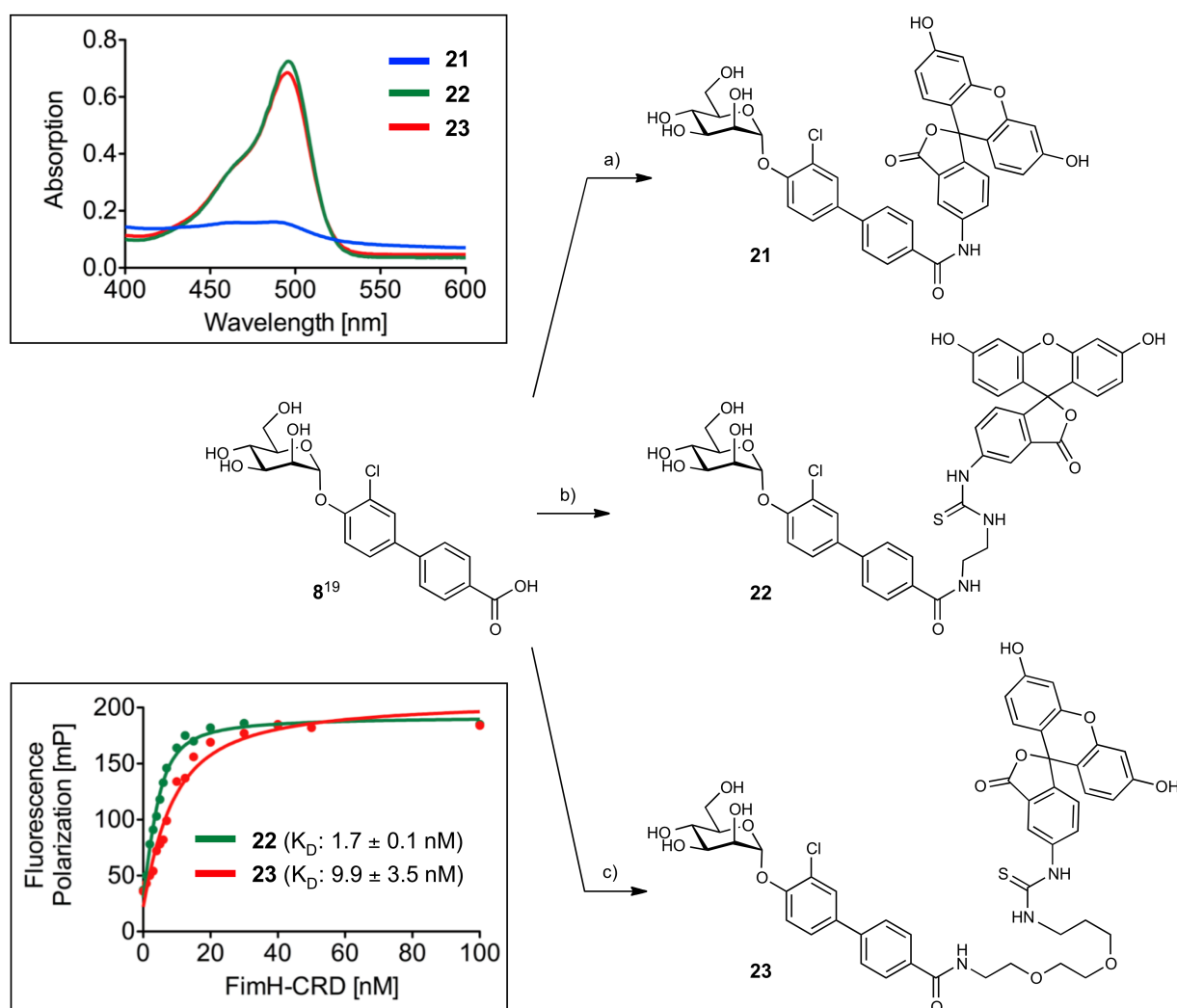
the second aromatic ring by Miyaura-Suzuki coupling (\rightarrow **20**, 75%), deprotection yielded mannoside **11j** (Scheme 3).



Scheme 3. a) $\text{BF}_3 \cdot \text{Et}_2\text{O}$, CH_2Cl_2 , 40 °C (76%); b) $\text{Pd}(\text{Cl}_2)\text{dppf} \cdot \text{CH}_2\text{Cl}_2$, K_3PO_4 , DMF, 80 °C (75%); c) NaOMe, MeOH, rt, 4 h (48%).

Binding Affinity. The binding affinity of heptyl mannoside **1**, the biphenyl mannosides **5**, **6**, **10**, and the bioisosteres **11a-j** was determined in a competitive fluorescence polarization assay (FP-assay) and with isothermal titration calorimetry (ITC). A protein construct consisting of the CRD with a C-terminal His-tag with a thrombin cleavage site (FimH-CRD-Th-His₆) was used for all experiments.³³

Competitive Fluorescence Polarization Assay. For the rapid evaluation of binding affinity, we established a competitive binding assay based on fluorescence polarization (FP). Similar formats have been applied before for the detection of carbohydrate-lectin interactions.^{18,34} In this assay, the antagonist of interest displaces a fluorescently labeled competitor from the binding site, thereby causing a reduction in fluorescence polarization.³⁵ To identify the optimal competitor, fluorescein isothiocyanate (FITC) was connected to the FimH ligand **8** by three linkers of different lengths (\rightarrow **21-23**, Scheme 4). For optimal sensitivity and signal-to-noise ratio, three main parameters need to be considered: (i) the affinity of the competitor should not be impaired by the fluorescent label, (ii) the conformational flexibility of the label upon binding of the competitor to the CRD should be low and (iii) the fluorescence properties of the label should not be affected by the connected ligand.³⁶⁻³⁸ A change in fluorescence properties was observed for reporter ligand **21** in which the label was linked to the biphenyl aglycone by an amide bond. The absorption spectrum revealed a lack of the characteristic fluorescein absorption peak at 494 nm (Scheme 4), likely due to an extension of the conjugated system to the biphenyl moiety of the ligand. The elongated saturated spacer groups in competitors **22** and **23** ensured that the expected spectral properties of the dye were retained (Scheme 4).



Scheme 4. a) 1-[(1-(Cyano-2-ethoxy-2-oxoethylideneaminoxy)-dimethylamino-morpholinomethylene)] methanaminium hexafluorophosphate (COMU), NEt_3 , fluoresceinamine, DMF, rt, 7 h (**21**, 19%); b) i. DIC, NHS, *N*-Boc-ethylenediamine, DMF, rt, 12 h; ii. TFA, DCM, rt, 10 min (68% over two steps), iii. fluorescein isothiocyanate (FITC), NEt_3 , DMF, rt, 3 h (**22**, 48%); c) i. DIC, NHS, *N*-Boc-PEG2- NH_2 , DMF, rt, 14 h; ii. TFA, DCM, rt, 30 min (62% over two steps); iii. FITC, DMF, rt (**23**, 65%).

For the determination of their binding affinity, fixed concentrations of the reporter ligands **22** and **23** were incubated for 24 h with a linear dilution of the FimH-CRD (0-100 nM). FP was measured using a plate reader, with polarized excitation at 485 nm, and emission at 528 nm measured through appropriately oriented polarizers. Fitting the single-site binding function of Cooper³⁹ to the observed FP data resulted for compound **22** in a dissociation constant ($K_D = 1.7$ nM, Figure 3A) similar to that of the unlabeled parent compound **8**,¹⁹ whereas **23** showed a five-fold lower affinity (9.9 nM) (Scheme 4). Therefore, the reporter ligand **22** fulfills all characteristics as an optimal competitor and was used for the FP assay.

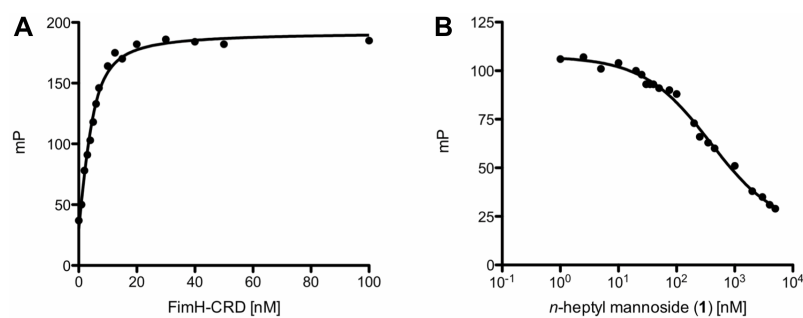


Figure 3. A) Direct binding curve of the labeled competitor **22** obtained by adding a linear dilution of FimH-CRD (0-100 nM) and a constant concentration of competitor **22** (5 nM). The K_D was determined by fitting the experimental data to a single-site binding fit that accounts for ligand depletion. In three FP based direct binding experiments the K_D of competitor **22** was determined to be 1.7 nM. B) Inhibition curve of *n*-heptyl mannoside (**1**) from the competitive FP assay. The IC_{50} value was determined by nonlinear least-squares fitting to a standard 4-parameter equation. A modified Cheng-Prusoff equation was used to calculate the corresponding K_D value ($K_D = 28.3$ nM).

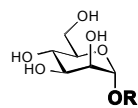
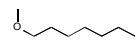
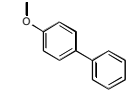
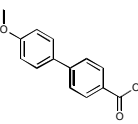
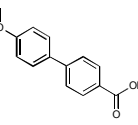
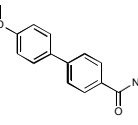
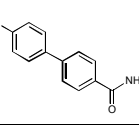
For the test compounds **1**, **5**, **6**, **10**, and **11a-j**, a 24 h incubation time was applied before FP was measured due to the long residence time of FimH antagonists ($t_{1/2} > 3.5$ h, Figure 3B⁴⁰). The 24 h incubation period was empirically determined to be necessary to reach equilibrium between reporter ligand and compound of interest. IC_{50} values were obtained by nonlinear least-squares regression (standard four-parameter dose response curve) and converted to K_D values using a modified Cheng-Prusoff equation.³⁵ This equation accounts for the ligand depletion effect in competitive titrations involving high-affinity interaction partners present in similar concentrations. Under these conditions, the free concentration of an interacting species cannot be assumed to equal the total concentration.

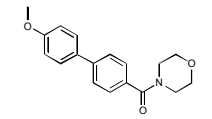
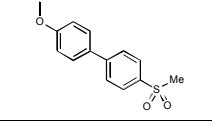
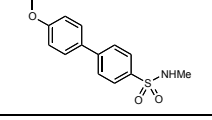
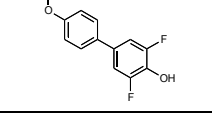
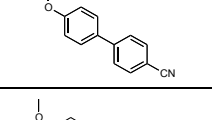
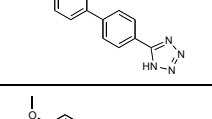
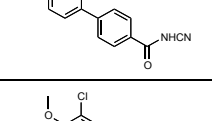
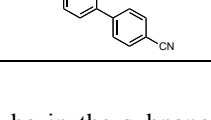
The K_D values determined for the test compounds **1**, **5**, **6**, **10**, and **11a-j** are summarized in Table 1. Against our expectations, the biphenyl mannosides **6** and **10** exhibit similar affinities (Table 1), despite the presence of an electron withdrawing carboxylate substituent in antagonist **6**. According to the crystal structure of FimH co-crystallized with the sulfonamide derivative **11e** (Figure 4A), the outer aromatic ring of the biphenyl aglycone forms π - π interactions with the electron rich Tyr48, which is part of the tyrosine gate of FimH.¹⁵ A reduction of electron density of the aglycone by the electron withdrawing carboxylate was expected to enforce these π - π stacking interactions and lead to improved affinity. However, this beneficial effect might be compensated by an entropic penalty originating from the improved π - π stacking to Tyr48 that might lead to the reduced flexibility of both protein and antagonist. Furthermore, a beneficial enthalpy effect might be partially compensated by an enthalpy penalty originating from the desolvation of the charged **10** carboxylate⁴¹ (see also

experimental part). Although this substituent is solvent exposed, at least a partial desolvation may be necessary upon antagonist binding. To prove this assumption, we replaced the carboxylate by the corresponding methyl ester (\rightarrow **5**)¹⁹ in order to reduce the desolvation penalty and, as predicted by the Hammett constant σ_p ,⁴² to further improve the π - π stacking. Indeed, a six-fold improvement in affinity was achieved. However, since the methyl ester undergoes rapid enzyme-mediated hydrolysis *in vivo*,¹⁹ it will not be available at the place of action in the urinary bladder. The methyl ester was therefore replaced by metabolically stable bioisosteres²⁹ exhibiting comparable electron withdrawing properties⁴² (Table 1, entries 5-13). The most potent derivatives **11d**, **11e** and **11g** showed affinities in the low nanomolar range.

As previously reported,²⁴ a chloro substituent in the *ortho*-position of the aromatic ring adjacent to the anomeric oxygen is favorable for affinity and improves the physicochemical properties relevant for oral bioavailability. Indeed, the corresponding antagonist **11j** was the most potent compound tested in this study.

Table 1. Affinities (K_D) of FimH antagonists to FimH-CRD-Th-His₆; dissociation constants (K_D) were determined in a competitive fluorescence polarization assay.

Entry	Compd		Affinity K_D [nM]
1	1		28.3 ± 5.0
2	10		15.1 ± 2.2
3	6		17.9 ± 1.5
4	5		3.6 ± 0.9
5	11a		2.8 ± 0.3
6	11b		2.9 ± 0.5

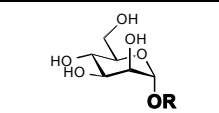
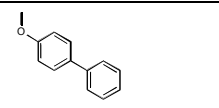
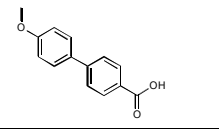
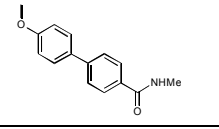
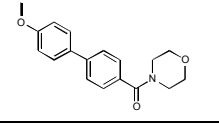
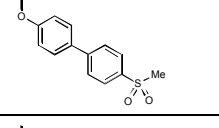
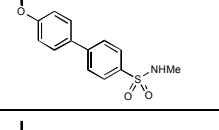
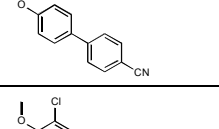
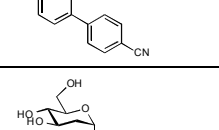
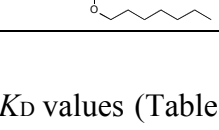
7	11c		3.0 ± 0.1
8	11d		1.7 ± 0.2
9	11e		2.7 ± 0.4
10	11f		3.7 ± 0.2
11	11g		2.0 ± 0.6
12	11h		5.7 ± 0.1
13	11i		8.4 ± 0.3
14	11j		$< 1^{\text{a}}$

^{a)} The K_D value of **11j** was approximated to be in the subnanomolar range. The IC_{50} value obtained in the competitive FP assay was equal to the lowest value that can be resolved by the assay, indicating stoichiometric titration of **11j** due to its high affinity. Consequently, its K_D must be below the K_D of competitor **22**.

Isothermal Titration Calorimetry (ITC). To further confirm our hypothesis regarding π - π stacking and desolvation, we performed ITC experiments with unsubstituted biphenyl mannoside **10**, the carboxylic acid **6**, and the bioisosteres **11b-e, g** and **j** (Table 2). ITC allows the simultaneous determination of the stoichiometry (N), the change in enthalpy (ΔH) and the dissociation constant (K_D) for ligand-protein binding.^{43,44} The reliable determination of these three parameters requires well-defined sigmoidal titration curves characterized by the dimensionless Wiseman parameter c ($c = Mt(0) K_D^{-1}$, where $Mt(0)$ is the initial macromolecule concentration).⁴⁵ To be sure that data can be fitted with confidence, the c -value should be between 1 and 1,000 (ideally between 5 and 500),⁴⁶ which could be achieved for the antagonists **6** and **10**. For titrations involving low micromolar $Mt(0)$ and interactions in the low nanomolar or picomolar range, as suggested for the bioisosteres **11b-j**, c -values

above 1,000 were expected. Since these conditions lead to steep titration curves that do not allow the determination of the curve slope representing $1/K_D$, we applied an alternative, competitive format referred to as displacement assay.^{47,48} First, FimH-CRD-Th-His₆ was pre-incubated with the low affinity antagonist *n*-heptyl 2-deoxy- α -D-mannopyranoside (**24**, for synthesis see supporting information). The high-affinity bioisosteres of interest were titrated into the protein-ligand complex giving well-defined sigmoidal titration curves.

Table 2. Thermodynamic parameters from ITC for selected FimH-antagonists binding to FimH-CRD-Th-His₆; n, stoichiometric correction factor; CI, confidence interval from fitting.

Entry	Compd		K_D [nM] (95 % CI)	ΔG [kJ/mol]	ΔH [kJ/mol] (95 % CI)	$-T\Delta S$ [kJ/mol]	n	Type of measurement
1	10		17.7 (14.1 – 22.3)	-44.2	-45.0 (-44.5 – -45.6)	0.8	1.07	direct
2	6		15.0 (13.4 – 16.7)	-44.7	-48.7 (-48.4 – -49.0)	4.0	1.05	direct
3	11b		4.3 (3.2 – 5.6)	-47.8	-54.5 (-54.1 – -54.9)	6.7	1.02	competitive vs. 24
4	11c		5.0 (3.8 – 6.6)	-47.4	-54.5 (-54.1 – -54.8)	7.1	0.97	competitive vs. 24
5	11d		3.0 (2.1 – 4.2)	-48.7	-52.3 (-51.5 – -53.1)	3.6	0.99	competitive vs. 24
6	11e		3.5 (2.9 – 4.3)	-48.2	-52.2 (-51.6 – -52.8)	3.9	1.06	competitive vs. 24
7	11g		2.8 (2.3 – 3.3)	-48.8	-58.2 (-57.8 – -58.6)	9.4	1.00	competitive vs. 24
8	11j		1.3 (1.1 – 1.6)	-50.7	-60.9 (-60.4 – -61.4)	10.1	1.01	competitive vs. 24
9	24		9'386 (8'555 – 10'287)	-28.7	-19.5 (-19.1 – -20.0)	-9.1	1.00	direct

The resulting K_D values (Table 2) correspond well with the data obtained from the FP assay (Table 1). A comparison of the thermodynamic fingerprints of antagonists **10** and **6** reveals

that the more favorable enthalpic contribution resulting from facilitated π - π stacking leads to a net enthalpy gain ($\Delta\Delta H$: -3.7 kJ/mol). However, an even greater increase in enthalpy is likely countered by the enthalpy costs for desolvation of the electron withdrawing carboxylate.

The gain in enthalpy is in turn compensated by an unfavorable entropy ($-T\Delta\Delta S$: 3.2 kJ/mol) as a result of the reduced flexibility of both the antagonist and the Tyr48 side-chain caused by the improved interaction. This is not entirely outweighed by the beneficial entropy contribution related to the partial desolvation of the carboxylate and the related release of water into the bulk. Added together, the enthalpy and entropy contributions of antagonists **10** and **6** result in similar affinities (K_D : 17.7 and 15.0 nM, respectively).

In contrast, the replacement of the carboxylate group by various neutral bioisosteres (entries 3-6) reduces the enthalpy costs for desolvation (see calculated free energies of desolvation, experimental part) and therefore leads to a markedly improved enthalpy ($\Delta\Delta H$: -3.5 to -5.8 kJ/mol). As a result, an up to fivefold improvement of the K_D values was achieved. Finally, with a cyano substituent (entries 7 & 8), the enthalpy term was further improved ($\Delta\Delta H$: -3.7 kJ/mol) due to a reduced desolvation penalty and improved π - π stacking interactions. However, this beneficial component is again partially compensated by a decrease in entropy. This can be attributed, first, to the loss of flexibility of the tightly bound ligand (Figure 4B) and, second, to the smaller surface area of the cyano substituent compared to amide, sulfonamide and sulfone, which results in a smaller number of water molecules being released to bulk upon binding.

X-ray Crystallography. To determine the binding poses of the bioisosteres, we co-crystallized the compounds **11e** or **11j** with FimH-CRD (Figure 4). Atomic resolution crystal structures were obtained at 1.07 Å (**11e**) and 1.10 Å (**11j**). As observed in previous mannoside co-crystal structures,^{15,18,27} the mannose moiety forms an extensive hydrogen bond network to the well-defined binding site with all of its hydroxyl groups. The biphenyl aglycone is located between the tyrosine gate residues (Tyr48/Tyr137). The π - π stacking of the second aromatic ring of the aglycone to the side chain of Tyr48 contributes most to the interaction energy of the aglycone moiety. Interactions to the Tyr137 side-chain on the other hand are only limited. Whereas a previously published crystal structure of a biphenyl mannoside in complex with FimH-CRD suffers from crystal contacts of binding site residues (Tyr48 side-chain to backbone oxygen of Val27) possibly causing the distortion of the

binding site,¹⁸ the binding site of our structures are mostly solvent exposed. This revealed the flexibility of the aglycone in the FimH-CRD/**11e** structure, since the electron density towards the solvent-exposed sulfonamide indicates that there is not one single orientation. Therefore, the aglycone was modeled in two distinct poses. In contrast, in the FimH-CRD/**11j** structure the amino acid side chain of Y48 can be modeled in two distinct rotamers, suggesting flexibility also of the receptor.

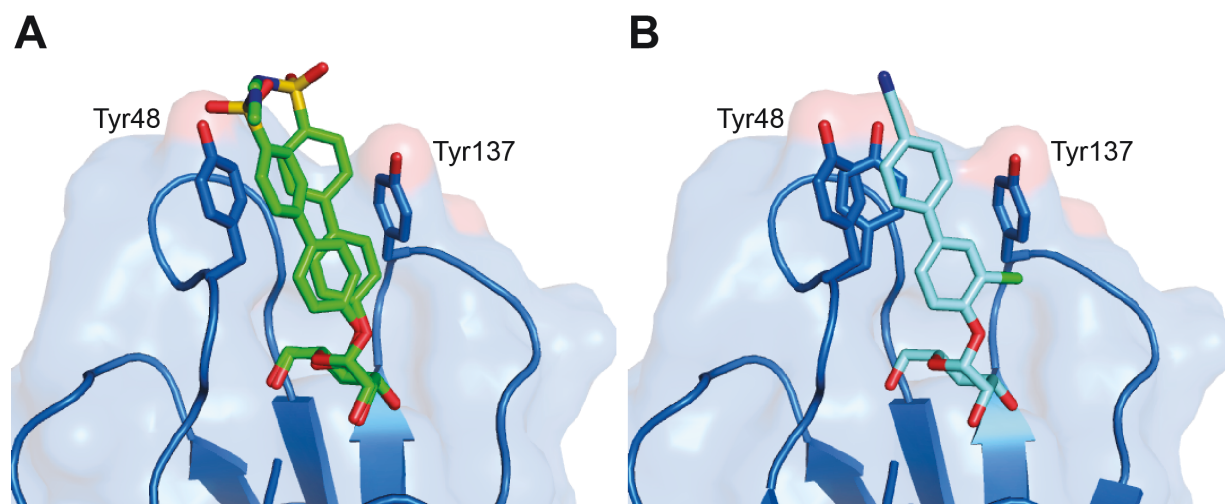


Figure 4. Ligand binding poses determined by X-ray co-crystallization with compounds **11e** resolved to 1.07 Å (A) and **11j** resolved to 1.10 Å (B). The electron density surrounding the aglycone of **11e** indicates flexibility of the aglycone and was modeled in two poses. Both compounds bind in a similar pose with a well-defined hydrogen network surrounding the mannose moiety and π - π stacking interactions between the second aromatic ring and Tyr48 side-chain (A). In contrast, in the FimH-CRD/**11j** structure the amino acid side chain of Y48 can be modeled in two distinct rotamers, suggesting flexibility also of the receptor (B).

Physicochemical Properties and *In Vitro* Pharmacokinetics. Intestinal absorption and renal excretion are prerequisites for a successful oral treatment of UTI with FimH antagonists. Furthermore, reabsorption of antagonist from the renal ultrafiltrate is desirable for maintaining the minimal anti-adhesive concentration in the target organ, namely the bladder, over an extended period of time. To estimate the influence of the bioisostere approach on oral bioavailability and the rate of renal excretion, we determined lipophilicity by means of the octanol-water distribution coefficient ($\log D_{7.4}$),⁴⁹ aqueous solubility, and membrane permeability in the artificial membrane permeability assay (PAMPA)⁵⁰ and the colorectal adenocarcinoma (Caco-2) cell monolayer model.⁵¹

Table 3. Physicochemical and *in vitro* pharmacokinetic parameters.

Compd	pK _a ^{a)}	log D _{7.4} ^{b)}	Solubility [μg/mL] / pH ^{c)}	PAMPA log P _e [cm/s] / pH ^{d)}	Caco-2 P _{app} [10 ⁻⁶ cm/s] ^{e)}		PPB f _b [%] ^{f)}	Metabolic stability t _{1/2} [min] ^{g)}
					a→b	b→a		
1	---	1.65	> 3000	-4.89	7.0 ± 0.6	9.4 ± 0.2	81	13
10	---	2.1 ± 0.1	21 ± 1 / 7.4	-4.7 ± 0.1 / 7.4	10.0 ± 0.9	19.0 ± 1.2	93 ± 1	n.d.
5	---	2.14	33.8 / 6.51	-4.7	4.23	n.d.	93	1.0
6	3.88	< -1.5	> 3000 / 6.61	no permeation	n.d.	n.d.	73	> 60
11a	---	0.5 ± 0.1	12 ± 1 / 7.4	-6.8 ± 0.3 / 7.4	0.12 ± 0.01	0.61 ± 0.03	n.d.	n.d.
11b	---	0.8 ± 0.0	122 ± 13 / 7.4	-9.2 ± 1.4 / 7.4	1.10 ± 0.82	0.87 ± 0.15	n.d.	n.d.
11c	---	0.2 ± 0.1	> 250 / 7.4	-7.8 ± 0.3 / 7.4	0.18 ± 0.07	1.30 ± 0.03	48 ± 2	> 60
11d	---	0.4 ± 0.0	246 ± 17 / 7.4	-7.2 ± 0.0 / 7.4	0.36 ± 0.01	1.76 ± 0.12	99 ± 1	> 60
11e	---	0.7 ± 0.1	> 250 / 7.4	-8.6 ± 0.2 / 7.4	0.28 ± 0.23	1.82 ± 0.14	> 99	> 60
11f	6.5	1.1 ± 0.0	> 150 / 3.0 > 150 / 7.4	-7.7 ± 0.8 / 5.0 -8.8 ± 0.1 / 7.4	0.40 ± 0.02	1.90 ± 0.17	n.d.	n.d.
11g	---	1.4 ± 0.0	186 ± 4 / 7.6	-5.7 ± 0.0 / 7.4	2.0 ± 0.1	13.2 ± 2.1	99 ± 0	> 60
11h	3.7	-1.4 ± 0.1	11 ± 0 / 3.0 273 ± 2 / 7.4	-9.3 ± 1.4 / 5.0 -8.8 ± 1.4 / 7.4	0.17 ± 0.00	0.22 ± 0.01	n.d.	n.d.
11i	2.5	-1.1 ± 0.1	> 150 / 3.0 > 150 / 7.4	-6.8 ± 0.2 / 5.0 -7.0 ± 0.1 / 7.4	0.22 ± 0.14	0.29 ± 0.03	n.d.	n.d.
11j	---	2.1 ± 0.0	192 ± 5 / 7.4	-5.2 ± 0.0 / 7.4	2.2 ± 0.4	22.1 ± 1.5	89 ± 1	> 60

a) pK_a values were determined by NMR spectroscopy; b) Octanol-water distribution coefficients (log D_{7.4}) were determined by a miniaturized shake-flask procedure at pH 7.4, values represent the mean ± SD of sextuplicate measurements;⁴⁹ c) Kinetic solubility was measured in a 96-well format using the μSOL Explorer solubility analyzer at the indicated pH in triplicate; d) P_e = effective permeability: passive permeation through an artificial membrane was determined by the parallel artificial membrane permeation assay (PAMPA), values represent the mean ± SD of quadruplicate measurements performed at the indicated pH;⁵⁰ e) P_{app} = apparent permeability: permeation through a Caco-2 cell monolayer was assessed in the absorptive (a→b) and secretory (b→a) directions in triplicate;⁵¹ f) Plasma protein binding (PPB) was determined by equilibrium dialysis in triplicate;⁵² g) Metabolic stability was determined by incubating the compounds (2 μM) with pooled rat liver microsomes (RLM, 0.5 mg/mL) in presence of NADPH (1 mM, compounds **1**, **6**, **11c-e**, **g**, **j**) or without NADPH (compound **5**);⁵³ n.d. = not determined.

Oral Bioavailability. Oral bioavailability relies on compound dissolution in the gastrointestinal fluids, permeation through the membranes lining the intestine, and stability against first pass metabolism.^{54,55} In turn, permeability and potency define the minimum aqueous solubility required for an orally dosed compound.⁵⁶ For our FimH antagonist, we therefore aimed to exceed the solubility limit of 50 μg/mL in order to achieve substantial absorption through the intestinal mucosa. Sufficient aqueous solubility was reported for *n*-heptyl α-mannopyranoside (**1**).¹⁹ The unsubstituted biphenyl α-D-mannopyranoside **10** as

well as the antagonists bearing a methylcarboxylate, carboxamide, or tetrazole substituent in its unionized state (compounds **5**, **11a** and **11h**) were found to be scarcely soluble due to the apolar and planar character of the aglycone.^{24,57} By contrast, the polar carboxylic acid moiety present in antagonist **6** or the substituents in the bioisosteres **11b-j** enhanced the observed solubility beyond the limit of 50 µg/mL. Permeability data derived from PAMPA⁵⁸ and the Caco-2 model⁵⁹ suggest high permeation of the moderately lipophilic antagonists **1**, **10**, and **5** ($\log D_{7.4} > 1.6$) through the intestinal membranes. The bioisosteres **11a-f**, **h**, **i**, although slightly more permeable than the strongly hydrophilic carboxylic acid derivative **6**, show only moderate values of permeability compared to *n*-heptyl α -mannopyranoside (**1**) or the unsubstituted biphenyl mannoside **10**. However, the *para*-cyanobiphenyl derivatives **11g** and **11j** display elevated $\log D_{7.4}$ and effective permeability ($\log P_e$) in the range for successful intestinal absorption. Featuring both high aqueous solubility and elevated membrane permeability, the *para*-cyano substituted bioisosteres **11g** and **11j** are thus the most promising candidates for oral absorption. Moreover, combining the bioisosteric replacement with the addition of a chloro substituent in the *ortho*-position of the aromatic ring adjacent to the anomeric oxygen (\rightarrow **11j**)²⁴ resulted in the most advantageous physicochemical profile for oral bioavailability.

Renal Excretion. The rate of renal excretion depends on the rate of glomerular filtration and the propensity to tubular secretion and reabsorption of an antagonist.⁶⁰ Only the fraction that is not bound to plasma proteins is expected to enter the glomerular filtrate.⁶¹ Plasma protein binding (PPB) data indicating the fraction bound (f_b) are listed in Table 2.⁵² The biphenyls **6** and **11c** were identified as moderate binders to plasma proteins ($f_b \leq 65\%$), which suggests a low impact of PPB on antagonist filtration. The f_b values of the antagonists **1**, **10**, **5**, and **11j** were between 80 and 93%, whereas the bioisosteres **11d**, **e**, and **g** showed particularly high protein binding ($f_b \geq 99\%$) implying slow compound entry into the primary urine. However, the kinetic aspects of PPB, that is, association and dissociation rate constants, remain to be determined to quantify precisely the influence of PPB on filtration.⁶²

Furthermore, $\log D_{7.4}$ was identified as key determinant of tubular reabsorption.⁶³⁻⁶⁵ Accordingly, lipophilic compounds are predominantly reabsorbed from the renal filtrate. Given that renal clearance is the major route of elimination, this will result in a slow but steady excretion into the bladder. In contrast, hydrophilic compounds are poorly reabsorbed and thus quickly renally eliminated, which leads to high initial compound levels in the urine

but narrows the time range where the minimal anti-adhesive concentration is maintained. Consequently, low $\log D_{7.4}$ as shown for the antagonists **6**, **11h**, and **11i** implies low tubular reabsorption and rapid elimination of the filtered molecules by the urine. Otherwise, $\log D_{7.4}$ between 0.2 and 0.7, such as determined for the bioisosteres **11a-e**, suggests increasing propensity to tubular reuptake, whereas $\log D_{7.4} > 1$ as shown for heptyl mannoside **1** and the biphenyl mannosides **10**, **5**, **11g**, **11f**, and **11j** is optimal for tubular reabsorption from the glomerular filtrate and thus for slow renal clearance.

Metabolic Stability. Increasing lipophilicity is usually paralleled by increasing susceptibility to metabolism.⁶⁶ Liabilities towards metabolic clearance pathways which prevent the intact antagonist from reaching the target in the bladder were therefore of interest. To assess their propensity to cytochrome P450 (CYP450)-mediated metabolism, heptyl mannoside **1**, the carboxylic acid derivative **6**, and the bioisosteres **11c-e**, **g**, **j** were incubated with rat liver microsomes (RLM, 0.5 mg/mL) in presence of the cofactor β -nicotinamide adenine dinucleotide phosphate (NADPH).⁵³ To confirm the high propensity of the methyl ester present in antagonist **5** to carboxylesterase (CES)-mediated hydrolysis, this antagonist was incubated with RLM only. The profiles of unchanged compound versus time revealed high susceptibility of heptyl mannoside **1** to CYP450-mediated metabolism ($t_{1/2} = 13$ min) and rapid hydrolysis of the ester **5** by the hepatic CES ($t_{1/2} = 1.0$ min). Otherwise, the bioisosteres **11c-e,g & j** were stable against enzyme-mediated bioconversion ($t_{1/2} > 60$ min) suggesting lower propensity to metabolic, non-renal elimination pathways.

Considering PPB, lipophilicity, and metabolic stability data, we therefore expected (i) a steady release of compounds **11d**, **e**, **g**, **j** into the bladder because of high PPB decelerating glomerular filtration (**11d**, **e**, **g**) and/or high $\log D_{7.4}$ supporting tubular reabsorption (**11g**, **j**), (ii) a fast excretion of antagonist **6** and **11c** via the urine due to low PPB and low $\log D_{7.4}$, and (iii) a rapid clearance of heptyl mannoside **1** from the body by renal and metabolic pathways. Compounds featuring high propensity to renal excretion as major route of elimination (**11c**, **11e** and **11j**) were selected for *in vivo* PK studies in a mouse model.

Pharmacokinetic Studies in C3H/HeN Mice. This first part of our study explored the predicted effects of lipophilicity, PPB, and metabolic stability on antagonist disposition and elimination upon a single dose iv application (50 mg/kg) of compounds **11c** and **11e**. The PK parameters of these applications and those of the previously published carboxylate **6** are

summarized in Table 4. The Table also contains the results of the iv administration of compound **11j** (0.625 mg/kg).

Table 4. Pharmacokinetic parameters determined after a single iv application of compounds **6a**, **11c**, **11e** and **11j** in female C3H/HeN mice. Values were calculated using PKSolver.⁶⁷ C_0 , initial concentration; V_z , volume of distribution in terminal phase; AUC, Area under the curve; CL_{tot} , total clearance; C_{max} , maximal concentration.

Compd	Plasma						Urine
	C_0 ($\mu\text{g/mL}$)	Dose (mg/kg)	V_z (mL)	$t_{1/2}$ (h)	AUC_{0-inf} ($\mu\text{g} \times \text{h/mL}$)	CL_{tot} (mL/h)	C_{max} ($\mu\text{g/mL}$)
6 ¹⁹	40	50	25.2	0.33	23.5	53.1	300
11c	109.7	50	28.3	0.4	25.3	49.4	4611
11e	151.6	50	19.5	1.9	175.1	7.1	387
11j	0.36	0.625	52.8	0.17	0.07	218	10

In contrast to the fast plasma clearance of antagonists **6** and **11c** (Figure 5A), the methyl sulfonamide bioisostere **11e** attained higher initial concentration in plasma (C_0) and lower total clearance (CL_{tot}). Therefore, it could be detected until six hours post application, resulting in markedly higher plasma AUC. The observed high C_0 of compound **11e** may be attributed to a small volume of distribution (V_z) resulting from the high PPB ($f_b \geq 99\%$).⁶¹ In urine (Figure 5B), the carboxylic acid **6** and the morpholinomethanone **11c** displayed high levels immediately following administration and a rapid concentration decrease within the first two hours, reflecting the rapid elimination from plasma. Fast renal excretion as major route of elimination can be rationalized by the physicochemical properties of the antagonists **6** and **11c**, that is, moderate PPB and $\log D_{7.4}$, as well as high metabolic stability. Otherwise, the methyl sulfonamide bioisostere **11e** showed sustained compound levels in urine over a period of two hours and subsequent slow decrease until six hours post administration. This sustained renal excretion is a result of the interplay of the antagonist's elevated PPB and $\log D_{7.4}$.

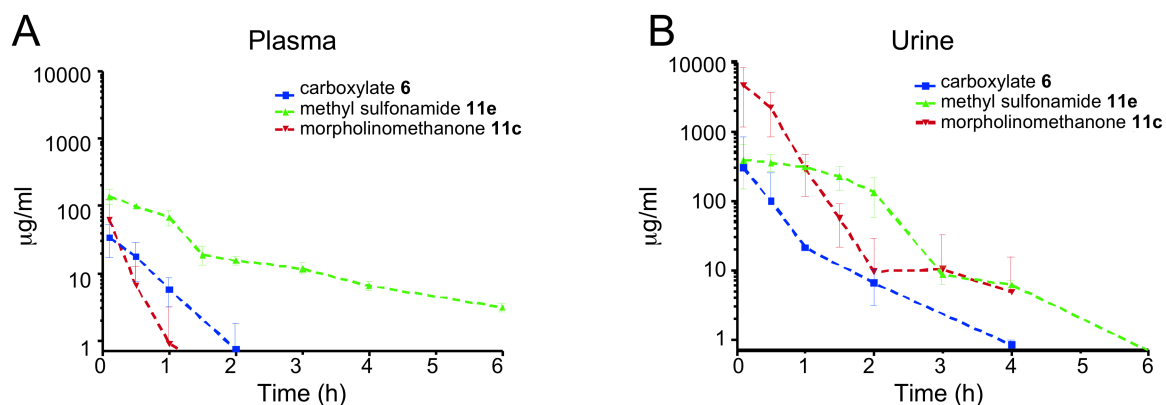


Figure 5. Antagonist concentrations in (A) plasma and (B) urine after a single iv application of **6**, **11c**, and **11e** (50 mg/kg).

In a second study, the *para*-cyano bioisostere **11j**, characterized by a high oral absorption potential, but low solubility, was administered as a single dose iv (0.625 mg/kg) and po (1.25 mg/kg). The plasma concentration curve upon iv dosing displays a steep decline within the first hour post application, while the po curve shows a prolonged period where absorption and elimination are in equilibrium (Figure 6A). The urine concentration profiles (Figure 6B) parallel the plasma curves obtained by the two modes of application, i.e. high plasma clearance upon iv bolus injection led to high initial antagonist levels in urine and a rapid concentration decline. By contrast, sustained plasma concentrations upon po administration resulted in prolonged urine levels. As a result, urine concentrations exceed the minimum level required for the anti-adhesive effect (minimal anti-adhesion concentration, MAC_{90}),²³ determined by flow cytometry⁶⁸ (0.094 $\mu\text{g/ml}$), for more than eight hours upon oral single-dose administration, proving the high potential of the *para*-cyano biphenyl mannoside for the oral treatment of UTI (Figure 6B).

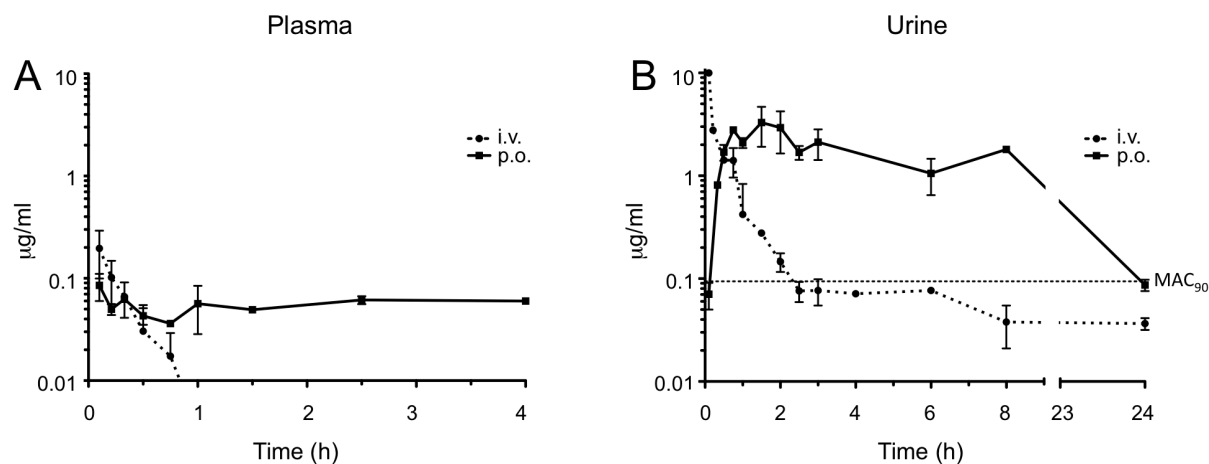


Figure 6. Antagonist concentrations in (A) plasma and (B) urine after a single iv and po application of compound **11j** (iv: 0.625 mg/kg; po: 1.25 mg/kg). MAC₉₀, minimal anti-adhesive concentration to inhibit 90% adhesion (0.094 µg/ml).

Infection study in C3H/HeN Mice. Based on the promising PK profile of **11j**, six mice were inoculated with UTI89 following an oral application of **11j** (1.25 mg/kg) 40 min prior to infection. Three hours after inoculation, animals were sacrificed and bladder and kidneys were removed. Organs were homogenized and analysed for bacterial counts. The results were compared to ciprofloxacin (CIP), used as standard antibiotic therapy against UTI89.⁶⁹ The median reduction in bacterial counts of the mice treated with **11j** and CIP compared to the control group are displayed in Figure 7.

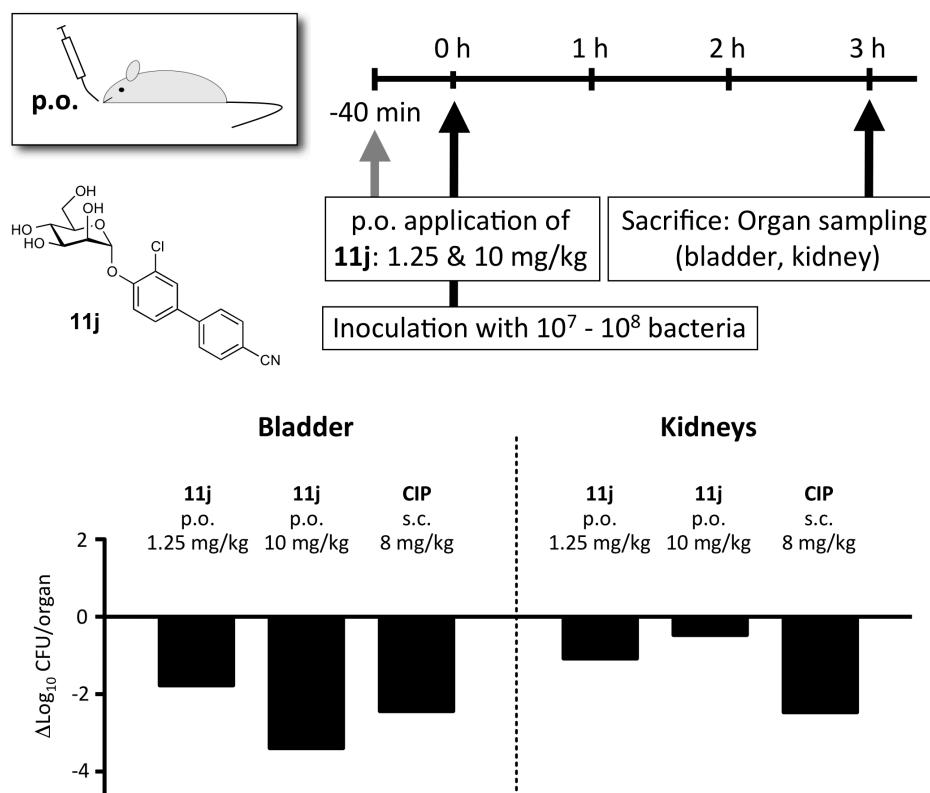


Figure 7. Treatment efficacy in the UTI mouse model 3 h after infection. The bars depict the median reduction of bacterial counts after application of 1.25 or 10 mg/kg **11j** p.o. or 8 mg/kg CIP s.c. (representing the murine dose equivalent to a human standard dose).⁷⁰ The baseline represents the median counts of the untreated control group.

The median value in the untreated control group showed bacterial counts of 6.6 Log_{10} colony forming units (CFU) in the bladder and 6 Log_{10} CFU in the kidneys. After oral application of 1.25 mg/kg of **11j**, bacterial loads in the bladder decreased by 1.7 Log_{10} CFU and 1.08 Log_{10} CFU in the kidneys. The lower reduction in the kidneys is most likely due to the differing adhesion mechanisms between bladder and kidneys (type 1 pili vs P-pili), which is not targeted by **11j**.⁷¹ With CIP (8 mg/kg s.c.) a substantial reduction in both, bladder and kidneys (median reductions of 2.44 Log_{10} and 2.47 Log_{10} , respectively) was observed. Despite the low oral dose of **11j**, the approximately 100-fold reduction of CFU in the bladder promised an even higher effect upon dose increase. To increase solubility of **11j**, a basic formulation was used. When 10 mg/kg were applied, bacterial loads in the bladder decreased by 3.4 Log_{10} CFU/ml, exceeding the effect of CIP, but only 0.5 Log_{10} CFU in the kidneys. Based on this large reduction after an oral application of 10 mg/kg, **11j** has a large potential for further development.

SUMMARY AND CONCLUSION

Recently, numerous monovalent alkyl and aryl α -D-mannopyranosides have been described as potent *FimH* antagonists. However, most of them suffer from insufficient pharmacokinetic properties, i.e. modest bioavailability and short duration of the therapeutic effect in the bladder, their site of action. As a consequence, high doses at short intervals are required to achieve anti-adhesive effects over an extended period of time. Therefore, the goal of the present study was an appropriate optimization of the pharmacokinetic profile of biphenyl α -D-mannopyranosides while keeping their high affinity to the CRD of *FimH*. The starting point was the biphenyl-carboxylate **6** where the critical carboxylate was replaced by bioisosteres.^{29,72}

With a series of bioisosteres a three- to fivefold improvement of affinity was achieved compared to **6**. Although binding necessitates only partial desolvation of the carboxylate and its bioisosteric replacements, a reduction of the enthalpy penalty for desolvation⁴¹ was identified as the source of the improved affinity exhibited by the bioisosteres. Thermodynamic evaluation of antagonists **11b-e** revealed almost identical enthalpy contribution to binding. However, for antagonists with the *para*-cyano substituent (**11g** & **11j**) an enhancement of up to -8.7 kJ/mol was observed, indicating a reduced desolvation penalty and an improved stacking as derived from the crystal structure of **11j** co-crystallized with the CRD of *FimH* (Figure 4B). On the other hand, higher affinity originating from a reduction of conformational flexibility of ligand and protein resulted in a concomitant entropy penalty of up to 6.5 kJ/mol.

In addition to the improved pharmacodynamics, the relevant pharmacokinetic parameters (solubility, permeability, renal excretion) could also be substantially improved. With 3'-chloro-4'-(α -D-mannopyranosyloxy)-biphenyl-4-carbonitrile (**11j**), a *FimH* antagonist with an optimal *in vitro* PK/PD profile was identified. The *para*-cyano substituent conferred lipophilicity and high binding to plasma proteins, which slowed down the rate of renal excretion. Despite higher lipophilicity, antagonist **11j** was unsusceptible to CYP450 mediated metabolism, and therefore predominantly eliminated via the renal pathway. *In vivo* experiments confirmed the excellent PK-profile of **11j** with steady renal excretion for more than eight hours after oral application, suggesting a long-lasting anti-adhesive effect. Finally, orally applied **11j** (10 mg/kg) was effective in a mouse model of UTI by reducing the bacterial load in the bladder by over 1000-fold. Improvement of solubility, enabling the

application of higher dosages of **11j**, will possibly lead to an even higher bacterial reductions, which will be the subject of future investigations.

EXPERIMENTAL SECTION

Synthesis

The synthesis of compounds **11a-f**, **11i**, **14a-f**, **16**, **19**, and **24**, including compound characterization data, can be found in the Supporting Information.

General methods. NMR spectra were recorded on a Bruker Avance DMX-500 (500.1 MHz) spectrometer. Assignment of ^1H and ^{13}C NMR spectra was achieved using 2D methods (COSY, HSQC, HMBC). Chemical shifts are expressed in ppm using residual CHCl_3 , CHD_2OD or HDO as references. Optical rotations were measured using Perkin-Elmer Polarimeter 341. Electron spray ionization mass spectra (ESI-MS) were obtained on a Waters micromass ZQ. The LC/HRMS analysis were carried out using a Agilent 1100 LC equipped with a photodiode array detector and a Micromass QTOF I equipped with a 4 GHz digital-time converter. Microwave-assisted reactions were carried out with a CEM Discover and Explorer. Reactions were monitored by TLC using glass plates coated with silica gel 60 F₂₅₄ (Merck) and visualized by using UV light and/or by charring with a molybdate solution (a 0.02 M solution of ammonium cerium sulfate dihydrate and ammonium molybdate tetrahydrate in aqueous 10% H_2SO_4). MPLC separations were carried out on a CombiFlash Companion or Rf (Teledyne Isco) equipped with RediSep normal-phase or RP-18 reversed-phase flash columns. LC-MS separations were done on a Waters system equipped with sample manager 2767, pump 2525, PDA 2525 and micromass ZQ. All compounds used for biological assays are at least of 95% purity based on HPLC analytical results. Commercially available reagents were purchased from Fluka, Aldrich, Alfa Aesar or abcr GmbH & Co. KG (Germany). Solvents were purchased from Sigma-Aldrich or Acros and were dried prior to use where indicated. Methanol (MeOH) was dried by refluxing with sodium methoxide and distilled immediately before use. Dimethoxyethane (DME) was dried by filtration over Al_2O_3 (Fluka, type 5016 A basic).

4'-(2,3,4,6-Tetra-O-acetyl- α -D-mannopyranosyloxy)-biphenyl-4-carbonitrile (14g). A Schlenk tube was charged with aryl iodide **12**²⁴ (330 mg, 0.60 mmol), 4-cyanophenylboronic acid (**13g**, 96 mg, 0.65 mmol), $\text{Pd}(\text{dppf})\text{Cl}_2 \cdot \text{CH}_2\text{Cl}_2$ (15 mg, 0.018 mmol), K_3PO_4 (192 mg,

0.90 mmol) and a stirring bar. The tube was closed with a rubber septum and was evacuated and flushed with argon. This procedure was repeated once, and then anhydrous DMF (2 mL) was added under a stream of argon. The mixture was degassed in an ultrasonic bath and flushed with argon for 5 min, and then stirred at 80 °C overnight. The reaction mixture was cooled to rt, diluted with EtOAc (50 mL), and washed with water (50 mL) and brine (50 mL). The organic layer was dried over Na₂SO₄ and concentrated *in vacuo*. The residue was purified by MPLC on silica gel (petroleum ether/EtOAc) to afford **14g** (187 mg, 59%) as colorless oil. $[\alpha]_D^{20} +72.9$ (*c* 0.8, MeOH); ¹H NMR (500 MHz, CD₃OD): $\delta = 7.73-7.71$ (m, 2H, Ar-H), 7.65-7.64 (m, 2H, Ar-H), 7.57-7.53 (m, 2H, Ar-H), 7.21-7.19 (m, 2H, Ar-H), 5.60-5.57 (m, 2H, H-1, H-3), 5.47 (dd, *J* = 1.9, 3.4 Hz, 1H, H-2), 5.40 (t, *J* = 10.1 Hz, 1H, H-4), 4.30 (dd, *J* = 5.1, 12.2 Hz, 1H, H-6a), 4.14-4.08 (m, 2H, H-6b, H-5), 2.22, 2.07, 2.06, 2.04 (4 s, 12H, 4 COCH₃); ¹³C NMR (126 MHz, CD₃OD): $\delta = 170.62, 170.14, 170.11, 169.83$ (4 CO), 156.16, 144.87, 134.05, 132.77, 128.64, 127.46 (Ar-C), 119.05 (CN), 117.15, 110.77 (Ar-C), 95.86 (C-1), 69.42 (2C, C-2, C-5), 68.90 (C-3), 65.94 (C-4), 62.16 (C-6), 21.01, 20.84, 20.82 (4C, 4 COCH₃); ESI-MS: *m/z*: Calcd for C₂₇H₂₇NNaO₁₀ [M+Na]⁺: 548.2, found: 548.2.

4'-(α -D-Mannopyranosyloxy)-biphenyl-4-carbonitrile (11g). To a solution of **14g** (40 mg, 0.08 mmol) in dry MeOH (5 mL) was added freshly prepared 1 M NaOMe/MeOH (0.1 eq) under argon. The mixture was stirred at rt until the reaction was complete (monitored by TLC), then neutralized with Amberlyst-15 (H⁺) ion-exchange resin, filtered and concentrated *in vacuo*. The residue was purified by MPLC on silica gel (DCM/MeOH, 10:1-7:1) to afford **11g** (16 mg, 60%) as white solid. ¹H NMR (500 MHz, CD₃OD): $\delta = 7.82-7.75$ (m, 4H, Ar-H), 7.69-7.63 (m, 2H, Ar-H), 7.30-7.23 (m, 2H, Ar-H), 5.58 (d, *J* = 1.7 Hz, 1H, H-1), 4.05 (dd, *J* = 1.8, 3.4 Hz, 1H, H-2), 3.94 (dd, *J* = 3.4, 9.5 Hz, 1H, H-3), 3.83-3.71 (m, 3H, H-4, H-6a, H-6b), 3.62 (ddd, *J* = 2.5, 5.3, 9.8 Hz, 1H, H-5). The spectroscopic data were in accordance with literature values.¹⁸

5-(4'-(2,3,4,6-Tetra-*O*-acetyl- α -D-mannopyranosyloxy)-biphenyl-4-yl)-1*H*-tetrazole (15). A Schlenk tube was charged with **14g** (30 mg, 0.06 mmol), trimethylsilyl azide (16 μ L, 0.12 mmol), dibutyltin oxide (2 mg, 0.006 mmol), DME (1 mL) and a stirring bar. The mixture was heated to 150 °C for 10 min by microwave irradiation. The reaction mixture was cooled to rt, and then concentrated *in vacuo*. The residue was purified by MPLC on silica gel (DCM/MeOH, 9:1-8:1) to afford **15** (26 mg, 81%) as colorless oil. $[\alpha]_D^{20} +56.1$ (*c* 0.3,

MeOH); ^1H NMR (500 MHz, CDCl_3): δ = 8.25-8.15 (m, 2H, Ar-H), 7.75-7.65 (m, 2H, Ar-H), 7.60-7.55 (m, 2H, Ar-H), 7.20-7.17 (m, 2H, Ar-H), 5.64-5.55 (m, 2H, H-1, H-3), 5.49 (dd, J = 1.7, 3.3 Hz, 1H, H-2), 5.40 (t, J = 10.1 Hz, 1H, H-4), 4.31 (dd, J = 5.3, 12.4 Hz, 1H, H-6a), 4.17-4.06 (m, 2H, H-5, H-6b), 2.22, 2.07, 2.06, 2.05 (4 s, 12H, 4 COCH_3); ^{13}C NMR (126 MHz, CDCl_3): δ = 170.67, 170.14, 170.11, 169.81 (4 CO), 155.61, 128.36, 127.84, 127.49, 116.93 (Ar-C), 95.78 (C-1), 69.36 (C-5), 69.26 (C-2), 68.90 (C-3), 65.89 (C-4), 62.12 (C-6), 20.92, 20.76, 20.73 (4 COCH_3); ESI-MS: m/z : Calcd for $\text{C}_{27}\text{H}_{28}\text{N}_4\text{NaO}_{10}$ $[\text{M}+\text{Na}]^+$: 591.2, found: 591.1.

5-(4'-(α -D-Mannopyranosyloxy)-biphenyl-4-yl)-1H-tetrazole (11h). Prepared according to the procedure described for **11g** from **15** (26 mg, 0.03 mmol). Yield: 18 mg (quant.) as a white solid. $[\alpha]_{\text{D}}^{20}$ +112.1 (c 0.1, MeOH/ H_2O , 2:1); ^1H NMR (500 MHz, CD_3OD): δ = 7.98-7.96 (m, 2H, Ar-H), 7.72-7.71 (m, 2H, Ar-H), 7.58-7.54 (m, 2H, Ar-H), 7.16-7.13 (m, 2H, Ar-H), 5.46 (d, J = 1.7 Hz, 1H, H-1), 3.94 (dd, J = 1.9, 3.5 Hz, 1H, H-2), 3.83 (dd, J = 3.4, 9.5 Hz, 1H, H-3), 3.68-3.61 (m, 3H, H-4, H-6a, H-6b), 3.52 (ddd, J = 2.5, 5.4, 9.7 Hz, 1H, H-5); ^{13}C NMR (126 MHz, CD_3OD): δ = 158.19, 145.07, 134.97, 129.29, 128.74, 128.55, 118.26 (Ar-C), 100.13 (C-1), 75.52 (C-5), 72.42 (C-3), 71.98 (C-2), 68.33 (C-4), 62.69 (C-6); HRMS: m/z : Calcd for $\text{C}_{19}\text{H}_{21}\text{N}_4\text{O}_6$ $[\text{M}+\text{H}]^+$: 401.1456, found: 401.1450.

4'-(2,3,4,6-Tetra-*O*-acetyl- α -D-mannopyranosyloxy)-3'-chloro-biphenyl-4-carbonitrile (20). Prepared according to the procedure described for **14g** from aryl iodide **19**²³ (79 mg, 0.135 mmol), **13g** (22 mg, 0.15 mmol), $\text{Pd}(\text{dppf})\text{Cl}_2 \cdot \text{CH}_2\text{Cl}_2$ (3.3 mg, 4 μmol) and K_3PO_4 (57 mg, 0.27 mmol). Yield: 57 mg (75%) as a white solid. $[\alpha]_{\text{D}}^{20}$ +77.7 (c 0.5, CHCl_3); ^1H NMR (500 MHz, CDCl_3): δ = 7.72 (d, J = 8.3 Hz, 2H, Ar-H), 7.63 (m, 3H, Ar-H), 7.43 (dd, J = 2.2, 8.6 Hz, 1H, Ar-H), 7.27 (d, J = 8.6 Hz, 1H, Ar-H), 5.64-5.59 (m, 2H, H-1, H-2), 5.54 (dd, J = 1.9, 3.2 Hz, 1H, H-3), 5.41 (t, J = 10.1 Hz, 1H, H-4), 4.28 (dd, J = 5.2, 12.3 Hz, 1H, H-6a), 4.17 (ddd, J = 2.1, 5.1, 10.0 Hz, 1H, H-5), 4.10 (dd, J = 2.2, 12.3 Hz, 1H, H-6b), 2.21 (s, 3H, COCH_3), 2.12- 2.00 (m, 9H, 3 COCH_3); ^{13}C NMR (126 MHz, CDCl_3): δ = 170.54, 170.08, 169.90, 169.84, (4C, CO) 151.67, 143.61, 135.29, 132.87, 129.41, 127.53, 126.60, 125.20, 118.79, 117.36, 111.47 (Ar-C, CN), 96.72 (C-1), 70.00 (C-5), 69.39 (C-3), 68.82 (C-2), 65.86 (C-4), 62.16 (C-6), 20.98, 20.81, 20.79, 20.78 (4 COCH_3); ESI-MS: m/z : Calcd for $\text{C}_{27}\text{H}_{26}\text{ClNNaO}_{10}$ $[\text{M}+\text{Na}]^+$: 582.1, found: 582.1.

3'-Chloro-4'-(α -D-mannopyranosyloxy)-biphenyl-4-carbonitrile (11j). Prepared according to the procedure described for **11g** from **20** (36 mg, 0.06 mmol). Yield: 12 mg (48%) as a white solid. $[\alpha]_{\text{D}}^{20} +109.4$ (*c* 0.23, MeOH); ^1H NMR (500 MHz, CD_3OD): $\delta = 7.80$ - 7.72 (m, 5H, Ar-H), 7.59 (dd, $J = 2.2, 8.6$ Hz, 1H, Ar-H), 7.48 (d, $J = 8.7$ Hz, 1H, Ar-H), 5.62 (d, $J = 1.4$ Hz, 1H, H-1), 4.12 (dd, $J = 1.8, 3.3$ Hz, 1H, H-2), 4.00 (dd, $J = 3.4, 9.5$ Hz, 1H, H-3), 3.83 - 3.68 (m, 3H, H-4, H-6a, H-6b), 3.63 (ddd, $J = 2.3, 5.4, 9.6$ Hz, 1H, H-5); ^{13}C NMR (126 MHz, CD_3OD): $\delta = 153.65, 145.15, 135.42, 133.86, 129.82, 128.53, 127.87, 125.47, 119.70, 118.59$ (Ar-C), 111.97 (CN), 100.66 (C-1), 76.05 (C-5), 72.39 (C-3), 71.80 (C-2), 68.20 (C-4), 62.65 (C-6); IR (KBr), $\nu = 3400$ (OH), 2227 (C \equiv N), $1606, 1487$ (Ar-C=C) cm^{-1} ; HRMS: m/z : Calcd for $\text{C}_{19}\text{H}_{18}\text{ClNNaO}_6$ $[\text{M}+\text{Na}]^+$: 414.0715, found: 414.0721.

3'-Chloro-*N*-(3',6'-dihydroxy-3-oxo-3*H*-spiro[isobenzofuran-1,9'-xanthen]-5-yl)-4'-(α -D-mannopyranosyloxy)-biphenyl-4-carboxamide (21). Compound **8** (10.0 mg, 0.024 mmol), fluoresceinamine isomer I (12.7 mg, 0.037 mmol) and COMU (20.9 mg, 0.049 mmol) were dissolved in dry DMF (1 mL), then NEt_3 (10 μL , 0.073 mmol) was added and the mixture was stirred at rt for 7 h. 1 N HCl in DMF was added until acid reaction on pH paper and the mixture was concentrated. The residue was dissolved in DCM/MeOH (3:1) and loaded onto a silica gel column. The complex mixture of compounds was only partially resolved. The fractions containing the product were collected, concentrated and purified by preparative HPLC (gradient water/MeCN containing 0.2% HCO_2H), to afford compound **21** (5 mg, 19%). $[\alpha]_{\text{D}}^{20} +21.1$ (*c* 0.1, MeOH); ^1H NMR (500 MHz, CD_3OD): $\delta = 8.26$ (d, $J = 8.4$ Hz, 2H, Ar-H), 7.88 - 7.74 (m, 3H, Ar-H), 7.66 (dd, $J = 2.2, 8.6$ Hz, 1H, Ar-H), 7.51 (d, $J = 8.7$ Hz, 1H, Ar-H), 7.29 (dd, $J = 1.9, 5.3$ Hz, 2H, Ar-H), 7.19 (dd, $J = 2.1, 8.3$ Hz, 1H, Ar-H), 7.08 - 6.99 (m, 2H, Ar-H), 6.95 (d, $J = 8.7$ Hz, 1H, Ar-H), 6.72 (dd, $J = 5.5, 10.6$ Hz, 2H, Ar-H), 6.61 (dd, $J = 2.3, 8.7$ Hz, 1H, Ar-H), 5.65 (s, 1H, H-1), 4.15 (dd, $J = 1.8, 3.2$ Hz, H-2), 4.03 (dd, $J = 3.4, 9.5$ Hz, H-3), 3.87 - 3.72 (m, 3H, H-4, H-6a, H-6b), 3.65 (m, 1H, H-5); ^{13}C NMR (126 MHz, CD_3OD): $\delta = 137.50, 136.01, 131.90, 130.24, 130.20, 129.87, 129.24, 128.03, 127.91, 125.79, 125.46, 124.73, 118.99, 118.76, 118.65$ (Ar-C), 100.73 (C-1), 76.06 (C-5), 72.42 (C-3), 71.85 (C-2), 68.24 (C-4), 62.69 (C-2); ESI-MS: m/z : Calcd for $\text{C}_{39}\text{H}_{31}\text{ClNO}_{12}$ $[\text{M}+\text{H}]^+$: 740.2, found: 740.2.

3'-Chloro-*N*-(2-(3-(3',6'-dihydroxy-3-oxo-3*H*-spiro[isobenzofuran-1,9'-xanthen]-5-yl)-thioureido)ethyl)-4'-(α -D-mannopyranosyloxy)-biphenyl-4-carboxamide (22). To a stirred solution of compound **8** (25 mg, 0.061 mmol) in dry DMF (1 mL), NHS (21 mg, 0.183 mmol) was added, followed by DIC (9.2 mg, 0.073 mmol). The mixture was stirred at rt for 2 h, then *N*-Boc-ethylendiamine (10.7 mg, 0.067 mmol) was added and the reaction was stirred for 10 h. It was then cooled down to 0 °C, diluted with water and concentrated. Chromatography on silica gel (DCM/MeOH) yielded 23 mg (0.042 mmol, 68%) of *tert*-butyl (3'-chloro-4'-(α -D-mannopyranosyloxy)-biphenyl-4-yl-carboxamido)ethyl)carbamate. This product was dissolved in CH₂Cl₂ (3 mL) and TFA (1 mL) was added. The solid dissolved during addition of TFA. After 10 min the reaction was complete. The mixture was evaporated and excess TFA was removed in high vacuum. The intermediate *N*-(2-aminoethyl)-3'-chloro-4'-(α -D-mannopyranosyloxy)-biphenyl-4-carboxamide TFA salt (23 mg, 0.042 mmol, quant.) was used directly in the next step. It was dissolved in dry DMF (0.5 mL) and NEt₃ (12.8 mg, 0.127 mmol) was added. The mixture was cooled to 0 °C, then FITC (14.8 mg, 0.038 mmol) was added and the mixture was stirred for 3 h in the dark. The mixture was then co-evaporated with water, taken up in MeOH/10% aq. acetic acid and evaporated. Chromatography on silica gel (DCM/MeOH) yielded compound **22**, contaminated with triethylammonium acetate. The compound was then re-dissolved in MeOH, and 0.5 N HCl in MeOH was added. The mixture was evaporated and chromatographed on silica gel, to yield pure **22** (15 mg, 47%). $[\alpha]_D^{20} +12.1$ (*c* 0.3, MeOH); ¹H NMR (500 MHz, CD₃OD): δ = 8.12 (s, 1H), 7.92 (d, *J* = 8.3 Hz, 2H, Ar-H), 7.70 (dd, *J* = 5.0, 13.1 Hz, 2H, Ar-H), 7.64 (d, *J* = 8.3 Hz, 2H, Ar-H), 7.54 (dd, *J* = 2.2, 8.6 Hz, 1H, Ar-H), 7.46 (d, *J* = 8.7 Hz, 1H, Ar-H), 7.09 (d, *J* = 8.2 Hz, 1H, Ar-H), 6.74 (s, 2H), 6.69 (d, *J* = 1.4 Hz, 2H, Ar-H), 6.55 (d, *J* = 8.4 Hz, 2H, Ar-H), 5.63 (d, *J* = 1.3 Hz, H-1), 4.15 (dd, *J* = 1.8, 3.1 Hz, H-2), 4.03 (dd, *J* = 3.4, 9.5 Hz, H-3), 3.94 (s, 2H, CH₂), 3.86-3.64 (m, 6H, H-4, H-5, H-6, CH₂); ¹³C NMR (126 MHz, CD₃OD): δ = 153.21, 143.84, 136.41, 129.66, 129.18, 127.76, 127.70, 125.37, 118.64, 103.62 (Ar-C), 100.75 (C-1), 76.00 (C-5), 72.41 (C-3), 71.86 (C-2), 68.24 (C-4), 62.69 (C-6), 40.76 (CH₂); ESI-MS: *m/z*: Calcd for C₄₂H₃₇ClN₃O₁₂S [M+H]⁺: 842.2, found: 842.2.

3'-Chloro-*N*-(2-(2-(2-(3-(3',6'-dihydroxy-3-oxo-3*H*-spiro[isobenzofuran-1,9'-xanthen]-5-yl)thioureido)ethoxy)ethoxy)ethyl)-4'-(α -D-mannopyranosyloxy)-biphenyl-4-carboxamide (23). Compound **8** (280 mg, 0.68 mmol) was dissolved in dry DMF (5 mL) under argon, then NHS (235 mg, 2.04 mmol) was added, followed by DIC (0.12 mL, 0.78 mmol) and the mixture was stirred at rt for 4 h, then Boc-PEG2-NH₂ (186 mg, 0.75 mmol)

was added, and the mixture was stirred at rt under argon for 10 h. It was then slowly diluted with water and concentrated. The residue was purified by chromatography on silica gel (DCM/MeOH) to give *tert*-butyl (2-(2-(2-(3'-chloro-4'-(α -D-mannopyranosyloxy)-biphenyl-4-ylcarboxamido)ethoxy)ethoxy)ethyl)carbamate (300 mg, 0.468 mmol, 69%). Then, the carbamate was suspended in DCM (3 mL) and TFA (1 mL) was added dropwise at rt. After 30 min, the solvents were evaporated and the crude mixture was dissolved in CHCl₃/MeOH (6:4 + 0.5% conc. NH₄OH) and transferred to a silica gel column, eluting with the same solvent mixture, to yield *N*-(2-(2-(2-aminoethoxy)ethoxy)ethyl)-3'-chloro-4'-(α -D-mannopyranosyloxy)-biphenyl-4-carboxamide (228 mg, 90 %). A fraction of the amine (10 mg, 0.018 mmol) was dissolved in dry DMF (0.5 mL) and cooled to 0 °C. FITC (6.5 mg, 0.017 mmol) was added and the mixture was stirred for 1 h. The mixture was concentrated and the residue was purified by chromatography on silica (DCM/MeOH), to yield **23** (10 mg, 65%). ¹H NMR (500 MHz, CD₃OD): δ = 8.21 (d, *J* = 1.4 Hz, 1H, Ar-H), 7.88 (d, *J* = 8.3 Hz, 2H, Ar-H), 7.68 (d, *J* = 2.2 Hz, 2H, Ar-H), 7.63 (d, *J* = 8.3 Hz, 2H, Ar-H), 7.53 (dd, *J* = 2.2, 8.6 Hz, 1H, Ar-H), 7.43 (d, *J* = 8.7 Hz, 1H, Ar-H), 7.09 (d, *J* = 8.2 Hz, 1H, Ar-H), 6.68 (d, *J* = 2.3 Hz, 2H, Ar-H), 6.65 (dd, *J* = 2.6, 8.6 Hz, 2H, Ar-H), 6.53 (dd, *J* = 1.6, 8.7 Hz, 2H, Ar-H), 5.61 (d, *J* = 1.3 Hz, 1H, H-1), 4.14 (dd, *J* = 1.8, 3.2, Hz, 1H, H-2), 4.03 (dd, *J* = 3.4, 9.5 Hz, 1H, H-3), 3.93-3.53 (m, 16H), 3.37 (s, 2H, NCH₂), 1.30 (s, 2H, CH₂); ¹³C NMR (126 MHz, CD₃OD): δ = 170.01 (CO), 153.17, 143.72, 136.37, 134.37, 130.39, 129.69, 129.04, 127.78, 127.73, 125.35, 118.60, 103.60 (Ar-C), 100.72 (C-1), 75.97 (C-5), 72.41 (C-3), 71.86, 71.40, 70.59 (5C, C-2, OCH₂), 68.23 (C-4), 62.64 (C-6), 49.88, 45.49, 40.97 (CH₂); ESI-MS: *m/z*: Calcd for C₄₆H₄₅ClN₃O₁₄S [M+H]⁺: 930.2, found: 930.4.

Competitive Fluorescence Polarization Assay

Expression and purification of CRD of FimH. A recombinant protein consisting of the CRD of FimH linked to a 6His-tag via a thrombin cleavage site (FimH-CRD-Th-His₆) was expressed in *E. coli* strain HM125 and purified by affinity chromatography as previously described.³³

K_D determination of FITC-labeled ligands. The functionalized ligands (**22**, **23**) were prepared as a 10 mM stock solution in pure DMSO (Sigma Aldrich, Buchs, Switzerland). All further dilutions of compounds and FimH-CRD-Th-His₆ protein were prepared in assay buffer (20 mM HEPES, 150 mM NaCl, 50 μ g/mL BSA, pH 7.4). BSA was added to the assay buffer to prevent non-specific binding of protein to the plastic surface. Binding isotherms for

the fluorescent ligands were obtained in direct binding studies by adding a constant concentration of ligand (final concentration 5 nM) and a linear dilution of protein (final concentration 0-100 nM) to a final volume of 200 μ L in 96-well, black, flat bottom NBSTM plates (Corning Inc., Corning, NY, USA). After incubating the plate for 24 h at rt with gentle shaking, the fluorescence polarization was measured with the SynergyTM H1 Hybrid Multi-Mode Microplate Reader (BioTek Instruments Inc., Winooski, VT, USA) with polarized excitation at 485 nm and emission measured at 528 nm through polarizing filters parallel and perpendicularly oriented to the incident polarized light. K_D values were determined by plotting the FP readout as a function of the protein concentration and applying the following single-site binding equation (Equation 1) that accounts for ligand depletion:

$$S_{obs} = S_F + (S_B - S_F) \cdot \left(\frac{C_P + C_L + K_D - \sqrt{(C_P + C_L + K_D)^2 - 4C_P C_L}}{2C_L} \right) \quad (1)$$

where S_{obs} is the observed signal from the ligand, S_F is the signal from free ligand, S_B is the signal from bound ligand, C_P is the total concentration of protein, and C_L is the total concentration of ligand.³⁹

K_D Determination of FimH Antagonists. The fluorescently labeled ligand **22** was used for the competitive fluorescence polarization assay. A linear dilution of non-labeled FimH antagonist with final concentrations ranging from 0-10 μ M was titrated into 96-well, black, flat bottom NBSTM plates (Corning Inc.) to a final volume of 200 μ L containing a constant concentration of protein (final concentration 25 nM) and FITC-labeled ligand which was fixed at a higher concentration in competitive binding assays than in direct binding experiments to obtain higher fluorescence intensities (final concentration 20 nM). Prior to measuring the fluorescence polarization, the plates were incubated on a shaker for 24 h at rt until the reaction reached equilibrium. The IC_{50} value was determined with Prism (GraphPad Software Inc., La Jolla, CA, USA) by applying a standard four-parameter IC_{50} function. The obtained IC_{50} values were converted into their corresponding K_D values using the derivation of the Cheng-Prusoff equation.³⁵ This variation of the Cheng-Prusoff equation is applied to competition assays with tight-binding inhibitors, and includes terms to correct for ligand depletion effects. However, the K_D for antagonists having a higher affinity towards FimH than the labeled ligand could not be accurately determined.³⁵

Isothermal Titration Calorimetry (ITC)

All ITC experiments were performed with the FimH-CRD-Th-His₆ protein using a VP-ITC instrument from MicroCal, Inc. (GE Healthcare, Northampton, MA, USA) with a sample cell volume of 1.4523 mL. The measurements were performed with 2.5 or 5% DMSO at 25 °C, a stirring speed of 307 rpm, and 10 μcal s⁻¹ reference power. The protein samples were dialyzed in assay buffer prior to all experiments. Compounds **6**, **10**, and **24** were measured in a direct fashion by titration of ligand (120-2,000 μM) into protein (10-55 μM) with injections of 3-6 μL at intervals of 10 min to ensure non-overlapping peaks. The quantity $c = Mt(0) K_D^{-1}$, where $Mt(0)$ is the initial macromolecule concentration, is of importance in titration microcalorimetry. The c -values of the direct titrations were below 1'000 and thus within the reliable range. For the compounds **11b-e**, **11g** and **11j** additional competitive ITC experiments were performed due to their high affinity resulting in c -values above 1'000 for direct titrations. These ligands (600 μM) were titrated into protein (30 μM), which was preincubated with compound **24** (300 μM) resulting in sigmoidal titration curves. Due to slow reaction kinetics, titration intervals of 20 min were used.

Baseline correction and peak integration was performed using the Origin 7 software (OriginLab, Northampton, MA, USA). An initial 2 μL injection was excluded from data analysis. Baseline subtraction and curve-fitting with the three variables N (concentration correction factor), K_D (dissociation constant), and ΔH° (change in enthalpy) was performed with the SEDPHAT software version 10.40 (National Institute of Health). A global fitting analysis was performed for the competition titration (compounds **11b-e**, **11g** or **11j** competing for the protein binding site with compound **24**) and the direct titration of the competitor (compound **24** binding to protein) to fit for K_D , ΔH° and N were fitted from direct titrations of compounds **11b-e**, **11g** or **11j** into protein. For the compounds **6**, **10** and **24** binding to protein all variables could be determined from a global analysis of the direct titration.

The thermodynamic parameters were calculated with the following equation (Equation 2):

$$\Delta G^\circ = \Delta H^\circ - T\Delta S^\circ = RT \ln K_D = -RT \ln K_A \quad (2)$$

where ΔG° , ΔH° , and ΔS° are the changes in free energy, enthalpy, and entropy of binding, respectively, T is the absolute temperature, and R is the universal gas constant (8.314 J mol⁻¹ K⁻¹). The 95 %-confidence intervals of the measurements were calculated for the two

variables K_D and ΔH° with the 1-dimensional error surface projection within the SEDPHAT software.

Calculation of the Free Energy of Desolvation. The three dimensional representation for each of the aglycons (4-methoxy biphenyl scaffold, Figure 7) was built in the Maestro⁷³ modeling environment and the global minimum conformation was identified by performing 500 iterations of the mixed torsional/low-mode conformational sampling in combination with the OPLS-2005 force-field and the implicit solvent model (water) as implemented in the Macromodel 9.9.⁷⁴ The global minimum structures were used as input for the AMSOL 7.1 program⁷⁶ to obtain the free energy of desolvation ΔG_{des} (Table 5) with the SM5.4A solvation model⁷⁶ and the AM1⁷⁷ level of theory (used keywords “AM1 SM5.4A SOLVNT=WATER TRUES”).

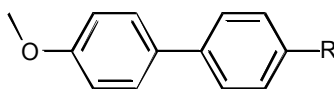


Figure 7. The 4-methoxy biphenyl scaffold of aglycons.

Table 5. Aqueous free energy of desolvation.

R	ΔG_{des} [kJ/mol]
<i>neutral</i>	
H	15.6
CONHCH ₃	39.9
COOCH ₃	23.0
SO ₂ NHCH ₃	65.5
SO ₂ CH ₃	56.4
4-morpholine amide	45.3
CN	22.0
<i>deprotonated</i>	
COO ⁻	298.2
SO ₂ -N ⁻ -Me	342.0

Determination of the MAC₉₀ by flow cytometry

The MAC₉₀ was determined in principle as in the previously published flow cytometry assay,⁶⁸ but with some modifications. The human epithelial bladder carcinoma cell line 5637 (DSMZ, Braunschweig, Germany) was grown in RPMI 1640 medium, supplemented with 10% fetal calf serum (FCS), 100 U/mL penicillin and 100 µg/mL streptomycin at 37 °C, 5% CO₂. All solutions were purchased from Invitrogen (Basel, Switzerland). The cells were

subcultured 1:6 twice per week [using Trypsin/EDTA (Sigma-Aldrich) for the detachment]. Two days before infection, 1.8×10^5 cells were seeded in each well of a 24-well plate in RPMI 1640 containing 10% FCS without antibiotics. The cell density was approximately $3\text{-}5 \times 10^5$ cells/well at the assay day.

For infection, the GFP-expressing clinical *E. coli* isolate UTI89⁷⁸ (UTI89 wt) and the GFP-expressing FimA-H knock-out strain UTI89 Δ *fimA-H* were used (strains were provided by Prof. Urs Jenal, Biocenter, University of Basel, Switzerland).⁶⁸ Bacteria were cultivated at 37 °C in 10 mL Luria-Bertani (LB) broth (Becton, Dickinson and Company) overnight, harvested by centrifugation (3800 rpm, 10 min) and washed three times in phosphate buffered saline (PBS, Sigma-Aldrich) and a bacterial solution of OD₆₀₀ of 0.75 in RPMI + 10% FCS was prepared. For the determination of the MAC₉₀ value, the IC₉₀, linear dilutions of the FimH-antagonist were prepared in 5% DMSO and PBS. Bacteria and antagonists were pre-incubated for 10 min at 37 °C, before cells were infected with either only 200 µL bacterial solution of UTI89 or UTI89 Δ *fimA-H* (positive and negative controls), or 225 µL of the pre-incubated bacteria-antagonist mixture. Infection lasted for 1.5 h, during this time infected cells were incubated at 37 °C. Then, cells were washed with PBS and detached from wells by the addition of 150 µL trypsin and incubation at 37 °C for 10 min, before flushing from wells PBS containing 2% FCS and transferred to tubes. To dilute the trypsin, cells were centrifuged at 13000 rpm, 1 min, 600 µL of the supernatant was discarded and the pellet was re-suspended in the remaining 300 µL PBS containing 2% FCS. Samples were stored on ice until measurement. Before analysis with the flow cytometer (Becton Dickinson, FACSCanto II), the samples were gently mixed and filtered using a 35 µm nylon mesh (Corning Life Sciences) to prevent cellular aggregation. Cells were gated with linear scaling for side scatter (SSC) and forward scatter (FSC) and GFP intensity of live cells was evaluated. IC₉₀ values were determined by plotting the concentration of the antagonist in a logarithmic mode versus the mean fluorescence intensity (MFI) of living cells and by fitting a dose response curve (variable slope, four parameters) with the prism software (GraphPad Prism).

X-ray analysis of the antagonists 11e and 11j co-crystallized with FimH-CRD

FimH-CRD-11e co-crystallization. Initial FimH-CRD (18 mg/mL in 20 mM HEPES pH 7.4) crystals were obtained in complex with 4-(5-nitroindolin-1-yl)phenyl α -D-mannopyranoside (5 mM).²³ Crystals were grown in sitting-drop vapor diffusion at 20 °C

with 200 nL of protein-antagonist mixture together with 200 nL precipitant solution in well D3 (0.2 M sodium phosphate monobasic monohydrate, 20% w/v PEG 3,350) of the PEG/Ion HT™ screen (Hampton Research, CA, USA). Cubic crystals appeared within one week, which served as cross-seeding crystals. A solution of FimH-CRD (20 mg/mL) and **11e** (5 mM) was mixed with 0.2 M sodium phosphate monobasic monohydrate, 20% w/v PEG 400 with 0.5 μ L of each solution. Streak-seeding was performed after one day of incubation. Cubic FimH-CRD-**11e** crystals formed within 24 h. Crystals were flash cooled to 100 K with perfluoropolyether cryo oil (Hampton Research, CA, USA) as cryoprotectant. Data was collected with synchrotron radiation ($\lambda = 0.99999 \text{ \AA}$) at the PXIII beamline, Swiss Light Source, Switzerland.

FimH-CRD-11j co-crystallization. Co-crystals were initially grown in sitting-drop vapor diffusion at 20 °C with 0.5 μ L of a mixture of FimH-CRD (20 mg/mL) and **11j** (5 mM) together with 0.5 μ L of 0.1 M HEPES pH 7.5, 2 M ammonium sulfate. Plate-like crystals formed within two weeks and were used as seeds for subsequent crystallization. Diffraction quality crystals were grown by streak-seeding in 0.5 μ L of FimH-CRD (10 mg/mL) with **11j** (2.5 mM) and 0.5 μ L of 0.1 M HEPES pH 7.5, 1.25 M ammonium sulfate. The drops were covered with perfluoropolyether cryo oil prior to flash cooling to 100 K. Data was collected with synchrotron radiation ($\lambda = 1.00003 \text{ \AA}$) at the PXIII beamline, Swiss Light Source, Switzerland.

Structure Determination and Refinement. Data were indexed and integrated with the XDS package⁷⁹ for the FimH-CRD-**11e** co-crystal structure, and with mosflm⁸⁰⁷ for the FimH-CRD-**11j** co-crystal structure. Scaling was performed with XDS and SCALA included in the CCP4 suite, respectively.⁸¹ Structures were solved by molecular replacement with PHASER⁸² using the FimH-CRD-butyl α -D-mannopyranoside complex (PDB code 1UWF) as search model. The structures were iteratively built using the COOT software⁸³ and refined with the PHENIX software.⁸⁴ Geometric restraints for **11e** and **11j** were generated with PRODRG.⁸⁵ The models were validated using molprobity.⁸⁶ Residues 113-115 were not modeled in the **11e** structure due to disorder. Furthermore, the ligand was modeled in two possible conformations. For both ligands, electron density is reduced on the second aromatic ring due to flexibility of the ligand.

Table 6. Data Collection and Refinement Statistics for *FimH*-CRD-11e and *FimH*-CRD-11j co-crystals.

	<i>FimH</i> -CRD-11e	<i>FimH</i> -CRD-11j
PDB code	4CSS	4CST
Space group	P 2 ₁ 2 ₁ 2 ₁	P 2 ₁ 2 ₁ 2 ₁
No. of molecules in the asymmetric unit	1	1
Cell dimensions		
<i>a</i> , <i>b</i> , <i>c</i> (Å)	48.38, 56.23, 61.59	48.84, 55.89, 61.00
<i>a</i> , <i>b</i> , <i>c</i> (°)	90, 90, 90	90, 90, 90
Data Collection		
Beamline	Swiss Light Source PXIII	Swiss Light Source PXIII
Resolution range (Å) ^a	30.0 - 1.07 (1.13 – 1.07)	23.5 – 1.10 (1.12 – 1.10)
Unique observations ^a	72000 (9354)	66470 (2500)
Average multiplicity ^a	10.9 (3.7)	5.4 (2.4)
Completeness (%)	96.1 (78.0)	97.2 (76.5)
R _{merge} ^a	0.056 (0.57)	0.051 (0.305)
Mean I / σ(I) ^a	21.5 (2.22)	15.5 (2.9)
Refinement		
Resolution range (Å)	15.7 – 1.07	23.5 – 1.10
<i>R</i> , <i>R</i> _{free}	11.2, 13.2	11.4, 13.0
Rms deviation from ideal bond length (Å)	0.010	0.010
Rms deviation from ideal bond angle (deg)	1.170	1.420

^aValues in parentheses are for highest-resolution shell.

Physicochemical and *in vitro* pharmacokinetic studies.

Materials. Dimethyl sulfoxide (DMSO), 1-propanol, 1-octanol, Dulbecco's Modified Eagle's Medium (DMEM) - high glucose, L-glutamine solution, penicillin-streptomycin solution, Dulbecco's Phosphate Buffered Saline (DPBS), trypsin-EDTA solution, magnesium chloride hexahydrate, and reduced nicotinamide adenine dinucleotide phosphate (NADPH) were purchased from Sigma-Aldrich. MEM nonessential amino acid (MEM-NEAA) solution, fetal bovine serum (FBS), and DMEM without sodium pyruvate and phenol red were bought from Invitrogen (Carlsbad, CA, USA). PRISMA HT universal buffer, GIT-0 Lipid Solution, and Acceptor Sink Buffer were ordered from pIon (Woburn, MA, USA). Human plasma was bought from Biopredic (Rennes, France) and acetonitrile (MeCN) and methanol (MeOH) from Acros Organics (Geel, Belgium). Pooled male rat liver microsomes were purchased from BD Bioscience (Franklin Lakes, NJ, USA). Tris(hydroxymethyl)-aminomethane (TRIS) was obtained from AppliChem (Darmstadt, Germany). The Caco-2 cells were kindly provided by Prof. G. Imanidis, FHNW, Muttentz, and originated from the American Type Culture Collection (Rockville, MD, USA).

pK_a. The pK_a values were determined as described elsewhere.⁸⁷ In brief, the pH of a sample solution was gradually changed and the chemical shift of protons adjacent to ionizable centers was monitored by ¹H nuclear magnetic resonance (NMR) spectroscopy. The shift was plotted against the pH of the respective sample, and the pK_a was read out from the inflection point of the resulting sigmoidal curve.

Log D_{7.4}. The in silico prediction tool ALOGPS⁸⁸ was used to estimate log *P* values of the compounds. Depending on these values, the compounds were classified into three categories: hydrophilic compounds (log *P* below zero), moderately lipophilic compounds (log *P* between zero and one) and lipophilic compounds (log *P* above one). For each category, two different ratios (volume of 1-octanol to volume of buffer) were defined as experimental parameters (Table 7).

Table 7. Compound classification based on estimated log *P* values.

Compound type	log <i>P</i>	ratio (1-octanol / buffer)
hydrophilic	< 0	30:140, 40:130
moderately lipophilic	0 - 1	70:110, 110:70
lipophilic	> 1	3:180, 4:180

Equal amounts of phosphate buffer (0.1 M, pH 7.4) and 1-octanol were mixed and shaken vigorously for 5 min to saturate the phases. The mixture was left until separation of the two phases occurred, and the buffer was retrieved. Stock solutions of the test compounds were diluted with buffer to a concentration of 1 μM. For each compound, six determinations, that is, three determinations per 1-octanol/buffer ratio, were performed in different wells of a 96-well plate. The respective volumes of buffer containing analyte (1 μM) were pipetted to the wells and covered by saturated 1-octanol according to the chosen volume ratio. The plate was sealed with aluminum foil, shaken (1350 rpm, 25 °C, 2 h) on a Heidolph Titramax 1000 plate-shaker (Heidolph Instruments GmbH & Co. KG, Schwabach, Germany) and centrifuged (2000 rpm, 25 °C, 5 min, 5804 R Eppendorf centrifuge, Hamburg, Germany). The aqueous phase was transferred to a 96-well plate for analysis by LC-MS.

The log *D*_{7.4} coefficient was calculated from the 1-octanol/buffer ratio (o:b), the initial concentration of the analyte in buffer (1 μM), and the concentration of the analyte in buffer (*c_B*) with Equation 3:

$$\log D_{7.4} = \log \left(\frac{1\mu\text{M} - c_B}{c_B} \times \frac{1}{o:b} \right) \quad (3)$$

Aqueous Solubility. Solubility was determined in a 96-well format using the μ SOL Explorer solubility analyzer (pIon, version 3.4.0.5). For each compound, measurements were performed at pH 3.0 and 7.4 in triplicates. For this purpose, six wells of a deep well plate, that is, three wells per pH value, were filled with 300 μ L of PRISMA HT universal buffer, adjusted to pH 3.0 or 7.4 by adding the requested amount of NaOH (0.5 M). Aliquots (3 μ L) of a compound stock solution (10-50 mM in DMSO) were added and thoroughly mixed. The final sample concentration was 0.1-0.5 mM, the residual DMSO concentration was 1.0% (v/v) in the buffer solutions. After 15 h, the solutions were filtrated (0.2 μ m 96-well filter plates) using a vacuum to collect manifold (Whatman Ltd., Maidstone, UK) to remove the precipitates. Equal amounts of filtrate and 1-propanol were mixed and transferred to a 96-well plate for UV/Vis detection (190 to 500 nm, SpectraMax 190). The amount of material dissolved was calculated by comparison with UV/Vis spectra obtained from reference samples, which were prepared by dissolving compound stock solution in a 1:1 mixture of buffer and 1-propanol (final concentrations 0.017-0.083 mM).

Parallel Artificial Membrane Permeation Assay (PAMPA). Effective permeability ($\log P_e$) was determined in a 96-well format with the PAMPA.⁵⁰ For each compound, measurements were performed at pH 5.0 and 7.4 in quadruplicates. Eight wells of a deep well plate, that is, four wells per pH-value, were filled with 650 μ L of PRISMA HT universal buffer adjusted to pH 5.0 or 7.4 by adding the requested amount of NaOH (0.5 M). Samples (150 μ L) were withdrawn from each well to determine the blank spectra by UV/Vis-spectroscopy (190 to 500 nm, SpectraMax 190). Then, analyte dissolved in DMSO was added to the remaining buffer to yield 50 μ M solutions. To exclude precipitation, the optical density was measured at 650 nm, with 0.01 being the threshold value. Solutions exceeding this threshold were filtrated. Afterwards, samples (150 μ L) were withdrawn to determine the reference spectra. Further 200 μ L were transferred to each well of the donor plate of the PAMPA sandwich (pIon, P/N 110163). The filter membranes at the bottom of the acceptor plate were infused with 5 μ L of GIT-0 Lipid Solution, and 200 μ L of Acceptor Sink Buffer was filled into each acceptor well. The sandwich was assembled, placed in the GutBoxTM, and left undisturbed for 16 h. Then, it was disassembled and samples (150 μ L) were transferred from each donor and acceptor well to UV-plates for determination of the UV/Vis spectra. Effective permeability ($\log P_e$) was calculated from the compound flux deduced from the spectra, the filter area, and the initial sample concentration in the donor well with the aid of the PAMPA Explorer Software (pIon, version 3.5).

Colorectal Adenocarcinoma (Caco-2) Cell Permeation Assay. Caco-2 cells were cultivated in tissue culture flasks (BD Biosciences) with DMEM high glucose medium, containing L-glutamine (2 mM), nonessential amino acids (0.1 mM), penicillin (100 U/mL), streptomycin (100 µg/mL), and fetal bovine serum (10%). The cells were kept at 37 °C in humidified air containing 5% CO₂, and the medium was changed every second day. When approximately 90% confluence was reached, the cells were split in a 1:10 ratio and distributed to new tissue culture flasks. At passage numbers between 60 and 65, they were seeded at a density of 5.3×10^5 cells per well to Transwell 6-well plates (Corning Inc.) with 2.5 mL of culture medium in the basolateral and 1.8 mL in the apical compartment. The medium was renewed on alternate days. Permeation experiments were performed between days 19 and 21 post seeding. Prior to the experiment, the integrity of the Caco-2 monolayers was evaluated by measuring the transepithelial electrical resistance (TEER) with an Endohm tissue resistance instrument (World Precision Instruments Inc., Sarasota, FL, USA). Only wells with TEER values higher than $250 \Omega \text{ cm}^2$ were used. Experiments were performed in the apical-to-basolateral (absorptive) and basolateral-to-apical (secretory) directions in triplicates. Transport medium (DMEM without sodium pyruvate and phenol red) was withdrawn from the donor compartments of three wells and replaced by the same volume of compound stock solution (10 mM in DMSO) to reach an initial sample concentration of 62.5 µM. The Transwell plate was then shaken (600 rpm, 37 °C) on a Heidolph Titramax 1000 plate-shaker. Samples (40 µL) were withdrawn from the donor and acceptor compartments 30 min after initiation of the experiment and the compound concentrations were determined by LC-MS (see below). Apparent permeability (P_{app}) was calculated according to Equation 4:

$$P_{\text{app}} = \frac{dQ}{dt} \times \frac{1}{A \times c_0} \quad (4)$$

where dQ/dt is the compound flux (mol s^{-1}), A is the surface area of the monolayer (cm^2), and c_0 is the initial concentration in the donor compartment (mol cm^{-3}).⁵⁰ After the experiment, TEER values were assessed again for each well and results from wells with values below $250 \Omega \text{ cm}^2$ were discarded.

Plasma Protein Binding (PPB). PPB was determined in a 96-well format using a high throughput dialysis block (HTD96b; HTDialysis LCC, Gales Ferry, CT, USA). For each compound, measurements were performed in triplicate. Dialysis membranes (MWCO 12-14 K; HTDialysis LCC) were hydrated according to the instructions of the manufacturer and placed into the dialysis block. Human plasma was centrifuged (5800 rpm, 5 °C, 10 min), the

pH of the supernatant (without floating plasma lipids) was adjusted to 7.4 by adding the requested amount of HCl (4 M), and analyte was added to yield a final concentration of 10 μ M. Equal volumes (150 μ L) of plasma containing the analyte or TRIS-HCl buffer (0.1 M, pH 7.4) were transferred to the compartments separated by the dialysis membrane. The block was covered with a sealing film and left undisturbed (5 h, 37 °C). Afterwards, samples (90 μ L) were withdrawn from the buffer compartments and diluted with plasma (10 μ L). From the plasma compartments, samples (10 μ L) were withdrawn and diluted with TRIS-HCl buffer (90 μ L). The solutions were further diluted with ice-cooled MeCN (300 μ L) to precipitate the proteins and centrifuged (3600 rpm, 4 °C, 10 min). The supernatants (50 μ L) were retrieved, and the analyte concentrations were determined by LC-MS (see below). The fraction bound (f_b) was calculated as follows (Equation 5):

$$f_b = 1 - \frac{c_b}{c_p} \quad (5)$$

where c_b is the concentration of the analyte withdrawn from the buffer compartment before dilution and c_p is the concentration in the plasma compartment. The values were accepted if the recovery of analyte was between 80 and 120% of the initial amount.

Cytochrome P450-mediated metabolism. Incubations consisted of pooled male rat liver microsomes (0.5 mg microsomal protein/mL), test compound (2 μ M), MgCl₂ (2 mM), and NADPH (1 mM) in a total volume of 300 μ L TRIS-HCl buffer (0.1 M, pH 7.4) and were performed in a 96-well plate on a Thermomixer Comfort (Eppendorf). Compounds and microsomes were preincubated (37 °C, 700 rpm, 10 min) before NADPH was added. Samples (50 μ L) at $t = 0$ min and after an incubation time of 5, 10, 20, and 30 min were quenched with 150 μ L of ice-cooled MeOH, centrifuged (3600 rpm, 4 °C, 10 min), and 80 μ L of supernatant was transferred to a 96-well plate for LC-MS analysis (see below). The metabolic half-life ($t_{1/2}$) was calculated from the slope of the linear regression from the log percentage remaining compound versus incubation time relationship. Control experiments without NADPH were performed in parallel.

LC-MS measurements. Analyses were performed using an 1100/1200 Series HPLC System coupled to a 6410 Triple Quadrupole mass detector (Agilent Technologies, Inc., Santa Clara, CA, USA) equipped with electrospray ionization. The system was controlled with the Agilent MassHunter Workstation Data Acquisition software (version B.01.04). The column used was an Atlantis® T3 C18 column (2.1 x 50 mm) with a 3- μ m particle size (Waters Corp.,

Milford, MA, USA). The mobile phase consisted of eluent A: H₂O containing 0.1% formic acid (for **11a-f, h-i**), or 10 mM ammonium acetate, pH 5.0 in 95:5, H₂O/MeCN (for **11g, j**); and eluent B: MeCN containing 0.1% formic acid. The flow rate was maintained at 0.6 mL/min. The gradient was ramped from 95% A/5% B to 5% A/95% B over 1 min, and then hold at 5% A/95% B for 0.1 min. The system was then brought back to 95% A/5% B, resulting in a total duration of 4 min. MS parameters such as fragmentor voltage, collision energy, polarity were optimized individually for each analyte, and the molecular ion was followed for each compound in the multiple reaction monitoring mode. The concentrations of the analytes were quantified by the Agilent Mass Hunter Quantitative Analysis software (version B.01.04).

***In Vivo* Pharmacokinetic Studies.**

Materials. DMSO and PBS were purchased from Sigma-Aldrich. The 96-well plates were bought from Agilent Technologies (0.5 mL, polypropylene). The gavage was obtained from Fine Science (Heidelberg, Germany) and the syringes (BD Micro Fine, U-100 Insuline, 30 G) and needles (BD Microlance 3, 25 G) from Becton Dickinson (USA, Ireland) and Henke Sass Wolf in Germany (Soft-Ject, 1 mL syringes).

Animals. Female C3H/HeN mice weighing between 19 and 25 g were obtained from Charles River Laboratories (Sulzfeld, Germany) and were housed three or four per cage. The mice were kept under specific pathogen-free conditions in the Animal House of the Department of Biomedicine, University Hospital of Basel, and animal experimentation guidelines according to the regulations of the Swiss veterinary law were followed. After 7 d of acclimatization, 9-10 week old mice were used for the studies. Animals had free access to chow and water at any time and were kept in a 12h/12h light/dark cycle. For administration volumes and sampling the good practice guidelines were followed.⁸⁹

Pharmacokinetic studies. The single-dose studies for the first experiment set were performed by intravenous application of FimH antagonists at a dosage of 50 mg/kg body weight, followed by plasma and urine sampling. Antagonists were diluted in PBS for injection into the tail vein. Blood and urine samples (10 µL) were taken at 6 and 30 min, and 1, 2, 4, 6, and 8 h after injection. For the PK studies with **11j**, the antagonist was dissolved in PBS with 5 % DMSO and injected into the tail vein (0.625 mg/kg) or given orally (1.25 mg/kg) using a gavage. Blood and urine were sampled (10 µL) after 7, 13, 20, 30, 45 min,

and 1, 1.5, 2, 2.5, 3, 4, 6, 8, and 24 h. Both, blood and urine samples, were directly diluted after sampling with MeOH to precipitate the proteins and centrifuged for 11 min at 13000 rpm. The supernatants were transferred to a 96-well plate and the analyte concentrations were determined by LC-MS (see above).

Infection study. For all infection studies, the drinking water of the mice was replaced by 5% glucose (monohydrate from AppliChem, BioChemica) containing water, three days before the start of the experiment. **11j** was dosed at 1.25 mg/kg (in 5% DMSO and PBS) and 10 mg/kg (5% DMSO in PBS containing 1% Tween 80) applied orally to 6 and 4 mice, respectively, as described in the pharmacokinetic studies, 40 min prior to infection. Ciprofloxacin was dosed with 8 mg/kg, which would correspond to a human dose of 400 mg,⁷⁰ subcutaneously 10 minutes prior to infection with UTI89 to 4 mice. Control values resulted from the infection of 11 mice. Before infection, remaining urine in the bladder was expelled by gentle pressure on the abdomen. Mice were anaesthetised in 2.5 vol% isoflurane/oxygen mixture (Attane, Minrad Inc, Buffalo, NY, USA) and placed on their back. Infection was performed transurethrally using a polyethylene catheter (Intramedic polyethylene tubing, inner diameter 0.28 mm, outer diameter 0.61 mm, Beckton Dickinson, Allschwil, Switzerland), on a syringe (Hamilton Gastight Syringe 50 µl, removable 30G needle, BGB Analytik AG, Boeckten, Switzerland). After gentle insertion of the catheter into the bladder, 50 µl of bacterial suspension of UTI89 (5.5×10^9 - 2.25×10^{10} CFU/ml) was slowly injected. This corresponded to approximately 10^7 - 10^8 CFU per mouse. Mice were killed by CO₂ three hours after inoculation and bladder and kidneys were aseptically removed. Organs were homogenized in 1 ml PBS using a tissue lyser (Retsch, Haan, Germany). Serial dilutions of bladder and kidneys were plated on Levine Eosin Methylene Blue Agar plates (Beckton Dickinson, France) and CFU were counted after overnight incubation at 37°C.

Acknowledgement

The authors thank Prof. Dr. med. Radek Skoda, Department of Biomedicine, University Hospital Basel, Switzerland, for giving us access to the animal facility. The financial support by the Swiss National Science Foundation (SNF interdisciplinary grant K-32K1-120904) is gratefully acknowledged.

References

- (1) Foxman, B.; Barlow, R.; D'Arcy, H.; Gillespie, B.; Sobel, J. D. Urinary tract infection: self-reported incidence and associated costs. *Ann. Epidemiol.* **2000**, *10*, 509-515.
- (2) Ronald, A. The etiology of urinary tract infection: traditional and emerging pathogens. *Am. J. Med.* **2002**, *113 Suppl. 1A*, 14S-19S.
- (3) Fihn, S. D. Acute uncomplicated urinary tract infection in women. *N. Engl. J. Med.* **2003**, *349*, 259-266.
- (4) Hooton, T. M.; Besser, R.; Foxman, B.; Fritsche, T. R.; Nicolle, L. E. Acute uncomplicated cystitis in an era of increasing antibiotic resistance: a proposed approach to empirical therapy. *Clin. Infect. Dis.* **2004**, *39*, 75-80.
- (5) Sanchez, G. V.; Master, R. N.; Karlowsky, J. A.; Bordon, J. M. In vitro antimicrobial resistance of urinary *Escherichia coli* isolates among U. S. outpatients from 2000 to 2010. *Antimicrob. Agents Chemother.* **2012**, *56*, 2181-2183.
- (6) Clatworthy, A. E.; Pierson, E.; Hung, D. T. Targeting virulence: a new paradigm for antimicrobial therapy. *Nature Chem. Biol.* **2007**, *3*, 541-548.
- (7) Mulvey, M. A.; Schilling, J. D.; Martinez, J. J.; Hultgren, S. J. Bad bugs and beleaguered bladders: interplay between uropathogenic *Escherichia coli* and innate host defenses. *Proc. Natl. Acad. Sci. U S A* **2000**, *97*, 8829-8835.
- (8) Schilling, J. D.; Mulvey, M. A.; Hultgren, S. J. Structure and function of *Escherichia coli* type 1 pili: new insight into the pathogenesis of urinary tract infections. *J. Infect. Dis.* **2001**, *183 Suppl. 1*, S36-40.
- (9) Wiles, T. J.; Kulesus, R. R.; Mulvey, M. A. Origins and virulence mechanisms of uropathogenic *Escherichia coli*. *Exp. Mol. Pathol.* **2008**, *85*, 11-19.
- (10) Capitani, G.; Eidam, O.; Glockshuber, R.; Grütter, M. G. Structural and functional insights into the assembly of type 1 pili from *Escherichia coli*. *Microbes Infect.* **2006**, *8*, 2284-2290.
- (11) Le Trong, I.; Aprikian, P.; Kidd, B. A.; Forero-Shelton, M.; Tchesnokova, V.; Rajagopal, P.; Rodriguez, V.; Interlandi, G.; Klevit, R.; Vogel, V.; Stenkamp, R. E.; Sokurenko, E. V.; Thomas, W. E. Structural basis for mechanical force regulation of the adhesin FimH via finger trap-like β sheet twisting. *Cell* **2010**, *141*, 645-655.
- (12) Sharon, N. Carbohydrates as future anti-adhesion drugs for infectious diseases. *Biochim. Biophys. Acta.* **2006**, *1760*, 527-537.
- (13) Firon, N.; Itzhak, O.; Sharon, N. Interaction of mannose-containing oligosaccharides with the fimbrial lectin of *Escherichia coli*. *Biochem. Biophys. Res. Commun.* **1982**, *105*, 1426-1432.
- (14) Firon, N.; Ofek, I.; Sharon, N. Carbohydrate specificity of the surface lectins of *Escherichia coli*, *Klebsiella pneumoniae*, and *Salmonella typhimurium*. *Carbohydr. Res.* **1983**, *120*, 235-249.
- (15) Bouckaert, J.; Berglund, J.; Schembri, M.; De Genst, E.; Cools, L.; Wuhler, M.; Hung, C.-S.; Pinkner, J.; Slättegård, R.; Zavialov, A.; Choudhury, D.; Langermann, S.; Hultgren, S. J.; Wyns, L.; Klemm, P.; Oscarson, S.; Knight, S. D.; De Greve, H.

- Receptor binding studies disclose a novel class of high-affinity inhibitors of the *Escherichia coli* FimH adhesin. *Mol. Microbiol.* **2005**, *55*, 441-455.
- (16) Firon, N.; Ashkenazi, S.; Mirelman, D.; Ofek, I.; Sharon, N. Aromatic alpha-glycosides of mannose are powerful inhibitors of the adherence of type 1 fimbriated *Escherichia coli* to yeast and intestinal epithelial cells. *Infect. Immun.* **1987**, *55*, 472-476.
- (17) Sperling, O.; Fuchs, A.; Lindhorst, T. K. Evaluation of the carbohydrate recognition domain of the bacterial adhesin FimH. Design, synthesis and binding properties of mannoside ligands. *Org. Biomol. Chem.* **2006**, *4*, 3913-3922.
- (18) Han, Z.; Pinkner, J. S.; Ford, B.; Obermann, R.; Nolan, W.; Wildman, S. A.; Hobbs, D.; Ellenberger, T.; Cusumano, C. K.; Hultgren, S. J.; Janetka, J. W. Structure-based drug design and optimization of mannoside bacterial FimH antagonists. *J. Med. Chem.* **2010**, *53*, 4779-4792.
- (19) Klein, T.; Abgottspon, D.; Wittwer, M.; Rabbani, S.; Herold, J.; Jiang, X.; Kleeb, S.; Lüthi, C.; Scharenberg, M.; Bezençon, J.; Gubler, E.; Pang, L.; Smiesko, M.; Cutting, B.; Schwardt, O.; Ernst, B. FimH antagonists for the oral treatment of urinary tract infections: from design and synthesis to in vitro and in vivo evaluation. *J. Med. Chem.* **2010**, *53*, 8627-8641.
- (20) Schwardt, O.; Rabbani, S.; Hartmann, M.; Abgottspon, D.; Wittwer, M.; Kleeb, S.; Zalewski, A.; Smiesko, M.; Cutting, B.; Ernst, B. Design, synthesis and biological evaluation of mannosyl triazoles as FimH antagonists. *Bioorg. Med. Chem.* **2011**, *19*, 6454-6473.
- (21) Cusumano, C. K.; Pinkner, J. S.; Han, Z.; Greene, S. E.; Ford, B. A.; Crowley, J. R.; Henderson, J. P.; Janetka, J. W.; Hultgren, S. J. Treatment and prevention of urinary tract infection with orally active FimH inhibitors. *Sci. Transl. Med.* **2011**, *3*, 109-115.
- (22) Han, Z.; Pinkner, J. S.; Ford, B.; Chorell, E.; Crowley, J. M.; Cusumano, C. K.; Campbell, S.; Henderson, J. P.; Hultgren, S. J.; Janetka, J. W. Lead optimization studies on FimH antagonists: discovery of potent and orally bioavailable ortho-substituted biphenyl mannosides. *J. Med. Chem.* **2012**, *55*, 3945-3959.
- (23) Jiang, X.; Abgottspon, D.; Kleeb, S.; Rabbani, S.; Scharenberg, M.; Wittwer, M.; Haug, M.; Schwardt, O.; Ernst, B. Anti-adhesion therapy for urinary tract infections – a balanced PK/PD profile proved to be key for success. *J. Med. Chem.* **2012**, *55*, 4700-4713.
- (24) Pang, L.; Kleeb, S.; Lemme, K.; Rabbani, S.; Scharenberg, M.; Zalewski, A.; Schädler, F.; Schwardt, O.; Ernst, B. FimH antagonists: structure-activity and structure-property relationships for biphenyl α -D-mannopyranosides. *ChemMedChem.* **2012**, *7*, 1404-1422.
- (25) Choudhury, D.; Thompson, A.; Stojanoff, V.; Langermann, S.; Pinkner, J.; Hultgren, S. J.; Knight, S. D. X-ray structure of the FimC-FimH chaperone-adhesin complex from uropathogenic *Escherichia coli*. *Science* **1999**, *285*, 1061-1066.
- (26) Hung, C.-S.; Bouckaert, J.; Hung, D.; Pinkner, J.; Widberg, C.; DeFusco, A.; Auguste, C. G.; Strouse, R.; Langermann, S.; Waksman, G.; Hultgren, S. J. Structural basis of tropism of *Escherichia coli* to the bladder drug in urinary tract infection. *Mol. Microbiol.* **2002**, *44*, 903-915.

- (27) Wellens, A.; Garofalo, C.; Nguyen, H.; Van Gerven, N.; Slättegård, R.; Henalsteens, J.-P.; Wyns, L.; Oscarson, S.; De Greve, H.; Hultgren, S. J.; Bouckaert, J. Intervening with urinary tract infections using anti-adhesives based on the crystal structure of the FimH-oligomannose-3 complex. *PLoS One* **2008**, *3*, e2040.
- (28) Wellens, A.; Lahmann, M.; Touaibia, M.; Vaucher, J.; Oscarson, S.; Roy, R.; Remaut, H.; Bouckaert, J. The tyrosine gate as a potential entropic lever in the receptor-binding site of the bacterial adhesin FimH. *Biochemistry* **2012**, *51*, 4790-4799.
- (29) Meanwell, M. A. Synopsis of some recent tactical application of bioisosteres in drug design. *J. Med. Chem.* **2011**, *54*, 2529-2591.
- (30) Prieto, M.; Zurita, E.; Rosa, E.; Luñoz, L.; Lloyd-Williams, P.; Giralt, E. Arylboronic acids and arylpinacolboronate esters in Suzuki coupling reactions involving indoles. Partner role swapping and heterocycle protection. *J. Org. Chem.* **2004**, *69*, 6812-6820.
- (31) Schulz, M. J.; Coats, S. J.; Hlasta, D. J. Microwave-assisted preparation of aryltetrazoleboronate esters. *Org. Lett.* **2004**, *6*, 3265-3268.
- (32) Devos, A.; Remion, J.; Frisque-Hesbain, A. M.; Colens, A.; Ghosez, L. Synthesis of acyl halides under very mild conditions. *J. Chem. Soc. Chem. Commun.* **1979**, 1180-1181.
- (33) Rabbani, S.; Jiang, X.; Schwardt, O.; Ernst, B. Expression of the carbohydrate recognition domain of FimH and development of a competitive binding assay. *Anal. Biochem.* **2010**, *407*, 188-195.
- (34) Waetherman, R.V.; Kiessling, L.L. Fluorescence anisotropy assay reveals affinities of C- and O-glycosides for concanavalin A. *J. Org. Chem.* **1996**, *61*, 534-538.
- (35) Cer, R. Z.; Mudunuri, U.; Stephens, R.; Lebeda, F. J. IC50-to-Ki: a web-based tool for converting IC50 to Ki values for inhibitors of enzyme activity and ligand binding. *Nucleic Acids Research*, **2009**, *37*, W441-W445.
- (36) Lynch, B. A.; Loiacono, K. A.; Tiong, C. L.; Adams, S. E.; MacNeil, I. A. A Fluorescence Polarization Based Src-SH2 Binding Assay. *Anal. Biochem.* **1997**, *247*, 77-82.
- (37) Wu, P.; Brasseur, M.; Schindler, U. A High-Throughput STAT Binding Assay Using Fluorescence Polarization *Anal. Biochem.* **1997**, *249*, 29-36.
- (38) Huang, X. Fluorescence Polarization Competition Assay: The Range of Resolvable Inhibitor Potency Is Limited by the Affinity of the Fluorescent Ligand *J. Biomol. Screen.* **2003**, *8*, 34-38.
- (39) Cooper, A. *Biophysical Chemistry, 2nd Edition*. RSC Publishing. Cambridge UK. **2011**, pp. 122-123.
- (40) Scharenberg, M.; Jiang, X.; Pang, L.; Navarra, G.; Rabbani, S.; Binder, F.; Schwardt, O.; Ernst, B. Kinetic properties of carbohydrate-lectin interactions: FimH antagonists. *ChemMedChem* **2014**, *9*, 78-83.
- (41) Cabani, S.; Gianni, P.; Mollica, V.; Lepori, L. Group contribution to the thermodynamic properties of non-ionic solutes in dilute aqueous solution. *J. Solution Chem.* **1981**, *10*, 563-595.
- (42) Hansch, C.; Leo, A.; Taft, R.W. A survey of Hammett substituent constants and resonance and field parameters. *Chem. Rev.* **1991**, *91*, 165-195.

-
- (43) Chen, A.; Wadso, I. Simultaneous determination of delta G, delta H and delta S by an automatic microcalorimetric titration technique: application to protein ligand binding. *J Biochem Biophys Meth*, **1982**, *6*, 307-316.
- (44) Freire, E.; Mayorga, O.L.; Straume, M. Isothermal titration calorimetry. *Anal Chem*, **1990**, *62*, 950A-959A.
- (45) Wiseman, T.; Williston, S.; Brandts, J. F.; Lin, L.-N. Rapid measurement of binding constants and heats of binding using a new titration calorimeter. *Anal. Biochem.* **1989**, *179*, 131-137.
- (46) Turnbull, W. B.; Daranas A.H. On the value of c: can low affinity systems be studied by isothermal titration calorimetry? *J. Am. Chem. Soc.* **2003**, *125*, 14859-14866.
- (47) Sigurskjold B. W. Exact analysis of competition ligand binding by displacement isothermal titration calorimetry. *Anal. Biochem.* **2000**, *277*, 260-266.
- (48) Velazquez-Campoy A.; Freire E. Isothermal titration calorimetry to determine association constants for high-affinity ligands. *Nat. Protoc.* **2006**, *1*, 186-191.
- (49) Dearden, J. C.; Bresnen, G. M. The measurement of partition coefficients. *QSAR Comb. Sci.* **1988**, *7*, 133-144.
- (50) Kansy, M.; Senner, F.; Gubernator, K. Physicochemical high throughput screening: parallel artificial membrane permeation assay in the description of passive absorption processes. *J. Med. Chem.* **1998**, *41*, 1007-1010.
- (51) Hubatsch, I.; Ragnarsson, E. G. E.; Artursson, P. Determination of drug permeability and prediction of drug absorption in Caco-2 monolayers. *Nat. Protoc.* **2007**, *2*, 2111-2119.
- (52) Banker, M. J.; Clark, T. H.; Williams, J. A. Development and validation of a 96-well equilibrium dialysis apparatus for measuring plasma protein binding. *J. Pharm. Sci.* **2003**, *92*, 967-974.
- (53) Obach, R. S. Prediction of human clearance of twenty-nine drugs from hepatic microsomal intrinsic clearance data: an examination of in vitro half-life approach and nonspecific binding to microsomes. *Drug Metab. Dispos.* **1999**, *27*, 1350-1359.
- (54) Chaturvedi, P. R.; Decker, C. J.; Odinecs, A. Prediction of pharmacokinetic properties using experimental approaches during early drug discovery. *Curr. Opin. Chem. Biol.* **2001**, *5*, 452-463.
- (55) Di, L.; Kerns, E. H. Profiling drug-like properties in discovery research. *Curr. Opin. Chem. Biol.* **2003**, *7*, 402-408.
- (56) Lipinski, C. A. Drug-like properties and the causes of poor solubility and poor permeability. *J. Pharmacol. Toxicol. Methods* **2000**, *44*, 235-249.
- (57) Ishikawa, M.; Hashimoto, Y. Improvement in aqueous solubility in small molecule drug discovery programs by disruption of molecular planarity and symmetry. *J. Med. Chem.* **2011**, *54*, 1539-1554.
- (58) Avdeef, A.; Bendels, S.; Di, L.; Faller, B.; Kansy, M.; Sugano, K.; Yamauchi, Y. PAMPA – critical factors for better predictions of absorption. *J. Pharm. Sci.* **2007**, *96*, 2893-2909.

- (59) Artursson, P.; Karlsson, J. Correlation between oral drug absorption in humans and apparent drug permeability coefficients in human intestinal epithelial (Caco-2) cells. *Biochem. Biophys. Res. Commun.* **1991**, *175*, 880-885.
- (60) Feng, B.; LaPerle, J. L.; Chang, G.; Varma, M. V. S. Renal clearance in drug discovery and development: molecular descriptors, drug transporters and disease state. *Expert Opin. Drug. Metab. Toxicol.* **2010**, *6*, 939-952.
- (61) Schmidt, S.; Gonzalez, D.; Derendorf, H. Significance of protein binding in pharmacokinetics and pharmacodynamics. *J. Pharm. Sci.* **2010**, *99*, 1107-1122.
- (62) Weisiger, R. A. Dissociation from albumin: A potentially rate-limiting step in the clearance of substances by the liver. *Proc. Natl. Acad. Sci. USA* **1985**, *82*, 1563-1567.
- (63) Smith, D. A.; Jones, B. C.; Walker, D. K. Design of drugs involving the concepts and theories of drug metabolism and pharmacokinetics. *Med. Res. Rev.* **1996**, *16*, 243-266.
- (64) Van de Waterbeemd, H.; Smith, D. A.; Beaumont, K.; Walker, D. K. Property-based design: optimization of drug absorption and pharmacokinetics. *J. Med. Chem.* **2001**, *44*, 1313-1333.
- (65) Varma, M. V. S.; Feng, B.; Obach, R. S.; Troutman, M. D.; Chupka, J.; Miller, H. R.; El-Kattan, A. Physicochemical determinants of human renal clearance. *J. Med. Chem.* **2009**, *52*, 4844-4852.
- (66) Waring, M. J. Lipophilicity in drug discovery. *Expert Opin. Drug Discov.* **2010**, *5*, 235-248.
- (67) Zhang Y.; Huo M.; Solver, P.K. An Add-in program for pharmacokinetic and pharmacodynamic data analysis in Microsoft Excel, *Computer Methods and Programs in Biomedicine* **2010**, *99*, 306-314.
- (68) Scharenberg, M.; Abgottspon, D.; Cicek, E.; Jiang, X.; Schwardt, O.; Rabbani, S.; Ernst, B. Cytometry-Based Assay for Screening FimH Antagonists. *Assay and Drug Development Technologies* **2011**, *9*, 455-464.
- (69) Hooton, T. M. Fluoroquinolones and resistance in the treatment of uncomplicated urinary tract infection. *Int. J. Antimicrob. Agents* **2003**, *22*, 65-72.
- (70) Jakobsen, L.; Cattoir, V.; Hammerum, A. M.; Nordmann, P.; Frimodt-Møller N.; Impact of low-level fluoroquinolone resistance genes qnrA1, qnrB19, and qnrS1 on ciprofloxacin treatment of *Escherichia coli* urinary tract infection in murine model. Poster presented at ICAAC 2010. 50th Interscience Conference on Antimicrobial Agents and Chemotherapy, 2010, Sep 12–15, Boston, MA.
- (71) Mulvey, M. A. Adhesion and entry of uropathogenic *Escherichia coli*. *Cell Microbiol.* **2002**, *4*, 257– 271.
- (72) Ballatore, C.; Huryn, D. M.; Smith, A. B. Carboxylic acid (bio)isosteres in drug design. *ChemMedChem* **2013**, *8*, 385-395.
- (73) Maestro, version 9.3, Schrödinger, LLC, New York, NY, 2012.
- (74) MacroModel, version 9.9, Schrödinger, LLC, New York, NY, 2012.
- (75) AMSOL, version 7.1, Hawkins, G. D.; Giesen, D. J.; Lynch, G. C.; Chambers, C. C.; Rossi, I.; Storer, J. W.; Li, J.; Thompson, J. D.; Winget, P.; Lynch, B. J.; Rinaldi, D.; Liotard, D. A.; Cramer, C. J.; Truhlar, D. G. University of Minnesota, Minneapolis, 2003; based in part on AMPAC, version 2.1, Liotard, D. A.; Healy, E. F.; Ruiz, J. M.; Dewar, M. J. S.

- (76) Chambers, C. C.; Hawkins, G. D.; Cramer, C. J.; Truhlar, D. G. Model for aqueous solvation based on class IV atomic charges and first solvation shell effects. *J. Phys. Chem.* **1996**, *100*, 16385-16398.
- (77) Dewar, M. J. S.; Zoebisch, E. G.; Healy, E. F.; Stewart, J. J. P. AM1 - A new general-purpose quantum-mechanical molecular-model (Vol. 107, PG 3902, 1985). *J. Am. Chem. Soc.* **1993**, *115*, 5348-5348.
- (78) Mulvey, M. A.; Schilling, J. D.; Hultgren, S. J. Establishment of a persistent *Escherichia coli* reservoir during the acute phase of a bladder infection. *Infect. Immun.* **2001**, *69*, 4572-4579.
- (79) Kabsch, W. Automatic Processing of Rotation Diffraction Data from Crystals of Initially Unknown Symmetry and Cell Constants. *J. Appl. Crystallogr.* **1993**, *26*, 795-800.
- (80) Leslie, A. G. W. The integration of macromolecular diffraction data. *Acta Crystallogr. D* **2006**, *62*, 48-57.
- (81) Winn, M. D.; Ballard, C. C.; Cowtan, K. D.; Dodson, E. J.; Emsley, P.; Evans, P. R.; Keegan, R. M.; Krissinel, E. B.; Leslie, A. G. W.; McCoy, A.; McNicholas, S. J.; Murshudov, G. N.; Pannu, N. S.; Potterton, E. A.; Powell, H. R.; Read, R. J.; Vagin, A.; Wilson, K. S. Overview of the CCP4 suite and current developments. *Acta Crystallogr. D* **2011**, *67*, 235-242.
- (82) McCoy, A. J. Solving structures of protein complexes by molecular replacement with Phaser. *Acta Crystallogr. D* **2007**, *63*, 32-41.
- (83) Emsley, P.; Cowtan, K. Coot: model-building tools for molecular graphics. *Acta Crystallogr. D* **2004**, *60*, 2126-2132.
- (84) Adams, P. D.; Grosse-Kunstleve, R. W.; Hung, L.-W.; Ioerger, T. R.; McCoy, A. J.; Moriarty, N. W.; Read, R. J.; Sacchettini, J. C.; Sauter, N. K.; Terwilliger, T. C. PHENIX: building new software for automated crystallographic structure determination. *Acta Crystallogr. D Biol. Crystallogr.* **2002**, *58*, 1948-1954.
- (85) van Aalten, D. M. F.; Bywater, R.; Findlay, J. B. C.; Hendlich, M.; Hooft, R. W. W.; Vriend, G. PRODRG, a program for generating molecular topologies and unique molecular descriptors from coordinates of small molecules. *J. Comput. Aided Mol. Des.* **1996**, *10*, 255-262.
- (86) Chen, V. B.; Arendall, W. B.; Headd, J. J.; Keedy, D. A.; Immormino, R. M.; Kapral, G. J.; Murray, L. W.; Richardson, J. S.; Richardson, D. C. MolProbity: all-atom structure validation for macromolecular crystallography. *Acta Crystallogr. D* **2010**, *66*, 12-21.
- (87) Bezençon, J.; Wittwer, M. B.; Cutting, B.; Smiesko, M.; Wagner, B.; Kansy, M.; Ernst, B. pK_a determination by ¹H NMR spectroscopy – an old methodology revisited. *J. Pharm. Biomed. Anal.* **2014**, in press; <http://dx.doi.org/10.1016/j.jpba.2013.12.014>.
- (88) (a) VCCLAB, Virtual Computational Chemistry Laboratory, 2005, <http://www.vcclab.org> (accessed August 14, 2012); (b) Tetko, I. V.; Gasteiger, J.; Todeschini, R.; Mauri, A.; Livingstone, D.; Ertl, P.; Palyulin V. A.; Radchenko, E. V.; Zefirov, N. S.; Makarenko, A. S.; Tanchuk, V. Y.; Prokopenko, V. V. Virtual computational chemistry laboratory – design and description. *J. Comput. Aided Mol. Des.* **2005**, *19*, 453-463.

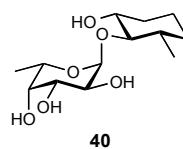
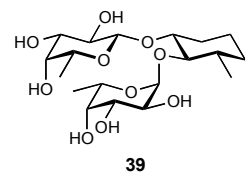
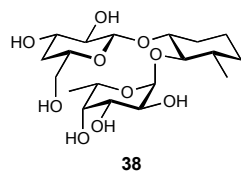
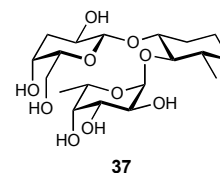
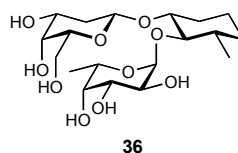
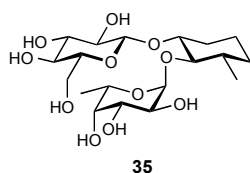
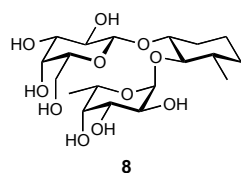
- (89) Diehl K-H.; Hull R. A. Good Practice Guide to the Administration of Substances and Removal of Blood, Including Routes and Volumes. *J. Appl. Toxicol.* **2001**, *21*, 15-23.

4. Compound Index

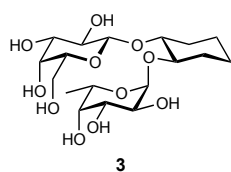
In the following, an overview of the lectin antagonists synthesized in the course of this thesis is given. The formulas are numbered as they appear in the corresponding sections.

DC-SIGN

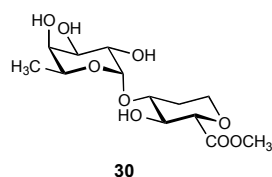
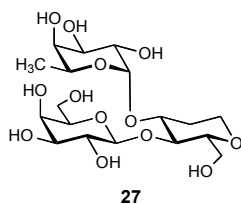
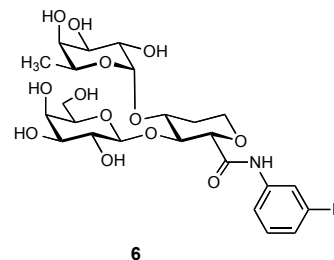
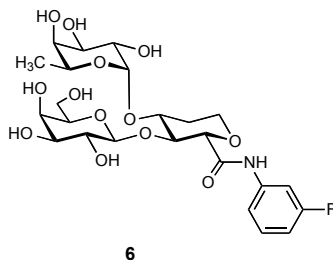
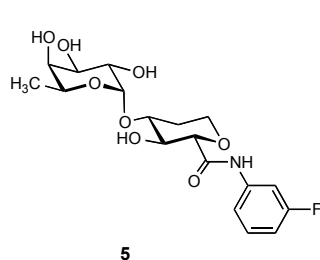
Chapter 2.3.1



Chapter 2.3.2

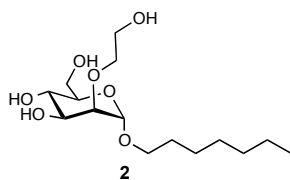


Chapter 2.3.3



FimH

Chapter 3.2.1



Chapter 3.2.2 and 3.2.3

